LOCALIZATION AND CHARACTERIZATION OF HYDROTHERMAL ALTERATION ZONES IN A GEOTHERMAL RESERVOIR AND THEIR SIGNIFICANCE FOR ROCK MECHANICS

Zur Erlangung des akademischen Grades eines

DOKTORS DER NATURWISSENSCHAFTEN

von der Fakultät für

Bauingenieur-, Geo- und Umweltwissenschaften des Karlsruher Instituts für Technologie (KIT) genehmigte

DISSERTATION

von

Dipl.-Geol. Carola Meller

Aus Mühlacker

Tag der mündlichen Prüfung: 17.11.2014

Referent: Prof. Dr. Thomas Kohl

Korreferentin: Prof. Béatrice Anne Ledésert

Karlsruhe 2014

ABSTRACT

With its potential to provide base-load electricity, geothermal energy can take an important share of the future energy mix. As estimated by the International Energy Agency, geothermal power can contribute to 3.5 % to the world-wide power production by 2050. To reach this goal, the development of Enhanced Geothermal Systems (EGS) is a major challenge. This technology allows the exploitation of low-enthalpy reservoirs developed in depths of up to several kilometers. For an economic operation of such reservoirs, pre-existing fractures are widened and new fractures are created by high pressure injection of fluids, thus creating and enhancing fluid pathways. With only a small number of EGS power plants installed world-wide, the technology is still in an early stage of development. The intended upscaling of power plant capacities from currently below 10 MW to future 100 MW meets severe obstacles including the assurance of efficiency, profitability and safety of geothermal facilities. The safety aspect mainly addresses the creation of microseismicity during hydraulic stimulation and the accidental creation of perceptible events. Key to control microseismicity is a deeper understanding of processes induced by high pressure fluid injection into and production from a geothermal reservoir. The understanding of such processes is the basis for mitigation of large seismic events, while optimizing the economic efficiency of the power plant.

This thesis is a contribution to an improved understanding of the relation between geological structures, rock mechanics and induced seismicity in EGS. The object of research is the EGS pilot facility in Soultz-sous-Forêts (France). This geothermal site stands out due to the experience of more than 25 years of development, testing and operation, which makes it a worldwide unique basis for EGS research. The PhD project was partly conducted within the portfolio topic GEOENERGIE of the Helmholtz Association of German Research Centres and it was funded by Energie Baden-Wuerttemberg (EnBW), Germany. The database for the studies formed several geophysical logs and drill core samples, courtesy of GEIE Heat Mining in Soultz, drilled rock cuttings provided by BRGM in Orléans, and catalogues of induced seismicity from the wells GPK1 [*Jones et al.*, 1995] and GPK3 [*Dorbath et al.*, 2009; *Dyer et al.*, 2003].

The main focus of this work is on hydrothermal alteration zones in the granitic rock mass of the geothermal reservoir in Soultz. These zones are affecting large parts of the reservoir rock, yet little is known about their precise location and their significance for reservoir mechanics. The first of four analyses aims at the localization of such hydrothermally altered zones and the quantification of their clay contents. A novel method based on a neural network is developed, which derives the clay content of fractures along the borehole wall from spectral gamma ray and fracture density derived from image logs. The neural network is trained on the correlation between the

fracture density, the density of clay-filled fractures, and spectral gamma ray signatures. Synthetic clay content logs (SCCLs) are created, indicating the clay-content along the boreholes. Calibration with reference data from the drill-core of the well EPS1 demonstrates a good accordance of the generated SCCL with the reference and underpins the potential of this method.

The application of the neural network on the deep Soultz wells GPK1-GPK4 and the characterization of hydrothermal alteration on the basis of drilled rock cuttings is the focus of the second study. It is demonstrated that magnetic susceptibility measured along the drill core of the reference well EPS1 is inversely correlated with the SCCL. Therefore, optical and magnetic mineralogical investigations of drilled rock cuttings, which reflect the magnetic signature of their original host rock, reveal to be suitable to characterize hydrothermal alteration of the Soultz granite. An alteration index from temperature dependent susceptibility measurements represents the alteration grade of the granite and is used to calibrate the SCCLs for GPK1-GPK4.

The calibrated SCCLs are subsequently used to investigate the mechanical significance of alteration zones. The main focus of this study is on the interpretation of borehole breakout analyses and observations during and after reservoir stimulation on the basis of the SCCLs. The study reveals a cumulative occurrence of breakouts in clay rich zones, indicative of a mechanical weakening of the rock. The deviation of the breakout orientation from their mean orientation in intervals with high SCCL might be an indicator of a stress field manipulation in clay rich zones. It is shown that there is a correlation between the occurrence of aseismic movements and increased clay contents in the rock. An influence of clay on induced seismic events is emphasized by the inverse correlation of the clay content with the maximum magnitude of induced seismic events, which has never been shown before on the scale of a geothermal reservoir.

The significance of clay-filled fractures on induced seismicity is further investigated in the fourth study, which aims on the characterization of seismicity induced during the 1993 stimulation of GPK1. In this study the critical pressure of fractures is determined by applying different mechanical properties according to the fracture clay filling. A probabilistic model of fracture orientations in the open-hole section of GPK1 is created and the fracture clay content is determined from the SCCL. Accordingly, decreasing mechanical strength is attributed to the fractures with high clay contents and the critical pressure of the fractures is determined. Comparison with the characteristics of induced seismicity during stimulation demonstrates that both, the occurrence of seismic events at low stimulation pressure, and the evolution of induced seismic events could be explained by discriminating fractures with different mechanical properties. Although based on a simplified model, the result of this analysis highlights the significance of hydrothermal alteration zones for reservoir mechanics and seismic events induced during reservoir stimulation and operation. It can be used as a basis for more complex geomechanical models of processes related to pore pressure changes in rock masses.

ZUSAMMENFASSUNG

Als eine der wenigen erneuerbaren Energien ist die Geothermie in der Lage, Grundlaststrom zu liefern, weshalb sie einen wichtigen Stellenwert im zukünftigen Energiemix einnehmen kann. Die Internationale Energiebehörde schätzt, dass im Jahre 2050 ein Beitrag der geothermischen Energie zur weltweiten Energieversorgung von bis zu 3,5 % möglich ist. Die größte Herausforderung um dieses Ziel zu erreichen, ist die Weiterentwicklung von Enhanced Geothermal Systems (EGS). Diese Technologie ermöglicht es, Niederenthalpie-Lagerstätten zu nutzen, die in Tiefen bis zu mehreren Kilometern erschlossen werden. Für eine wirtschaftliche Nutzung solcher Reservoire, werden durch das Einbringen von Fluiden unter hohem Druck bestehende Kluftsysteme erweitert und neue Klüfte geschaffen, um den Durchfluss durch das Gestein zu erhöhen. Mit bisher nur wenigen installierten EGS Kraftwerken weltweit, steht die Technologie jedoch noch am Anfang ihrer Entwicklung. Die angestrebte Erhöhung der Kraftwerkskapazitäten von derzeit 10 MW auf zukünftige 100 MW stößt auf erhebliche Hindernisse, wie zum Beispiel die gleichzeitige Gewährleistung der Effizienz, der Wirtschaftlichkeit und der Sicherheit geothermischer Systeme. Der Sicherheitsaspekt zielt vor allem auf die Erzeugung mikroseismischer Ereignisse während der hydraulischen Stimulation, wobei in seltenen Fällen auch spürbare Ereignisse auftreten. Ein Schlüsselfaktor, um die Mikroseismizität kontrollieren zu können ist ein tiefgehendes Verständnis der Prozesse, die durch das Injizieren von Flüssigkeiten unter hohem Druck oder während der Produktion aus einem geothermischen Reservoir in Gang gesetzt werden. Nur so können größere seismische Ereignisse verhindert werden, während jedoch gleichzeitig die Wirtschaftlichkeit des Kraftwerks optimiert wird.

Diese Dissertation liefert einen Beitrag zu einem besseren Verständnis der Zusammenhänge zwischen geologischen Strukturen, der Gesteinsmechanik und induzierter Seismizität in EGS. Im Mittelpunkt der Untersuchungen steht das EGS Pilotprojekt in Soultz-sous-Forêts (Frankreich). Dieser Geothermie-Standort zeichnet sich durch die Erfahrung von über 25 Jahren Entwicklung, Erprobung und Betrieb aus, was ihn zu einer weltweit einzigartigen Grundlage für EGS-relevante Forschung macht. Die Studien wurde zum Teil innerhalb des Portfolios GEOENERGIE der Helmholtz-Gemeinschaft Deutscher Forschungszentren durchgeführt und wurde von der Energie Baden-Württemberg (EnBW) mitfinanziert. Die Datengrundlage für diese Arbeit bilden mehrere geophysikalische Logs und Bohrkernproben, die von GEIE Heat Mining, Soultz zur Verfügung gestellt wurden. Bohrklein wurde bereitgestellt vom französischen geologischen Dienst (BRGM) in Orléans. Außerdem werden Seismizitätskataloge der Bohrungen GPK1 [*Jones et al.*, 1995] und GPK3 [*Dorbath et al.*, 2009] verwendet.

Der Fokus dieser Arbeit liegt auf hydrothermalen Alterationszonen im Granit des geothermischen Reservoirs in Soultz. Große Teile des Reservoirgesteins sind von hydrothermaler Alteration betroffen, jedoch ist nur wenig über deren genaue Lage und ihre Bedeutung für die Reservoirmechanik bekannt. Das Ziel der ersten von vier Untersuchungen ist daher zunächst die Lokalisierung der alterierten Bereiche und die Quantifizierung ihrer Tongehalte. Dazu wird eine neuartige Methode basierend auf einem neuronalen Netz entwickelt, die dazu in der Lage ist, den Tongehalt aus Spektralen Gamma Ray und Kluftdichte-Logs abzuleiten. Das neuronale Netz wird hierbei auf die Korrelation zwischen der Kluftdichte, der Dichte tongefüllter Klüfte und den Signaturen des Spektralen Gamma Ray Logs trainiert. Anschließend werden synthetische Tonlogs (SCCLs) erzeugt, die den Tongehalt entlang der Bohrung anzeigen. Die Kalibrierung der SCCL mit Referenzdaten des Bohrkerns aus der Bohrung EPS1 bestätigt die geringe Abweichung des erzeugten SCCLs von der Referenz und untermauert das Potenzial dieser Methode.

Die Anwendung des neuronalen Netzwerkes auf die tiefen Bohrungen GPK1-GPK4 und die Charakterisierung der hydrothermalen Alteration anhand von Bohrklein steht im Mittelpunkt der zweiten Studie. Es wird gezeigt, dass die magnetische Suszeptibilität, die entlang des Bohrkerns der Referenzbohrung EPS1 gemessen wurde, invers mit dem entsprechenden SCCL korreliert. Daher erweisen sich optische und magnetische Untersuchungen des Bohrkleins, das die magnetische Signatur seines Herkunftsgesteins widerspiegelt, als geeignet, um die hydrothermale Alteration des Soultz Granits zu charakterisieren. Ein Alterationsindex, der aus thermomagnetischen Messungen bestimmt wird, repräsentiert den Alterationsgrad des Gesteins und dient der Kalibrierung der SCCLs für die Bohrungen GPK1-GPK4.

Die kalibrierten SCCLs werden im Folgenden genutzt, um die mechanische Bedeutung von Alterationszonen zu untersuchen. Der Schwerpunkt dieser Untersuchung liegt auf der Interpretation von Bohrlochrandausbrüchen und verschiedenen Beobachtungen, die während und nach der Reservoir-Stimulation gemacht wurden, auf Grundlage der SCCLs. Die Studie offenbart ein gehäuftes Auftreten von Bohrlochrandausbrüchen in tonreichen Zonen, was auf eine Schwächung des Gesteins in solchen Bereichen hindeutet. Die Abweichung der Orientierung der Randausbrüche vom durchschnittlichen Mittel in Bereichen mit hohen SCCL-Werten könnte ein Hinweis auf eine Veränderung des Spannungsfeldes in tonreichen Zonen sein. Weiterhin zeigt sich ein Zusammenhang zwischen dem Auftreten aseismischer Bewegungen und erhöhten Tongehalten im Gestein. Eine Beeinflussung der induzierten Seismizität durch Ton zeigt sich in der inversen Korrelation zwischen der maximalen Eventmagnitude induzierter Beben und dem Tongehalt, was bisher noch nie auf der geothermischen Reservoirskala gezeigt werden konnte.

Die Bedeutung von tongefüllten Klüften für die induzierte Seismizität wird in der vierten Untersuchung näher betrachtet, in der eine Charakterisierung der Seismizität, die während der Stimulation der Bohrung GPK1 im Jahre 1993 aufgezeichnet wurde, angestrebt wird. Dazu wird der kritische Druck von Klüften bestimmt, wobei je nach

Tongehalt der Klüfte verschiedene mechanische Parameter zugewiesen werden. Es wird ein Wahrscheinlichkeitsmodell der Kluftorientierungen im Open-Hole Bereich der GPK1 erstellt, wobei der Tongehalt der Klüfte anhand des SCCLs bestimmt wird. Entsprechend der SCCL Werte wird den Klüften mit höheren Tongehalten dann eine geringere mechanische Festigkeit zugewiesen und anschließend der kritische Druck berechnet. Ein Vergleich der Ergebnisse mit den Eigenschaften der induzierten Mikroseismizität zeigt, dass sowohl das Auftreten von seismischen Ereignissen bei geringen Stimulationsdrücken als auch der Verlauf der induzierten Seismizität mit der Unterscheidung zwischen Klüften mit unterschiedlichen mechanischen Eigenschaften erklärt werden könnte. Obwohl die Berechnungen auf einem vereinfachten Modell beruhen, unterstreicht das Ergebnis der Studie die Bedeutung der hydrothermalen Alterationszonen für die Reservoir-Geomechanik und die Seismizität, die während der Stimulation und dem Betrieb eines Reservoirs induziert wird. Es kann als Basis für komplexere Modelle von Prozessen dienen, die im Zusammenhang mit Porendruckänderungen im Gestein stehen.

TABLE OF CONTENTS

1 INTRODUCTION

The recently published report of the Intergovernmental Panel on Climate Change (IPCC) of the United Nations (UN) confirmed an advancing climate change, wherein the emission of carbon dioxide is seen as the main initiator of this process [*IPCC*, 2014]. Renewable energy forms replacing fossil fuels are a key factor towards halting the climate change. During the stepwise transition from the fossil and atomic power production to renewables, a challenging goal is the insurance of base-load power without additional CO_2 impact of interim technologies. Among a wide range of renewables, geothermal energy can take an important share in the reduction of greenhouse gases. This quasi-inexhaustible energy source can replace fossil fuels for electricity production and heating and cooling of buildings. In contrast to other renewables, which are based on fluctuating resources, geothermal energy is permanently available and can provide CO_2-neutral base-load electricity. Geothermal energy production is totally controllable and as a domestic resource it is independent from imports.

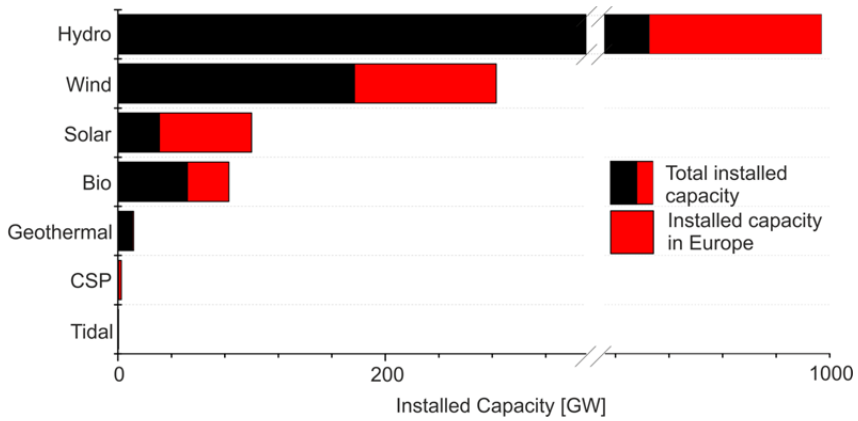

Figure 1-1: Installed capacity of renewable powers worldwide and in Europe. CSP = concentrated solar power. Hydropower has by far the largest share in renewables, followed by wind and solar power. However, besides hydropower and under certain circumstances biomass, geothermal energy is the only non-fluctuating energy amongst the presented. Data is from REN21 [2013]

According to the REN21 [2013] report, geothermal electric generating capacity grew by an estimated 300 MW in 2012, resulting in a total capacity of 11.7 GW_e and generating at least 72 TWh_e. The total capacity of geothermal contributing to renewable energy production is estimated to 223 TWh, corresponding to only ~2.4 % of the total installed capacity of renewables (Figure 1-1). The small share of geothermal to the total renewable energy production is mainly originating from the localized occurrence of high enthalpy reservoirs. Whereas geologically favored countries like Iceland, Indonesia, New Zealand, Kenya or the Philippines can cover a substantial part of their

electricity demand by direct use of hydrothermal resources, the major part of developed nations are located in low-enthalpy regions, where underground temperatures are too low for direct geothermal use.

The harvesting of energy from low-enthalpy reservoirs requires drilling of deep wells into low-permeable basement rocks. The concept of enhanced geothermal systems (EGS) allows economic energy production in low-enthalpy regions, like the major part of Central Europe (Figure 1-2). With the exception of a small high-enthalpy area in western Italy, where the first electricity producing power plant was installed in Larderello in 1913, geothermal electricity production in Central Europe is restricted to EGS. The first EGS pilot project in Europe was started in 1987 with the drilling of the well GPK1 in Soultz-sous-Forêts at the Western border of the Upper Rhine Graben. Today, the total installed geothermal capacity in Europe is ~1.6 MW (as in 2010) with 11.4 TWh/a electricity production [*EGEC*, 2011].

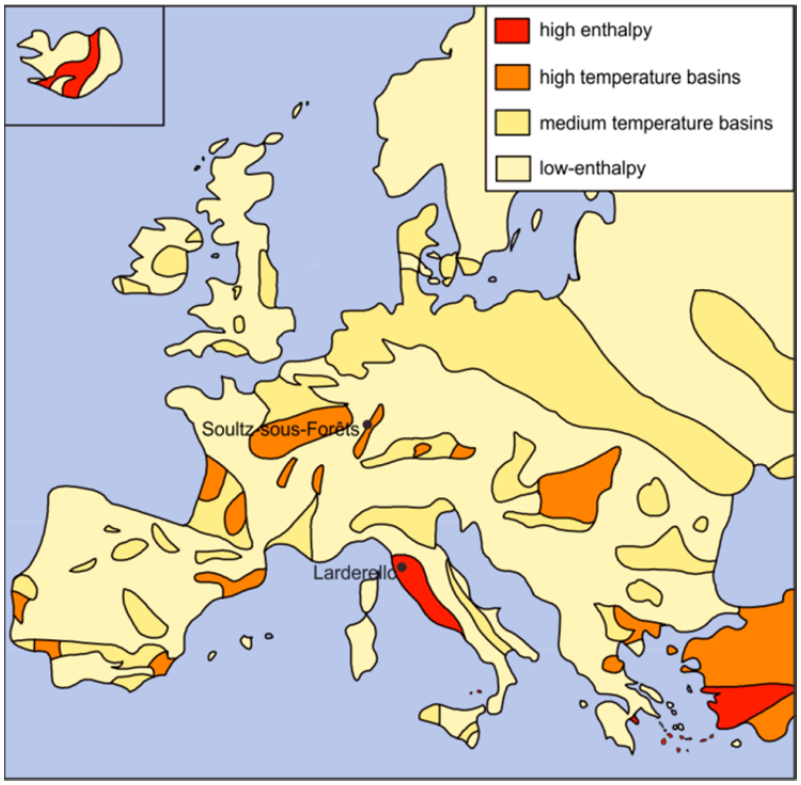

Figure 1-2: Main geothermal resources in Europe [modified after Antics and Sanner*, 2007]. The major part of Europe is characterized by a medium temperature to low-enthalpy underground suited for EGS only. In 1913, a high-enthalpy reservoir in Larderello (Italy) was for the first time used for geothermal electricity production. In the 1990s, a European EGS prototype was installed in the crystalline basement of the Upper Rhine Graben (Soultz-sous-Forêts, France).*

1.1 ENHANCED GEOTHERMAL SYSTEMS

The principle of EGS is the circulation of fluids through artificially created or enhanced fluid pathways in primary low-permeable reservoir rock. Circulation is either accomplished by the extraction and re-injection of natural geothermal brine or, in the case of dry reservoirs, by the injection of water from the surface. Hydrofracturing [*Sharma et al.*, 2004] or thermal fracturing [*Charlez et al.*, 1996], which aim at the creation of new fractures as fluid pathways, are mostly restricted to tight sedimentary rocks [*Stober and Bucher*, 2012]. More common is the forced shearing and dilation of naturally occurring fractures by the injection of water [*Baumgärtner et al.*, 2004] or chemicals [*Nami et al.*, 2008] into the reservoir. Chemical stimulation is based on the dissolution of minerals on fracture surfaces to enhance the fracture permeability. The injection of high-pressurized water into the reservoir during hydraulic stimulation aims at inducing faulting of fractures and increasing permeability until economic flow rates are reached. Figure 1-3 illustrates the principle of an EGS system. Hot water from the geothermal reservoir is extracted through a production well. It is used to produce electricity with a steam turbine or at lower temperatures with a binary power plant system. This way, energy in the form of heat is dissipated from the geothermal fluid and its temperature is reduced. The loop is closed by the re-injection of the fluid into the reservoir, where it is heated up again.

The vision of the International Energy Agency (IEA) is a contribution of geothermal of 3.5 % to the global electricity production by 2050, thus avoiding 800 megatons of CO_2, whereas half of the expected increase is made up by EGS [*IEA*, 2011]. The IEA aims at installing minimum 50 EGS research power plants and at upscaling EGS capacity by a factor of 3 until 2025. Eventually 100 MW_e power plants are planned to be realized in 2050 by the serial installation of EGS modules. This challenging goal can only be reached by an improved networking between scientists, engineers, governments and the public in order to face the obstacles that currently inhibit the development of geothermal energy.

Among the most important challenges and milestones for EGS development as defined by IEA are

- The reduction of drilling costs by advancing the development of cheaper drilling technologies,
- Arousing investors' interest and confidence in geothermal projects by defining medium- and long-term targets for geothermal energy technologies,
- The economic harvesting of geothermal energy from different geological environments,
- Improving social acceptability of the technology by controllability, i.e. facing the problems of environmental impacts and safety.

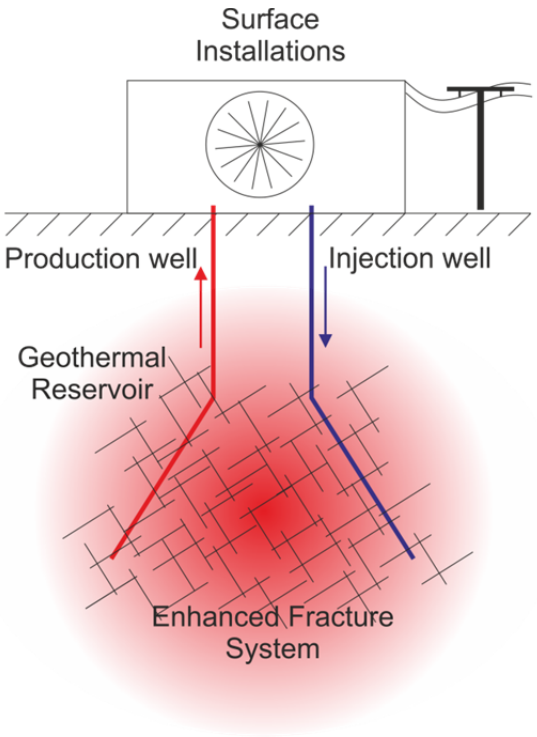

Figure 1-3: Principle of an enhanced geothermal system. Cool water is injected into an enhanced connected fracture network penetrating the geothermal reservoir. The heated water is extracted by a production well. A steam turbine by a binary power plant system on the surface produces electricity, which is directly delivered to the power network. With the re-injection of the cooled down water, the loop is closed.

In addressing these challenges, the installation of large-scale EGS projects is an essential step. The first EGS pilot project in Europe was installed in the 1990s in Soultz-sous-Forêts. In more than 25 years of research, a world-wide unique scientific database and experience has accumulated. The large-scale experiment in Soultz provided and still provides the possibility to test exploration and monitoring techniques, borehole methods and components of the power plant and to explore the short-term and long-term response of the geothermal reservoir to fluid circulation and heat extraction. Today, Soultz is the only geothermal site world-wide exploiting a reservoir at depths below 5000 m. Several important milestones were reached during the development of the reservoir. Amongst these is the increase of productivity by the factor 1000 after hydraulic stimulation of the reservoir at 3.6 km in 1997 [*Kohl et al.*, 1997]. The productivity of the lower reservoir (<5000 m) was increased by the factor 100 by chemical and hydraulic stimulation in 2007 [*Tischner et al.*, 2007], and 4 years later, circulation experiments achieved a further increase by the factor 2 [*Genter et al.*, 2013]. Successful prediction of the reservoir response to stimulation was accomplished in 2007 [*Kohl and Mégel*, 2007]. In 2011, the occurrence of seismic events during production could be reduced by a factor 0.04, as well as the magnitude of events.

The Soultz site was the first successful installation of EGS world-wide, yet new questions arose during its operation. It is for example still not fully understood, why seismicity during stimulation of the well GPK4 was different from those of the remaining wells [*Calò et al.*, 2014]. Whereas the seismic cloud of the GPK4 stimulation reached its full dimension in an early stage of injection and the wellhead pressure curve was rather flat, the spatial extension of induced seismicity during the stimulation of GPK1 developed with increasing injection pressure. A key factor towards a better characterization of the related processes is the understanding of the fluid mechanics during and after hydraulic stimulation. There is evidence that the processes before and after stimulation are different [e.g. *Schoenball et al.*, 2012; *Schoenball et al.*, 2014]. A further aspect, which remains unsolved, is the role of aseismic movements contributing to the total displacement on fractures during stimulation [*Cornet et al.*, 1997]. The assessment of their role for reservoir geomechanics and the prediction of their occurrence is a subject of research. The mentioned tasks are only some of the challenges of the EGS technology, which are related to the reservoir structure. A sound analysis of the reservoir rock is therefore fundamental to face these challenges. The present thesis aims at an improved characterization of the Soultz reservoir with the objective to better understand related mechanical processes.

1.2 MOTIVATION

25 years' experience during EGS development in the Upper Rhine Graben (URG) in Central Europe highlighted the importance of a sound reservoir characterization for safety and success of an EGS power plant installation and operation. In recent years, the large exploration risk, problems with wellbore stability and the occurrence of induced seismicity caused the failure of several projects and hampered the implementation of the EGS technology in the Upper Rhine area. Especially, avoiding perceptible seismic events with their immediate impact on the environment of a geothermal power plant has become a major task in EGS associated research.

The opening of fractures, which is the goal of hydraulic stimulation, is accompanied by small seismic events. Such events are wanted as they indicate shear movements on fractures, which are needed to enhance the fracture permeability, and they are a useful tool for the characterization of a reservoir. However, if large perceptible earthquakes occur, anxiousness can be caused amongst the local resident population. This happened for example during stimulation of the Basel Deep Heat Mining Project in 2006, where a M_L=3.4 earthquake occurred [e.g. *Häring et al.*, 2008] or during operation of the Landau geothermal power plant, when a M_L=2.4 and a M_L=2.7 earthquake happened [*Groos et al.*, 2013]. As a consequence, the Deep Heat Mining Project in Basel was abandoned and the Landau power plant had to reduce the injection pressure, thus reducing its economic efficiency.

A key factor to promote development of the EGS technology is an efficient exploitation of geothermal reservoirs to reach economic flow rates while keeping environmental impacts controllable and reducing them to a minimum. The role of scientists is to provide the basis for an understanding of the coupled processes in a geothermal reservoir during its development and exploitation. Knowledge of these processes is fundamental for the application of new technologies and stimulation techniques. Their analysis requires the combination of reliable characterization methods and reservoir models. For the creation of reservoir models the establishment of more detailed structural and geological databases is needed. Present techniques have to be refined and novel approaches are required to extract more information from available data.

In Germany, the crystalline basement provides the largest potential for EGS due to elevated temperatures and profound fracturation [*Schill et al.*, 2011]. However, the exploration and characterization of crystalline geothermal reservoirs is a major challenge due to their complex structure and mineralogy. The Soultz geothermal reservoir is located in the crystalline basement of the Upper Rhine Valley and is therefore representative of crystalline EGS reservoirs. Due to its long-term operation experience and its huge database, the Soultz site is predestined for the development and testing of techniques applicable to crystalline reservoirs and it was therefore selected as a basis for this thesis.

1.3 THESIS STRUCTURE

In the context of the social and energy-economic framework of EGS related science, the present thesis aims at presenting novel approaches to contribute to a deeper understanding of interrelated processes of geological structures, mineralogy and rock mechanics. The focus is on hydrothermal alteration zones in crystalline rock. The thesis is presented as a cumulative dissertation comprising four individual studies addressing hydrothermal alteration and associated rock mechanical phenomena. Three of the studies have been published in a scientific journal and one of them is accepted as a reviewed conference paper of the World Geothermal Congress in 2015. It is currently prepared for publication in a scientific journal.

The first part of the thesis will provide fundamentals about hydrothermal alteration and related rock mechanics, which highlight the relationship between different processes and the importance of hydrothermal alteration. Following, the benchmark data of the EGS pilot project in Soultz-sous-Forêts are reported. The second part consists of four studies, which build on each other, and which address the following questions:

- Is it possible to localize and quantify clay zones in a crystalline geothermal reservoir? (chapter 4)

- Which methods are suitable to characterize hydrothermal alteration in the absence of core samples? (chapter 5)

- Are alteration effects on geomechanics directly observable in a reservoir? (chapter 6)

- Can the evolution of induced seismicity be explained and assessed with the occurrence of alteration zones and resulting mechanical contrasts? (chapter 7)

The following outline provides an overview of the four studies, which are supposed to provide answers to these questions.

Localization of hydrothermally altered zones (chapter 4)
This study has been published in *Geophysical Journal International*.

The first study involves the development of a method to localize hydrothermally altered fracture zones in crystalline reservoir rocks on the basis of standard borehole logging techniques. The localization of these zones is a basis for estimating the mechanical friction of rock. The lack of sample material and extensive logging in geothermal projects was the incentive to find a method to derive information about the location of hydrothermally altered zones from standard logs measured in boreholes. The developed method is based on a neural network using the Kohonen algorithm and proved to be very successful in creating synthetic logs (SCCL) from spectral gamma ray data. These logs semi-quantitatively indicate the density of clay-filled fractures along a borehole in five groups. More than 90 % of a core-derived reference log could be reproduced with a deviation of ≤1 SCCL group. The created synthetic logs serve as a basis for further investigations to characterize the significance of clay zones in the Soultz granite.

Characterization of hydrothermal alteration (chapter 5)
This study has been published in *Geophysical Journal International*.

On the basis of the SCCL, magnetic mineralogical investigations are performed on cutting material from the deep geothermal wells GPK1, GPK3 and GPK4. The focus of this study is on the calibration of the SCCL on the basis of magnetic susceptibility measurements combined with optical microscopy and on a characterization of hydrothermal alteration without core material. The study shows that magnetic susceptibility is strongly correlated with the alteration degree of the Soultz granite. An alteration index on the basis of κ-T curves could be derived indicating the alteration degree of the sample. The combination of magnetic susceptibility investigations with optical microscopy is necessary in order to correctly interpret the susceptibility measurements.

A major finding of this study is that the SCCLs are also valid in the deep Soultz geothermal wells and can be calibrated with magnetic susceptibility measurements. Furthermore, it is highlighted that cutting material can provide valuable information about the geothermal reservoir, if no core samples are available.

Significance of hydrothermal alteration for rock mechanics (chapter 6)
This study has been published in *Geothermal Energy*.

The role of hydrothermal alteration for the frictional behavior of fractures and the mechanical strength of rock have been extensively studied on-site or in laboratories around the globe. The third study provides a review of the most important findings with respect to the relation between hydrothermal alteration and rock mechanics, the stress field, and induced seismicity. The role of hydrothermal alteration on the rock mechanical properties in Soultz is investigated by interpreting observations from earlier studies on the basis of the SCCL logs. It is shown that hydrothermally altered rock has a lower mechanical strength, depending on the grade of alteration. There is evidence for a stress decoupling in hydrothermally altered zones, which results in a change of magnitude and orientation of the stress field. Furthermore, weak zones are assumed to affect the evolution of induced seismicity and the occurrence of aseismic movements. A major finding of this study is an inverse correlation between the clay content of fractures and the maximum magnitude of seismic events induced on the fractures. This has never been demonstrated before on the scale of a geothermal reservoir.

Critical pressure of fractures (chapter 7)
This study has been accepted as a proceedings paper of the WGC in 2015 and is currently prepared for publication in a scientific journal.

The final study describes an approach to reconstruct the evolution of induced seismicity during the 1993 stimulation of GPK1 with a probabilistic model of the critical pressure of fractures. A preliminary study on the failure probability of fractures revealed that more information about the frictional properties of fractures is necessary in order to better estimate their critical pressure. Therefore, the SCCL logs are used in this study to assess the frictional properties of the fractures in Soultz. With a probabilistic distribution of fracture orientations and clay content, the number of fractures shearing at a certain pore overpressure is determined for the open hole section of GPK1. The results of the critical pressure distribution derived from applying different frictional parameters are compared to induced seismicity during hydraulic stimulation of the well in 1993. The results show that the presence of weak fractures with low friction coefficients and/or low cohesion could explain the evolution of induced seismic events. This approach can be used as a basis for more sophisticated models of induced seismicity.

2 HYDROTHERMAL ALTERATION IN FAULTS AND ITS NEURO-INFORMATIC CHARACTERIZATION

The modification of the rock structure and mineralogy during hydrothermal alteration has two major effects: The impact on the mechanical properties of rock due to the weakness of hydrothermal alteration zones, and the influence of the hydraulic properties of hydrothermally altered fluid pathways. Due to the importance of these effects for reservoir performance, the characterization of alteration effects and their localization in rock structures has become a major task for EGS. This chapter provides fundamentals about the most important aspects of hydrothermal alteration for rock mechanics and hydraulics. In the second part of the chapter, the principle of neural networks and self-organizing maps is introduced as a tool to characterize rock masses and the occurrence of hydrothermal alteration on the basis of logging data.

As these fields of research are rather complex, only an outline of the state of research relevant for this thesis is provided. For the fundamentals of geomechanics related to faults and earthquakes, mainly the works of Scholz [2010], Kanamori and Brodsky [2004], and Jaeger et al. [2007] were consulted. Fundamentals about clay minerals and hydrothermal alteration were mainly taken from Meunier [2005] and Velde [1995] and for neural networks, the works of Haykin [1999], Galushkin [2007] and Kohonen [1984; 2001] were used.

2.1 HYDROTHERMAL ALTERATION

The fracturation of rock masses during their tectonic history creates pathways for the percolation of hot fluids. Even, when these fluids have disappeared in recent days, they have left their marks in the form of hydrothermal alteration zones. The basic principles of hydrothermal alteration processes will be described in this section.

Velde [1995] defines rock alteration as the transformation of a rock mineral assemblage into a new set of minerals, which is more stable under the ambient hydrothermal conditions. The transformation of the rock forming minerals is induced by their local interaction with hot fluids having temperatures, which are more than 5°C warmer than the surrounding environment.

The fluids in a hydrothermal system are aqueous solutions of various phases like salts and gases. Their temperature can range from several tens of degrees to a maximum fluid temperature of 400°C and the salinity ranges between 0 to several wt-%. The pressure of the fluid is close to the hydrostatic pressure of its original environment with a maximum of 100 MPa [*Velde*, 1995]. At its original place, equilibrium established between the fluid and the surrounding rock. When the fluid rises to shallower depths, the conditions change and a new equilibrium state is approached, which includes chemical and mineralogical changes of the fluid and the surrounding rock. Hydrothermal alteration is the response of the pre-existing mineral assemblage to the temperature and/or chemical changes under the influence of an aqueous solution. In this process, mainly hydrous minerals are formed and especially clay minerals are preferred, whereas the number of newly formed phases is usually small [*Inoue et al.*, 1992]. The formation of new minerals can result from the transformation of primary silicates and clay minerals or from their precipitation from the fluid.

These processes are controlled by the changing thermo-chemical conditions, which causes the formation of alteration fronts characterized by specific mineral assemblages. Such alteration fronts form a zonation around hydrothermally altered fracture zones, the so-called alteration halos.

2.1.1 GEOMECHANICAL PROPERTIES OF ALTERATION ZONES

The importance of clay zones for the geomechanical structure and earthquake mechanics in brittle rock became an important issue in the framework of mitigation studies of natural and man-made disasters. A strong focus was given to hydrothermal alteration in crystalline rock and its effect on mechanical friction. Recent studies on the San Andreas Fault revealed the significant impact of clay inside faults and fractures on their mechanical and hydraulic properties. Evidence for the role of clay as zones of weakness or some kind of lubricant on faults promoting aseismic movements has been described by Schleicher et al [2006b], Dolan et al [1995], and Wu et al [1978]. Clay minerals are a characteristic of creeping faults with rates of up to 30 mm/a assumed for the San Andreas Fault [*Chang et al.*, 2013]. Studies on the slipping behavior of the San Andreas Fault suggest that the fault is not merely creeping but it rather consists of creeping patches, which build up stress on other patches with high friction. If the stress is large enough, these high friction patches rupture and cause seismic events [e.g. *Chang et al.*, 2013]. This theory is supported by the work of Amelung and King [1997], who observed a continuous earthquake activity on creeping faults. A major result of their study is that creep and earthquakes are not two separated phenomena, but two processes, which go hand in hand. This has been reported earlier for numerous faults and continental margins [e.g. *Brune*, 1968; *Mulargia et al.*, 2004; *Voisin et al.*, 2004].

Mechanical friction

The stress state of a rock mass mainly originates from tectonic forces, topography and geologic structures. At any point, it can be described by the magnitude and the orientation of the three principal stress components: the vertical stress S_v, the maximum horizontal stress S_H, and the minimum horizontal stress S_h. In addition to its rock mechanical properties, the mechanical strength of a fracture is significantly affected by its orientation relative to the principal stress. According to the Mohr-Coulomb criterion, the stress on a fracture can be expressed as

$$\tau = c + S_n \cdot \tan\varphi \qquad (2\text{-}1)$$

where τ is the shear force on the fracture plane, c is the cohesion, S_n is the normal force on the fracture plane, and φ is the internal friction angle.

In terms of the maximum and minimum principal stress S_1 and S_3, the shear and normal force acting on a fracture are given by

$$S_n = \frac{1}{2}(S_1 + S_3) + \frac{1}{2}(S_1 - S_3)\cos 2\beta \qquad (2\text{-}2)$$

$$\tau = \frac{1}{2}(S_1 - S_3)\sin 2\beta \qquad (2\text{-}3)$$

$$\beta = \frac{\pi}{4} + \frac{\varphi}{2} \qquad (2\text{-}4)$$

where β is the critical plane of failure for the respective rock mass.

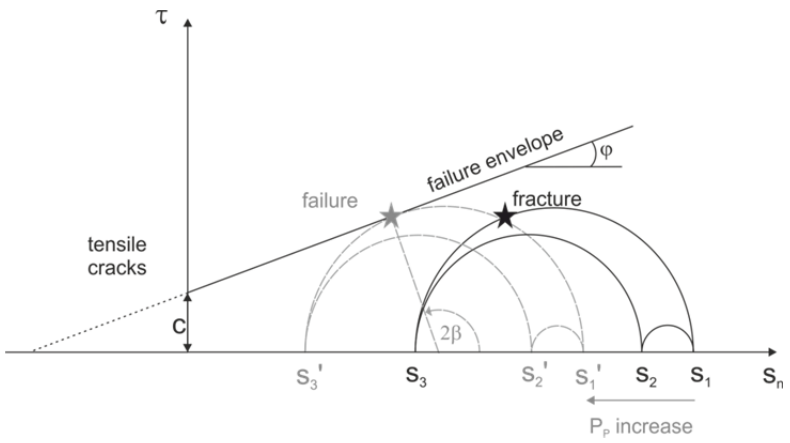

Figure 2-1: Mohr-circle representing the stress state on a fracture (black circle). A pore pressure increase shifts the circle towards the failure envelope (grey circle) and induces shear, when the fracture (star) cuts the envelope. S_n is the normal stress, τ the shear stress, S_1-S_3 and S_1'-S_3' the maximum, intermediate and minimum principal stress before and after pore pressure (P_p) increase respectively, 2β is the failure angle of the fracture, φ is the internal friction angle of the rock and c is its cohesion.

These correlations can be graphically expressed by the Mohr circle. Figure 2-1 is a sketch of the Mohr circle representing the stress state in a rock mass at a certain depth. Each fracture plane inside the reservoir can be represented by the normal on this plane as a point inside the circle. Depending on its orientation in the ambient stress field, a fracture can occur anywhere inside the Mohr circle. The failure envelope is the threshold between the stable state of the fracture and its failure, whereas the distance to the failure envelope is a measure of the required change of the current state to cause failure. The gradient and the intersection of the failure envelope with the y-axis are determined by the mechanical friction and the cohesion of the rock or the fracture surfaces. As a result, fractures at any orientations can shear upon a change of the effective stress (S-P_p), if their specific failure envelope is crossed. Without knowing the frictional properties of each fracture, there is no control of the parameters, which cause failure of the fracture. These parameters include

- The magnitude and orientation of the principal stress components,
- Pore pressure,
- Fracture orientation, and
- Friction and cohesion.

Especially, friction and cohesion of a fracture, which are characteristic factors for its mechanical properties, are hard to determine. Numerous studies were conducted to investigate these parameters. An early study by Byerlee [1978] revealed a uniform friction coefficient of rocks independent from the rock type. In his experiments, he found that the friction of different rocks depends on the confining pressure rather than on the rock type. He defined the following rules, which are known as Byerlee's law:

$$10\,MPa \leq s_n \leq 200\,MPa, \qquad \tau = 0.85 s_n \tag{2-5}$$

$$200\,MPa \leq s_n \leq 1500\,MPa, \qquad \tau = 50 + 0.6 s_n \tag{2-6}$$

However, Byerlee discovered that, if the gouge zone formed during slip on fracture surfaces is large enough, it can control the mechanical properties rather than the rough fracture surfaces. Then, the minerals, of which the gouge consists, determine the mechanical properties of the fracture. Especially, some clay minerals can have much lower friction coefficients than those specified by Byerlee's law [*Byerlee*, 1978; *Byerlee and Savage*, 1992]. As a result, hydrothermal alteration and the occurrence of clay can reduce the mechanical friction of rock. This was confirmed in several experiments. Zoback et al. [2012] and Kohli and Zoback [2013] for example investigated the relationship between clay content and mechanical friction of shale gas reservoir samples under wet conditions. They observed a linear decrease of the friction coefficient with increasing clay content from 0.8 at 10 wt-% clay to 0.4 at ~50 wt-% clay. Similar results were obtained by Tembe et al. [2010] for artificial clay gouge samples of quartz and illite and for natural soil samples tested by Akayuli et al. [2013]. The friction coefficients they measured for different clays vary and are much lower than those of other minerals like quartz or feldspars.

Earthquakes and the a- and b-value

Further characteristic parameters describing the frictional properties of rock are the *a*- and *b*-value from the Gutenberg-Richter law. Gutenberg and Richter [1942] observed that the occurrence of earthquakes with a certain magnitude in a region follows a logarithmic law and they described this relationship:

$$log_{10}N = a - bM \qquad (2\text{-}7)$$

with N the number of earthquakes with magnitude ≥M, a and b are constants. In seismogenic regions, the parameter b is typically equal to 1. Depending on the tectonic regime, b can vary between 0.5 and 1.5, but also values of >2 are observed in earthquake swarms, where a significantly higher proportion of small earthquakes occurs. The *a*-value is a representative of the total seismicity rate of a region.

As the frictional properties of rocks determine their slipping behavior, a correlation between the weakness of rocks and the occurrence of large and small earthquakes is expected. A *b*-value of 1 represents a logarithmic relationship between the magnitude of events and their frequency, whereas *b*-values > 1 reflect an increased number of small earthquakes. Hence, high *b*-values are expected in areas, where no large differential stress can build up. Schorlemmer et al. [2005] compared the results of numerous earthquakes from different settings and of laboratory data. They found that the *b*-value differs systematically with the faulting regimes. The highest *b*-values are observed in normal faulting regimes (up to 1.2), whereas the lowest *b*-values occur in thrusting regimes (as small as 0.6), and strike-slip regimes are in between. Based on the stress prevailing in the respective regimes, Schorlemmer et al. concluded that the *b*-value inversely correlates with differential stress levels. This was also confirmed by laboratory experiments performed by Amitrano [2003], who observed a decreasing *b*-value with increasing differential stress. Creeping fault sections exhibit high *b*-values around 1.3 [*Schorlemmer and Wiemer*, 2005]. Based on these results altered and fractured areas ought to be characterized by the occurrence of small events and creep, rather than by large earthquakes. This theory was for example posed by Heinicke et al. [2009] who investigated the correlation between hydrothermal alteration and the occurrence of earthquake swarms. They observed in the Vogtland Region of northwestern Bohemia that in addition to increased pore pressure and shear stress the mechanical weakening of rocks and the dissolution of fracture walls plays an important role for the evolution of earthquake swarms. Interestingly, the maximum magnitude of such earthquake swarms is limited to 5 [*Heinicke et al.*, 2009], which supports the theory of earthquakes with limited magnitudes occurring in regions with rocks of low friction coefficients. When analyzing *b*-values, one has to consider that this value is affected by numerous parameters, not least by the way it is computed. Besides the strength of the rock, the main affecting parameters of *b* are the stress field, the focal mechanism of the earthquakes and the presence of large geologic structures [*Scholz*, 2010 and references herein].

In geothermal reservoirs, the *b*-value is not constant throughout different operational stages. Large variations of *b*-values in time and space were for example observed by Bachmann et al. [2012]. They calculated the *b*-value for the time period during injection and after injection in the former EGS project in Basel, Switzerland. The *b*-values varied from 1.58 during injection to 1.15 after injection, which indicates a larger proportion of small earthquakes during injection.

Sliding on a fault

The rupture behavior of a fault from the Dietrich-Ruina constitutive model [*Dieterich*, 1978; *Ruina*, 1983] describes the frictional evolution of a fault for different sliding velocities with the material parameter $(a\text{-}b)$ representing the difference in steady-state friction. It indicates stable sliding of fault surfaces during slip, if $(a\text{-}b) > 0$, or unstable sliding, if $(a\text{-}b) < 0$. The synonyms for stable and unstable sliding are velocity strengthening and velocity weakening behavior, respectively. The effect of clay on the rupture behavior of faults has been studied in many laboratory experiments. Ikari et al. [2011] found experimental evidence for a relationship between the weakness of rocks and their frictional stability: rock samples with a low friction coefficient exhibit velocity strengthening behavior, whereas samples with high friction coefficients show velocity weakening behavior.

This indicates the occurrence of brittle failure only on rocks with high friction coefficients. Biegel et al. [1989] and Scholz et al. [1972] investigated the sliding behavior depending on the evolution of fault gouge. They observed velocity weakening during the initial sliding stage but with increased sliding displacement, when a gouge has formed, it evolved to velocity strengthening. Zoback et al. [2012] observed experimentally on shale gas samples that faults with clay contents higher than 30 % slide stable (i.e. $(a\text{-}b) > 0$), whereas faults with a lower clay content slip unstable (i.e. $(a\text{-}b) < 0$). They reasoned that such clay-rich faults slide aseismically, whereas the faults with lower clay contents produce microseismic events. Such results suggest that the filling of a fracture with gouge or hydrothermally formed clay minerals not only affects its friction coefficient, but also its frictional evolution during sliding. Higher clay contents and fine material inside fractures favor velocity strengthening behavior.

2.1.2 ALTERATION EFFECTS ON THE HYDRAULIC PROPERTIES OF A FRACTURE

Hydraulic flow through fractures is commonly described by the cubic law [*Boussinesq*, 1877]. In this approach, fractures are represented by two parallel plates with aperture a_m (Figure 2-2a). The transmissivity through the fracture strongly depends on its aperture and it can be expressed by

$$T = \frac{a_m^3}{12\mu} \qquad (2\text{-}8)$$

$$K = \frac{T}{a_h} \qquad (2\text{-}9)$$

for an even surface and for a rough surface, respectively, where μ is the fluid viscosity. The hydraulic aperture a_h of a rough surface is reduced by the presence of irregularities generally referred to as asperities (Figure 2-2b). The transformation of minerals during hydrothermal alteration can increase the aperture of a fracture by the dissolution of asperities (Figure 2-2c), or it can reduce it by the precipitation of secondary minerals, thus strongly enhancing or reducing the flow through the fracture (Figure 2-2d).

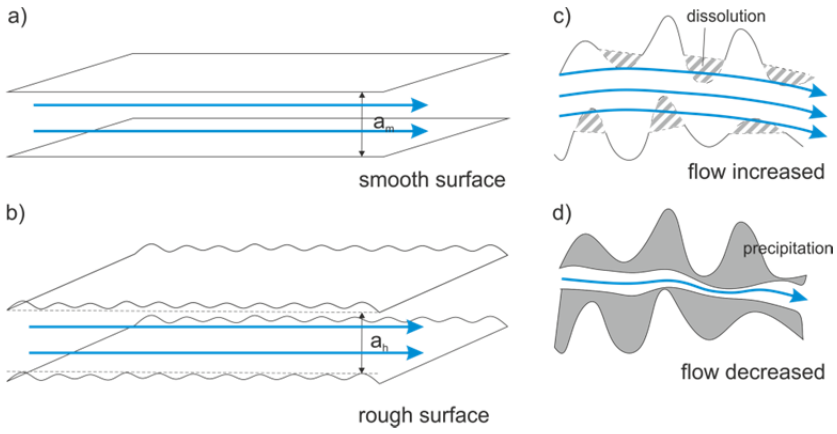

Figure 2-2: Flow through fractures represented by two parallel plates. a) Flow through an even fracture with aperture a_m. b) Flow through an uneven fracture, when the hydraulic aperture is used instead of a_m (a_h<a_m). c) The dissolution of asperities during hydrothermal alteration increases a_h and enhances the fracture transmissivity d) The precipitation of secondary minerals on the fracture surface during hydrothermal alteration can reduce a_h, thus strongly reducing the transmissivity of a fracture.

Being key factors for the success of an EGS system, the controlling parameters of permeability and transmissivity must be characterized to improve the efficacy of hydraulic and chemical stimulations. However, the effect of hydrothermal alteration on hydraulic flow through fractures is more complex than just a change of the fracture aperture, while most of the relevant processes are interrelated. The following section provides an overview of hydraulic effects of hydrothermal alteration.

Fault zones rich in phyllosilicate material tend to have lower permeabilities than quartz or framework silicate-rich gouges [*Faulkner et al.*, 2010]. The permeability of fault gouge is strongly controlled by the fraction of clay. However, due to grain size effects and compaction characteristics, there is a non-linear relation between permeability and the fault zone clay content under hydrostatic conditions. For example, in a quartz-clay mixture with a clay-content increase between 25 and 40 vol.-%, the clay particles sit in the pore space between quartz, and the compaction characteristics are largely controlled by the quartz framework [*Revil et al.*, 2002]. In experiments of Takahashi et al. [2007] and Crawford et al. [2008], the permeability reduction during deformation increased with increasing clay content from 0 to 24 vol.-%. Between 18 and 24 vol.-% clay, a dramatic permeability reduction of ~2.5 orders of magnitude occurred. In a gouge with more than 29 vol.-% clay content in contrast, deformation reduced permeability by only 0.5 orders of magnitude. This indicates that at larger percentages of clay, permeability is less sensitive to the magnitude of the clay fraction. Besides the fraction of clay, the permeability through clay-filled fractures depends on the clay structure. Fibrous illite for example, which precipitates in pores, was observed to reduce the permeability of oil reservoirs much more than platy crystals [*Wilkinson and Haszeldine*, 2002]. Due to their often platy structure, the alignment of clay crystals can result in a permeability anisotropy [*Faulkner and Rutter*, 1998]. Faulkner and Rutter [2000; 2003] showed that also temperature and pore fluid chemistry can strongly affect the permeability of natural clay-rich rocks by altering physico-chemical interactions between the rocks and the aqueous pore fluid. Chemical processes can for example cause the precipitation of calcite, which reduces the permeability. Calcite precipitation is not only limited to carbonatic rocks or sediments. It is also commonly observed in granite, even when it is not covered by carbonate sediments [*Fourcade et al.*, 2002].

Low permeability of clays inside fractures can cause pore pressure increase and reduce the fault strength [*Ikari et al.*, 2009], which is important for the forced circulation of fluids through rock masses. Fault zones can act as impermeable barriers, which keep up high pore fluid pressure [*Byerlee and Savage*, 1992; *Rice*, 1992]. Due to increased pore pressure, impermeable fractures are prone for shearing. Therefore, they are major target zones for hydraulic stimulation and permeability can be increased by orders of magnitude due to induced shearing [e.g. *Economides et al.*, 1989]. On the contrary, shearing in a gouge with coarse grains and high initial permeability can reduce the permeability significantly due to comminution [*Zoback et al.*, 2012].

The sealing of fractures with quartz makes them impermeable and rigid and the initially low permeability cannot be increased by hydraulic stimulation [*Economides et al.*, 1989]. Fractures bearing carbonates as an alteration product in contrast are observed to be good candidates for hydraulic stimulation in oil fields [*Warpinski et al.*, 2009]. In such fractures, chemical stimulation with hydrochloric acid can produce excellent results [*Kalfayan*, 2008].

Hydrothermal alteration also affects the surface structure of fractures. A fresh natural fracture has sharp edges and asperities providing numerous contact surfaces between the fracture walls. Dissolution and precipitation processes during hydrothermal alteration cause a smoothing of the fracture surface by dissolution of asperities and the precipitation of fine material in between [e.g. *Morrow et al.*, 2001; *Sausse*, 2002]. The increase of contact surfaces between the fracture walls leads to a decrease in permeability. Furthermore, the flow paths through rough and smooth surfaces are quite different. While smooth surfaces exhibit a regular flux, a large number of asperities and contact surfaces leads to pronounced channeling of the flow through fresh fracture surfaces [*Sausse*, 2002].

2.2 ARTIFICIAL NEURAL NETWORKS FOR LOG INTERPRETATION

When analyzing borehole logs, to characterize petrophysical properties of reservoir rocks, one is confronted with a large number of data. Conventional log interpretation techniques often reach their limits upon complex issues like the localization and characterization of hydrothermally altered facies. Novel techniques are required to make better use of available data, which is often limited in geothermal drillings. Neural networks have the potential to extract information from multidimensional data, which cannot be obtained from common methods. This chapter provides an outline of the fundamentals and the operation mode of neural networks.

The organization and operating mode of an artificial neural network (NN) is based on the features of a biological brain. According to Haykin [1999], an artificial neural network is defined as a massively parallel distributed processor, which consists of simple processing units. It has a natural propensity for the storage of experimental knowledge and makes it available for use. The resembling of the artificial brain covers two aspects:

1) The network uses a learning process to acquire knowledge from its environment.
2) The acquired knowledge is stored in interneuron connection strengths (synaptic weights).

There is a clear analogism between the elements of biological neurons and those of artificial neurons, which is schematically shown in Figure 2-3. Incoming information is weighted by the synaptic weights, which determine, in which way a single signal contributes to the net input. The knowledge of a network is stored in these weights. The transfer of the net input from a neuron to another is determined by a threshold function. This function controls, when and what kind of output is transferred to the connected neurons. Knowledge of a network can be acquired in three ways: supervised learning, unsupervised learning, and reinforcement learning.

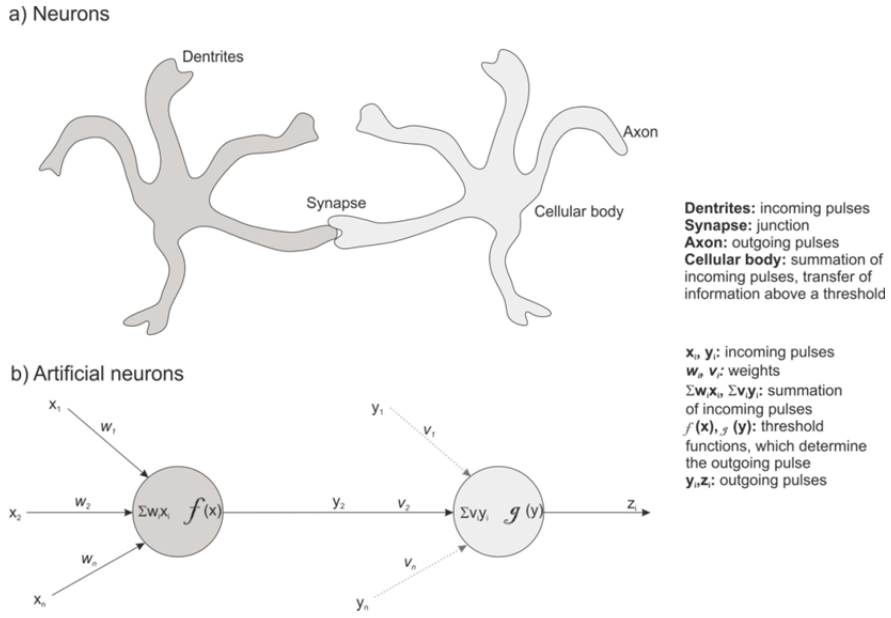

Figure 2-3: Schematic sketch of the connection between two natural neurons and two artificial neurons of a neural network. The dendrites of a natural neuron correspond to the input vectors of an artificial neuron. In the cellular body and in the artificial neuron, the incoming information is summed up. Above a certain threshold the information is passed to a neighboring neuron, which is connected by a synapse. In the natural neuron this is accomplished by an action potential. The artificial analogue is the activation function. In this way, many neurons are connected to each other and information can be transferred in a directed manner.

Supervised learning is accomplished by proposing the correct solution to the network. The weights between the neurons are adjusted to best approximate the provided solution. Unsupervised learning, i.e. learning without providing a solution, clusters the input on the basis of similarities between the parameters (self-organization). Reinforcement learning is a hybrid method between supervised and unsupervised learning. Here, the correct solution is not provided, but the network obtains feedback, if a released solution was right or wrong. The following two chapters will briefly describe the principles of supervised learning and unsupervised learning. Reinforcement learning was not used in this thesis and is therefore not discussed. Details on reinforcement learning can be found for example in Haykin [1999] or Galushkin [2007].

2.2.1 SUPERVISED LEARNING

For supervised learning, the user serves as a teacher by providing input pairs of data and the corresponding solution. There are various learning algorithms, each of them serving best for certain applications. Different algorithms are discussed in Haykin [1999]. The most commonly used algorithm is back-propagation. Here, information from the real world is passed to a layer of neurons, the so-called input neurons. This neuron layer is connected to a further hidden layer of neurons, which in turn is connected to the output layer. Each layer communicates with the following layer by weighted connections. During the training, the output layer is taught to give the correct result depending on the data given to the input-layer. At the beginning of the training phase, the network is provided a pair of corresponding input-output data. In order to retrieve the connection characteristics between input and output, the network uses a two-phase propagation-adapt cycle. This means that as soon as the input pattern is provided to the input layer, it is propagated through the layers and an output is generated. This output is then compared to the reference dataset and for each output unit an error is computed (first phase). In the second phase, these errors are communicated to each node, which is directly connected to the output. Then, the error propagates back to the input layer and each neuron receives its specific error. This error signal is then used to update (adapt) the respective connection weights in order to better approach the training dataset. The weight is modified according to

$$\Delta w_{ij} = \varepsilon \cdot \delta_i \cdot a_j \qquad (2\text{-}10)$$

where Δw_{ij} is the modification of the weight w between the neurons i and j, ε is a predefined learning parameter, δ_i is the delta value of the neuron i and a_j is the output of neuron j. The delta value is a measure of the deviation of a neuron from the desired output.

It is determined for output neurons by

$$\delta_i = f'_{act}(input_i) \cdot \left(a_{i,desired} - a_{i,observed}\right) \qquad (2\text{-}11)$$

and for hidden neurons by

$$\delta_i = f'_{act}(input_i) \cdot \sum_L \left(\delta_l \cdot w_{ij}\right) \qquad (2\text{-}12)$$

with $f'_{act}(input)$ the first derivative of the activity function of the neuron i, a_i the activity level of neuron i, L is the layer following layer I, and l is the neuron following neuron i *[Rey and Wender, 2011]*. The procedure is repeated until a predefined deviation from the real data or a predefined number of iterations are reached. The information stored in the network can now be applied and recalled on any dataset.

2.2.2 SELF-ORGANIZING NETWORKS

Self-organization plays a role in almost every aspect of science. The characteristics of self-organization are that it happens spontaneously, it is not directed and it is not controlled by any intrinsic or extrinsic factors. The organization of a system evolves by the mutual interaction of its components. In this way, the system can evolve, learn and adapt. An often unconscious example of self-organization is the coaction of differential cells to form organs and life-forms, or the creation of life itself by a spontaneous self-organization of molecules. In geology, the spontaneous crystallization of minerals, or stick slip patterns between interfaces incorporate self-organizing patterns.

The flexible and manifold application of self-organization is used in self-organizing neural networks for pattern identification in complex data. In contrast to networks using supervised learning, self-organizing networks are trained without supervision. The network tries to find patterns and regularities in the input data and to organize them in a predefined way. The self-organizing network consists of an input-layer and an output layer of neurons, which are connected by weighted junctions. Typically these two layers are a two-dimensional array of neurons. These 2D feature maps are mostly rectangular or hexagonal and are called Kohonen-maps [after *Kohonen*, 1984]. In the training phase of the network, the input vectors are presented sequentially in time. The desired output is not specified. When enough input vectors have been presented, the network defines clusters by adapting the weights of the neuron connections w_{ij} in a way that the point density functions of the clusters approximates the probability density function of the input vectors:

$$\Delta w_{ij}(n+1) = \Delta w_{ij}(n) + \theta_{ij}(n) \cdot \varepsilon \qquad (2\text{-}13)$$

where n is the current iteration number and θ is the neighborhood function, which is specific for a neuron. The neighborhood function is often Gaussian, and it determines how much the neighboring neurons are affected by the weight modification of a node. This way, the topological distance of the neurons determines, how their connection weights are changed. Close neurons are sensitive to physically similar inputs. Thus, the topology of the input is preserved in the two-dimensional representation of the data. The number of iterations should be predefined with respect to the size of the self-organizing map. According to Kohonen [2001] the number of iterations should be at least 500-fold the number of output neurons.

3 THE SOULTZ GEOTHERMAL SITE

The EGS pilot power plant in Soultz-sous-Forêts is located in the northeastern part of France (Alsace) at the western border of the Upper Rhine Graben, 40 km linear distance from Karlsruhe (Figure 3-1). An unusually high geothermal gradient in this area was discovered during oil exploration drillings between 1888 and 1970 [*Dezayes et al.*, 2005a]. This temperature anomaly together with a profound interconnected fracture network was the determining factor for the initiation of a geothermal pilot project for energy production. It started with the drilling of the first well GPK1 in 1987. The elementary facts about the Soultz EGS project will be provided in this chapter.

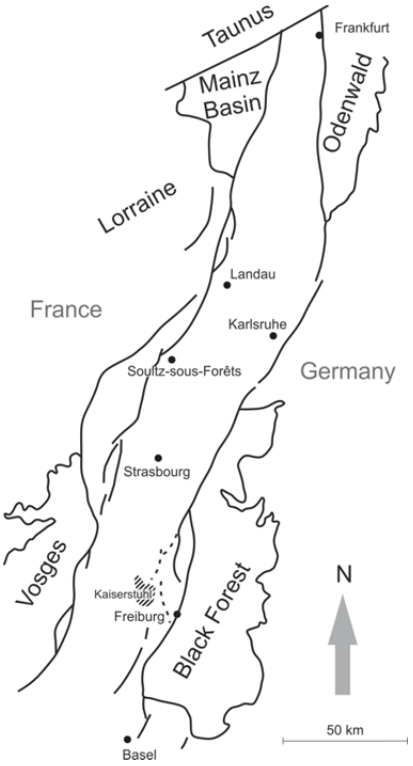

Figure 3-1: Location map of the Upper Rhine Graben.

3.1 GEOLOGICAL CONTEXT: UPPER RHINE GRABEN TECTONICS

The Upper Rhine Graben (URG, Figure 3-1) is a 300 km long and 30-40 km wide NNE trending structure of the European Cenozoic rift system (ECRIS) [e.g. *Illies*, 1975]. The Graben structure developed from an intracontinental foreland rifting contemporarily with the collisional phases of the Alpine and Pyrenean orogenies [*Schumacher*, 2002], which started about 65 million years ago in Late Mesozoic. The north-northeast trend of the Rhine Graben developed in parallel to the graben systems of southeastern France, which follow the strike of the alpine deformation front [e.g. *Brousse and Bellon*, 1983]. The large scale geological structures, which can be encountered in the URG rocks, can be related to various stress regimes evolving subsequently to the Alpine and Pyrenean collisions.

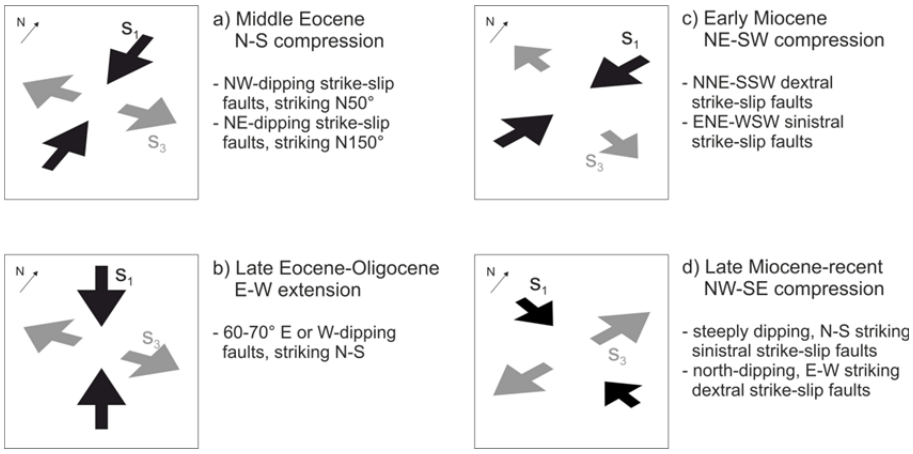

Figure 3-2: Sketch of the different stress regimes prevailing in the URG from mid Eocene to recent times and the fracture systems evolving from the different regimes.

During Middle and Late Eocene, the area of the URG was subject to N-S compression (Figure 3-2a), which originated from the collisional forces of the Alpine orogeny. Reactivation of large Permo-Carboniferous and Mesozoic faults during these times indicate a horizontal S_1 orientation of N19°E [*Dezayes et al.*, 1996]. The following main rifting stage of the URG deformation during Late Eocene to Late Oligocene is characterized by an E-W extension (Figure 3-2b) resulting from an exchange of the stress magnitudes of S_1 and S_2 upon a collisional coupling in the collision zones [*Dèzes et al.*, 2004]. The evolution of steeply dipping N-S oriented faults is associated with this stage, as well as graben subsidence and the deposition of thick sedimentary beds in the southern part of the URG.

This extensional phase was followed by a NE-SW compressional phase in Early Miocene (Figure 3-2c). It was accompanied by an uplift of the Black-Forest and Vosges and increased sedimentation rates in the northern part of the URG. The recent stress field of the URG is NW-SE compressional (Figure 3-2d) and developed in Late Miocene from the counter clockwise convergence of Africa-Arabia with Europe and the North Atlantic ridge push [*Dèzes et al.*, 2004]. The associated faults are steeply dipping, N-S striking sinistral strike-slip or E-W striking dextral strike-slip faults [*Dezayes et al.*, 1996]. The seismic activity of the Cenozoic Rift System is evidence of its ongoing tectonic evolution.

3.2 THE THERMAL ANOMALY AT SOULTZ-SOUS-FORÊTS

The hydrocarbon exploration of the Pechelbronn area from the 15th century on revealed the occurrence of bitumen at shallow depths, which can be attributed to an increased thermal gradient. Haas and Hoffmann [1929] characterized this thermal anomaly and found that locally temperatures can reach 50 °C at shallow depths of 400 m.

The ECRIS hosts some of the major geothermal anomalies in Europe in extensional settings away from active volcanic areas. Heat flow rates can exceed 150 mWm^{-2} with temperatures reaching 120 °C at 1000 m depth. The occurrence of high temperature anomalies is usually attributed to the circulation of hot fluids. Hydrothermal convection at the Graben scale can be observed in the URG and is also occurring along major faults in the Soultz area [*Dubois et al.*, 1996]. As this convection is restricted to fault and fracture systems, temperature is not homogeneously distributed in the URG. For the origin of the geothermal anomaly at Soultz, two hypotheses exist. The first attributes the increased temperature gradient to hydrothermal circulation along favorably oriented fracture zones in the basement and through the overlying highly permeable sandstone aquifer. These fractures are propped open by recent compressive shear strain parallel to the central graben segment. The second hypothesis identifies inherited fractures in the basement as circulation paths [*Baillieux*, 2012 and references herein].

Both hypotheses suppose that the hydrothermal water originates from meteoric water infiltrating into fractures at the graben shoulders or into the sedimentary cover and descending to greater depths, where it is heated up and circulates through connected fracture systems, transferring the heat to shallower depths. It is assumed that the infiltration of meteoric water and the formation of hydrothermal water are ongoing processes, as well as hydrothermal alteration of rocks around the flow paths [*Dubois et al.*, 2000; *Dubois et al.*, 1996].

3.3 GEOTHERMAL PILOT PROJECT

3.3.1 DEVELOPMENT

The drilling of GPK1 in 1987 was the initiation of the geothermal project in Soultz-sous-Forêts. The well was drilled to a depth of 2000 mTVD (true vertical depth), where a temperature of 140 °C was encountered. Several injections and tracer tests followed and temperature and flow logs were measured. A downhole seismic network was installed to monitor and to locate microseismic events induced during injection [*Dezayes et al.*, 2005a]. An important step for the characterization of the geothermal reservoir was the deepening of the former oil well EPS1 to 2227 mTVD in 1990/1991 with a full drill core recovery from 930 m to the bottom hole. In 1992, GPK1 was deepened to 3600 mTVD and large scale hydraulic tests were performed. In 1995, a third well (GPK2) was drilled to a depth of 3900 mTVD. Several hydraulic tests and hydraulic stimulations of GPK1 and GPK2 followed in order to enhance the reservoir permeability. GPK2 was deepened to 5084 mTVD in 1999 and finally, two more wells (GPK3 and GPK4) were drilled in 2002 and 2004, to depths of 5031 mTVD and 4982 mTVD, respectively. Permeability in these wells was increased by hydraulic stimulations (Table 3-1). In the 25 years of development and operation, a huge database of borehole logging, seismic monitoring, scientific publications, PhD theses, laboratory and operation data have accumulated. The huge database characterizes the Soultz geothermal site as a unique and outstanding project for scientific research.

3.3.2 RESERVOIR GEOLOGY AND HYDROTHERMAL ALTERATION

The geothermal system in Soultz-sous-Forêts exploits mainly two geothermal reservoirs in the crystalline basement, which is covered by 1.4 km Mesozoic sediments. The upper reservoir at around 3500 m depth is hosted by a Hercynian coarse-grained porphyritic monzogranite, which is characterized by large kalifeldspar megacrysts in a matrix of quartz, feldspars, plagioclase, biotite, amphibole and accessory minerals like magnetite, titanite, apatite, allanite and zircon. The lower reservoir is located in fine-grained two-mica granite with primary muscovite flakes [*Hooijkaas et al.*, 2006], which is encountered at depths greater than 4600 m. Both granites underwent several stages of hydrothermal alteration, which caused the formation of pronounced alteration zones.

The porphyritic granite has a weathering surface resulting from an exhumed stage in the formation history, when meteoric water could infiltrate the rock mass. This paleo-weathering caused a pronounced reddening of the granite by the precipitation of hematite (Figure 3-3a), but it plays no role in the deeper parts of the rock, where the

geothermal reservoirs are located. The complex alteration history of the granitic body is an ongoing process, which started in Variscan times. Mainly two types of alteration are distinguished: pervasive alteration and vein alteration. The earlier propylitic alteration is a weak isochemical alteration of the granitic matrix without a change in the granite texture (Figure 3-3b). It incorporates the partial transformation of biotite and hornblende into chlorite, the replacement of plagioclase by illite and the formation of hydrogarnet and epidote within the granite.

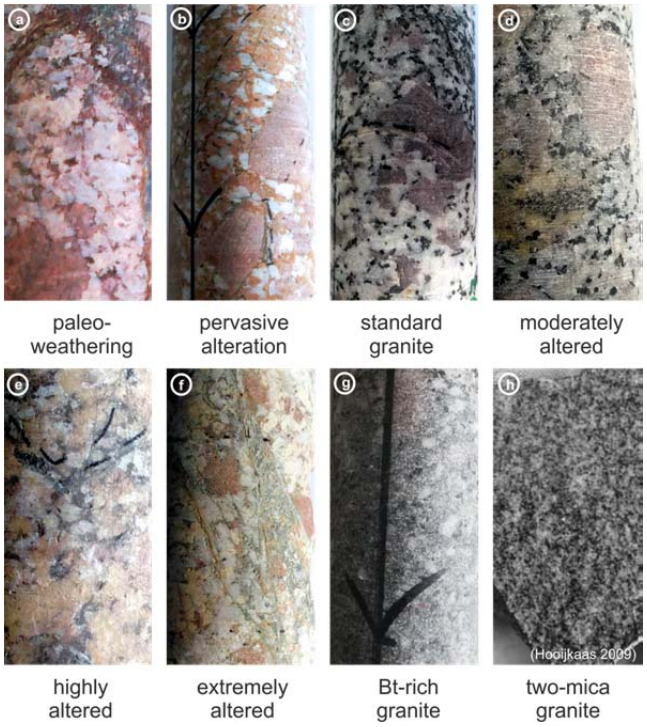

Figure 3-3: Different alteration types and grades of the porphyritic Soultz granite as observed on drill core samples (a-g) and a sample of the lower two-mica granite (h).

The second alteration, superposing the earlier stages involves strong chemical and textural changes mainly in and in the vicinity of fractures. The fractured zones in the Soultz granite are characterized by a specific structure. Around the quartz vein, which often seals the center of the fracture, a distinct zonation is observed. In the brecciated and cataclased zone, the original structure of the granite is lost and hydrothermal alteration has transformed feldspars or biotite into clay minerals. Depending on the respective minerals that have formed, the granite becomes greenish in the case of chlorite or epidote, reddish, if hematite has formed or yellowish if the dominating clay mineral is illite [*Genter et al.*, 2000]. This vein alteration is significantly changing the mechanical and structural properties of the rock [*Valley and Evans*, 2006]. Along with the mineralogy the physical parameters like porosity, bulk density and P-wave velocity of the rock change [*Ledésert et al.*, 2010].

In some altered zones, quartz, biotite, plagioclase and hornblende are totally dissolved [*Ledésert et al.*, 2010]. The precipitations in veins contain secondary quartz, barite, illite, carbonates, iron oxides, and locally illite-smectite and chlorite-smectite mixed-layers [*Genter et al.*, 2000; *Schleicher et al.*, 2006a]. Various alteration grades can be distinguished on core samples and cuttings ranging from low to extreme alteration (Figure 3-3c-f). The same kinds of alteration are also observed in the biotite-rich granite, a facies variation of the porphyritic granite (Figure 3-3g), and the deeper two-mica granite (Figure 3-3h).

3.3.3 HYDRAULIC PROPERTIES OF THE SOULTZ RESERVOIR

During circulation tests in the Soultz-sous-Forêts geothermal reservoir, large fracture zones gathered more than 20 % of the fluid [*Dezayes et al.*, 2010a]. Along with the dimension and geometry of a fracture, its surface and its filling are affecting its permeability. Sausse and Genter [2005] found that hydrothermal alteration results in smoothing of the fracture surfaces and prevents the channeling of flow inside the fracture. The average porosity of the fresh standard granite is below 1 % [*Genter et al.*, 2000]. The porosity values measured for hydrothermally altered samples are often higher than those of breccia and microbreccia. For altered samples, Genter et al. [2000] determined porosities between 1.7 % and 25 % by mercury porosity measurements. Altered plagioclase, which makes up to 40 % of the rock volume [*Ledésert et al.*, 1999], has porosities between 20 % and 27 %.

The filling of fractures with clay minerals in contrast can result in significant reduction of the fault permeability, which can cause increased pore pressures and reduce the frictional strength [*Ikari et al.*, 2009]. The importance of hydrothermally altered zones for fluid circulation was highlighted earlier by Evans et al. [2005b], who found that permeability creation during stimulation of the well GPK1 was limited to the interior of hydrothermally altered structures. Evans et al. [2005a] discovered that all fractures in GPK1 whose permeability could be enhanced during stimulation show evidence of shear.

They analyzed flow logs and temperature logs for the GPK1 stimulations in order to find primary permeable zones and those zones, which became permeable during stimulation. The major findings of their study were: (1) Flow is switching between the neighboring fractures of a fault zone, (2) Permeable fractures tend to be hydrothermally altered, but shearing could damage fracture fillings and thus make the fillings prone to be washed out and (3) Permeability creation/enhancement is focused on cataclastic shear zones with hydrothermal alteration. On the contrary, gouging can also lead to ineffective stimulation due to asperity indentation and clogging of apertures.

3.3.4 OPERATION AND CONFIGURATION OF THE SOULTZ EGS

Since the start of the geothermal project in Soultz in 1987, scientists from various countries are working on the exploration of the Soultz geothermal reservoir and on the optimization of the power plant installations. Between 2000 and 2007, several circulations, injections, and hydraulic and chemical stimulations were performed in the four deep wells GPK1-GPK4. An overview of the stimulation and circulation activities before 2010 is provided in Table 3-1.

The surface installations of the power plant were built up between 2007 and 2008 as an Organic-Rankine-Cycle (ORC) power plant for production of electricity and heat. Today, water is produced at ~175 °C and re-injected with ~70 °C, whereas the pumping rate is between 25-35 ls^{-1}. Heat from the working fluid is extracted by a tube bundle heat exchanger and the net thermal power is 21 MW. The ORC cycle for electricity production works with isobutane and an air cooling system. The inlet pressure at the single level radial flow turbine is 1.9 MPa. With the current triplet configuration of GPK2 as production well and GPK3 and GPK4 as injectors, around 2.1 MW electrical power can be produced [*Genter, 2014, pers. comm.*]. A scheme of the ORC configuration and the well trajectories in Soultz is presented in Figure 3-4. Figure 3-5 provides an overview of the logs, which were available for this thesis.

Table 3-1: Overview of the circulation and stimulation activities on the Soultz wells GPK1-4. Data: BRGM

	stimulation	circulation
GPK1	**1993**: packer and open-hole, 40 ls^{-1} and 50 ls^{-1}	**1996**: GPK2→GPK1: 15 ls^{-1} and 22 ls^{-1} **1997**: GPK1→GPK2: 12 ls^{-1} and 24 ls^{-1} **1998**: GPK1→GPK2: 24 ls^{-1}
GPK2	**1995**: stimulation test, 12 ls^{-1} and 56 ls^{-1} **1996**: massive stimulation, 25 ls^{-1} and 78 ls^{-1} **2003**: Chemical stimulation with chloric acid, 12 ls^{-1} and 30 ls^{-1} **2003**: stimulation with 0.5 MPa backpressure in GPK3, 15 ls^{-1} and 39 ls^{-1}	**1996**: GPK2→GPK1: 15 ls-1 and 22 ls^{-1} **1997**: GPK1→GPK2: 12 ls-1 and 24 ls^{-1} **2005**: GPK3→GPK2, GPK4: 15 ls^{-1} **1998**: GPK1→GPK2: 24 ls^{-1} **2008/2009**: GPK2→GPK3: 25 ls^{-1} **2008/2009**: GPK2→GPK3: 25 ls^{-1}
GPK3	**2003**: hydraulic stimulation, 15 ls-1 and 30 ls^{-1} **2005**: chemical stimulation with chloric acid, 27 ls^{-1}	**2003**: GPK3→GPK2: 15 ls-1 and 20 ls^{-1} **2005**: GPK3→GPK2, GPK4: 15 ls^{-1} **2008/2009**: GPK2→GPK3: 25 ls^{-1} **2008**: GPK2→GPK3, GPK4, 25 ls^{-1}, 17,5 ls^{-1}
GPK4	**2004**: hydraulic stimulation, 30 ls^{-1} **2005**: hydraulic stimulation, 30 ls^{-1}, 45 ls^{-1} and 25 ls^{-1}	**2005**: GPK3→GPK2, GPK4: 15 ls^{-1} **2008**: GPK2→GPK3, GPK4, 25 ls^{-1}, 17,5 ls^{-1}

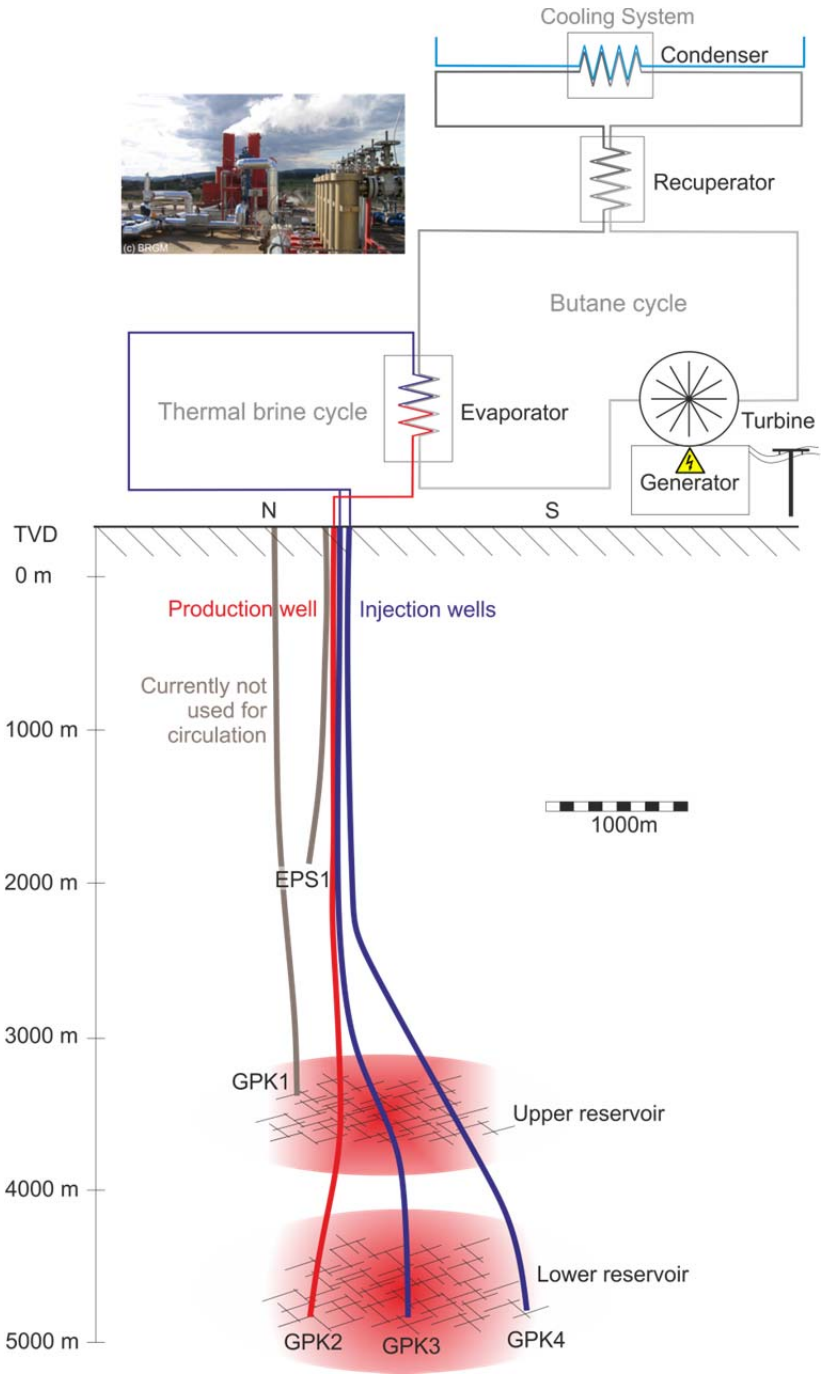

Figure 3-4: Schematic of the current configuration of the Soultz geothermal power plant. Electricity is produced with an Organic Rankine Cycle (ORC) using isobutane as working fluid. Currently, GPK2 is used as production well and GPK3 and GPK4 are injectors. The configuration of production and injection wells is flexible. The borehole trajectories are drawn to scale and geometry, the power plant cycle is only schematic.

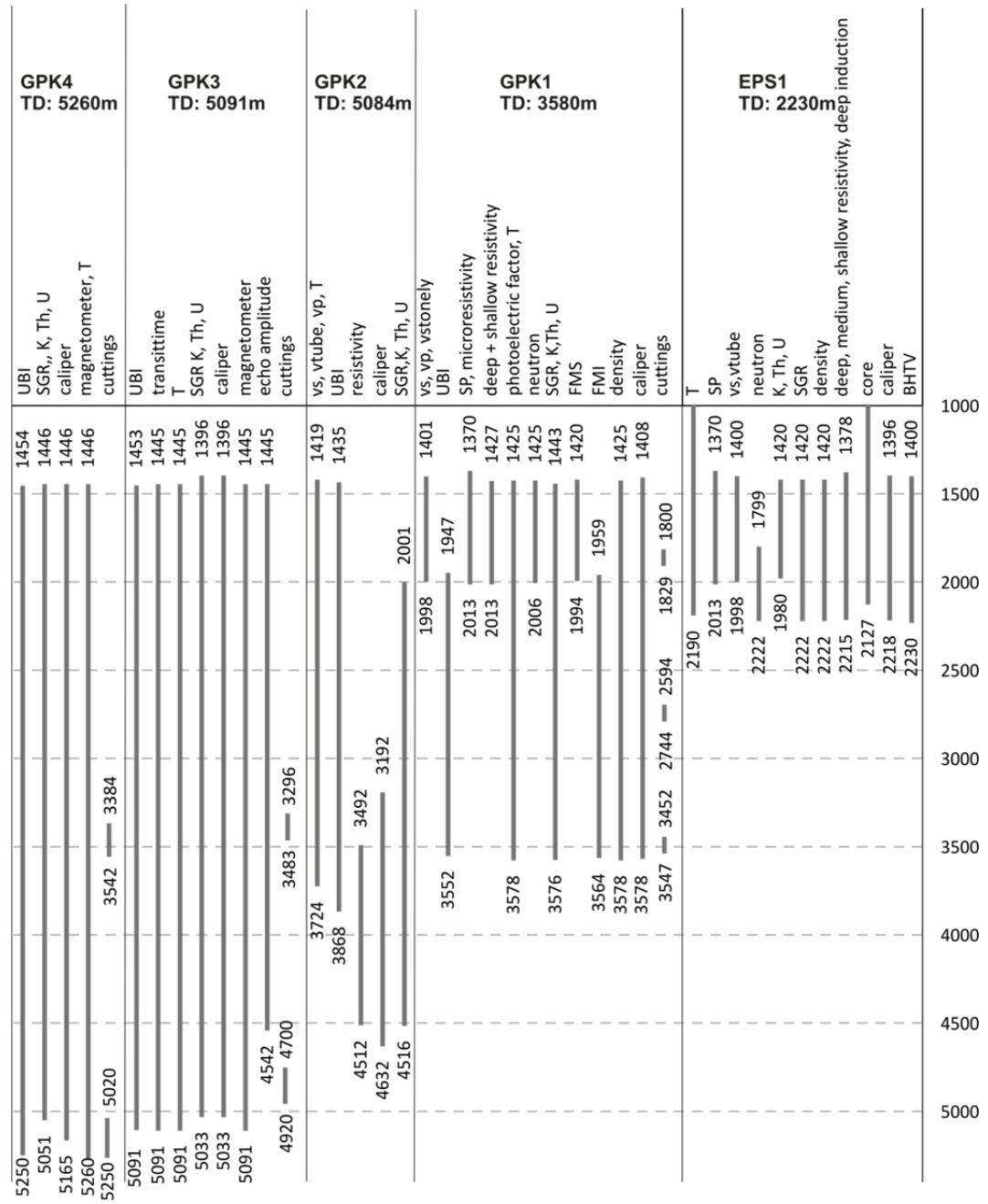

Figure 3-5: Overview of the logs and data in the granite of the Soultz wells EPS1, GPK1, GPK2, GPK3, and GPK4, which were available for this thesis including the respective covered depth ranges. BHTV=Borehole Televiewer, SGR = Standard Gamma Ray, FMI = Fullbore Formation Micro Imager, FMS = Formation Micro Scanner (resistivity), T = temperature, echo amplitude = amplitude of reflected acoustic signal, vs = shear wave velocity, vtube = tubewave velocity, SP = Spontaneous Potential, UBI = Ultrasonic Borehole Imager, vstonely = stonely wave velocity, SGR=Spectral Gamma Ray

3.3.5 CRITICAL PRESSURE

It is supposed in the Soultz reservoir that a large proportion of fractures is optimally oriented in the present stress field and are therefore critically stressed [*Cornet et al.*, 2007; *Evans*, 2005]. With the profound knowledge of the state of stress and the fracture orientations derived from image logs in the Soultz geothermal reservoir, the Mohr-Coulomb criterion can be used to estimate the critical pressure of fractures defined as their distance from the friction line (see Figure 2-1):

$$P_c = \sigma - \frac{(\tau - c)}{tan\,\varphi} \qquad (3\text{-}1)$$

where P_c is the critical pressure, σ is the effective normal stress acting on the fracture, τ is the effective shear stress acting on the fracture, c is its cohesion and φ the friction angle. This relation derived from the Mohr-Coulomb criterion is used to calculate for fracture families with certain orientations their respective critical pressure in the stress field of their depth [*Meller et al.*, 2012].

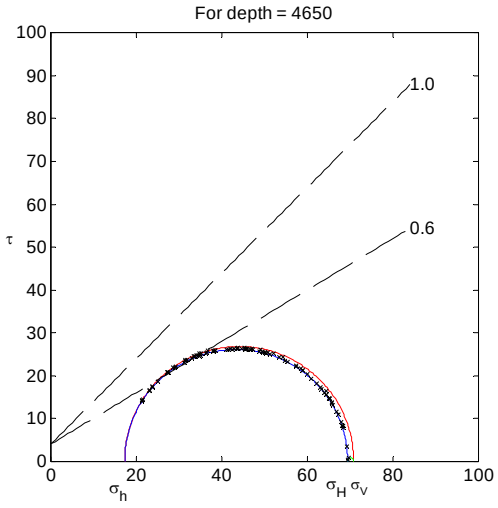

Figure 3-6: Mohr diagram for the fractures in a 150m interval of GPK3 in a depth interval of 4500m to 4650m and the state of stress at 4650m.

The Mohr-circle plot of the fractures in the Soultz reservoir (Figure 3-6) shows that the difference between S_v and S_H is small and the majority of fractures lies on the left side of the circle, which means they are close to the failure line. A pressure increase in the order of 10 MPa would shear a large proportion of the fractures, if a friction coefficient between 0.6 and 1.0 is defined. These coefficients represent the upper and lower bound for crystalline rock as defined from observations and laboratory tests [*Byerlee*, 1978; *Reches et al.*, 1992].

Figure 3-7 shows the resulting distribution of the critical pressure in the well GPK3 between 4500 and 4650 m, which is obtained from the Terzaghi corrected fracture density [*Terzaghi*, 1965]. The plot shows that a large proportion of fractures have critical pressures close to 0 MPa indicating they are critically stressed. These results are in accordance with studies from Cornet et al. [2007] and Evans [2005] who identified a high number of fractures in Soultz, which are close to failure.

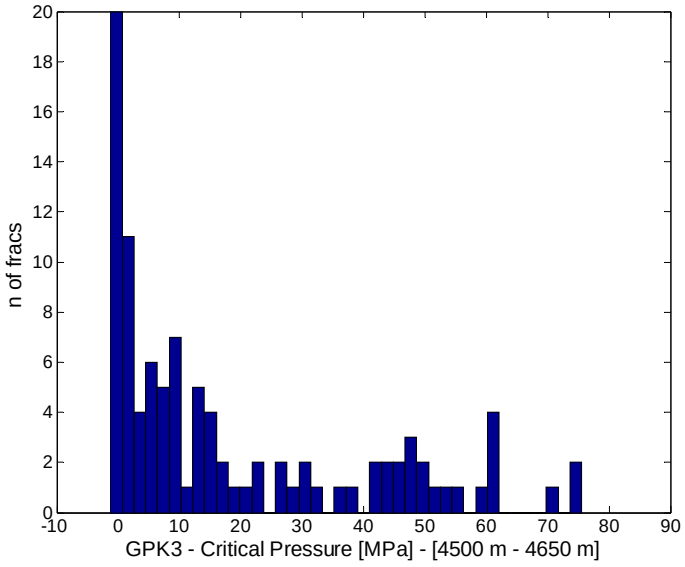

Figure 3-7: Distribution of the critical pressure in the depth interval of 4500 to 4560m of GPK3. A friction coefficient of 0.6 was used. Low values of P_p are evidence of critically stressed fractures that can shear due to small pore pressure changes.

With Mohr-Coulomb, the number of fractures prone for shearing upon applying a certain stimulation pressure can be estimated for each well and depth section. However, in order to do so, the frictional properties of the fractures have to be known. The major challenge for such approaches is in the predefinition of a friction coefficient and cohesion for all fractures inside the reservoir. As the fractures inside the Soultz granite are affected by various grades of hydrothermal alteration (chapter 3.3.2), studies by Zoback et al. [2012] and Tembe et al. [2010] suggest that fractures with different alteration grades have different friction coefficients while friction is decreasing with increasing clay contents. In order to discriminate between fractures of different alteration grades (and hence friction), a tool is required to localize hydrothermal alteration zones and to identify clay inside fractures. The identification of hydrothermally altered zones to create an improved model of the critical pressure in Soultz was the incentive of the following chapters.

4 THE APPLICATION OF A NEURAL NETWORK TO MAP CLAY ZONES IN CRYSTALLINE ROCK

This study has been published in *Geophysical Journal International.*

MELLER, C., A. GENTER, AND T. KOHL [2014]. The application of a neural network to map clay zones in crystalline rock. *Geophys J Int*, 196 (**2**), 837-849, doi: 10.1093/gji/ggt423.

ABSTRACT

The appearance of clay in fractures is an important issue of applied geoscience as it not only affects the stability but also the flow paths through rocks. Forming a link between hydraulic, geochemical and mechanical processes, clay structures need to be thoroughly investigated. The growing importance of clay for waste disposal, petroleum research, geothermal exploration, and geotechnical engineering necessitates tools to find and to characterize clay structures and clay minerals indirectly from geophysical measuring methods. Particularly, there is need for a technique enabling to map clay-rich zones from geophysical well logs acquired on-site in order to assess the mechanical and hydraulic properties of rocks. In the present study we present a neural network based method to map clay bearing fracture zones in crystalline facies. The study has been performed on the basis of geophysical and geological data acquired at the geothermal site of Soultz-sous-Forêts (France), in the granitic reservoir. A neural network was trained on geophysical logs from the fully cored exploration well EPS1. Calibration of the network was done on reference logs derived from the drill core. The effective calibration enabled the creation of synthetic clay content logs, which predict the clay amount in fractures along the well with >74 % accordance with a reference log.

High clay contents could be located in faults, on which aseismic movements have been identified. The validation of this relationship destines the synthetic logs to help identifying potentially weak zones from geophysical logging methods. With application on non-cored wells, this tool can become a powerful means for assessing the probability of aseismic movements on faults caused by the presence of clay and estimating the hydraulic properties of fractures.

4.1 INTRODUCTION

4.1.1 THE IMPORTANCE OF CLAY IN APPLIED GEOSCIENCES

Clay bearing structures are of major importance in applied geoscience. A peculiarity of the material is the linkage between geomechanical, hydraulic and geochemical processes. In terms of geomechanics, clay is both a blessing and a curse. Commonly, clay structures in sedimentary rock are of major interest for the safe storage of waste deposits [e.g. *Cho et al.*, 2010]. Due to its flexible structure, clay can enclose dumped material and seal it from the environment. Therefore, clay formations are regarded particularly suitable for nuclear waste disposal. Contrary, the soft behavior of clay can be problematic, if its appearance lowers the structural stability of reservoirs, boreholes, slopes or fundaments [e.g. *Cappa and Rutqvist*, 2012; *Koleini et al.*, 2012; *Mokni et al.*, 2012].

However, clay does not only appear as a sedimentary rock structure, but it also plays a major role as a geochemical alteration product of certain minerals. As such, it appears e.g. in fractured rock, where the appearance of clay minerals on fracture surfaces can hamper the migration of fluids along flow paths [e.g. *Velde*, 1977]. As clay plays an important role as a host rock for oil and gas as well as for the migration and retention of hydrocarbons, especially the hydrocarbon industry has put major efforts into the investigation of clay minerals and structures and into techniques for their localization [e.g. *Titov et al.*, 2010]. Clay mineral identification and localization requires a large variety of geophysical and laboratory methods. As such, geophysical borehole logging is broadly applied using radiometric or electric methods like resistivity logs or induced polarization, neutron scattering and gamma ray logs. Due to their clear signature on K, Th, U logs, clay is often used for stratigraphic correlation in sedimentary rocks, but the complexity of crystalline rocks requires new methods of clay identification and location in the subsurface. The present paper focusses the importance of clay for crystalline geothermal systems.

4.1.2 CLAY IN CRYSTALLINE GEOTHERMAL RESERVOIR ROCKS

The heat stored in the crystalline basement rock is considered to be the major geothermal resource in wide areas [*Kohl et al.*, 2005]. Faults and fractured systems in crystalline rocks present hydraulic pathways for hydrothermal fluids. Enhanced Geothermal Systems target fractures to efficiently produce and inject geothermal brine. Because of their high permeability and heat supply, fractured crystalline settings

provide ideal conditions for their exploitation as geothermal reservoirs and the production of heat and electricity [e.g. *Genter et al.*, 2003].

For EGS both, the presence of hydraulic pathways and the mechanical behavior of a reservoir are of major importance for the success of hydraulic stimulation and the operation of a power plant. The permeability of a reservoir is one of the limiting factors to the production and injection flow rates. Permeability is not only affected by the dimension and geometry of the fracture, but also by its surface and its filling. The appearance of fractures filled with clay minerals remarkably decreases the permeability of a geothermal reservoir. The hydraulic properties of a fracture play also an important role for the appearance of large earthquakes during hydraulic stimulation [*Charléty et al.*, 2007].

"Fracture" is a generic term describing a natural discontinuity without visible displacement. It corresponds generally to small-scale discontinuities. At Soultz, many individual fractures were observed and measured from the cores of the EPS1 well [e.g. *Genter and Traineau*, 1992; *Genter and Traineau*, 1996] in which we conducted our study. They analyzed 800 m length of granitic cores and a full structural characterization was conducted. On core, small-scale fractures were systematically filled by carbonates, chlorite, iron oxides, epidote or sulfides mainly. Fractures are mode 1 (opening) fractures. The term fault defines a natural discontinuity with a significant off-set. On the cores, it was possible to identify faults due to the occurrence of striations, off-set or other structural criteria [*Genter and Traineau*, 1996]. Faults were generally filled by secondary hydrothermal minerals such as geodic quartz, carbonates, barite and clay minerals (illite). Faults are mode 2 (shearing) fractures. The concept of fracture zone is also used in this study. It corresponds to a spatial concentration of both fractures (Mode 1) and faults (Mode 2) visible at core scale associated with a significant hydrothermal alteration and the appearance of clay minerals [*Genter et al.*, 2000].

Clay minerals inside fractures are formed during alteration of the reservoir rock fostered by the circulation of geothermal brine throughout the history of the reservoir. In fractures of igneous crustal rocks the dissolution of primary minerals and the crystallization of clay minerals are the most significant and the most common fluid-rock interactions [*Meunier*, 2005]. The most common geochemical reactions are the alteration of silicates into trioctahedral illite and smectite or dioctahedric chlorite.

There are also other processes observed like the recrystallization of phengite and an illitization of previously formed clay minerals. Along with the prevailing stress field and the structure of a reservoir, these processes are supposed to considerably affect the strength of crystalline rock [*Valley and Evans*, 2006] and thus change its mechanical behavior. Janecke and Evans [1988] found for example that under certain temperature-pressure-strain rate conditions altered feldspars behave ductile instead of brittle in an altered shear zone in southeastern Arizona.

Tembe et al. [2006] tested the mechanical properties of cuttings from the SAFOD borehole in central California. They prepared the samples as artificial gouge on granite/sandstone forcing block containing sawcuts. With triaxial frictional sliding tests a profile of the friction coefficient along the borehole was obtained. Samples containing clay minerals had a considerably smaller friction coefficient than quartzo-feldspathic rocks. As together with the laboratory setup many sample preparation parameters could have affected the measurements, it is questionable, if the obtained data is transferable to in-situ scales. Duebendorfer et al. [1998] suggest alteration processes as an origin of aseismic shortening in Southern California. Some other authors also found evidence that the presence of clay in fractures as gouge plays an important role for the occurrence of aseismic movements on fault zones and fractures [e.g. *Dolan et al.*, 1995; *Schleicher et al.*, 2006b; *Wu et al.*, 1975]. Due to their major importance for reservoir mechanics and in order to be able to plan effective stimulation while mitigating the risk for large earthquakes., it is desirable to be able to map in a geothermal well potentially weak zones correlated with the appearance of clay minerals.

Present approaches to locate weak zones in a reservoir often use P- and S-wave velocities [e.g. *Freund*, 1992] or electrical tools [e.g. *Titov et al.*, 2010]. One shortcoming of the seismic approach is the low resolution, which makes it impossible to map clay-zones in the scale of few meters. Moreover, the impedance contrast between fractured crystalline rock and clay-bearing fractures is not large enough to differentiate between them both. The identification of clay from electrical logs is difficult, when (conductive) hydrothermal waters fill the reservoir pores or when Fe- bearing minerals occur in the rock matrix. As a consequence, one must always use several log types for interpretation. Unfortunately, they are not always available. Therefore, the goal is to be able to characterize clay-bearing zones based on standard geophysical data. The evaluation of complex interaction between manifold parameters makes it necessary to find a method, which is able to deal with multidimensional input data, to reduce its dimension and to extract the desired information.

With the present study, a characterization of the clay distribution along a borehole using geophysical logging data is performed. We introduce a tool for the detection of clay in wellbores on the basis of various geophysical logging techniques. With the help of a neural network analysis (NNA) applied on radioactive log profiles and fracture density curves, synthetic clay content logs (SCCL) are created for geothermal wells in Soultz-sous-Forêts (Alsace, France). After a rough review of the available data, reference clay content logs (index-SCCLs, iSCCLs) are created from core data of the investigation well EPS1. These logs are reference datasets, which represent the real clay content inside faults of the granite derived from core analysis. The neural network is then trained on the logging data of the well based on information from the iSCCL. The network is calibrated and different input parameters are tested in order to find the configurations that yield the best result. Finally, the benefit of the present results on the estimation of reservoir hydraulics and geomechanics is discussed.

4.2 THE GEOTHERMAL SITE IN SOULTZ-SOUS-FORÊTS

4.2.1 GEOLOGY AND ALTERATION PROCESSES

The geothermal site in Soultz sous Forêts at the western boundary of the Upper Rhine Graben is a multi-well system with the two injection wells reaching a depth of 5100 m (GPK3) and 3600 m (GPK1) respectively and the production well reaching 5080 m (GPK2). Two more wells were drilled to 5260 m (GPK4) and 2230 m (EPS1) depth respectively. The elaborately investigated pilot well EPS1 will be of major importance for this study.

The reservoir rock is an intrusion of a post-tectonic Variscan monzogranite overlain by a sedimentary cover of 1400 m thickness. The mineralogical composition of the granite is mainly characterized by large K-feldspar megacrysts in a matrix of quartz, biotite, plagioclase and amphibole. Accessory minerals are titanite, apatite and magnetite [*Genter and Traineau*, 1991]. During the multi-phase tectonic history of the opening of the Upper Rhine Graben a pronounced fracture network formed in the granitic rock. Simultaneously, several stages of fluid inflow can be reconstructed [*Schleicher et al.*, 2006a], during which primary minerals have been dissolved and secondary mineral phases precipitated. The earlier propylitic alteration is a weak isochemical alteration of the granitic matrix without a change in the granite texture. It incorporates the partial transformation of biotite and hornblende into chlorite, the replacement of plagioclase by illite and the formation of hydrogarnet and epidote within the granite. The second alteration, superposing the earlier stages involves strong chemical and textural changes mainly in and in the vicinity of fractures. In some altered zones, quartz, biotite, plagioclase and hornblende are totally dissolved [*Ledésert et al.*, 2010]. The precipitations in veins contain secondary quartz, barite, illite, carbonates, iron oxides, and locally illite-smectite and chlorite-smectite mixed-layered minerals [*Genter et al.*, 2000; *Schleicher et al.*, 2006a].

The fractured zones in the Soultz granite have a specific structure, which can be seen in Figure 4-1. Around the quartz vein, which often seals the center of the fracture, a distinct zonation is observed. In the brecciated and cataclased zone, the original structure of the granite is lost and hydrothermal alteration has transformed feldspars or biotite into clay minerals. Depending on the respective minerals that have formed, the granite becomes greenish in the case of chlorite or epidote, reddish, if hematite has formed or yellowish if the dominating clay mineral is illite [*Genter et al.*, 2000]. This vein alteration is significantly changing the mechanical and structural properties of the rock. Along with the mineralogy the physical parameters like porosity, bulk density and P-wave velocity of the rock change [*Ledésert et al.*, 2010].

Valley and Evans [2006] found from laboratory measurements that the uniaxial compressive strength of the granite is lower for samples showing vein alteration. These altered zones are therefore of major interest in terms of rock mechanical properties.

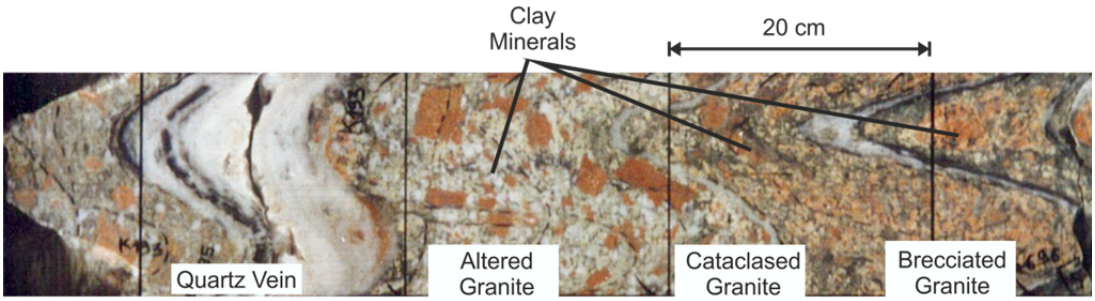

Figure 4-1: The zonation of an altered fault. Unrolled photograph of the EPS1 core K195, at 2156 m depth (top). The picture represents a scanned core, which means that planar lines become sinusoidal if they cut the core at an angle, which is not horizontal. Clay minerals occur mainly in the zone of hydrothermally altered granite, but they can also occur in the remaining zones. Two consecutive horizontal lines represent 20 cm

4.2.2 THE SOULTZ LOG DATABASE

During many years of scientific research at Soultz, a huge database of logging data, research results and scientific publications has been accumulated for the geothermal wells [*Genter et al.*, 2010]. The five wells have been logged with different logging techniques. Some of them cover the whole wells, but many of them are only available for intervals. The 2227 m deep well EPS1, located 40 m to the northeast of the GPK2-4 wellheads, has been fully cored from 930 m depth. The core covers 487 m of sandstone and 810 m of granite. Because of this unique data record, the well EPS1 plays an important role in the following analysis although it is not part of the multi-well geothermal production. The top of the granite is at about 1400 m.

The sedimentary cover will not be part of this study. There are different logs available for the five wells. An overview is given in Figure 4-2. Most log types have been conducted in the shallowest well EPS1 as this was intended to be an investigation well. The deepest wells GPK3 and GPK4 have only been logged by the standard logs, i.e. the spectral gamma ray, which incorporates the standard gamma ray (SGR), the potassium (K), thorium (Th) and uranium (U) logs. The borehole wall has been investigated by Ultrasonic Borehole Imager (UBI) logs. Therefore, SGR, K, Th, U, image logs, and the caliper are the only logging data available for all five wells.

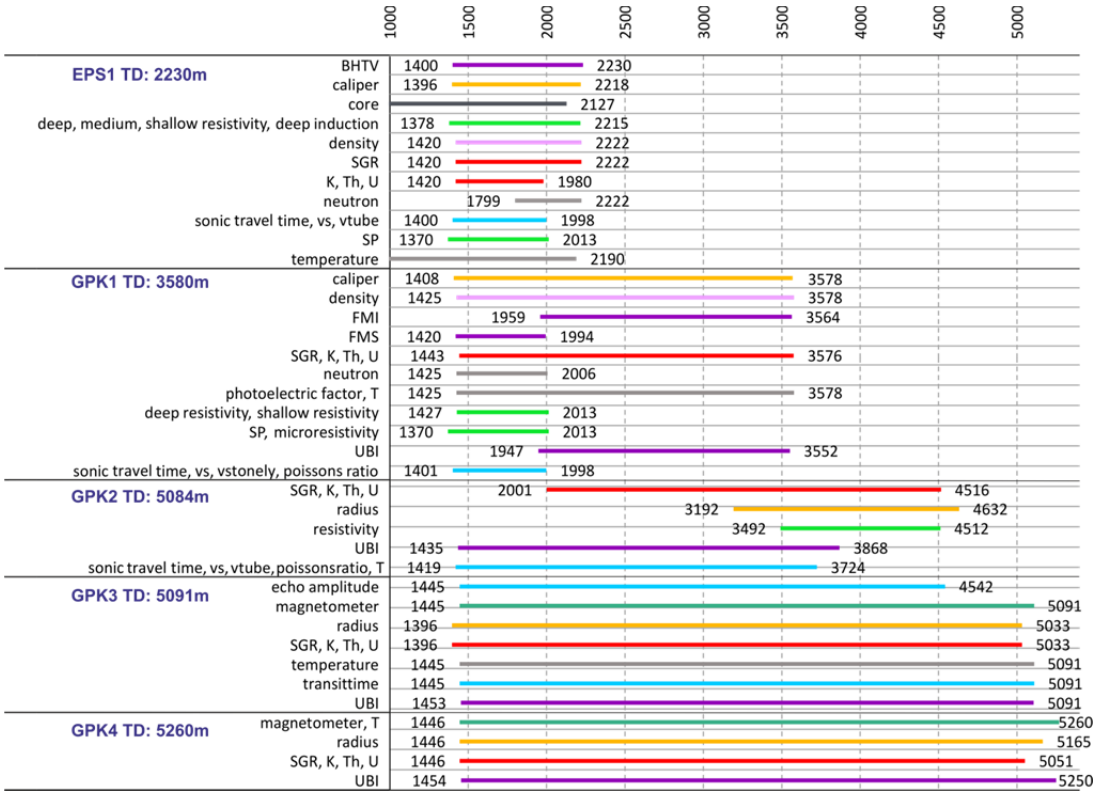

Figure 4-2: Overview of logs available for EPS1. BHTV=Borehole Televiewer, SGR = Standard Gamma Ray, FMI = Fullbore Formation Micro Imager, FMS = Formation Micro Scanner (resistivity), T = temperature, echo amplitude = amplitude of reflected acoustic signal, vs = shear wave velocity, vtube = tubewave velocity, SP = Spontaneous Potential, UBI = Ultrasonic Borehole Imager, vstonely = stonely wave velocity.

4.3 FIRST DATA ASSESSMENT

Because of their various physical and chemical properties, clay minerals can be identified from geophysical borehole logs (after Ellis and Singer [2007]):

- Resistivity logs are sensitive to the structurally bound water inside the clay layers or on the surface of clay minerals.
- The neutron porosity log is sensitive to hydrogen contained in water molecules.
- Gamma ray logs identify abundances of radioactive isotopes included in the structure of clay minerals. Illite for example has a high K-content, montmorillonite integrates Th.

As the occurrence of clay minerals is strongly correlated with the vein alteration, one would expect higher clay content and consequently higher SGR values with increasing alteration grades. Vein alteration occurs mainly on big fractures or on zones with a high fracture density. In order to further investigate this correlation, a fracture density log for EPS1 is computed. This is achieved by counting the fracture density along the well in a sliding window of 1 m length and a sampling rate of 0.1 m. The limitation for fractures larger than the sampling rate is overcome by counting them also in the neighboring interval. For calibration purposes, EPS1 is especially suited as data can be directly be derived from the core. The fracture fillings have been determined and a synthetic clay content log (SCCL) for the density of clay filled fractures was computed for EPS1. Henceforth, this log will be referred to as Index-Synthetic Clay Content Log (Index-SCCL or iSCCL). Following, the granite is subdivided into 5 groups of different alteration grades in order to investigate the relationship between alteration (i.e. clay content) and SGR values (Table 4-1).

*Table 4-1: Classification of the different lithologies into five qualitative alteration grades visually described from cutting analysis [*Genter and Tenzer*, 1995].*

alteration grade	description of lithology from the litholog (cuttings)
0 – fresh granite	porphyritic granite, biotite-rich granite, K-feldspar megacrysts, kalifeldspar-rich granite, xenolith, K-feldspar cumulate, microgranite, two-mica granite, hematized granite, leucogranite and propylitized granite
1 – low alteration	Poorly hydrothermalized granite and altered porphyritic granite
2 – moderate alteration	moderately altered granite and cataclased granite
3 – highly altered	highly altered granite, breccia and crushed microbreccia
4 – extremely altered	extremely altered granite, quartz vein, protomylonite, mylonitised granite and fracture zones

Previous assumptions regarding higher SGR values with increasing clay content and higher alteration grade cannot be verified easily (Figure 4-3). The computed Index-SCCL is plotted versus the SGR data of EPS1 and the alteration grade is illustrated color-coded. The effect is probably caused by various primary minerals in the granitic matrix like biotite or K-feldspar, which can also incorporate radioactive isotopes. This makes it necessary to use the whole gamma spectrum of K, Th and U logs and to find a method to resolve the complex interaction of granitic matrix and clay minerals from these multidimensional logging data.

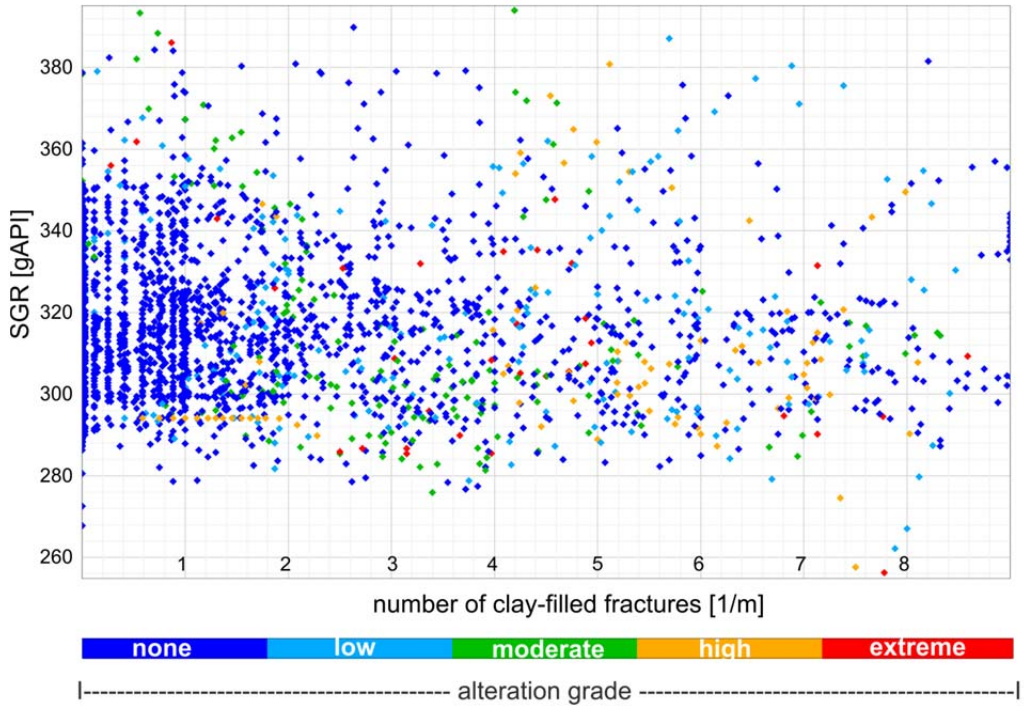

Figure 4-3: Crossplot of the clay-filled fracture density counted from the EPS1 core vs. SGR. The color of the dots represents the alteration grade of the host rock. There is no correlation visible between the clay content, alteration grade and the SGR counts. The vertical lines occurring between 0 and 1 fracture per meter are artifacts of the 0.1 m precision of the clay-filled fracture density calculation.

4.4 BACKGROUND AND METHODOLOGY

The neural network analysis is a method, which has proven itself in the application on multidimensional data in many fields. It is for example a common method in face recognition [e.g. *Lawrence et al.*, 1997] or in image processing [e.g. *Cochocki and Unbehauen*, 1993], but it has also been used for geological tasks. In geological context, it has among others been applied for earthquake prediction [*Alves*, 2006]. Alves used a tool originally developed for financial analysis and applied it on the seismicity occurrence of the Azores. With this method, he successfully predicted the July, 1998 and the July, 2004 earthquakes. Singh [2005] applies an NNA on conventional logs like gamma ray, neutron and density logs for the porosity/permeability prediction of the Uinta Basin. Maiti et al. [2007], Chawathe [1994], Nikravesh [1998], Benaouda et al. [1999], Baldwin et al. [1990] and Rolon et al. [2009] use the NNA technique for facies prediction in different geological settings. Their works have in common that the NNA technique is used for the creation of synthetic logs for wells, where measurements are missing. More specifically, Rolon et al. [2009], Ayala Marín and García-Yela [2010], Dingding et al. [2006] train the network on wells, for which all desired logs are available and create synthetic logs by applying it on wells, where the data is incomplete. The obtained logs can replace real loggings, which cannot be measured as a consequence of low budgeting or technical reasons. An overview of the applications of NNA in the petroleum industry is given by Ali [1994]. To our knowledge this study is the first application to use NNA for the detection of clay zones and the estimation of the amount of clay minerals in altered igneous rock for geothermal purposes.

Because of its flexibility and versatileness, the application of a neural network is suited to meet the challenge of identifying complex correlations between wall rock and measurements in multidimensional geophysical logging data. In this section the different aspects, which make the neural network suitable for the problem of identifying clayey fracture zones, are explained.

For the present study the Schlumberger Software Techlog64 (version 2011.2.1) is used. The Techlog software package allows handling and interpreting a multitude of multi-well data. In addition to common statistical methods the software provides the possibility to evaluate logging data with more complex approaches like the neural network analysis called *IPSOM*.

Basically, a neural network consists of an input and an output layer of numerous units called neurons. Each neuron is able to receive process and transmit information. While connected, input-units receive signals from the environment and output-units pass information to the environment. The kind of connection between these units is manipulated by weights, which control the transmission of information.

The weights can be positive and negative and they can be of various magnitudes. Thus, the input of a neuron depends on the output or activity of the connected neurons and on the weight between them.

For our study, the Kohonen-algorithm [*Kohonen*, 1984] is used. This algorithm works with a self-organizing map (SOM), which is a two-dimensional representation of the multidimensional network. It helps understanding, how data is organized and it allows basic manipulations of the computed network. The computing of the SOM consists of a training phase, where the network analyses the given input, and a propagation phase, where the acquired knowledge is tested.

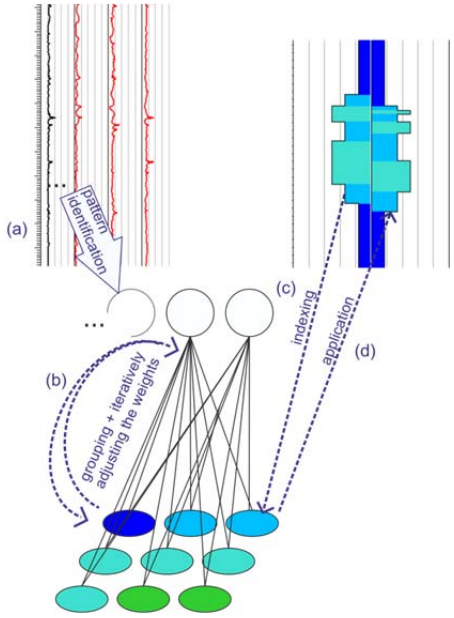

Figure 4-4: The neural network analysis with a Kohonen map from the input log (a) to the synthetic log (d). In detail: (a) Input logs give their information to the input neurons (empty circles) and the input data is classified in a map according to close patterns. (b) The weights between input and output neurons (colored circles) are adjusted and the network unravels. The nodes can be illustrated on a 2D SOM. (c) The indexing dataset controls the clustering of the nodes. Each node is assigned to a certain group (illustrated by the different colors). (d) The network identifies similar patterns in the application dataset and assigns them to the groups given by the index.

In the training phase, the input logs are classified, i.e. each neuron is assigned different patterns of log response (Figure 4-4a). Initially, the weights between the neurons are arbitrarily chosen. Then, the network selects an input vector and the activity of the output-neurons is calculated. The unit, which is most excited, is the one with the closest properties and the minimum distance to the input pattern.

Then, the weights to this unit are adjusted in a way that the input vector is better approximated (Figure 4-4b). The same, but in a weaker form, happens to the

neighboring units. The learning parameter, which determines, how much the weights are changed, is reduced after each cycle, so that the changes to the weights become smaller and smaller. This process is repeated until the predefined number of iterations is reached. If the number of cycles is large, the changes become continuously smaller, and the network approaches a stable state.

First, the network learns how the petrophysical properties and the reference classification (index) are correlated; this is the so-called supervised mode. In order to create synthetic logs representing the groups of the index-log, the nodes of the SOM have to be assigned to the respective index groups. This process is called the indexation of the map and it is done with the minimal distance method. Each pattern identified in the log corresponds to a certain index group given by the reference log. Nodes with similar properties are assigned to the same group, if the distance between the properties of the node and the group is minimal. Thus, each node of the SOM is assigned to the index node with the closest properties. The result of this process can be directly seen on the two-dimensional map (Figure 4-4c), where the different groups are represented by different colors.

In the following propagation phase, the knowledge of the network stored in the weights of the neurons is tested in order to check its quality. Herein, this is achieved by applying the network on the input data and comparing it with the index log, which was initially given as a basis for learning. With application of the trained network on itself, patterns in the logs are grouped into neurons assigned to the group of the respective index neuron (Figure 4-4d). By comparing the resulting log of the propagation phase with the index log, wrongly assigned units can be corrected and the result of the created synthetic log can be improved.

Among the parameters which affect the performance of the Kohonen map, are the number of iterations, the radius and the algorithm of the neighborhood function, the learning parameter, the size of the SOM, and the dimension of the network. The number of neurons should be adapted to the data. It should be considerably smaller than the number of input samples in order to achieve a proper learning and indexation. The number of iterations should be high enough for the network to converge to a stable state during the learning process. Kohonen [2001] suggests that the number of iterations should be at least 500-fold the number of output units. These parameter-effects will be discussed in the following section.

4.4.1 METHODOLOGY FOR THE IDENTIFICATION OF CLAY-BEARING FRACTURE ZONES USING AN NNA

Training of the NNA on the Reference Logs of EPS1

In the learning phase, the network is trained on the gamma ray logging data and the core fracture density log. The NNA is tested with SOM sizes of 10x10, 15x15, 20x20, and 25x25 nodes. After Kohonen [2001] the iteration numbers should then be at least 50'000, 112'500, 200'000, and 312'500. In this study, 120'000, 1'000'000, 3'000'000 respectively 5'000'000 cycles are applied and their results are compared in order to find optimum settings. The result of the learning process is a map of nodes with each of them representing a spectral composition of SGR, K, Th, U, and fracture density data. Following, the nodes are indexed according to the Index-SCCL log. This way, the neurons of the map are categorized into five clay content groups (corresponding to 0-20 %, 20-40 %, 40-60 %, 60-80 % and 80-100 % of the maximum Index-SCCL value and numbered from 1 (low density) to 5 (maximum density)). In the following propagation phase, the result will be processed in order to improve the correlation between the index and the modeled log. The procedure will be explained in the next chapter.

Testing the Quality of the Network by its Application on the Input Data

The processing of the NNA is necessary to reassign nodes to the proper facies, which have been wrongly indexed. This is done in the propagation phase, where the network is reapplied on the input data to compare the reference log with the synthetic log. Improvement of the results is done manually by working on the SOM, on a two-dimensional representation of the network, the spectra for the index groups and the model log. As an example, the procedure is explained for an NNA with 100 nodes (Figure 4-5).

Manual processing is necessary to avoid misinterpretations caused by influences of the rock matrix, but it has to be thoroughly decided, which combinations of log intensities show clay and which are caused by the granitic matrix. Different clay minerals, which have miscellaneous characteristics, excite different log responses that are mixed with the influence of the host rock. Therefore, the matrix lithology has always to be considered before reassigning a node.

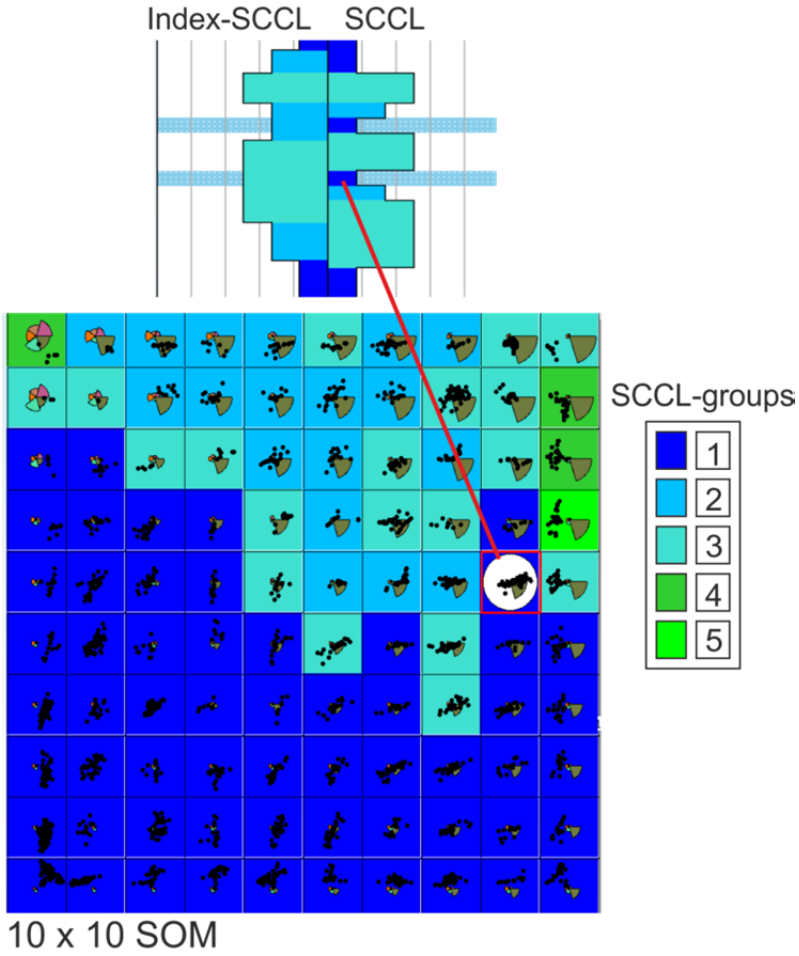

Figure 4-5: Self-organizing map: Each square of the map represents one node. Each node of the SOM reflects a specific spectral composition, which is displayed as a pie chart. The size of each portion is related to the intensity of the log response. The node color represents the respective iSCCL group. Dots on the spectra of each square represent samples that define a node. The closer the dots are to the center of the square, the closer their properties are to those of the index node. During processing the node responsible for the classification of a specific depth to one of the 5 clay content groups can be displayed. The corresponding node is marked with a white circle in the SOM and the depth interval is highlighted in light blue. By comparing for each group the probability to fit a node, poorly defined nodes can be redistributed to a different group.

4.5 RESULTS

The resulting SCCLs for different SOM sizes agree closely with the Index-SCCL (Figure 4-6). The synthetic log for the map size of 25x25 nodes provides the best results. The synthetic clay log named SCCL 25x25 presented in Figure 4-6 was created with a SOM of 625 nodes using 5'000'000 iterations for the network training.

Table 4-2: Percentage of depth intervals of the SCCL deviating by varying degrees from the Index-SCCL (rounded values). No deviation means that the SCCL matches the Index-SCCL i.e. the prediction of the SCCL is correct.

deviation from Index-SCCL	depth intervals
none	74.3%
1 group	16.4%
2 groups	5.6%
3 groups	3.1%
4 groups	0.6%

To quantitatively analyze the quality of the modeled log, the percentage of correctly determined index groups is calculated. The model provides a great accordance with the index (Table 4-2). A major portion (74.3 %) of depth intervals has been correctly assigned and 90.7 % of the depth intervals deviates maximum 1 group from the index.

The network cannot only reconstruct the largest densities of clay-bearing fractures, but it is also able to assess their quantity (Figure 4-6). The upper zone of high clay content and fracture density between 1400 m and 1540 m is characterized by the formation of clay minerals from feldspars and a superposition of paleo-weathering. The medium part between 1540 m and 1980 m penetrates porphyritic granite of different alteration and fracturation grades, while all gamma ray logs are available. The big fracture zone between 1620 and 1640 m, at 1660 m and at 1700 m depth are very well reconstructed in the SCCL. Even for the paleo-alteration zone at the top of the granite to a depth of about 1550 m, where logs are sometimes very sensitive to the various alteration products, the model shows great accordance with the Index-SCCL.

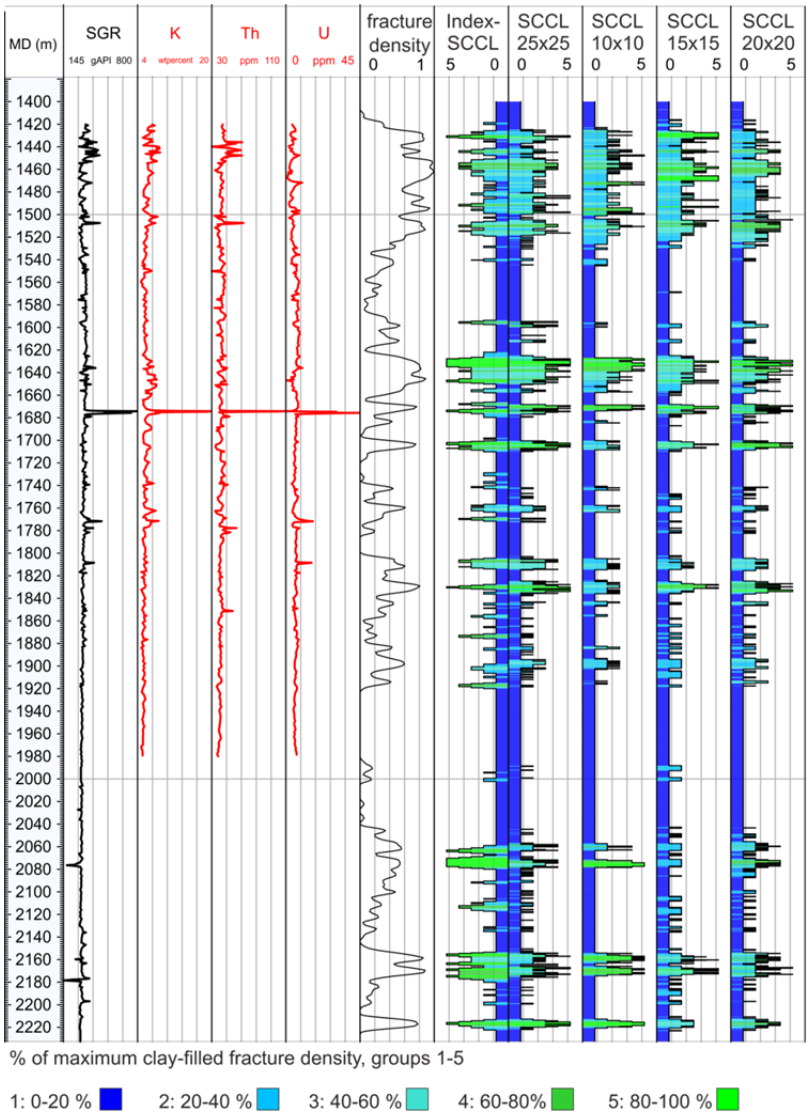

Figure 4-6: SCCLs for various SOM dimensions for EPS1 and the input logs SGR, K, Th, U, normalized core fracture density and the Index-SCCL. The fracture density and the Index-SCCL have been computed from core data and serves as a reference. The SCCL are the logs modeled using a SOM with different sizes. Accordance between Index-SCCL and SCCL: 10 x 10: 62.9 %, 15 x 15: 66.2 %, 20 x 20: 69.9 %, 25 x 25: 74.3 %.

The quality of the SCCL is not the same for the prediction of clay groups 1-5 (Figure 4-7). The diagram shows for each iSCCL group the respective predicted group. The pie chart illustrates the sum of depth intervals covered by the respective groups. The prediction is most accurate for group 1 where the clay-filled fracture density is low (Figure 4-7 (left)). If group 1 has been determined from core data, for 87 % of the respective depth intervals this group is really predicted by the SCCL. The prediction of group 2 is more uncertain and it is to 31.5 % misinterpreted as group 1. For the interpretation of the statistics it is also important to consider the decreasing number of depth intervals for higher density of clay-filled fractures. Even though the correct amount of clay is not in all cases properly determined, the deviations of the predicted model groups from the real ones are mostly only by one group, that is no more than 20 % more or fewer total clay content. So, the present model can distinguish between clay-filled fractures and fractures without clay. For the purpose of mapping potentially weak zones, this is a prerequisite.

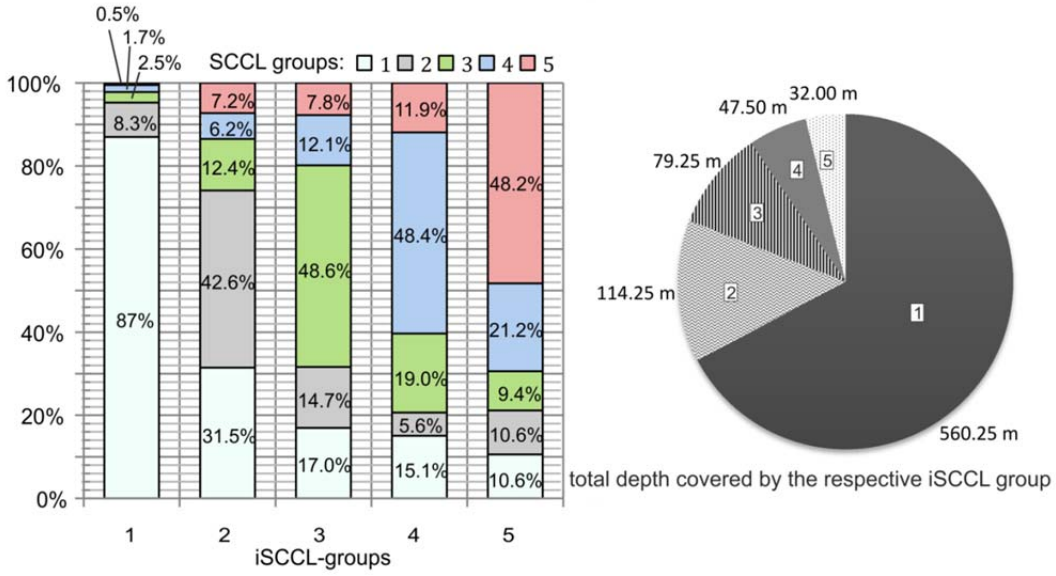

Figure 4-7: Left: The graph shows for each Index-SCCL group belonging to a depth interval, which group is predicted by the model. The numbers inside the bars give percentage for each group rounded to one decimal. Right: The figure shows for each group the total depth covered.

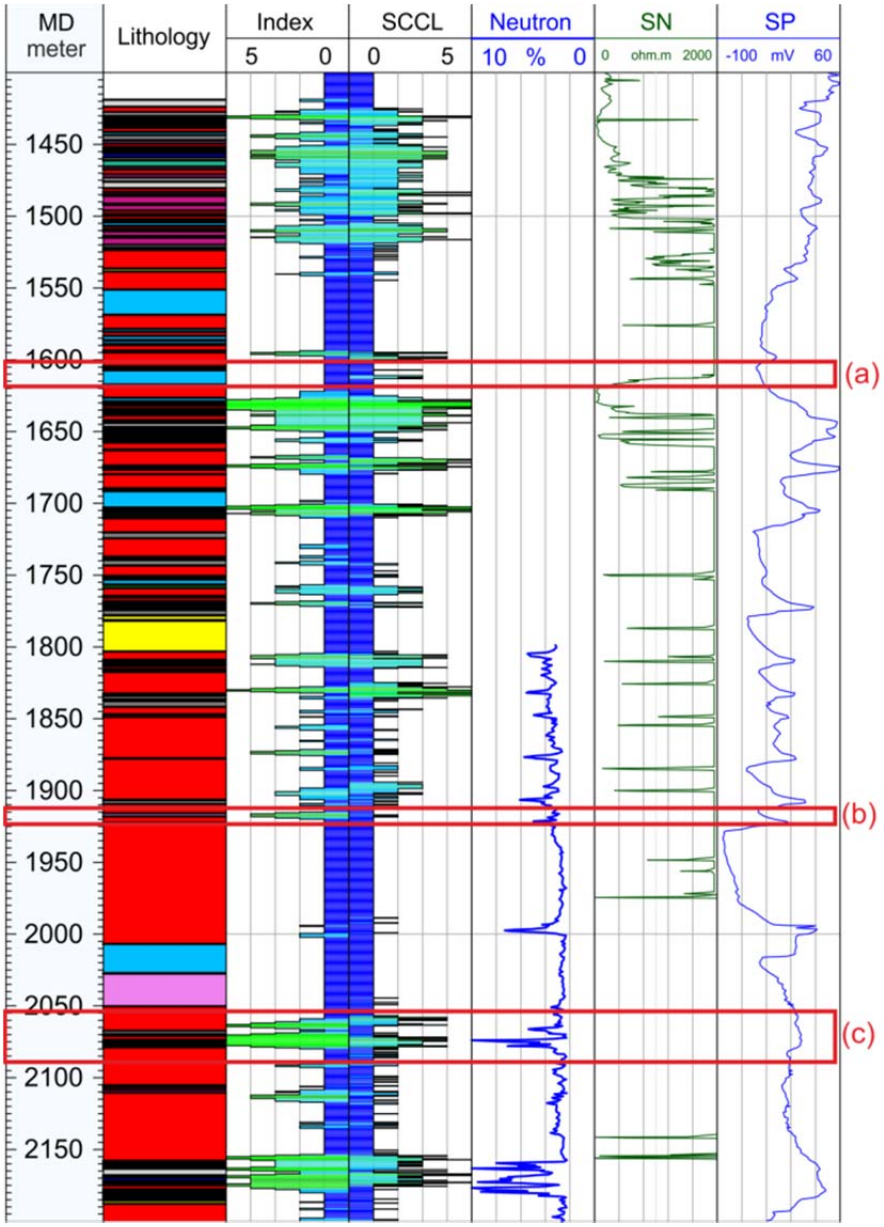

Figure 4-8: Comparison of the clay model with other measured logs (lithology, neutron, short normal resistivity (SN), spontaneous potential (SP). The intervals (a), (b) and (c) marked with the red rectangle are zones, where the model predicts too much clay (rectangle (a)) or too little clay-(rectangles (b) and (c)). In the lithology log, red intervals are standard granite, yellow is biotite-rich granite, light-blue is kalifeldspar cumulate, purple is xenolith, green is hydrothermalized granite.

4.6 DISCUSSION

4.6.1 ORIGIN OF DEVIATIONS FROM THE ISCCL

The largest clay-bearing fracture zones and the zones without clay can be reconstructed very well. Smaller zones are not fitted by the model. Examples for such zones are shown in Figure 4-8. In some intervals, the model predicts more clay-filled fractures than there are (Figure 4-8a). One reason for that is in the granitic rock matrix. The mentioned interval lies in a kalifeldspar cumulate (light-blue interval in the lithology log) with a naturally high K content. Therefore, the SGR and K readings of this zone are increased and the NNA interprets this as enrichment in clay minerals.

In a few zones the predicted density of clay-filled fractures is lower than it is observed in the core (Figure 4-8b). The respective interval is in xenolithe, which possibly gives a different background signal than the standard granite and thus leads to an overestimation of the clay-fracture density. However, in some zones, where we observe such behavior (e.g. Figure 4-8c), the input data are incomplete. If one or more of the gamma ray logs is missing, the indexation is difficult and the prediction of the model has to be carefully assessed.

4.6.2 THE SENSITIVITY OF THE NNA CONFIGURATIONS

Depending on the NNA configurations, the result of the model may change. In order to test the influence of the different parameters, the network was run several times using different numbers of nodes and clay groups. The results are discussed below.

The models for SOM sizes of 10 x 10, 15x15, 20 x 20 and 25 x 25 maps are compared in order to investigate the effect of a higher number of nodes. The respective SCCLs are shown in Figure 4-6. Sizes larger than 25 x 25 are physically not reasonable as the number of input samples is too small to guarantee a proper learning and indexing. Using a higher number of nodes improves the resolution of the data and it gives the possibility to better assign the log responses to different groups (Table 4-3). This way, small nuances between index groups and nodes can be better captured. Figure 4-6 compares the logs modeled with different SOM sizes. The resolution and the quality of the logs increase with increasing number of nodes (larger map). This is also confirmed by the statistical evaluation of correctly determined depth intervals (Table 4-3).

Table 4-3: Comparison of the percentage of correctly modeled clayey fracture density groups for different input parameters of the NNA. The learning phase span 5'000'000 iterations.

Parameters	**Ex. 1**	**Ex. 2**	**Ex. 3**	**Ex. 4**	**Ex. 5**	**Ex. 6**
size of SOM	10 by 10	15 by 15	20 by 20	25 by 25	25 by 25	25 by 25
number of clay groups	5	5	5	3	5	10
correctly determined intervals	62.9 %	66.2 %	69.9 %	84.2 %	74.3 %	50.0 %
nodes : samples	1:33	1:15	1:8	1:5.3	1:5.3	1:5.3

For the present model, five clay content groups (0-20 % to 80-100 % of maximum clay-bearing fracture density) are used. Using more groups makes the processing of the model a lot more complicated and the model is worse than for the model with only five groups. Only 50 % of the depth intervals can be correctly modeled by using 10 clay content groups. One reason for that is that the number of samples which are the basis for the definition of an index group is much lower (down to 3 samples) and no more representative. Furthermore, the sampling rate of the logs sets a limitation to the depth intervals belonging to the same clay content group. They are often as small as 0.25 m. When comparing this to the sampling rate of 0.15 m for gamma ray logging, such groups cannot be resolved from these logs as they are characterized by only one sampling point. Therefore, it is not considered reasonable to refine the resolution by using more index groups. A smaller number of groups (Ex. 4, Table 4-3) can improve the correlation between index and model, but the resolution is worse and informative value gets lost.

The NNA was run with different numbers of iterations. Different orders of magnitude between 100'000 and 5'000'000 have been compared and the learning process of the map been observed. At the beginning of the learning phase there are large changes in the spectra defining the nodes of the SOM until a nearly stable state is reached. After a sufficiently high number of iteration cycles, we can only observe very small changes in the map. The large number of degrees of freedom for larger sized maps is reflected by the required number of iterations. For the 10 x 10 map, the stable state was reached after 500'000 cycles, for the 25 x 25 map we used 5'000'000 iterations. Although a higher number of cycles also involves a longer computing time, it is better to use a preferably high number of iterations. Otherwise, the neuronal network has not completely adjusted to the input data and the result is neither representative nor reproducible. For the present study the computing time was only few minutes, so we could easily apply high numbers of iterations, but for larger datasets this could be an important factor to consider.

Compared to the minimum 312'500 iterations postulated by Kohonen [2001], a factor 10 higher number was used During the learning process we could observe that the stable state for a 25x25 map was not reached at all after 312'500 iterations From this it is obvious that the postulated minimum is really an absolute minimum to obtain reproducible results but it is better to use a preferably high number of cycles and to observe the learning process in order to find the optimum settings.

Because of its iterative learning character, the exact weight distribution of a neural network can never be exactly reproduced in a further run. However, the resulting models and statistics of different runs of the SOM are very stable. This is a big advantage in the usage of NNA, as there are many ways to reach the goal. This is not the case, if the number of iterations is chosen too small or if the number of nodes of the SOM is not adapted to the input data. However, once the parameters are thoroughly chosen and the network calibrated with a high number of cycles to reach the stable state, the result will be approximately the same for each NNA.

4.6.3 THE BENEFIT OF FURTHER GEOPHYSICAL LOGS FOR INTERPRETING SCCLS

In order to identify logs that are useful to assess the certainty of modeled clay-zones, log responses in real clay zones in EPS1 are investigated. It is found that there is no log, on which all clay zones can be identified. The peaks of resistivity logs, especially the short normal (SN) log, often coincide with large amounts of clay (Figure 4-8). The neutron log in contrast is sensitive to hydrogen atoms, which can be incorporated into the structure of clay minerals, but appears also in water molecules of fluids. However, peaks in the neutron log can only be observed in very large fracture zones with large amounts of clay. Smaller zones are not seen, which is possibly due to their low hydrogen content. From this log, we can only assess where the fractured zones are and where clay is likely to appear. The spontaneous potential (SP) log is one of the best indicators for clayey zones. Its peaks coincide with high clay amounts and the log resolution is also very good (Figure 4-8). Also on this log not all clay zones can be seen and unfortunately, we do not have neutron logs for the deepest wells. The effect of using these logs as an additional input for the NNA is following discussed.

As they were sensitive to some of the clay bearing fracture zones, the NNA is run again three times, each time adding the neutron log, the SP log and the shallow resistivity log respectively to the original input. The addition of the SP log could improve the correspondence between iSCCL and SCCL from 74.3 % to 78.0 %, while the SN log improved it to 75.5 %. The neutron log in contrast could not improve the result. The correspondence was only 61.1 %.

One reason for that may be that the neutron log is sensitive to fractures in general, not only to clay filled fractures. The SP and SN log however, are sensitive to the charged elements of clay minerals and are thus better indicators for clay-bearing zones. Unfortunately, these methods are not standard logging techniques anymore and might not be available for other wells, on which a NNA should be applied.

4.6.4 APPLICATION OF THE NNA TO OTHER WELLS AND ITS IMPLICATION FOR ROCK MECHANICS AND HYDRAULICS

By application of the trained network on GPK1-4, SCCLs are created for the remaining wells. Comparing the SCCL of GPK1 (Figure 4-9) with data of large microseismic events [*Charléty et al.*, 2007] reveals the occurrence of large earthquakes in GPK3 between 4500 and 4600 m depth, where the clay content is predicted very low. We observe brittle instead of ductile behavior, which might be fostered by clays, and apparently the flow paths are permeable in this clay-poor zone. Otherwise, a pressure sufficiently high to create large seismic events could not have built up.

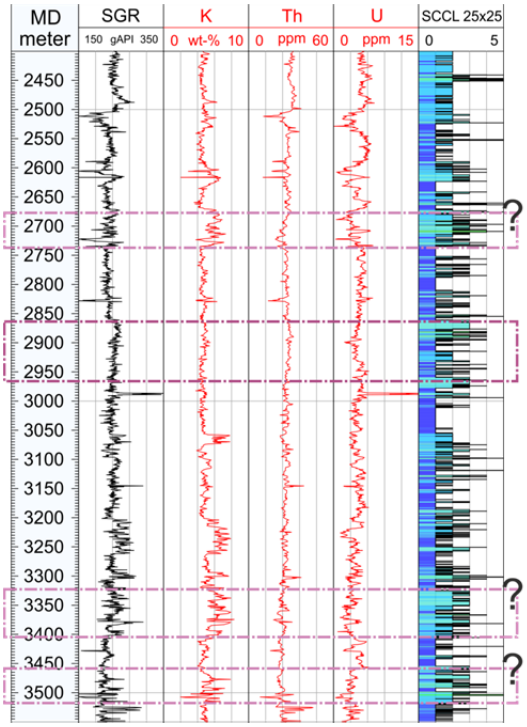

Figure 4-9: Section of the clay model for GPK1. Purple rectangle: aseismic zone after Cornet et al. [1997]. Rectangles with question marks might be also aseismic due to high clay content.

Cornet et al. [1997] found that near the bottom of GPK1 there is a zone, where aseismic movements took place on several fractures (Figure 4-9) after hydraulic stimulation of the bottom hole section. GPK1 is cased down 2840 m depth. Below the casing shoe, some clay is predicted, where Cornet et al. identified aseismic zones. In order to further investigate the correlation between clay minerals in fractures, hydraulic properties and aseismic creep, more detailed studies need to be conducted. Such studies might also clarify, if the predicted high clay content zones (Figure 4-8) are also potentially aseismic.

4.7 CONCLUSIONS AND OUTLOOK

A new methodology is presented, which can be used to predict the density of clay bearing fractures along boreholes with very good accuracy. The network has been trained on a dataset consisting of SGR, K, Th and U and fracture density logs derived from image logs. The clay content data gathered from the EPS1 core served as a reference log (iSCCL). In order to obtain the best possible results the parameters of the NNA have been selected according to the input data. The best results could be obtained by choosing a SOM size of 25 x 25, which corresponds to a network with 625 nodes. A number of 5'000'000 learning cycles was found to be sufficient for the network to converge. The most significant limitations of the neural network have been found to be incomplete logging data or a complex interaction between rock matrix and clay minerals, which affects the gamma ray logs. In such intervals, which rarely occurred, clay bearing fractures are missed by the model or clay zones are spuriously predicted by the model. More than 90 % of the modeled intervals deviate maximum 20 % from the core derived reference log and 74 % of the intervals maintaining clay-filled fractures could be exactly reconstructed. Using additional logs like SP or resistivity could improve the results, but they might not always be available. Other logs like neutron could not improve the model, but they can be helpful for the interpretation of the SCCL.

So far, clay-bearing facies could only be reliably mapped in sedimentary environments. This neural network based technique makes it possible to locate clay-bearing zones also in crystalline environments, where the contrast in physical parameters is not sufficiently large to easily identify clay on well logs. The big advantage of this method is that it only needs standard geophysical loggings and can thus be widely applied. The resolution of the SCCLs depends on the resolution of the input logs only, so the synthetic logs can see small clay-bearing fracture zones down to the decimeter scale. Compared to the clay-localization using S-waves/P-waves or electrical logs (resistivity, conductivity, SP) [*Freund*, 1992; *Titov et al.*, 2010], the neural network based method allows a semi-quantitative estimate of the amount of clay present.

The SCCL of the non-cored well GPK1 showed clay-filled fractures in potential aseismic zones and low clay content in intervals, where large microseismic events occurred. The connection between the appearance of clay and the occurrence of seismicity and aseismic movements makes the NNA a powerful tool to identify potentially weak zones and hydraulic pathways. An application on the remaining Soultz wells GPK2-4 might therefore be used as an indicator for reservoir mechanics and hydraulic properties. The implication for clay-filled fractures on geomechanics and hydraulic rock properties will be proven in future studies.

The flexibility of neural networks makes this technique easily applicable to all kinds of environments and well logs. Therefore, it is not only interesting for geothermics but for all applications exploring and using the underground.

ACKNOWLEDGEMENTS

The authors are grateful to the EnBW for the financial support of the research, to the BRGM for providing the Soultz structural data and core pictures from EPS1, and to the GEIE EMC for providing the various geophysical data from the Soultz wells.

5 IDENTIFICATION AND CHARACTERIZATION OF HYDROTHERMALLY ALTERED ZONES IN GRANITE

This study has been published in *Geophysical Journal International.*

MELLER, C., KONTNY, A., AND KOHLT, T. (2014). Identification and characterization of hydrothermally altered zones in granite by combining synthetic clay content logs with magnetic mineralogical investigations of drilled rock cuttings. *Geophys J Int*, **199** (1): 465-479, doi: 10.1093/gji/ggu278.

ABSTRACT

Clay minerals as products of hydrothermal alteration significantly influence the hydraulic and mechanical properties of crystalline rock. Therefore, the localization and characterization of alteration zones by downhole measurements is a great challenge for the development of geothermal reservoirs. The magnetite bearing granite of the geothermal site in Soultz-sous-Forêts (France) experienced hydrothermal alteration during several tectonic events and clay mineral formation is especially observed in alteration halos around fracture zones. During the formation of clay minerals, magnetite was oxidized into hematite, which significantly reduces the magnetic susceptibility of the granite from ferrimagnetic to mostly paramagnetic values. The aim of this study was to find out if there exists a correlation between synthetic clay content logs and measurements of magnetic susceptibility on cuttings in the granite in order to characterize their alteration mineralogy. Such a correlation has been proven for core samples of the EPS1 reference well.

Synthetic clay content logs were created from gamma ray and fracture density logs using a neural network. These logs can localize altered fracture zones in the GPK1-4 wells, where no core material is available. Mass susceptibility from 261 cutting samples of the wells GPK1-GPK4 was compared with the neural network derived synthetic logs. We applied a combination of temperature dependent magnetic susceptibility measurements with optical and electron microscopy, and energy dispersive X-ray spectroscopy to discriminate different stages of alteration.

We found, that also in the granite cuttings an increasing alteration grade is characterized by an advancing oxidation of magnetite into hematite and a reduction of magnetic susceptibility. A challenge to face for the interpretation of magnetic

susceptibility data from cuttings material is that extreme alteration grades can also display increased susceptibilities due to the formation of secondary magnetite. Low magnetic susceptibility can also be attributed to primary low magnetite content, if the granite facies changes. In order to interpret magnetic susceptibility from cuttings, contaminations with iron from wear debris of the drilling tools must be eliminated. Provided that the magnetic mineralogy of the granite is known in detail, this method in combination with petrographic investigations is suited to indicate and characterize hydrothermal alteration and the appearance of clay.

5.1 INTRODUCTION

The experience of more than 10 years of water circulation and several hydraulic stimulations in the geothermal reservoir of the geothermal power plant in Soultz-sous-Forêts (France) showed, that, in contrast to other enhanced geothermal systems like Basel or Landau [e.g. *Catalli et al.*, 2013], the magnitude of seismic events induced by circulation of fluids is rather low [e.g. *Baisch et al.*, 2010]. A possible reason for this behaviour is that clay minerals inside fractures can act as lubricants on fault zones and promote aseismic instead of seismic movements as it is observed on the San Andreas Fault [*Moore and Lockner*, 2013]. Due to their substantial effect on rock mechanics, such clay rich fracture zones are of major importance for the characterization and engineering of a reservoir. The objective of our study is the localization of these zones using a correlation between magnetic susceptibility of granite cuttings and the synthetic clay content logs and proving its reliability.

5.2 THE SOULTZ-SOUS-FORÊTS SITE

5.2.1 GEOLOGICAL SETTING

The geothermal project in Soultz-sous-Forêts at the western border of the Upper Rhine Graben targets a granitic intrusion of Variscan age overlain by 1.4 km Cenozoic and Mesozoic sediments. A porphyritic monzogranite hosts the geothermal reservoir and extends to a depth of ~4800 m forming the main granitic body of the Soultz geothermal system. It is characterized by large kalifeldspar crystals in a matrix of quartz, plagioclase, biotite, amphibole and accessories of magnetite, titanite, apatite, and allanite [e.g. *Hooijkaas et al.*, 2006]. The reservoir rock has been penetrated by five deviated wells with the deepest well reaching 5260 m measured depth (MD) and a pilot well (EPS1), which has been completely cored to a depth of 2300 m.

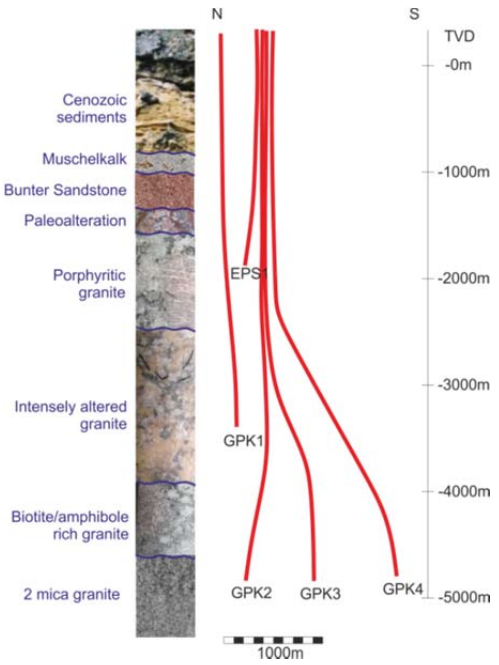

Figure 5-1: Overview of the trajectories of five deep wells at Soultz and the lithological profile to a depth of ~5000 m true vertical depth (TVD). Sketch is based on borehole trajectory data.

At 4800 m depth, fine-grained two-mica granite occurs hosting the second geothermal reservoir. It is interpreted as a younger intrusion into the older porphyritic granite and it contains primary muscovite and biotite while kalifeldspar is depleted [*Hooijkaas et al.*, 2006]. The well trajectories and the different facies are sketched in Figure 5-1. The Soultz intrusions belong to the magnetite series [*Ishihara*, 1977], with primary magnetite as the main carrier of susceptibility. Fresh granite contains ~1 wt-% multi-domain magnetite with a grain size between 300 and 500 µm. Magnetic susceptibility is between 10 and 80 x 10^{-3} SI depending on the wt-% of magnetite [*Just et al.*, 2004].

5.2.2 THE FORMATION OF CLAY MINERALS DURING HYDROTHERMAL ALTERATION

Due to large-scale wrench tectonics and block rotations during the Cretaceous, large fault zones were formed during the Variscan orogeny [e.g. *Edel et al.*, 2013]. Such zones provided pathways for fluids, which percolated large areas of the orogenic belt [e.g. *Guillou-Frottier et al.*, 2013] and altered the Soultz granite in two major alteration events. The first alteration stage occurred in Middle Carboniferous, when permeable zones formed inside the granite. This pervasive alteration event affected the granitic matrix, but had no influence on the structural properties of the rock [*Genter and*

Traineau, 1992]. Pervasive alteration is characterized by a transformation of plagioclase and biotite into illite, calcite and chlorite. Just and Kontny [2012] found that during circulation of O_2-rich fluids, magnetite was partially oxidized into martite in discrete zones near the fluid pathways. In such zones, the grain size of magnetite was reduced and magnetic susceptibility decreased from ferrimagnetic values ($<15 \times 10^{-3}$ SI) to paramagnetic values in the order of 10^{-8} SI. Secondary hematite precipitated from residual fluids.

The second alteration stage took place in Late Carboniferous, when early Variscan fault zones were reactivated. Subsequent circulation of hydrothermal fluids through fractures caused the formation of alteration zones around the fractures as large as several tens of meters. These fracture zones are significantly influencing the structural properties of the granite [*Genter and Traineau*, 1992]. The alteration halos are characterized by a central zone, sometimes sealed by quartz, surrounded by brecciated and altered rocks [*Genter and Traineau*, 1992]. The alteration intensity varies from fresh (no alteration) to extremely altered facies and is mainly characterized by a transformation of silicates into clay minerals [e.g. *Schleicher*, 2005] and by an increasing amount of secondary clay minerals and carbonates. The main secondary minerals are quartz, calcite, illite, hematite, and chlorite. Pyrite and Fe-carbonates were formed and the granite was exhumed to the surface in late Variscan times [*Fritz et al.*, 2010; *Ledésert et al.*, 1996]. In the upper part of the pluton, where meteoric waters infiltrated the paleo-surface, the Fe-carbonates and maghemite (γ-Fe_2O_3) decomposed and secondary fine-grained hematite precipitated [*Just and Kontny*, 2012]. Martite pseudomorphs formed after magnetite grains, whereas the size of the magnetite relics depends on the alteration intensity and on the intensity of stage I alteration. Martite was often fractured and a second hematite generation formed along the cracks. Magnetic susceptibility is mostly below 1×10^{-3} SI and hydrothermally altered wall rocks show the lowest magnetic susceptibility ($0.2\text{-}0.3 \times 10^{-3}$ SI) reflecting the most intense vein alteration. After deposition of the sedimentary cover in Mesozoic times, the infiltration of organic matter from the overlying sedimentary cover reduced martite back into secondary magnetite in the deeper part of the granite [*Just*, 2005].

5.2.3 RELEVANCE OF MAGNETIC SUSCEPTIBILITY FOR THE OCCURRENCE OF CLAY MINERALS

Just et al [2004] found that during hydrothermal alteration, which lead to the formation of clay minerals, there was also a transformation of magnetite (Fe_3O_4) into hematite (α-Fe_2O_3) (martitization). This process has previously also been observed elsewhere in granite, basalts and itabirites [e.g. *Angerer et al.*, 2011; *Lagoeiro*, 1998; *Oliva-Urcia et al.*, 2011]. Magnetite oxidation is accompanied by a reduction of magnetic susceptibility [*Genter and Traineau*, 1992].

Core material of the reference well EPS1 provided the unique opportunity to investigate in detail hydrothermal processes and fractures directly on samples. Just *et al.* [2004] compared the bulk magnetic susceptibility log along the EPS1 core of Rummel and König [1991] with the appearance of rock alteration and changes in the magnetic mineralogy. They found, that an increasing alteration grade was accompanied by decreasing magnetic susceptibility.

Meller et al. [2014b] developed a method to create synthetic clay content logs (SCCL) on the basis of spectral gamma ray measurements. Such logs provide a semi-quantitative measure of the appearance of clay minerals inside fractures related to hydrothermal alteration. The method to create such logs will be described in the following chapter. According to the results from Just *et al.* [2004], we expected a correlation between the SCCL and magnetic susceptibility of EPS1. Plotting the bulk magnetic susceptibility curve generated after data from Rummel & König [1991] against the SCCL reveals an inverse correlation between the amount of clay and magnetic susceptibility (Figure 5-2). This inverse correlation between results from two totally independent methods suggests that magnetic susceptibility can be used as a marker of hydrothermal alteration. The objective of this work is to create SCCL logs for the deep Soultz boreholes GPK1-4, where no direct observation of fracture mineralogy is possible due to the lack of core samples. With magnetic mineralogical investigations on cuttings of these wells we wanted to investigate, if the mineralogical changes due to hydrothermal alteration, which have been described on the EPS1 core, can also be observed in the deeper part of the geothermal reservoir.

The importance of clay as a control to fracture mechanics has been highlighted earlier [*Rummel and Schreiber*, 1993; *Rummel et al.*, 1991; *Valley and Evans*, 2003]. Clay can be localized by resistivity logs, spontaneous potential logs or sonic logs or it can be identified directly on core material. However, due to low budgeting, boreholes for geothermal applications are generally not cored and only standard (wireline) logs like calliper, image logs and spectral gamma ray are measured.

For certain scientific purposes, further logging analyses such as resistivity, spontaneous potential, flow-meter logs, etc. might be conducted. Unfortunately, this is often not the case and if so, these logs are only conducted as spot measurements for selected depth intervals. In contrast to drill cores, cuttings are obtained from each drilling without additional costs. Most of the structural information about the reservoir is lost in the rock chips of cuttings. Therefore, these rock chips are mainly used for the creation of lithology logs and for geochemical analyses. The loss of structural information, however, plays no role for bulk magnetic susceptibility of the cuttings, as it only depends on the mineralogical content of the sample. With the help of microscopic studies, drilled rock cuttings can provide important additional information about the composition of rocks and chemical processes in a reservoir.

Just [2005] verified that hydrothermal alteration is responsible for the transformation of silicates and magnetite oxidation in the granite. This process has also been observed by Pandarinath et al. [2013] for the Los Azufres geothermal system in Mexico. The authors found that with increasing depth, hydrothermal alteration increases and the fraction of magnetic minerals decreases. Thus, magnetic susceptibility was found to decrease with depth. Our study focusses on the localization and characterization of hydrothermally altered intervals along the wells GPK1-4 using the temperature-dependence of magnetic susceptibility in combination with microscopic methods on cuttings material.

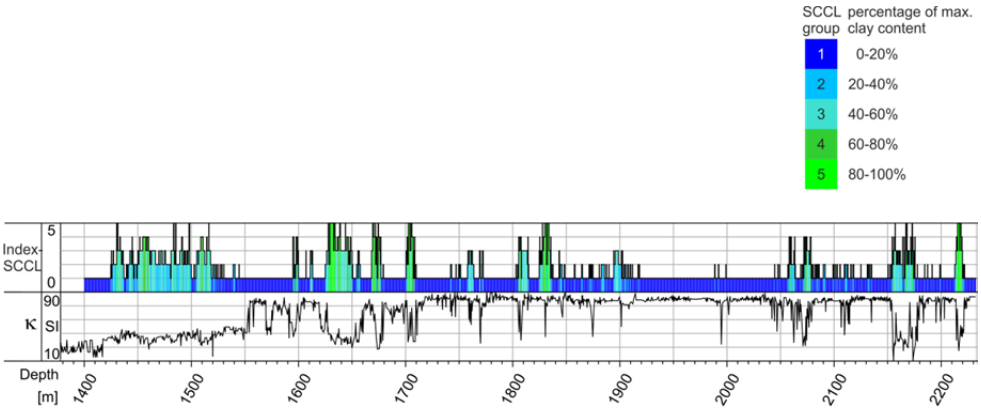

Figure 5-2: A comparison between the core derived synthetic clay content log representing the density of clay-filled fracture along the well with magnetic susceptibility (κ) in 10^{-3} SI of the EPS1 core reveals an excellent correlation between low magnetic susceptibility values and high clay content. Susceptibility data are taken from Rummel & König [1991] and the SCCL is from Meller et al. [2014b].Methods for the identification of vein alteration and its magnetic properties

5.2.4 DETECTING CLAY FROM SPECTRAL GAMMA RAY LOGS USING A NEURAL NETWORK

Meller et al. [2014b] described a method to find clay bearing fracture zones on the basis of spectral gamma ray and fracture-density logs by applying a neural network on the logging data. They created a reference dataset for the appearance of clay inside fractures on the basis of core data from the pilot well EPS1 at Soultz-sous-Forêts. The reference was used to train the neural network using a Kohonen-algorithm [*Kohonen*, 1984]. This algorithm uses a self-organizing map, which is a two-dimensional representation of the multidimensional network. In the training phase, the neural network classifies the input logs in a way that each pattern of log responses is assigned to a node of the neural network. This process is repeated until a certain number of iterations is reached and the network has optimally approximated the input. In the

subsequent indexing phase, the network learns how the log responses are correlated with the appearance of clay. For this purpose, the reference clay log is used to group the nodes of the neural network into the predefined SCCL classes. The nodes are distributed into the classes with the closest properties. After this indexing, the network has the knowledge about how clay, fracture density and spectral gamma ray are correlated. This knowledge can be recalled when applying the network on the logs from the remaining wells.

In order to investigate the correlation between alteration intensity, magnetite oxidation, and the formation of clay minerals in the deep wells GPK1, GPK2, GPK3 and GPK4, we applied the network, which was trained on the EPS1 spectral gamma ray and fracture density logs, on the respective logs of the deep Soultz wells.

5.2.5 MAGNETIC SUSCEPTIBILITY MEASUREMENTS FOR WELL CHARACTERIZATION

For measurement of magnetic susceptibility and temperature dependence of magnetic susceptibility 261 cutting samples from the following depth intervals of the wells GPK1, GPK3 and GPK4 were selected:

i) 147 samples for GPK1 from 1800-1829 m, 2594-2744 m and 3452-3547 m
ii) 43 samples for GPK3 from 3296-3482 m and 4704-4915 m and
iii) 71 samples for GPK4 from 3384-3542 m and 5030-5258 m.

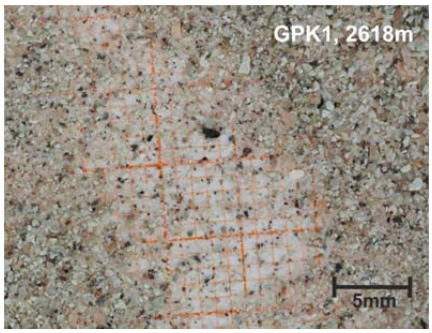

Figure 5-3: Photo of cuttings from porphyritic granite (GPK1, 2618 m) on millimeter paper.

The cuttings are very fine-grained with grain sizes between 0.1 mm to 1 mm (Figure 5-3). GPK2 cuttings were not used due to poor quality. Bulk magnetic susceptibility was measured with an AGICO KLY-2 Kappabridge with an applied magnetic field of 300 Am^{-1} at a frequency of 920 Hz. Magnetic susceptibility of each sample was measured three times and average of these three values is normalized by the sample density.

5.3 RESULTS

5.3.1 SYNTHETIC CLAY CONTENT LOGS FOR THE WELLS GPK1-4

The SCCL logs of the deeper wells provide a semi-quantitative log of the clay-filled fractures (Figure 5-4). They allow discriminating several zones with distinct clay content. This is indicated by five groups of increasing clay content, whereas group 1 represents 0-20 % of the maximum density of clay-filled fractures and group 5 represents the highest density (80-100 %). The groups are defined in the legends of Figure 5-2 and Figure 5-4.

Based on the synthetic logs, we can define several depth intervals with different characteristics from the top to the base of the wells: Interval I, which ends at about 1900 m depth, is characterized by high clay content with SCCL groups 4 and 5. It is followed by interval II, which contains ~150 m of low clay (SCCL 1 and 2) with a central structure with SCCL 4 and 5 indicating a clay-rich interval at about 2100 m. This interval can be observed in all four wells. In GPK1 and GPK2 (Figure 5-4 a and b), interval III contains a succession of small intervals with changing contents of clay-filled fractures. In interval III of the wells GPK3 and GPK4 (Figure 5-4 c and d) the SCCL is generally higher and it can be subdivided into two sub-intervals IIIa and IIIb. IIIa contains several broad and clay-rich structures alternating with intervals of low SCCL (little clay). Interval IIIb has high SCCL values in GPK3, but smaller SCCL values in GPK4. Interval IV is characterized by low SCCL in GPK2 and 3, whereas in GPK2 fracture information is missing in this depth and the SCCL log might not be correct. In GPK1 and GPK4, there are broad intervals of intermediate SCCL (groups 2 and 3) alternating with thick intervals without or with very little clay (SCCL group 1 and 2). The deepest interval V beginning at a depth of ~4600 m again shows an increased density of clay-filled fractures, which might be due to the transition of porphyritic granite to the fine-grained two-mica granite.

Resuming, the highest SCCL is expected in the upper parts of the wells (interval I) and around the structure at ~2100 m in all wells. Furthermore, clay-rich zones occur in GPK1 around 2700 m, 2900 m and 3300-3500 m. In GPK2, high SCCL values indicate high clay content between 4600 m and 4800 m. GPK3 has several clay-rich intervals between 2800 m and 3600 m and below 4600 m. GPK4 is the well with the highest SCCL, especially in the intervals IIIa, IV and V.

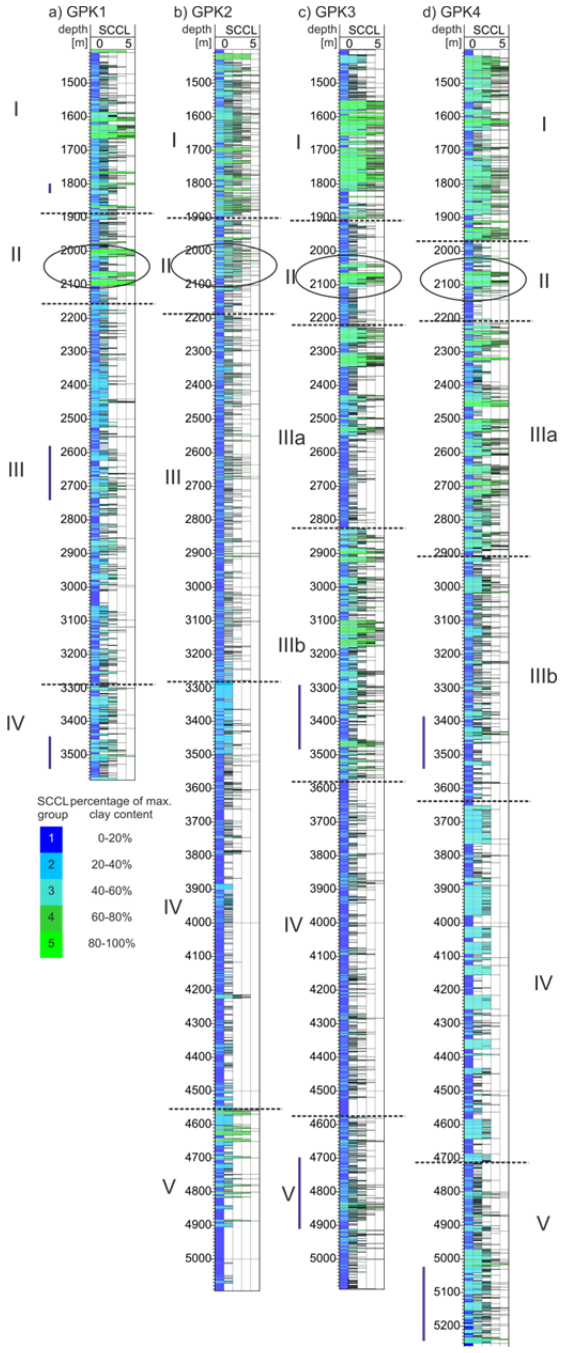

Figure 5-4: SCCLs for the wells GPK1-GPK4 created by the neural network application. The colors represent the different groups of increasing density of clay-filled fractures as explained by the legend. The blue lines beside the logs indicate the depth intervals, for which cuttings were available. The logs are subdivided into four respectively five depth intervals I to IV or V, which are similar in each well. The black ellipse in zone II highlights a clay-rich structure, which can be seen in each well.

5.3.2 MAGNETIC SUSCEPTIBILITY OF CUTTINGS

Large variations of mass magnetic susceptibility have been measured for the three wells, ranging from χ=0.16 to 7.35 x 10^{-3} m^3kg^{-1} for GPK1, χ=0.24 to 8.92 x 10^{-3} m^3kg^{-1} for GPK3, and χ=1.59 to 17.91 x 10^{-3} m^3kg^{-1} for GPK4. In the following, the symbol χ indicates mass susceptibility in $10^{-3}m^3kg^{-1}$, whereas κ in Figure 5-2 is bulk susceptibility in SI. From the described previous data we expected higher χ in fresh granite than in the altered granite. Figure 5-5 shows exemplary results for different reservoir depths with increasing depth from GPK1 to GPK4. The GPK1 interval around 1500 m is neglected as this interval is characterized by high paleo-alteration intensity. This alteration is not of interest for this study. A comparison between the measured χ and the respective lithology (Figure 5-5) indicate that the strong correlation between susceptibility and SCCL seen in Figure 5-2 is not always apparent. However, there is a tendency towards higher χ in the porphyritic granite than in altered facies (Figure 5-5a, b).

The SCCL can better explain intervals of low χ than the lithology log. In the depth interval 2625 to 2660 m of GPK1, the litholog indicates fresh porphyritic granite. χ is only high between 2625 and 2640 m followed by a slight decrease. In contrast to the lithology log, the SCCL log indicates the appearance of clay-filled fractures between 2640 and 2660 m, which are a sign for alteration in this interval. This is in accordance with low magnetic susceptibility. Poor correlation between χ and SCCL can be found, for example, in the extremely altered facies between 3490 and 3500 m in GPK1 (Figure 5-5b) or in the fresh porphyritic granite between 4780 and 4810 m in GPK3 (Figure 5-5c). In alternating sequences in the order of few meters, there is poor correlation between alteration and χ. We assume that this is a result of the large sampling interval, which is in the order of the thickness of lithological units. An important observation is that the transition between porphyritic and two mica granite correlates with a decrease of χ (Figure 5-5c). The two mica granite is characterized by lower magnetite content than the porphyritic granite.

With a statistical analysis of SCCL versus magnetic susceptibility we further investigated the correlation between magnetic susceptibility logs and the SCCL logs.

The cross-plot of SCCL group number versus mass susceptibility (Figure 5-6) reveals that χ is inversely correlated with the clay content indicated by the SCCL. The mean mass magnetic susceptibilities ($\overline{\chi}$) and their respective standard deviation (σ^2) measured for the five SCCL groups are:

Group 1: $\overline{\chi}$ =3.5 (σ^2=4.97)
Group 2: $\overline{\chi}$ =3.01 (σ^2=4.62)
Group 3: $\overline{\chi}$ =2.24 (σ^2=1.96)
Group 4: $\overline{\chi}$ =1.61 (σ^2=1.54)
Group 5: $\overline{\chi}$ =0.42 (σ^2=0.28).

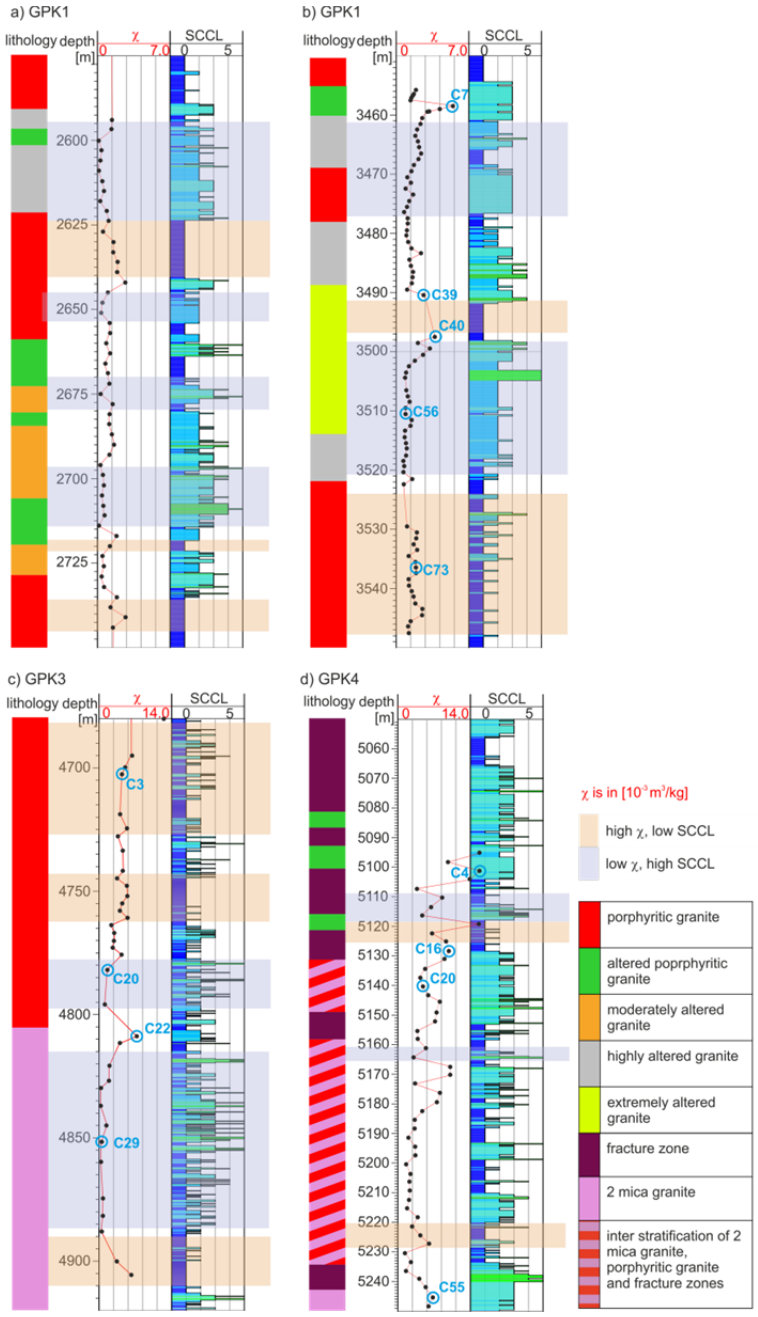

Figure 5-5: GPK1, GPK3 and GPK4 susceptibility logs derived from measurements of the mass susceptibility of cuttings. Shown is a comparison between SCCL and mass susceptibility of cuttings for certain depth intervals of GPK1, GPK3 and GPK4. The colored bars indicate where low magnetic susceptibility correlates with high clay content (blue) and vice versa (brown). The simplified lithology is created after the litholog derived from cuttings examination by Genter and Traineau [1993] for GPK1, Dezayes et al. [2003] for GPK3 and Dezayes et al. [2005b] for GPK4. The colors are explained in the legend. Blue circles indicate the selected samples for κ-T measurements and thin section analyses.

$\overline{\chi}$ is lower for higher clay content, which is in agreement with the results of the measurements done by Just et al. [2004]. Although the mean values indicate decreasing susceptibility with increasing clay content, there is a large scattering of χ in each SCCL group (Figure 5-7a), which is also reflected by the large standard deviation of $\overline{\chi}$ (Figure 5-6). According to the observation in EPS1 that magnetic susceptibility decreases with increasing clay content, we would expect the lowest χ for the SCCL groups 4 and 5, yet low χ is measured for all SCCL groups. This may be due to the varying amount of magnetite present in the samples, and the diluting effect on cuttings material by large phenocrysts of feldspar with diamagnetic to paramagnetic χ values. Alternatively, the blending of sample material from different depth intervals may dilute the χ intensity.

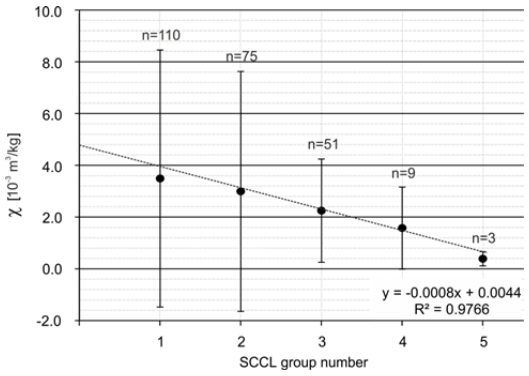

Figure 5-6: Synthetic Clay Content Log groups versus mass susceptibility of cuttings. With increasing group number, i.e. higher clay content, mass magnetic susceptibility (χ) is lower. Circles represent the mean values of measured magnetic susceptibility and bars indicate the standard deviations. The dashed line is the regression line. The equation of the regression line and the R2 value are given in the lower right corner of the diagram.

As a result, minerals from depth intervals with different alteration grades and different SCCLs can be mixed, which means that the SCCL assigned to a sample might not be representative for that interval. For GPK4, for example, the sampling interval was between three and 24 meters [*Dezayes et al.*, 2005b]. In GPK3, the maximum distance between two samples was 16 m. This might be the reason, why the largest scattering of χ vs. SCCL can be observed in GPK3 and GPK4 (Figure 5-7c and d), whereas scattering is lowest in GPK1 (Figure 5-7d). Here, the sampling interval was 1 m, the highest number of samples available. In the GPK1 well, a clear tendency towards higher χ was found in the fresh granite and towards lower values in the clay-rich sections (Figure 5-5).

Although the scattering of χ is high, we measured the highest χ only in fresh lithology (SCCL groups 1 and 2).For the well GPK4, the minimum χ in each SCCL group is considerably higher than for the GPK1 samples, but there is no clear indication from lithology explaining the different behaviours. We assume that magnetic susceptibility is increased due to contamination of the cuttings by wear debris from the drill bit or other drilling tools. This aspect has been further investigated by microscopic examination of the samples.

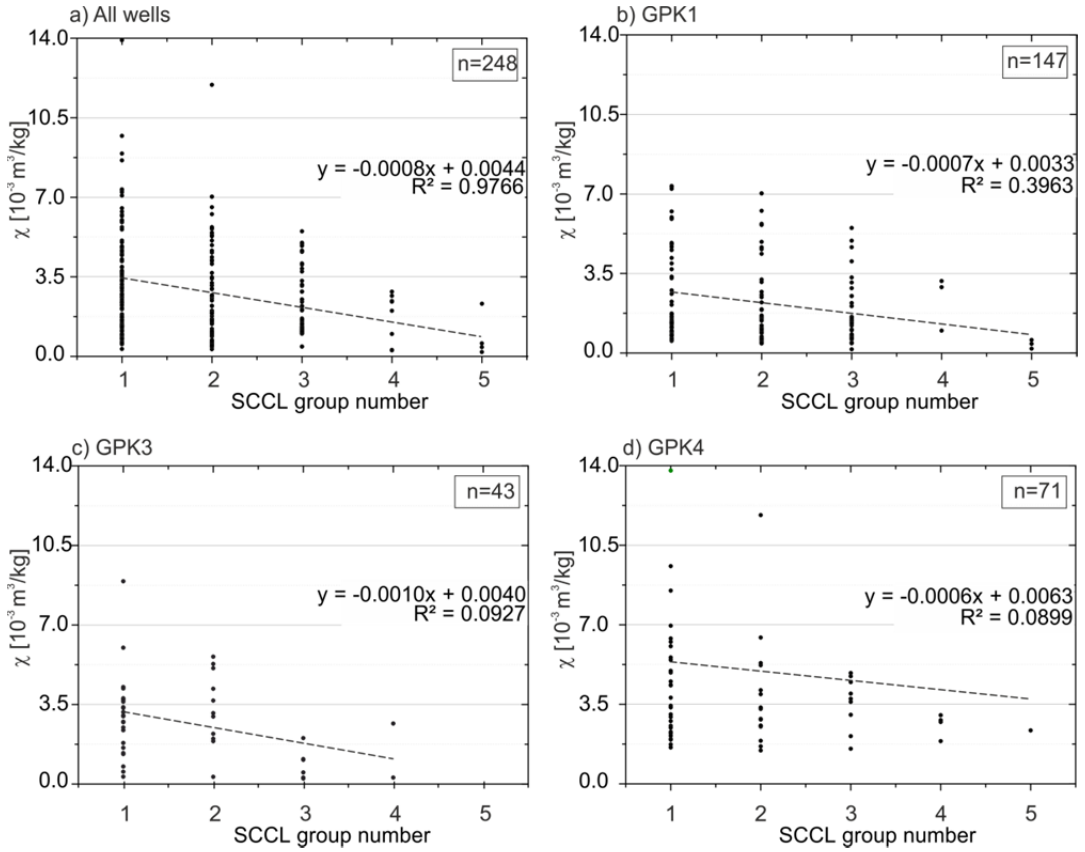

Figure 5-7: Measured susceptibility values for the different SCCL groups for all wells (a) and separated for GPK1 (b), GPK3 (c) and GPK4 (d). The dashed line is the regression line with the respective equations and R^2 value given in the diagram. For GPK4 four χ values of SCCL1 and SCCL2 are above ~14. These samples are not plotted here and are excluded for the regression calculation.

5.4 CHARACTERIZATION OF HYDROTHERMAL ALTERATION BY MAGNETIC MINERALOGICAL INVESTIGATIONS OF CUTTINGS

The excellent correlation between decreasing χ and the appearance of clay, which has been demonstrated on the EPS1 core (Figure 5-2), has not always been observed in the magnetic susceptibility measurements of cuttings. Therefore, a more detailed understanding of the magnetic mineralogy of cutting samples is necessary to correctly interpret the results. The following section summarizes the main aspects of our magnetic mineralogical investigations. These results are compared to earlier investigations on EPS1 core material by Just et al. [2004] and Just and Kontny [2012].

5.5 MINERALOGICAL AND MAGNETIC METHODS

Magnetic mineral assemblages in fresh and altered granite cuttings were studied from samples with very low and very high susceptibility, respectively (blue circles in Figure 5-5). Twelve samples were selected for thin section investigations under reflected and transmitted light using a Leitz Orthoplan optical microscope. Two samples were additionally investigated by electron microscopy (Quanta FEG 650 from FEI, with an acceleration voltage of 15 kV) and with energy dispersive X-ray spectroscopy (EDX) using a Quantax 400 with an XFlash-Detector, in combination with the software Esprit 1.9 from Bruker AXS Microanalysis GmbH. In order to explain the behaviour of samples with intermediate to high susceptibility but different degrees of alteration in the SCCL, the altered sample GPK1-C40 and the fresh sample GPK1-C73 from the porphyritic granite were selected. Our goals were to identify and to compare their carriers of magnetic susceptibility and the mineral assemblage.

Magnetic susceptibility as a function of temperature (κ-T curves) was measured for 16 samples (~0.2 g) in order to determine Curie points and to characterize mineral transformations, which is useful for the identification of magnetic minerals. κ-T curves were measured with a KLY-4S Kappabridge applying a magnetic field of 300 Am^{-1} and a frequency of 875 Hz. The sample was first heated from –192 °C to room temperature (low-temperature run) with a heating rate of approximately 4 °C/min. Afterwards, the sample was measured from ambient temperature to 700 °C and cooled back to room temperature with a heating rate of 10 °C/min. The measurements were conducted in an Argon atmosphere with a flow rate of 100 ml/min to minimize mineral reactions with atmospheric oxygen during heating. The raw data were corrected for the empty furnace and normalized to χ at room temperature.

5.6 RESULTS OF MAGNETIC MINERALOGICAL INVESTIGATIONS

5.6.1 MICROSCOPIC IDENTIFICATION OF MINERAL PHASES

Two distinct granite facies occur in the granitic body of the Soultz geothermal system the porphyritic granite and the two-mica granite (Figure 5-5). The main focus of our cuttings investigation involved the porphyritic granite because alteration stages are better defined in this facies. The porphyritic granite contains large phenocrysts of K-feldspar and a coarse grained matrix of quartz, biotite, and plagioclase. Accessory phases are mainly zircon, titanite, sometimes with inclusions of lamellar hemo-ilmenite grains and pyrite (Figure 5-8a and b), and magnetite.

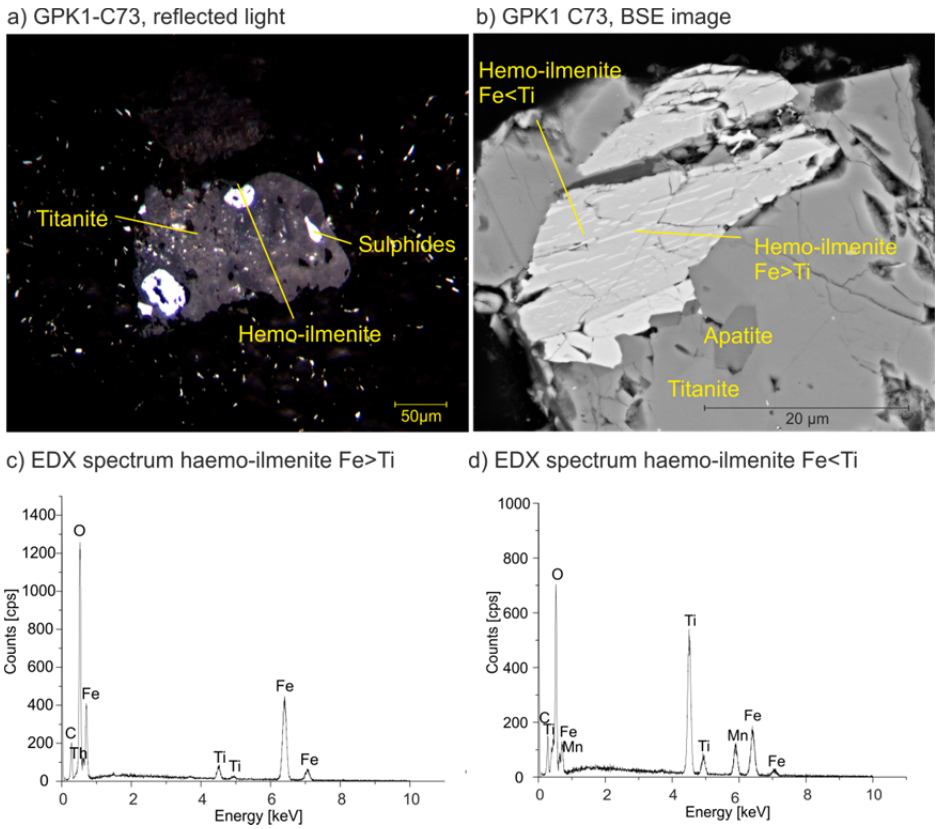

Figure 5-8: Microscopy of the sample GPK1-C73 (fresh granite). a) is in reflected light, b) is a back-scattered electron photograph, c) and d) are EDX spectra of hemo-ilmenites with different titanium contents.

Thin sections of cuttings of two-mica granite from the deeper part of the GPK4 well look different from those of the GPK1 and GPK3 wells. The occurrence of cross-hatched microcline and myrmekite is typical for the two-mica granite facies and has already been described by Dezayes et al. [2005b]. Microcline and myrmekite can be seen in thin sections as well as muscovite associated with biotite. In the two mica granite, we have also identified magnetite as the main magnetic mineral albeit its abundance seems to be less than in the porphyritic granite. However, we were not able to quantify the different contents of magnetite in the two granite facies as their distribution is heterogeneous.

Cutting samples from the altered granite are characterized by a higher amount of hematite than magnetite. Both minerals are always intergrown indicating a replacement relationship (Figure 5-9a). It is not clear if magnetite replaces hematite or if magnetite is transformed into hematite in these grains. Just and Kontny [2012] also observed an intergrowth of magnetite and hematite in thin sections of granite from stage I alteration [see Fig. 3d in *Just and Kontny*, 2012]. In addition to a higher amount of hematite, we observed iron-bearing carbonates in the more altered samples (Figure 5-9b and c).

A frequently observed paragenesis in altered samples is that of allanite, rutile, apatite and titanite with iron oxides (Figure 5-9 e and f). Goethite and hematite occur as alteration seams around the fractured cuttings. This alteration appears not to be a product of hydrothermal alteration, but rather a secondary effect due to humidity inside the stored samples. We recognized, that iron-oxide alteration seams are more pronounced in the samples of GPK1 than in those of GPK3 and GPK4. GPK1 was drilled in 1992 and therefore these samples are older than the samples from GPK3 and GPK4 that were drilled in 2002 and 2003/2004 respectively. This means, they have been exposed longer to atmospheric oxygen and moisture. Therefore, we attribute the more pronounced oxidation to the long storage time of the GPK1 samples. Such an alteration due to storage has also been observed around iron flakes, which occur as contaminations in the cuttings (Figure 5-9g). The EDX spectrum of the iron flake showed iron, oxygen, manganese, chromium, and silica (Figure 5-9h), which probably reflect the composition of the material of the drilling tool. The oxidation rim around the flakes only showed iron and oxygen.

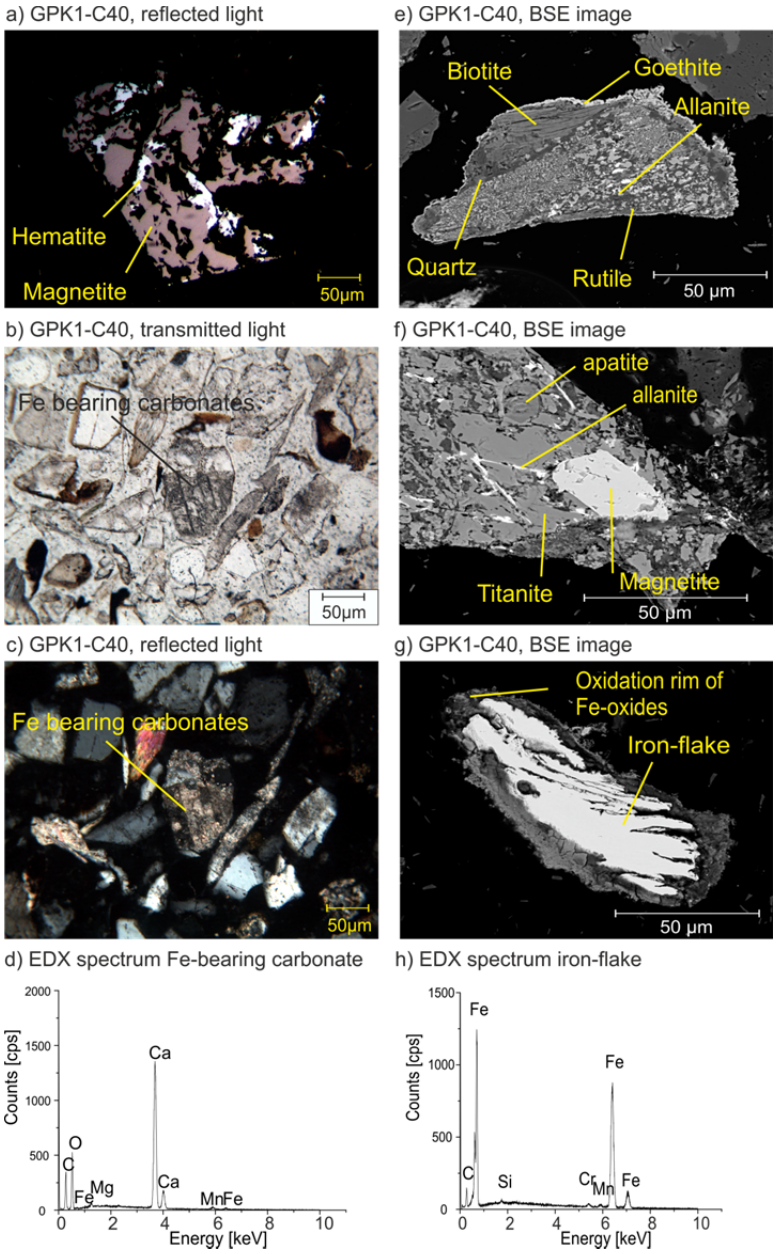

Figure 5-9: Microscopy, BSE images and EDX spectra of some minerals in the sample GPK1-C40 (altered granite).

5.6.2 κ-T CURVES

Figure 5-10 shows typical *κ-T* curves of fresh and altered porphyritic and two-mica granite from the GPK1-4 wells. In all samples, magnetite was identified as the main carrier of magnetic susceptibility, which is indicated by the occurrence of the Verwey transition (Tv) at 120 K (-153°C) and a Curie temperature at ~580°C.

Fresh and altered granite cuttings of well GPK3 and 4 are all contaminated iron debris (Figure 5-10a, b, d) indicated by the magnetic susceptibility behaviour between 600 and 700 °C where magnetic susceptibility does not reach zero. Even GPK1 cuttings stored for the last 20 years occasionally contain iron flakes (Figure 5-9g and h). These iron flakes were, however, no longer recognized in *κ-T* curves of GPK1 samples (Figure 5-10c), which indicates their oxidation (formation of rust) and therefore their rare survival over this time period.

In the altered sample of the porphyritic granite (Figure 5-10c), a transformation above 400 °C into a ferrimagnetic phase has been observed. This feature can be related to iron-bearing carbonates, which transform at this temperature into a ferrimagnetic spinel phase (Just and Kontny, 2012), and which is also in agreement with our microscopic observations (Figure 5-9b, c and d). This interpretation is supported by the cooling curve, which only shows magnetite and a ferrimagnetic phase with a Curie point at 499°C [inflection point method, *Tauxe*, 1998] and the features from the heating curves are destroyed.

The difference in the reversibility of the *κ-T* curves indicates that a degree of alteration occurred during the heating experiment. In the cooling run of the GPK1 samples, susceptibility is considerably higher than in the heating run. This indicates the formation of new ferrimagnetic mineral phases (e.g. magnetite from hematite or secondary Fe-bearing carbonates) during the heating run. The curves confirm the observation by Just and Kontny [2012], who found that more pronounced stage II alteration in the sample is reflected by less reversibility of the susceptibility curve. They defined an alteration index (AI) similar to that of Hrouda [2003] as a measure for the irreversibility of *κ-T* curves, calculated according to the formula $AI = \kappa_{CTroom} - \kappa_{HTroom}$, where κ_{CTroom} and κ_{HTroom} are the normalized susceptibility of the cooling respectively heating run at room temperature.

For less altered samples, *AI* is <1, whereas more altered samples have *AI* >1 with the highest values measured for stage II alteration (maximum of 4.8). Samples of GPK4 show a negative alteration index, which indicates the decomposition of magnetite or a transformation of the iron chips during heating. However, this behaviour is not observed in the *κ-T* curve of the separated iron chips (Figure 5-11), which have an alteration index of 0.04. This suggests that the iron chips increase the absolute value of magnetic susceptibility of the samples, but do not affect the alteration index.

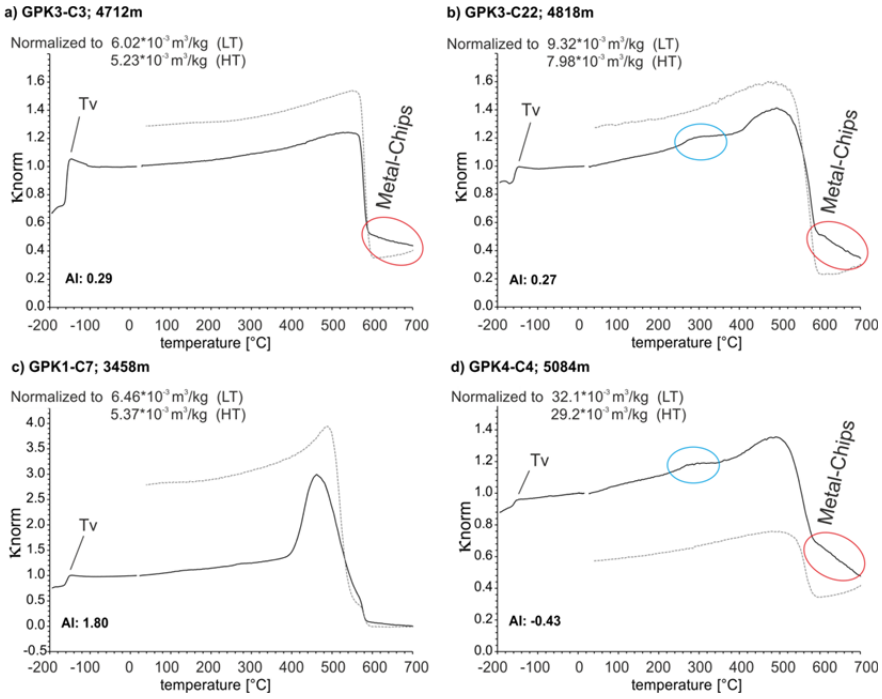

Figure 5-10: κ-T curves for the samples a) GPK3-C3 (porphyritic granite), b) GPK3-C22 (two-mica granite), c) GPK1-C7 (altered porphyritic granite) and d) GPK4-C4 (altered two-mica granite). Susceptibility is normalized to the susceptibility at room temperature for the low-temperature (LT) and high temperature run (HT) as indicated in the upper left corner of the graphs. The black curves show the heating run and the grey curves the cooling run, respectively. The alteration index (AI) is given for each curve.

Although identified by its red internal reflections in thin sections, hematite was not seen directly in *κ-T* curves. No Morin transition of hematite at ~263 K (-10 °C) or Néel temperature at 675 °C was observed. We assume that magnetite masks the Morin transition of hematite, whose susceptibility is three orders of magnitude weaker than that of magnetite. The missing Néel temperature and the increase of magnetite content during the heating experiment indicate that hematite is transformed into magnetite. Therefore, higher alteration indexes in the altered granite samples are mainly related to the transformation of hematite and iron-bearing carbonates into magnetite.

Some fresh and altered cutting samples of all wells, but most pronounced in GPK1 (Figure 5-12a and c), show a conspicuous increase in magnetic susceptibility at about 250 °C forming a peak at about 300 °C, which is followed by a decrease. Between about 400 and 580 °C magnetic susceptibility is higher than below 250 °C indicating that a phase with higher magnetic susceptibility must have formed. This phase is not stable during the heating procedure and transforms presumably into magnetite. An increase in magnetic susceptibility is for example observed at the λ-transition of minerals, which is a change in the magnetic state by a rearrangement of vacancies. Although the strong increase in susceptibility at 250 °C resembles the one observed for the λ-transition of

hexagonal pyrrhotite [e.g. *Kontny et al.*, 2000], where the magnetic state of the mineral changes from anti-ferromagnetic to ferrimagnetic, and the and the Curie temperature at about 350 °C might be indicative for ferrimagnetic iron sulphides like smythite or greigite [*Dunlop and Özdemir*, 1997], we have microscopically identified pyrite as the only occurring iron sulphide. Samples with the conspicuous peak at about 300 °C also do not show a pronounced field-dependence of magnetic susceptibility (Figure 5-12b and c), which would be a clear indication of ferrimagnetic pyrrhotite [e.g. *Hrouda*, 2003].

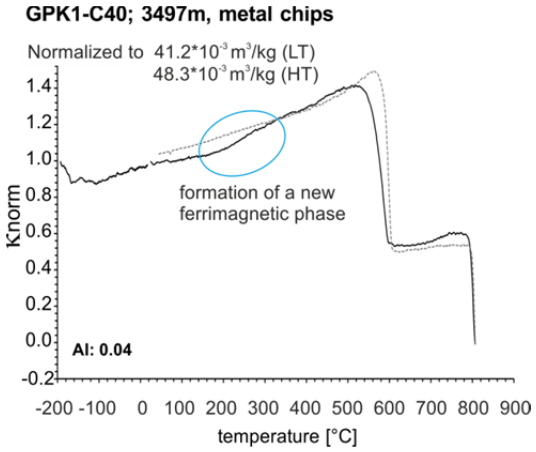

Figure 5-11: κ-T curve of iron chips separated from the sample GPK1-C40. The curve shows the formation of a new ferromagnetic phase (probably magnetite) during heating. The newly formed magnetite is indicated by its Curie-temperature. The sample becomes paramagnetic at 800°C.

A similar but not equivalent bump in *κ-T* curves was observed by Petronis et al. [2011] in the Western Granite from NW Scotland and is actually widespread for magnetite-bearing rocks [*Hrouda*, 2003]. This feature is in general attributed to maghemite, an oxidation product of magnetite. Because we clearly see that a new phase with higher magnetic susceptibility has formed at 250 °C (higher magnetic susceptibility level between 400 and 580 °C), we suspect that we see a two-stage phase transformation of a phase with lower magnetic susceptibility to a strong ferrimagnetic phase (or we see a Hopkinson peak of a ferrimagnetic phase with small grain sizes) and then to magnetite. We suspect that the peak might be attributed to the formation of maghemite from the oxidation products of the iron chips, which is transformed in the course of further heating to magnetite. Maghemite formation is often observed during heating of iron oxides like goethite or hematite [e.g. *Cornell and Schwertmann*, 2003].

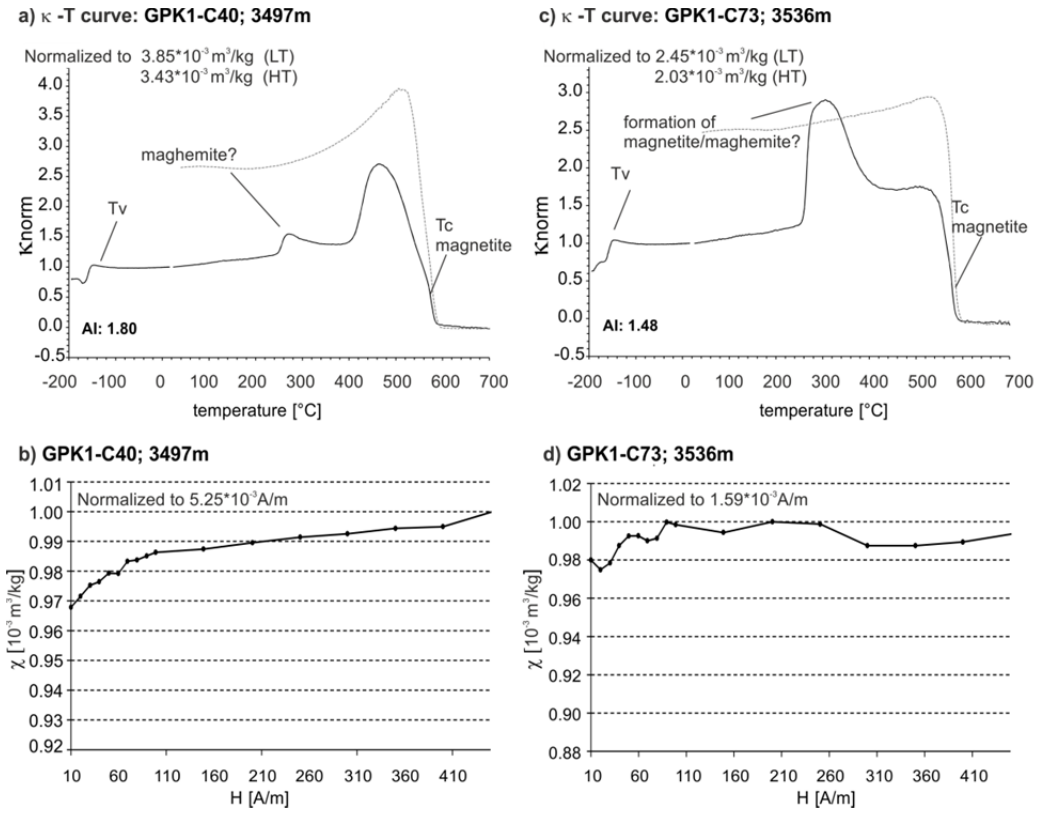

Figure 5-12: κ-T curves and field dependency of the samples GPK1-C40 and GPK1-C73. The κ-T curves (a and c) show the formation of several mineral phases during the heating run. The formation of pyrrhotite can be excluded, as the samples show no field dependency (b and d).

This interpretation would be in agreement with the observation that this behaviour is most pronounced in cutting samples from the GPK1 well, in which iron flakes are most oxidized. In order to find an evidence for this hypothesis we selected some iron chips from the sample GPK1-C40 (see Figure 5-12a) and measured a *κ-T* curve (Figure 5-11). Magnetic susceptibility increases continuously during heating of the iron chips, but below 300 °C the gradient of the curve becomes steeper reaching a maximum at around 260 °C and forming a peak at 280 °C. This is probably the same peak, which we observed in the *κ-T* curves of the cutting samples. Further heating clearly indicates the formation of magnetite, which is a major phase of the iron flakes. We relate this behaviour to the oxidation seams around the iron chips and take it as evidence for our hypothesis that the 300 °C peak in our samples is mainly related to oxidation products of the iron flakes.

5.7 DISCUSSION

5.7.1 SCCL LOGS FROM SPECTRAL GAMMA RAY DATA

The application of the neural network method [*Meller et al.*, 2014b] makes it possible to find altered and clay rich zones along the geothermal wells. In general, the logs allow discriminating between five different intervals of high and low clay content, respectively. The logs show a high content of clay-filled fractures in the upper part of all four deep wells. In the deeper parts of the reservoir, the patterns are different between the boreholes, which might be due to the fact that the upper parts of the wells are very close to each other, whereas below 3000 m the wells are increasingly deviated from each other. The change in lithology is not clearly visible in the SCCL logs, but the transition from intensely altered facies to two-mica and amphibole rich granite at ~3500 m and the transition to the fine-grained two-mica granite at ~4600 m are reflected by a change in clay content and in the pattern of clay appearance. Several structures can be identified, which might indicate fracture or alteration zones, and have not been taken into account in previous studies. This is for example a structure at 2100 m MD, which can be seen in all four deep wells and in EPS1. A large fracture zone has been identified in GPK3 and EPS1 [*Dezayes et al.*, 2000; *Genter and Traineau*, 1995], but not for the remaining wells. Such zones are related to vein alteration and the high clay content can weaken the granitic rock. The identification of these potentially weak zones is important as they most probably behave different than the intact or unaltered rock mass. Compared to previous petrographic approaches for the localization of altered zones, this SCCL method is independent from cutting losses or other drilling-related effects, which can lower the quality of the cutting material. It is based on standard logging techniques and provides the possibility to obtain complete synthetic logs in a rather short time.

5.7.2 CHARACTERIZATION OF ROCK ALTERATION BY MAGNETIC MINERALOGICAL INVESTIGATIONS

Magnetite was found in all samples from which we measured κ-T curves independent of granite type and degree of alteration, although the proportion is small in the altered samples. The strong decrease of magnetic susceptibility in the altered samples can be related to the oxidation of magnetite to hematite as already stated by Just et al. [2004] and Just and Kontny [2012]. According to these earlier studies on the EPS1 cores, a significant decrease of magnetic susceptibility occurs in stage II altered granite, which is restricted to fault zones with an intense brittle deformation and brecciation of the

granite as well as alteration halos in the adjacent wall rocks. Illite along with Fe-carbonates, pyrite and hematite (martite) occur as alteration minerals, which are shown to transform into ferrimagnetic magnetite during heating in κ-T curves and, therefore, can be recognized easily. The strong irreversibility of κ-T curves for the highly altered stage II samples observed by Just and Kontny [2012] was also seen in our κ-T measurements from the cuttings (Figure 5-10a). The most important transformation seen in κ-T curves is the one from hematite into magnetite. In addition, we found Fe-bearing carbonates in the cuttings, which are observed in the κ-T curves by the transformation into magnetite above 400 °C. In addition to these mineral transformations, we recognized in nearly all samples another phase with a peak in susceptibility at about 300 °C, which is not described from the EPS1 core material. This phase is most likely related to the oxidation products of iron flakes, which occur as contamination in the cuttings and could also be seen in κ-T curves of iron chips separated from the cuttings. The peak might reflect the formation of maghemite from oxidation products of the iron contaminants during heating of the samples [*Gendler et al.*, 2005; *Taylor and Schwertmann*, 1974].

Iron flakes have been observed microscopically (Figure 5-9a) and in some κ-T curves (Figure 5-10c). Especially in the cuttings from the longest stored GPK1, these iron flakes are strongly oxidized to a mixture of different Fe-oxides. Due to the lower content of fresh iron in GPK1 cuttings, the GPK1 sample portion separated for κ-T measurements might be free of original iron flakes and just contain the oxidation products. Therefore, GPK1 magnetic susceptibility decreases to paramagnetic values above 600 °C, while still showing the peak below 300 °C. The contamination of the cuttings by iron flakes can significantly disturb the correlation between magnetic susceptibility and SCCL. For example, GPK1-C40 (3485 m, see Figure 5-5b) from the altered granite shows a higher magnetic susceptibility than we might expect according to its alteration degree (Fe-bearing carbonates, high amount of hematite, few magnetite). Therefore, the iron contamination must be eliminated before magnetic susceptibility measurements, which was not done in this study. Our study has shown that high χ in combination with low alteration index (AI < 1) is typical for the porphyritic granite and low χ in combination with negative alteration index (AI < 0) is typical for the two-mica granite. Low magnetic susceptibility in combination with strongly irreversible κ-T curves (AI > 1) and the formation of magnetite above 400 °C clearly indicates alteration stage II, which has also produced the highest amount of clay minerals. There are several reasons for high magnetic susceptibility, which we identified by microscopic investigations. High magnetic susceptibility is either related to a high amount of fresh magnetite in unaltered rock or due to secondary formation of magnetite in extremely altered samples. Furthermore, high χ can be caused by contaminations with iron debris from the drilling tools. Low χ is a result of magnetite oxidation in the course of hydrothermal alteration, but it can also be attributed to a primary low magnetite proportion in cutting material. The latter effect explains why also fresh, unaltered granite have low χ (Figure 5-6).

5.7.3 CALIBRATION OF SCCLS

Magnetic susceptibility measurements from the EPS1 core and clay concentration calculated from borehole measurements (SCCL) show a strong correlation (Figure 5-2) suggesting that magnetic susceptibility can be used in the magnetite-bearing Soultz granite as an independent alteration indicator. One of the goals of this study was to investigate the applicability of magnetic susceptibility measurements on cuttings as a calibration tool for the SCCL logs of the deep wells GPK1-4. We found magnetite as the primary magnetic mineral in all samples independent of their facies. The degree of magnetite oxidation to hematite indicates rock alteration and thus the presence of clay minerals. In several depth intervals, SCCL and χ were inversely correlated, but we could identify several difficulties. In general we found a reasonable correlation between the different SCCL groups and magnetic susceptibility of cuttings (Figure 5-6), although there is a large scattering of magnetic susceptibility values, especially in the fresh granite. The reason for this large scattering is probably a mixture of rock chips from certain depth intervals and the inhomogeneous distribution of magnetite within the granite. The larger the sampling interval, the more different granite types (porphyritic vs. two-mica granite and fresh vs. altered granite) can be mixed and the resolution and quality of χ measurements is hampered. Petrographic changes smaller than few meters thickness cannot be seen. Some small rock pieces might also get lost during their vertical transport uphole and clay minerals may be dissolved. Furthermore, there can be enrichment in flaky minerals like biotite and muscovite. Due to their shape, they float on the mud, as it has for example been observed in GPK4 [*Dezayes et al.*, 2005b], where biotite was enriched. Washing of the cuttings of GPK3 and GPK4 could also have affected the mineralogical content by dissolving small particles. In terms of calibration of the SCCL we can state that it is not straightforward postulating high clay content for low χ samples and no clay in high χ samples respectively, but the analysis showed that high magnetic susceptibility is only systematically measured in fresh samples. It is possible to calibrate the SCCL at least for intervals, where no clay is expected. For the remaining intervals, susceptibility of cuttings can be used as an auxiliary means to calibrate the SCCL log.

5.8 CONCLUSION

In this study, we introduced a new method to identify altered and clay-rich zones within a magnetite-bearing granitic reservoir. For the first time, synthetic clay content logs (SCCL) have been created from borehole logs by a neural network analysis indicating the alteration along the deep wells in Soultz-sous-Forêts. These logs can be interpreted on the basis of magnetic mineralogical investigations of cuttings, describing the mineral transformations resulting from hydrothermal alteration in the deeper part

of the granitic reservoir. Magnetic susceptibility measurements on cuttings allow a calibration of SCCL logs. By comparing EPS1 core and GPK1-4 cuttings magnetic susceptibility data with the calculated SCCL, we were able to define intervals with fresh and altered granite albeit with different success. This study, however, revealed that petrographic investigations in combination with κ-T curves on cuttings material are powerful tools to decipher different granite types and different degrees of alteration. The degree of alteration is reflected by χ, which is lower for highly altered samples. Low χ can also be observed in fresh granite types with a primary low magnetite proportion, but can be discriminated by magnetic mineralogical investigations. For a better resolution of the data and for calibration measurements, we suggest a sampling interval for the cuttings of ideally 1 m. Furthermore, iron contaminations from the drill bit should be eliminated prior to magnetic mineralogical investigations in order to receive better results.

Being so far merely a by-product of drilling and only used for creating lithology logs and chemical analysis, cuttings should be paid more attention for reservoir characterization, as they provide significant information. Magnetic susceptibility of the cuttings is fast and easily measured. In order to be able to correctly interpret the measuring results, petrographic investigations like transmitted and reflected light microscopy of thin sections, REM, EDX and κ-T measurements are necessary. With these methods, the magnetic mineral assemblage can be identified and the alteration processes can be reconstructed.

Based on the results of this study, further investigations on fracture mechanics and hydraulics related to the appearance of clay inside fractures are made possible. The effect of clay inside fractures on induced seismicity is one of the major issues to be investigated. Furthermore, the influence of clay on fracture permeability needs to be further analysed and will be the topic of future work.

ACKNOWLEDGEMENTS

This research was conducted within the portfolio topic GEOENERGIE of the Helmholtz Association of German Research Centers and was funded by Energie Baden-Wuerttemberg (EnBW), Germany. The authors are grateful to GEIE Exploitation minière de la chaleur for providing the Soultz borehole data and to the French geological survey (BRGM) in Orléans, who provided us the cutting material, especially to Chrystel Dezayes, who made the effort to track the desired intervals out. Thin sections have been prepared by Stephan Unrein and Kristian Nikoloski. The work on the REM and EDX was made possible by the friendly support of Volker Zibat from the laboratory of electron microscopy (LEM) at KIT in Karlsruhe. Finally, we are grateful to the reviewers who contributed to an improvement of the quality of this manuscript.

6 THE SIGNIFICANCE OF HYDROTHERMAL ALTERATION ZONES FOR THE MECHANICAL BEHAVIOR OF A GEOTHERMAL RESERVOIR

This study has been published in *Characterization of Deep Geothermal Systems*, a special issue in *Geothermal Energy.*

MELLER, C. AND KOHL, T. (2014). The significance of hydrothermal alteration zones for the mechanical behavior of a geothermal reservoir. Geothermal Energy **2** (12). doi: 10.1186/s40517-014-0012-2

ABSTRACT

The occurrence of hydrothermally altered zones is a commonly observed phenomenon in brittle rock. The dissolution and transformation of primary minerals and the precipitation of secondary minerals affect rocks in terms of mechanics, stress conditions, and induced seismicity.

The present study investigates commonly observed phenomena of hydrothermal alteration and observations at the geothermal site of Soultz-sous-Forêts, which are related to the occurrence of hydrothermal alteration. Geomechanical observations at Soultz are interpreted on the basis of synthetic clay content logs, which are created from borehole logging data, and which identify clay in hydrothermally altered zones.

It is shown that hydrothermal alteration results in a reduction of the frictional strength of the reservoir rock. Weak zones can act as stress decoupling horizons, which locally perturb the stress field and affect the evolution of the microseismic cloud. For the first time it is shown on a reservoir scale that large magnitude seismic events are restricted to unaltered granites, whereas in clay zones only small magnitudes are observed. It is demonstrated that clay rich zones foster the occurrence of aseismic movements on fractures.

Secondary mineral precipitation during hydrothermal alteration has a great effect on the geomechanical properties of a geothermal reservoir. The identification of such zones is a first step towards understanding the relation between alteration and mechanical processes inside a reservoir and can help reducing induced seismicity during hydraulic stimulation of a reservoir.

6.1 INTRODUCTION

The importance of clay zones for the geomechanical structure and the earthquake mechanics in brittle rock became an important issue in the framework of mitigation studies of natural and man-made disasters [*Holmes et al.*, 2013]. A strong focus was given to hydrothermal alteration in crystalline rock and its effect on mechanical friction. Recent studies on the San Andreas Fault revealed the significant impact of clay inside faults and fractures on their mechanical and hydraulic properties. Faults and fractures are target zones for enhanced geothermal systems (EGS), as they provide pathways for geothermal fluids. In terms of mitigation of induced seismicity, while increasing the permeability of the geothermal reservoir, detailed understanding of hydraulic and mechanical processes of fractured rock is key for the success of an EGS project.

6.1.1 THE SIGNIFICANCE OF CLAY FOR GEOTHERMAL PROJECTS

The development of enhanced geothermal systems (EGS) in low-enthalpy regions like the Upper Rhine Graben in central Europe involves the application of hydraulic stimulation for permeability enhancement in the geothermal reservoir. Mostly located near residential areas, there is a claim for safety and controllability of the geothermal technology from the public. In the past, people were concerned by the occurrence of small perceptible earthquakes, caused by stimulation activities or during operation of geothermal power plants like the magnitude M_L=3.4 earthquake in Basel in 2006 [e.g. *Häring et al.*, 2008] the M_L=2.9, M_L=2.5 and M_L=2.3 in Soultz-sous-Forêts in 2003, 2000 and 2004 [*Dorbath et al.*, 2009] or the M_L=2.4 and M_L=2.7 earthquakes near Landau in 2009 [*Groos et al.*, 2013]. The injection of fluid into the underground changes the effective stress, thus inducing slips on fractures and faults associated with seismic events in brittle rock. In order to predict or even control the seismic behavior of a geothermal reservoir, the geomechanical structures and the associated processes must be known.

In fresh and homogeneous rock, the relation between stress and mechanical failure is commonly described by the Mohr-Coulomb criterion [*Scholz*, 2010] with flow through fractures to be characterized as sub-laminar by Darcy flow [*Sausse*, 2002]. In geothermal reservoirs however, the percolation by geothermal brine promotes the formation of hydrothermally altered zones around fluid pathways. The dissolution of primary rock-forming minerals and the precipitation of secondary minerals like quartz, clay or carbonates change the in-situ conditions with respect to mechanical strength of the rock. In such zones, simple models might no longer apply and the reservoir behavior is difficult to assess. Evidence, that simple rock mechanical models no longer

account during and especially after the shut-in of hydraulic stimulation, have been only recently highlighted by Schoenball et al. [2014], who demonstrated a change in the stress regime during stimulation.

Several studies demonstrate the relation between geomechanics, earthquake characteristics and the weakness of rocks on a crustal and regional scale. For geothermal projects, however, the geomechanical properties of a reservoir are to be known on a very local scale in the order of several meters. The size of hydrothermal alteration zones can range from millimeters to several kilometers. In order to characterize a geothermal reservoir and to assess its geomechanics, it is important to understand the significance of such alteration zones. Therefore, it is necessary to know and to understand, if and how large-scale geomechanical rules and observations can be transferred to the reservoir scale.

The present paper conducts an investigation on the significance of hydrothermal alteration in the granite of the geothermal site in Soultz-sous-Forêts (France) and the change of its mechanical parameters. The basis of the analyses is synthetic clay logs, which are created from spectral gamma ray logs using a technique introduced by Meller et al. [2014b]. These logs are indicative of the occurrence of clay bearing fractures along the boreholes. The newly derived results are investigated under the light of the existing geomechanical interpretation, which is summarized in the following chapter.

6.1.2 CURRENT STATE OF RESEARCH ON THE ROLE OF CLAY IN FAULT ZONES

Evidence for the role of clay as zones of weakness or some kind of lubricant on faults promoting aseismic movements has been described by Schleicher et al. [2006b], Dolan et al [1995], and Wu et al [1975]. Clay minerals are a characteristic of creeping faults with rates of up to 30 mm/a assumed for the San Andreas Fault [*Chang et al.*, 2013]. Studies on the slipping behavior of the San Andreas Fault however suggest that it is not merely creeping but it rather consists of creeping patches, which build up stress on patches with high friction. If the stress is large enough, these high friction patches rupture and cause seismic events [e.g. *Chang et al.*, 2013]. This theory is supported by the work of Amelung and King [1997], who observed a continuous earthquake activity on creeping faults. A major result of their study is that creep and earthquakes are not two separated phenomena, but two processes, which go hand in hand. This has been reported earlier for numerous faults and continental margins [e.g. *Brune*, 1968; *Mulargia et al.*, 2004; *Voisin et al.*, 2004].

Recent studies at the geothermal site in Soultz-sous-Forêts revealed similar mechanisms during shear movements on faults. Bourouis and Bernard [2007] observed in data of seismicity induced during GPK1 stimulation repeated shear movements on fault asperities surrounded by creeping zones. Schmittbuhl et al. [2014] observed in laboratory experiments a close relationship between seismic and aseismic movements on faults and conclude that aseismic processes can drive seismicity, almost independent from fluid pressure. The triggering of seismic events by creep movements is an important issue for EGS systems and needs to be considered for the mitigation of large seismic events.

Clay minerals, which are a main product of hydrothermal alteration [e.g. *Meunier*, 2005; *Velde*, 1995], sometimes have very low friction coefficients of ~0.3 [e.g. *Morrow et al.*, 1992 and references herein, and c.f. Figure 6-1b]. The frictional properties of clay minerals however, strongly depend on their structure and water content. Therefore, it is not easy to estimate the frictional properties of clay filled faults [*Moore and Lockner*, 2007]. Many studies have been conducted on the relationship between the nature of fracture fillings and fault mechanics. Zoback et al. [2012] and Kohli and Zoback [2013] investigated the relationship between clay content and mechanical friction of shale gas reservoir samples under wet conditions. They observed a linear decrease of the friction coefficient with increasing clay content (Figure 6-1a) from 0.8 with 10 wt-% clay to 0.4 at ~50 wt-% clay. Similar results have been obtained by Tembe et al. [2010] for artificial clay gouge samples of quartz and illite and for natural soil samples tested by Akayuli et al. [2013]. The friction coefficients they measured for different clays vary and are much lower than those of other minerals like quartz or feldspars (Figure 6-1b).

The rupture behavior of a fault from the Dietrich-Ruina constitutive model [*Dieterich*, 1978; *Ruina*, 1983] describes the frictional evolution of a fault for different sliding velocities with the material parameter $(a-b)$ representing the difference in steady-state friction. It indicates stable sliding of fault surfaces during slip, if $(a-b) > 0$, or unstable sliding, if $(a-b) < 0$. The synonyms for stable and unstable sliding are velocity strengthening and velocity weakening behavior, respectively. The effect of clay on the rupture behavior of faults has been studied by many laboratory experiments. Ikari et al. [2011] found experimental evidence for a relationship between the weakness of rocks and their frictional stability: rock samples with a low friction coefficient show velocity strengthening behavior, whereas samples with high friction coefficients show velocity weakening behavior (Figure 6-1). This indicates the occurrence of brittle failure only on rocks with high friction coefficients. Zoback et al. [2012] observed experimentally on shale gas samples that faults with clay contents higher than 30 % slide stable (i.e. $(a-b) > 0$), whereas faults with a lower clay content slip unstable (i.e. $(a-b) < 0$, Figure 6-1c). They reasoned that such clay-rich faults slide aseismically, whereas the faults with lower clay contents produce microseismic events.

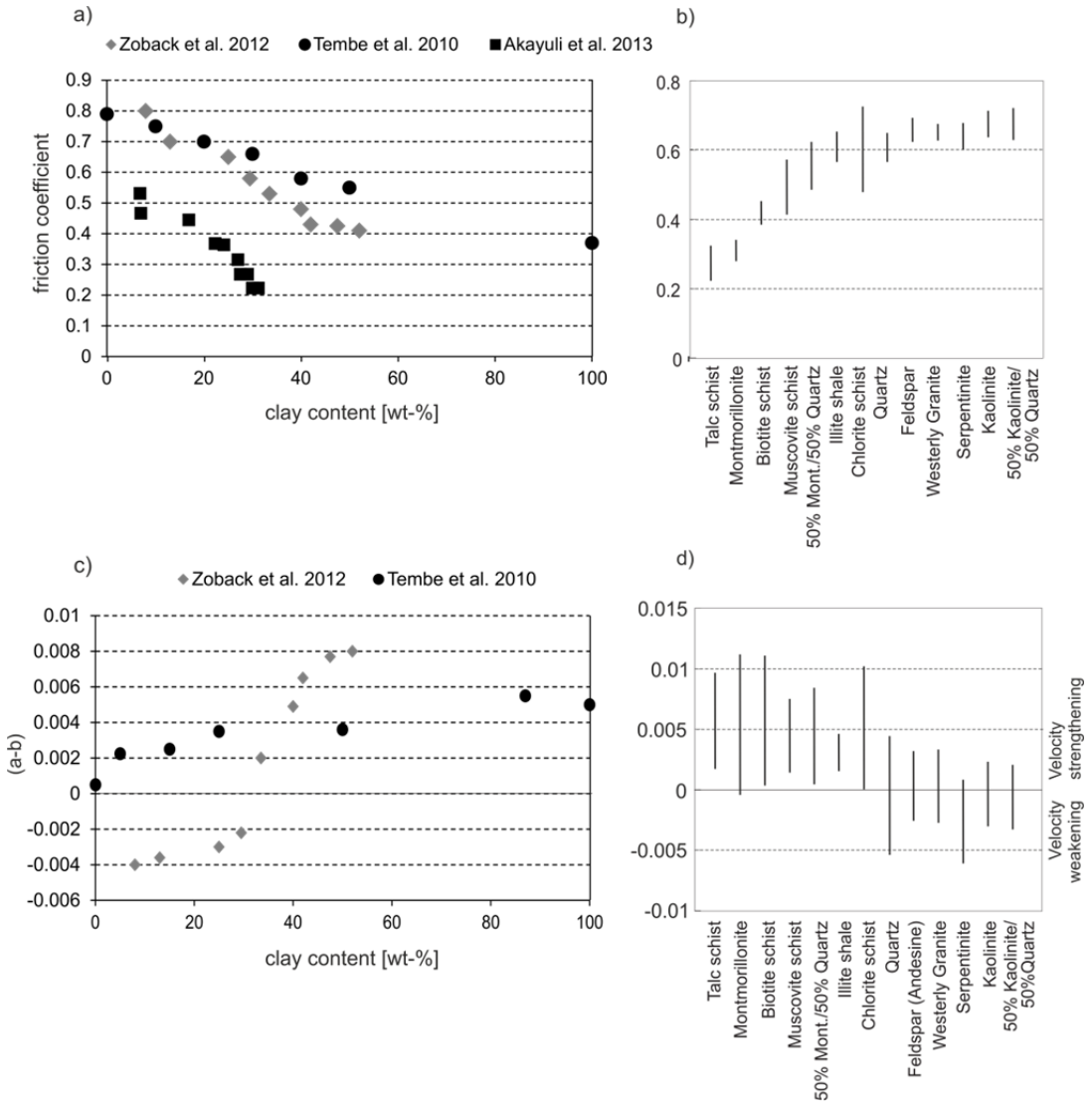

Figure 6-1: Friction coefficient and a-b for different rock types. a) Friction coefficient for rocks and a soil with different clay contents. Increasing clay content reduces the frictional strength. b) Range of measured friction coefficients for different rock types (data from Ikari et al. [2011]). c) (a-b) parameter for rocks and soil with different clay contents and d) (a-b) for different rock types. With increasing clay content the friction coefficient is reduced and (a-b) increases. High clay content and low friction results in velocity strengthening behavior. Rock types with low friction show velocity strengthening behavior. Experimental data from Zoback et al. [2012] is derived from measurements on shale and Tembe et al. [2010] measured artificial quartz-illite samples. Akayuli et al. [2013] did experimental studies on soil.

The dataset of Tembe et al. [2010] illustrates a dependence of *(a-b)* of illite-quartz samples on the illite content. For these samples, no velocity weakening behavior is observed. The reason for this is that quartz can behave both, velocity strengthening, and velocity weakening and under the experimental conditions it was velocity strengthening *(a-b)* > 0 (Figure 6-1c), but nevertheless the effect of the clay proportion of the samples on *(a-b)* is significant.

As the frictional properties of rocks determine their slipping behavior, a correlation between the weakness of rocks and the occurrence of large and small earthquakes is expected. The so-called *b*-value, which is derived from the Gutenberg-Richter law [*Gutenberg and Richter*, 1954], describes the proportion of small relative to large earthquakes. A *b*-value of 1 represents a logarithmic relationship between the magnitude of events and their frequency, whereas *b*-values > 1 reflect an increased number of small earthquakes. High *b*-values are expected in areas, where no large differential stress can build up. Schorlemmer et al. [2005] compared the results of numerous earthquakes from different settings and of laboratory data. They found that the *b*-value differs systematically with the faulting regimes. The highest *b*-values are found in normal faulting regimes (up to 1.2), whereas the lowest *b*-values occur in thrust events (as small as 0.6), and strike-slip events are in between. Based on the stress prevailing in the respective regimes, Schorlemmer et al. concluded that the *b*-value inversely correlates with differential stress levels. This was also confirmed by laboratory experiments performed by Amitrano [2003], who observed a decreasing *b*-value with increasing differential stress. Creeping fault sections show very high *b*-values around 1.3 [*Schorlemmer and Wiemer*, 2005]. Based on these results, the occurrence of small events and aseismic movements in strongly altered and fractured areas is expected, rather than large earthquakes. This assumption has also been proposed by Heinicke et al. [2009] who investigated the correlation between hydrothermal alteration and the occurrence of earthquake swarms. They observed in the Vogtland Region of northwestern Bohemia that in addition to increased pore pressure and shear stress the mechanical weakening of rocks and the dissolution of fracture walls plays an important role for the evolution of earthquake swarms. Interestingly, the maximum magnitude of such earthquake swarms is limited to 5 [*Heinicke et al.*, 2009], which supports the theory of only small earthquakes occurring in regions with rocks of low friction coefficients. When analyzing b-values, one has to consider that this value is affected by numerous parameters, not least by the way it is computed. Besides the strength of the rock, the main affecting parameters are the stress field, the focal mechanism of the earthquakes and the presence of large geologic structures [*Scholz*, 2010 and references herein]. In geothermal reservoirs, large variations of *b*-values in time and space have for example been observed by Bachmann et al. [2012]. They calculated the *b*-value for the time period during injection and after injection. The *b*-values varied from 1.58 during injection to 1.15 after injection, which represents a larger proportion of small earthquakes during injection.

Dorbath et al. [2009] calculated a *b*-value of >1.2 for the stimulations of the well GPK2 at Soultz, whereas for the well GPK3, which is maximum 500 m away from GPK2 it was determined to 0.9. They related this behavior to the presence of large fault zones in the vicinity of the well, which dominate their seismic evolution.

6.2 THE SOULTZ GEOTHERMAL SITE

The European geothermal project of Soultz-sous-Forêts (France) targets a geothermal anomaly at the western border of the Upper Rhine Graben. Five wells have been drilled to a maximum depth of 5 km. Three of these wells are currently used for operation with two wells as injectors (GPK3, GPK4) and one producing well (GPK2) [Genter, pers. comm]. The upper geothermal reservoir is hosted by a porphyritic Hercynian monzogranite (Figure 6-2a), overlain by 1.4 km of Mesozoic sediments. The lower reservoir lies in fine-grained two-mica granite, which can be encountered at depths greater than 4.6 km. The pluton has been affected by the Upper Rhine Graben tectonics, which caused the formation of large sets of faults and fracture zones. These faults and fractures are the main pathways for circulating fluids and are thus responsible for the permeability of the rock [*Genter and Traineau*, 1992]. Paleo-circulation of meteoric fluids from the Graben shoulders led to pronounced alteration of the Soultz granite. The first pervasive alteration affected the whole granitic matrix (Figure 6-2b), but had no effect on the structural properties of the granite. It involved the formation of mainly chlorite and hematite. A subsequent vein alteration event significantly changed the granite structure (Figure 6-2c). During this alteration event, primary minerals were dissolved and secondary minerals precipitated [*Schleicher*, 2005]. Alteration halos developed enfolding the zones around fractures affected by hydrothermal alteration. These halos can be several tens of meters thick and are characterized by the transformation of mainly silicates and the precipitation of secondary clay minerals, quartz, carbonates, sulfates and iron oxides [*Genter and Traineau*, 1996]. The dominating clay minerals of the vein alteration are several generations of illites and smectites, and minor tosudite and chlorite [e.g. *Bartier et al.*, 2008]

The sealing of fractures by secondary minerals and the transformation of silicates into clay minerals affected the hydraulic and mechanical properties of the rock [*Charléty et al.*, 2007; *Valley and Evans*, 2003], whereas the details of such processes are still subject to extensive research. Bartier et al. [2008] highlighted for example the importance of clay mineralogy for the permeability of the Soultz granite, which is reduced by illite precipitation, but enhanced by tosudite precipitation. Ledésert et al. [2010] highlighted the complexity of processed linked to porosity/permeability formation and decrease by the dissolution and transformation of primary minerals and the formation of new minerals. The type and structure of clay minerals is not only

important for the evolution of porosity and permeability, but also for the shearing properties of a fault filled with clays. The variation of hydro-mechanical properties of the rock with different alteration types and grades makes it important to first detect alteration zones and, second, to understand their significance for the performance of a reservoir.

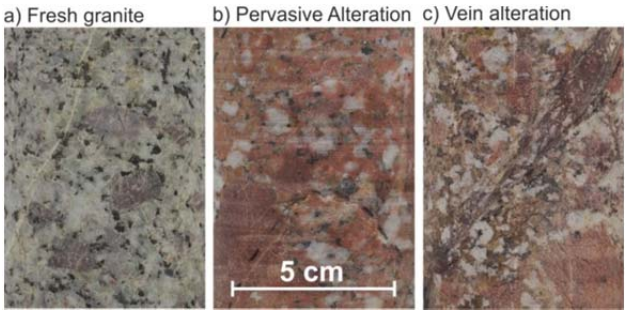

Figure 6-2: Core pictures of different facies of the Soultz granite. a) Fresh granite without evidence of hydrothermal alteration. b) Pervasive alteration with mainly formation of hematite and no structural influence. c) Vein alteration with dissolution of silicates and precipitation of clay minerals.

6.3 METHODS

The basis for the rock mechanical studies are neural network derived SCCL logs, which present the clay content along the borehole in a semi-quantitative way with five groups of increasing clay content. In sedimentary rocks, clay minerals can be easily identified from peaks in spectral gamma ray (SGR) logs. In crystalline rock in contrast, apart from clays numerous other minerals contain radioactive isotopes, which makes it difficult to identify clay minerals on SGR logs. Therefore, a neural network is used, which makes it possible to identify different signal patterns on logging data and to localize the clay-bearing zones. The resolution of the resulting SCCL logs is on the scale of decimeters.

The neural network for the creation of the synthetic clay content logs uses a self-organizing map working with a Kohonen algorithm [*Kohonen*, 1984]. The principle of this procedure is the grouping and indexing of patterns according to their spatial distance from each other. Each combination of n logs represents a vector in n dimensions. The location of these vectors in n dimensions determines their assignment to the nodes of a two-dimensional self-organizing map. Thus, their dimension is reduced, which makes it easier to classify them. The number of classes can be defined according to the desired resolution.

The network is trained using supervised learning, which means the grouping and classification of the nodes based on reference data. These reference data are used to teach the neural network how different parameters are correlated. For this study, the reference data consists of spectral gamma ray logs and a fracture density log. A log representing the density of clay-filled fractures was derived from core investigations of the EPS1 reference well and served as a template for the classification of the nodes. For the deep wells GPK1-GPK4, the fracture density log could be computed on the basis of fractures identified on borehole image logs. The resulting SCCLs (Figure 6-3) semi-quantitatively represent the density of clay-filled fractures along the boreholes with five groups. The major flow paths through the granite are marked by dashed lines. Group 1 represents the group with the lowest clay content and group 5 represents the highest clay content. The comparison with reference data has shown that only ~10 % of the logs deviate more than 1 SCCL group from real data and the vertical resolution of the logs is between 10 and 50 cm depending on the resolution of the SGR logs, from which they are derived.

The SCCL logs allow discriminating between zones of high and low clay contents. Whereas the upper parts of all wells are characterized by high SCCL values, representing the paleo-alteration surface, the lower parts are very different for the five wells. Intervals with high SCCL are mostly found around fractures, which have been identified as permeable on flow logs, but hydrothermal alteration also occurs away from such fractures. However, not all permeable fractures are located in altered zones. This might be due to the fact that extreme alteration leads to a clogging of fractures with clay minerals, thus reducing its permeability [*Sausse*, 2002]. The actually flowing fractures might not have been permeable in the past, which prevented the surrounding rock from being hydrothermally altered. Increased clay content is seen at the bottom of the wells below 4600 m at the transition between the porphyritic to two-mica granite. For details of this neural network method, the SCCL logs and the calibration of the logs by magnetic mineralogical investigations, refer to Meller et al. [2014b] and Meller et al. [2014a].

For the deep wells in Soultz, no core material is available. Therefore, petrophysical and geologic parameters can only be derived from borehole measurements and seismicity catalogs. This study is mainly based on breakout and fracture analyses conducted on borehole image logs, and on a catalogue of seismic events recorded during hydraulic stimulation. Borehole breakouts are enlargements and elongations of a borehole in a preferential direction and are formed by spalling of fragments of the wellbore during drilling. They generally form parallel to the minimum horizontal stress and their formation is facilitated in weak wall rocks [*Babcock*, 1978]. Their analysis can therefore provide information about the orientation of the stress field and on the mechanical properties of the penetrated rock. Seismic events induced during stimulation are an indication of structures in the geothermal reservoir. Their analysis provides indications about the stress state, fracture orientation, rock mechanics and fluid pathways.

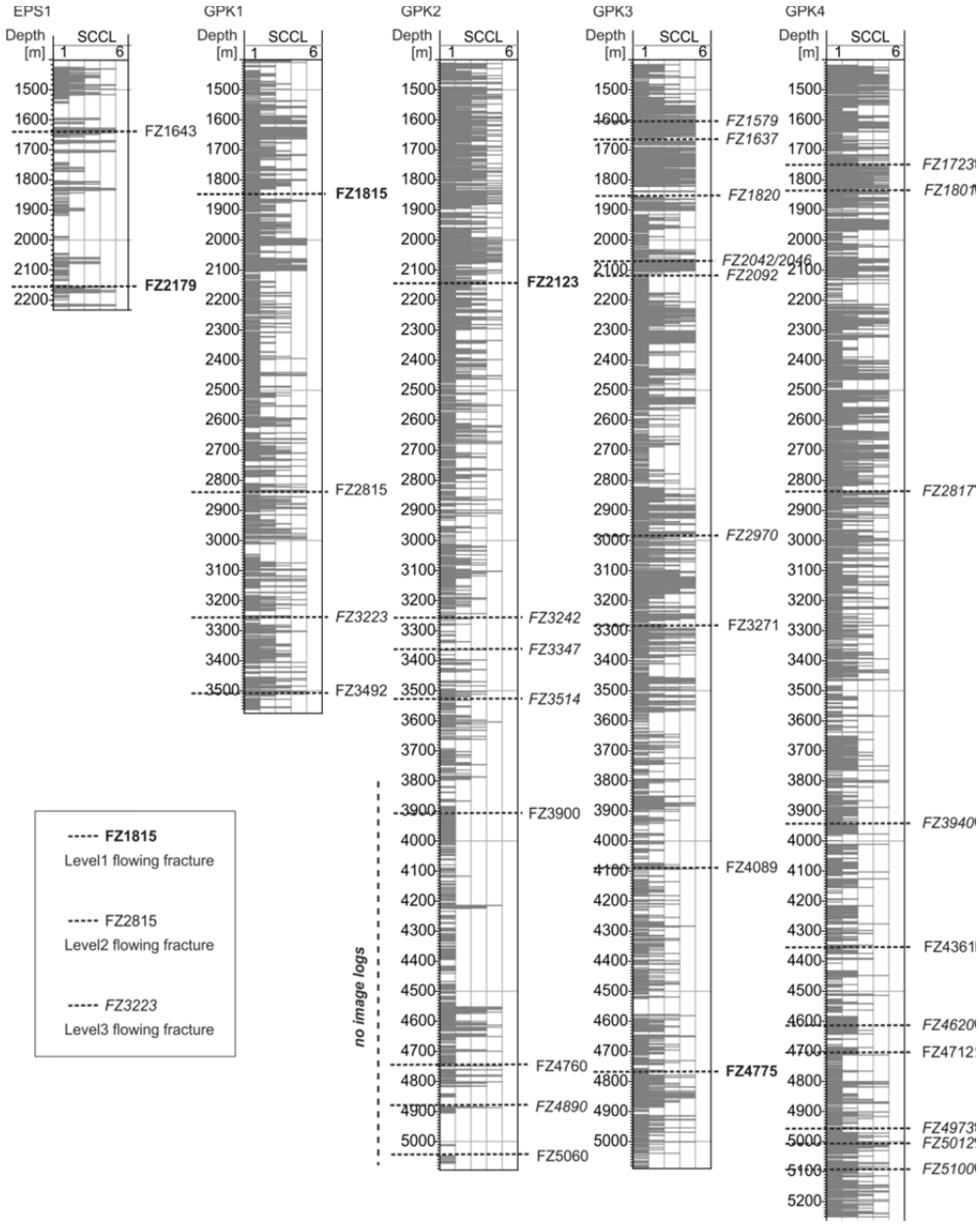

Figure 6-3: SCCL for the wells GPK1-GPK4. The SCCL is created on spectral gamma ray and the corrected fracture density log. FZXXXX denotes fracture zones after their depth of occurrence. Level1 flowing fractures: Major fracture zones with significant mud losses during stimulation, primary permeable. Level2 flowing fractures: >20 % water losses during stimulation. Level3 flowing fracture: small fracture zones with <20 % water loss (classification after Dezayes et al [2010b]). Higher SCCL indicates higher clay contents with SCCL=1 representing no clay and SCCL=5 the maximum density of clay-filled fractures.

6.4 RESULTS AND DISCUSSION

6.4.1 IMPACTS OF HYDROTHERMAL ALTERATION ON ROCK MECHANICS

Due to their preferential formation in weak rocks, a cumulative occurrence of breakouts in altered zones in the Soultz granite could be indicative of the weakness of alteration zones. This theory was investigated on the basis of breakouts, identified by Sahara et al. [2014]. They analyzed breakouts in the deeper part of the well GPK4. On Figure 6-6, a total of 2440 breakouts from Sahara et al. [2014] together with the SCCL for this depth interval is illustrated. A correlation between clay content and the appearance and size of breakouts is obvious. Whereas the density of breakouts is high in clay rich intervals, depth sections without clay are characterized by an absence of breakouts, as for example at 4180 m, 4480-4590 m and 4730-4800 m (BA in Figure 6-5). Obviously, the occurrence of breakouts is strongly related to the presence of hydrothermally altered zones. This suggests that hydrothermal alteration weakens the rock and thus promotes the formation of breakouts. Upon the transition from the porphyritic granite to the two-mica granite at around 4800 m, the breakout density clearly increases (2M in Figure 6-5). The cumulated occurrence of breakouts at this transition might originate from the mechanical contrast between the two granites. Such mechanical contrast occurs also at the transition between fresh granite and strongly altered granite.

The correlation of the clay zones with the occurrence of breakouts demonstrates their geomechanical significance. However, it is in contrast to present studies, which seem to identify rather high friction coefficients for the Soultz granite. By applying the Mohr-Coulomb failure criterion using effective stresses on the fractures, Cornet et al. [2007] obtained a minimum friction coefficient of 0.81. Evans et al [2005a] found that fractures in highly altered zones are surprisingly strong despite the presence of illite and ascribed this behavior to their internal architecture of intact rock bridges and jogs between weak zones. According to Byerlee [1978], rock samples with precut fault surfaces have a uniform friction coefficient of 0.85 and no cohesion at normal stress below 300 MPa, independent from the rock type. However, Byerlee observed that fractures filled with clay minerals are an exception from his law and have much lower friction coefficients. A gradual decrease in frictional strength with the addition of clay has also been observed in triaxial measurements of Berea sandstone under high temperature and high pressure conditions. Here, a sharp drop of the friction coefficient occurred at clay contents ~50 % [*Takahashi et al.*, 2007]. In these experiments, clay minerals inside fractures were observed to weaken faults, but also to stabilize their sliding behavior.

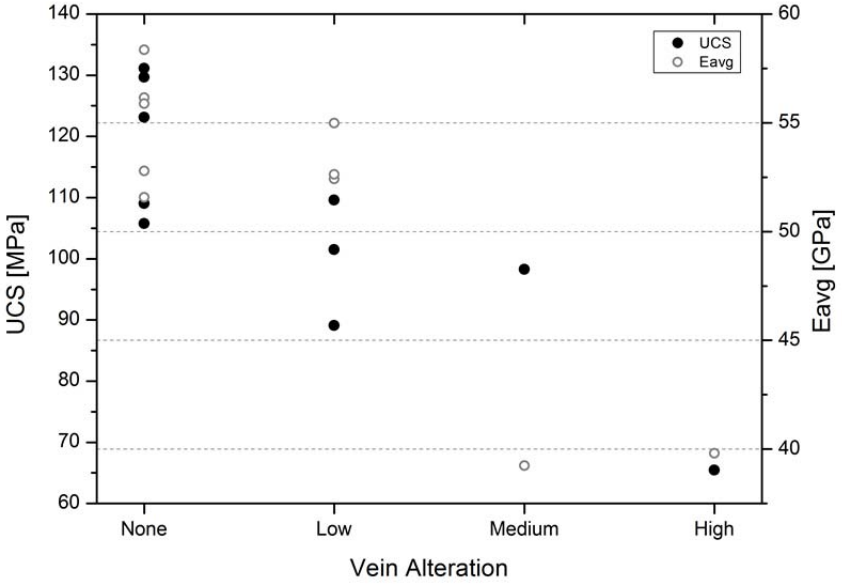

Figure 6-4: E-moduli and uniaxial compressive strength (UCS) of samples with different vein alteration grades. Data is taken from Valley and Evans [2003], who measured UCS and E-moduli for samples with different alteration grades. Alteration intensity is inversely correlated with E-modulus and UCS.

Crawford et al. [2008] performed experiments of quartz-kaolinite mixtures of different proportions and compared their strength. They also observed a reduction of frictional strength with an increasing clay fraction. Ikari et al. [2009] obtained low friction coefficients of fault gouges rich in phyllosilicates. These experimental results are in agreement with the breakout observations at Soultz, which indicate weakness of the hydrothermally altered zones, but which are in contrast to the high minimum friction coefficient of 0.81 determined by Cornet et al. [2007] for the whole granitic rock mass. It is therefore assumed that hydrothermal alteration causes a variation in the frictional properties of the Soultz granite on a meter-scale with higher frictional strength in unaltered rock and a lower frictional strength in altered rock.

Elastic properties of the Soultz granite have been experimentally studied by Valley and Evans [2003]. They selected samples of different alteration grades from the EPS1 core and measured the uniaxial compressive strength (UCS) of the core pieces. Furthermore they measured the S- and P-wave velocities of the samples in order to determine their E-moduli. They found an inverse correlation between alteration grade and UCS respectively the E-modulus of the samples (Figure 6-4). From the results of this study it is expected that the highly altered clay zones affect the frictional properties in Soultz and the friction coefficient is not uniform, but is lowered by hydrothermal alteration.

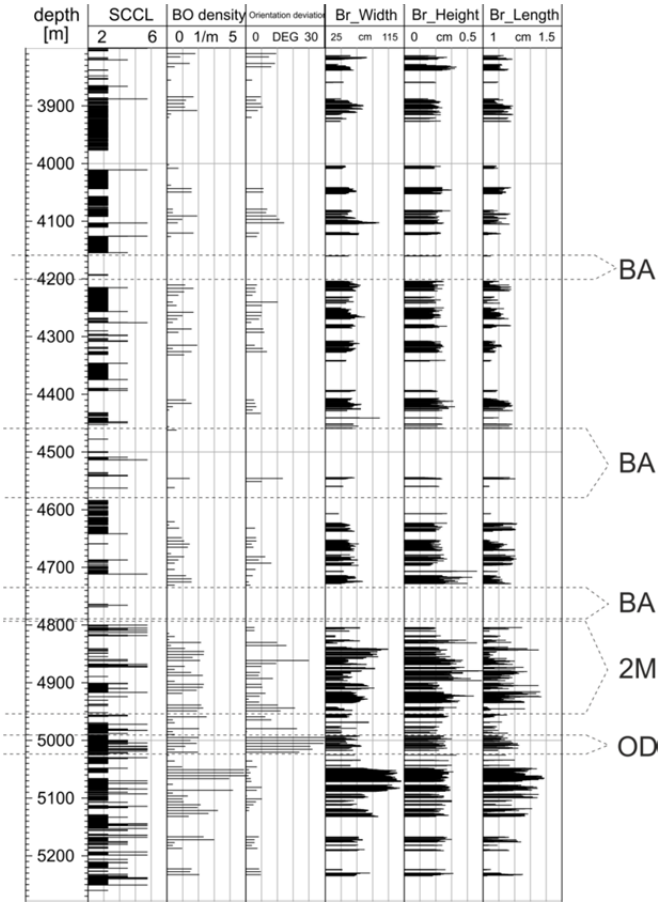

Figure 6-5: SCCL 2-5 of the well GPK4 compared to the breakout density, orientation deviation and breakout dimensions. There is a clear correspondence between breakout appearance and size and the SCCL (breakout data from Sahara et al [2014]). Intervals without clay are characterized by an absence of breakouts (BA). On the transition between standard granite and 2 mica granite at around 4800 m the orientation of the breakout changes (2M). This might be attributed to the mechanical contrast between the two granitic rock masses. A clay rich interval around 5000 m depth coincides with a large orientation deviation of the breakouts (OD).

Recent researches showed that a characteristic of such weak zones is that they can fail at low stress levels, as it is for example observed on a large scale on the San Andreas Fault in a strike slip regime, whose slip direction deviates 70° from the maximum horizontal stress [e.g. *Boness and Zoback*, 2006], the Zuccale normal Fault on Elba [e.g. *Smith et al.*, 2007] or some normal faults at the eastern side of the Sea of Japan [e.g. *Faulkner et al.*, 2010; *Sibson*, 2009]. If such observations can be transferred to the reservoir scale, hydrothermally altered zones might fail at lower stress levels than the surrounding intact rock mass. This is especially important in terms of hydraulic stimulation, as weak faults could shear at much lower stimulation pressure than unaltered rock and influence the evolution of induced seismicity.

6.4.2 IMPACTS OF HYDROTHERMAL ALTERATION ON THE STRESS FIELD

Clay layers inside rock masses give rise to large contrasts of mechanical properties. In contrast to intact crystalline or sedimentary rock masses, weak clay-rich zones cannot establish large differential stress [*Zoback and Harjes*, 1997].

The stress field in Soultz has been thoroughly investigated by many scientists [*Cornet et al.*, 2007; *Rummel*, 1995, and references herein; *Valley and Evans*, 2010]. This resulted in detailed knowledge of the magnitude and orientation of the principal stress components with depth. Based on the analysis of wellbore failure and hydraulic data as well as microseismic data, a linear stress model has been established for the Soultz reservoir [*Cornet et al.*, 2007; *Valley and Evans*, 2007]:

S_v = -1.3+0.255z; S_H = 0.98 (-1.3+0.255z); S_h = -1.78+0.01409z; P_p = 0.9+0.0098z

with P_p the pore pressure and z the depth in m. The S_H orientation is approximately north-south and the vertical stress S_V is equivalent to the overburden. However, in inhomogeneous rock masses with changing mechanical properties, the magnitude and orientation of the stress field change at the transition between layers of different mechanical strength. The Soultz granite is very heterogeneous due to its porphyritic structure, its lithological variations, hydrothermally altered zones and the profound fracturing. Borehole breakouts generally form in the direction of the minimum horizontal stress and are therefore useful indicators of the orientation of S_h and S_H. An analysis of borehole breakouts can give evidence about local stress variations. The high resolution of the SCCL logs in the order of decimeters for the first time allows a detailed analysis of indications for stress field variations at Soultz on the basis of breakouts. In the following, the occurrence of breakouts and their orientation is interpreted on the basis of the SCCL logs.

Evidence for a change in the direction of the principal stresses can be found in breakout data from Sahara et al. [2014] in the well GPK4. The transition from porphyritic to two-mica granite at around 4800 m (2M in Figure 6-5) is not only characterized by an increased breakout density, but also by a deviation of the mean breakout orientation. As breakouts generally form in the direction of the minimum principal stress, an orientation deviation of the breakout could be an indicator for a rotation of S_h. Another excursion of the breakout orientation is observed at a depth of 5000 m (OD in Figure 6-5). This deviation coincides with a very clay rich interval. This clay rich interval might act as a small stress decoupling horizon, which rotates the principal stress. According to the data of Sahara et al., stress rotations in clay rich intervals can be as large as ±30° from the mean orientation. Deviations of breakout orientations in hydrothermally altered zones have also been observed by Valley [2007] in the wells GPK3 and GPK4. He observed major stress perturbations occur at depths of 2000 m and 4700 m. The SCCLs show that these stress perturbations coincide with the

occurrence of clay-rich intervals related to large flowing fracture zones (FZ2123, FZ4760, FZ4775, Figure 6-3), but it cannot be ruled out that they could also be caused by the presence of the fracture zones as it was for example observed by Valley [2007]. The stress variation at ~4700 m is probably caused by the contrast in the elastic moduli of the rock between the standard porphyritic granite to two-mica granite at this depth and increased clay content.

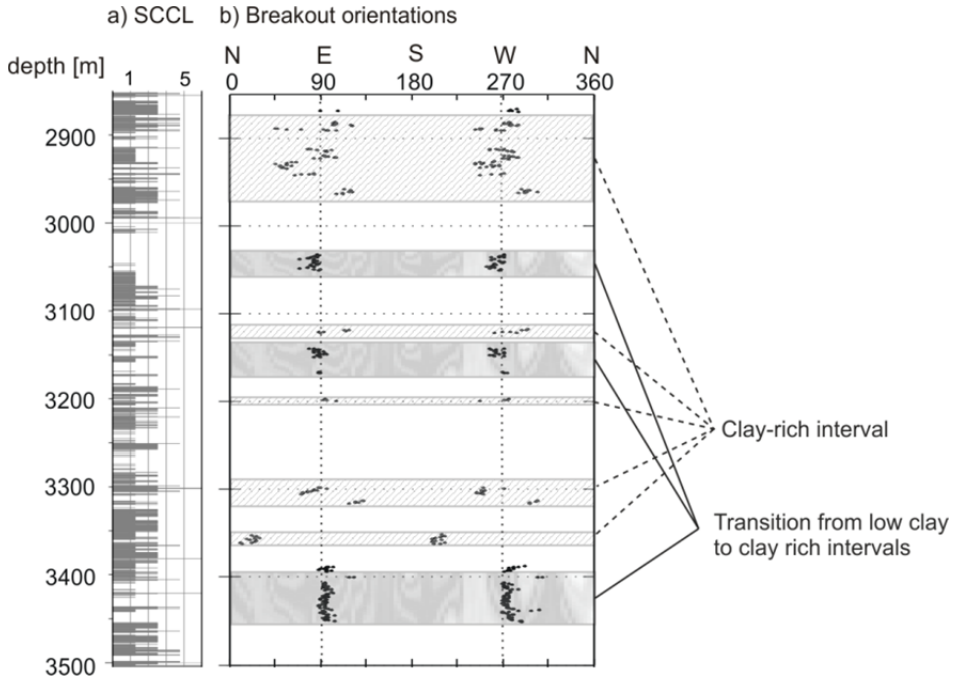

Figure 6-6: SCCL and breakouts for the well GPK1. A mean breakout orientation of 90°±19° was determined from 498 measurements (data from Valley and Evans [2000]). The occurrence of clay-rich intervals coincides with an accumulation of borehole breakouts. At the transition between fresh and altered granite, the breakout orientation rotates

Valley and Evans [2000] analyzing breakouts in the well GPK1 between 2840 m and 3510 m, found an increased breakout concentration at the top of this interval. This agrees with the occurrence of a clay rich interval in this section indicated by high SCCL (Figure 6-6). The mean S_H orientation determined from breakouts is 0°±19°, which is in agreement with the mean orientation of structures of the microseismic cloud. Excursions of the mean breakout orientation occur in the intervals 2890-2950 m, and 3300-3350 m, which are characterized by high SCCL values. The occurrence of breakouts in GPK1 between 2960 and 3500 m is not only restricted to high-clay zones, but high breakout-densities as for example at 3000-3050 m or at 3400-3450 m depth also occur, when a depth interval without or with very little clay is followed by a very clay-rich interval. Here, the contrast of elastic moduli of the two depth intervals might cause a cumulating appearance of breakouts.

This might also be represented in the different orientations of the microseismic cloud in the depth intervals 2700-2900 m, where it is oriented north-south, and 3200-3600 m, where its azimuth is 145-160° [*Cornet et al.*, 1997]. Cornet and his colleagues linked this orientation deviation to the higher pore pressure above 2900 m, but it could also be related to the presence of clay-rich zones. Such clay-rich zones could also lead to increased pore pressures [*Wu*, 1978].

Similar analyses have been conducted by Langenbruch and Shapiro [2014], who investigated stress states in boreholes from different regimes. Based on sonic logs, they created a model of the in situ elastic moduli to calculate the spatial distribution of in-situ stress within a rock mass. Their large spatial variations of the stress regime suggest that linear stress models are not sufficient for Coulomb failure within a rock mass. Economides et al. [1989] observed that within sedimentary formations the vertical gradient of the minimum horizontal principal stress does not vary linearly with depth. The authors found that elastic heterogeneity has a significant influence on stress magnitudes, which vary by up to more than ±20% of the externally applied stresses. Cornet and Roeckel [2012] observed this phenomenon in limestone layers of the Paris Basin and in the North German Basin. They saw that the local stress magnitudes are not linearly increasing with depth and they saw variations of ~15° in the stress directions. In contrast to Langenbruch and Shapiro [2014] and Economides et al. [1989], they assume that the stress magnitudes are controlled by the creeping characteristics of the various layers rather than by their elastic characteristics [*Cornet and Roeckel*, 2012].

The change of the local stress field in magnitude and orientation has previously been described for large fracture zones [e.g. *Brudy et al.*, 1997]. In the San Andreas Fault for example, a stress rotation of ~28° with respect to the stress field of the rigid crust has been measured [*Chéry et al.*, 2004] Cornet and Roeckel [2012] identified soft layers as decoupling layers introducing decoupling of stress fields in the layers above and below theses layers. This was also observed by Meixner et al. [2014], who documented a rotation of the maximum horizontal stress in different facies along the Bruchsal geothermal wells (c.f. Figure 7 in his article).

However, in those studies, stress field variations are only observed on large scales of several kilometers. The analysis of breakouts on the basis of SCCL logs provides indications that changes of the stress field both, in magnitude and orientation of the principal stress can also be induced by small scale soft alteration zones on the meter scale as observed in geothermal wells. Taking these observations into account, it is obvious that the estimation of mechanical properties on the basis of a linear stress field can only provide far field values, especially for zones, where the SCCL is high. So, in addition to the frictional parameters, the exact orientation of the stress field has to be constrained in hydrothermally altered zones in order to be able to assess their mechanical characteristics.

6.4.3 THE IMPACTS OF HYDROTHERMAL ALTERATION ON INDUCED SEISMICITY

At Soultz, 20 hydraulic and chemical stimulations have been performed and large catalogs of seismic events are available [*Genter et al.*, 2010]. During hydraulic stimulation, large amounts of water are injected into the geothermal reservoir in order to increase the pore pressure prevailing in the reservoir rock. If the pressure increase is large enough to overcome the frictional stability of fractures, shear movements are induced, which can be observed by the occurrence of microseismic events. A detailed summary of the background of hydraulic stimulation can for example be found in Economides et al. [1989] or Majer et al. [2007].

Parameters influencing the evolution of induced seismicity like the pressure of the fluid, the ambient stress field, the orientation of fractures, hydraulic properties, and the frictional characteristic of rock can be affected by hydrothermal alteration. Herein, the relation between hydrothermal alteration and induced seismicity at Soultz is investigated.

Except some new fractures, which are created during hydraulic stimulation at Soultz by hydrofracturing [*Cornet*, 2012], seismicity in the Soultz reservoir is mainly restricted to shear movements on existing geological structures, which can be observed during all stimulations performed on the Soultz wells [e.g. *Dorbath et al.*, 2009; *Evans et al.*, 2005b; *Fabriol et al.*, 1994]. However, it is not clear, why some structures are seismically more active than others. According to the Mohr-Coulomb failure criterion, the most important factor affecting the shearing behavior of a fracture or fault is its orientation relative to the ambient stress field. Favorably oriented fractures lie (sub)-parallel to the maximum principal stresses and can thus be easily sheared. The focal mechanisms at Soultz [cf. Figure 1 in *Schoenball et al.*, 2012] indicate that some fractures produce seismic events upon hydraulic stimulation unless they should be stable according to the Mohr-Coulomb failure criterion. A possible reason for that could be a very low shear strength of some fractures, which allows them to shear at large angles to the maximum stress. This gives further evidence, that the friction coefficient of fractures at Soultz is not homogeneous, but rather varies in a wide range.

Aseismic movements on fractures have been directly observed in Soultz by Cornet et al. [1997]. The SCCL of GPK1 indicates clay-rich intervals between 2800 and 3000 m, 3050 and 3100 m, 3180 and 3230 m, 3340 and 3410 m and 3450 and 3500 m (Figure 6-7). The stars in this figure mark the shear movements, which have been induced during stimulation of GPK1, and which have been identified on image logs. All shear zones lie close to flowing zones inside hydrothermally altered intervals, whereas most of the shear movements were aseismic (yellow stars).

The higher number of aseismic movements at shallower depths is most probably related to the higher density of (large) fractures. A comparison between the orientation of these fractures and the orientation of S_H (Figure 6-8) reveals that some of the creeping fractures strike at an angle of >30° to S_H. If the Mohr-Coulomb failure criterion accounts for these fractures, their friction coefficient must be very low that shear is induced under the present conditions.

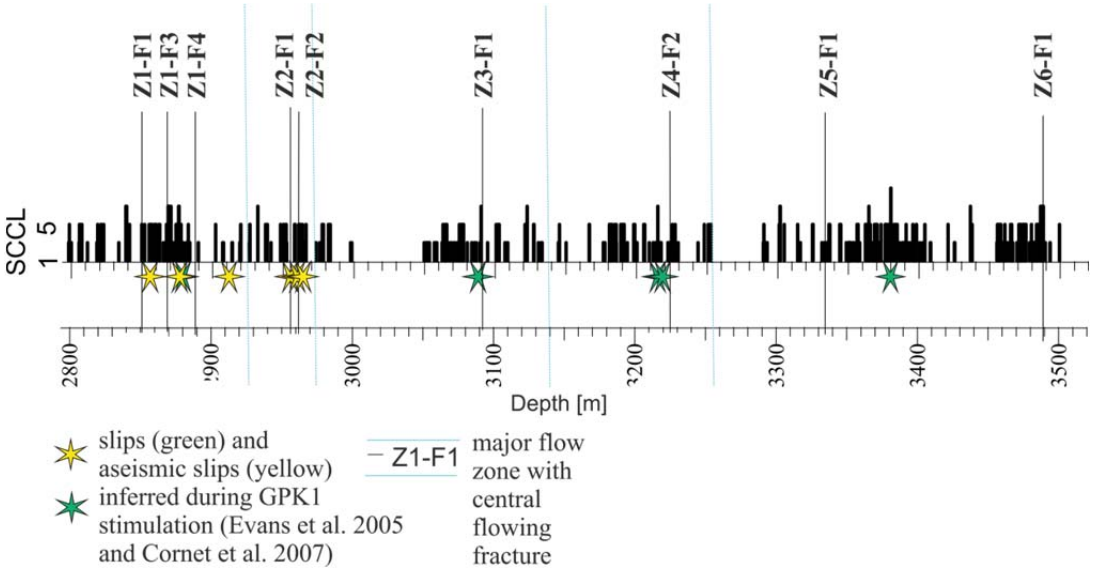

Figure 6-7: SCCL, major flow zones and the occurrence of aseismic fault slip in the well GPK1 between 2800 and 3500 m. SCCL and the location of (aseismic) slips during GPK1 stimulation have been identified by Cornet et al. [1997] and Evans et al. [2005a]. Major flow zones are surrounded by zones of high SCCL. Slip is restricted to hydrothermally altered clay zones with high SCCL. The occurrence of aseismic slips is restricted to clay rich flowing faults.

The correlation of aseismic movements with clay-rich intervals and their orientation at a significant angle to S_H supports the assumption of clay acting as some kind of lubricant on the fault zones. This makes these fractures prone for aseismic shearing, although they are not optimally oriented in the present stress field. Aseismic movements are assumed to take a big share of the movements induced during hydraulic stimulation and some authors even assume, that the major part of shearing happens aseismically [e.g. *Bourouis and Bernard*, 2007; *Schoenball et al.*, 2014]. Further evidence for aseismic movements in Soultz in GPK1 [*Bourouis and Bernard*, 2007; *Schmittbuhl et al.*, 2014; *Schmittbuhl et al.*, 2013b], GPK2 [*Calò et al.*, 2011; *Schoenball et al.*, 2014] and GPK3 [*Calò et al.*, 2011; *Nami et al.*, 2008] underlines the significance of clay on the structural reservoir evolution of the reservoir.

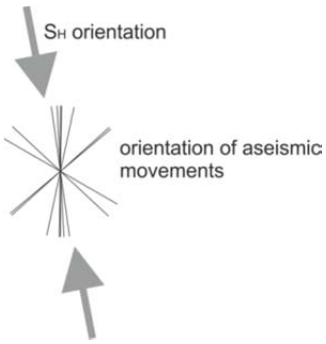

Figure 6-8: Strike of the aseismic movements observed by Cornet et al. (1997) vs. the orientation of SH. Some of the aseismic movements happened on fractures, which are oriented at an angle >30° to SH, which indicates weakness of these fractures, as they are not favorably oriented for shear.

The SCCLs provide the unique opportunity to investigate the relation between seismic events and clay inside the reservoir. It is best constrained by calibration in the well GPK1 and GPK3. In GPK2, the quality of the SCCL is bad due to the lack of logging data SCCL and for GPK4 the location uncertainty of seismicity is too large [*Gaucher, pers. comm.*]. Therefore, the analysis is focused on GPK1 and GPK3. In the well GPK1, the location and magnitude for several 19000 seismic events have been determined [*Jones et al.*, 1995] and for GPK3 22000 events have been located [*Dorbath et al.*, 2009; *Dyer et al.*, 2003]. As the SCCL logs can only indicate clay in the proximity of the wells, the events in a radius of 100 m around the borehole are selected. For the remaining 5600 events (4200 for GPK1 and 1400 for GPK3) the respective SCCL value of the depth, where they occurred is determined. Then, the magnitude of the respective event is plotted against the SCCL value (Figure 6-9). The exciting result of this plot is that with increasing clay content, the maximum magnitude of seismic events is decreasing. Recent observations of Schorlemmer et al. [2005], Langenbruch and Shapiro [2014], and others suggest that low differential stress in weak zones prevents large seismic events and it has long been assumed that the occurrence of large events in Soultz is restricted to fresh, i.e. unaltered granite, but it could never be directly observed. This figure suggests that the *b*-value in Soultz, although not constant in time, is also affected by the occurrence of hydrothermally altered zones. The *b*-value of the entire 2000 stimulation test of GPK2 was determined to 1.29 by Cuenot et al. [2008] and for the GPK3 stimulation Dorbath et al. [2009] determined a *b*-value of 0.94. It would be interesting to compare the total clay content in both wells in order to find a correlation between the total clay content and the b-value. Unfortunately, the SCCL of the lower part of GPK2 could not be properly created due to missing image logs. The rather large value of 1.29 for GPK3 might be indicative of weak structures, as such high values are normally only found in regions of crustal weakness [*Amitrano*, 2003].

Therefore, the presence of large faults is most probably not the only reason for the different seismic behavior of GPK2 and GPK3 as it was observed by Dorbath et al [2009]. The different *b*-values, which can be obtained from the seismic events induced during stimulation of these wells, could also be affected by the presence/absence of alteration zones.

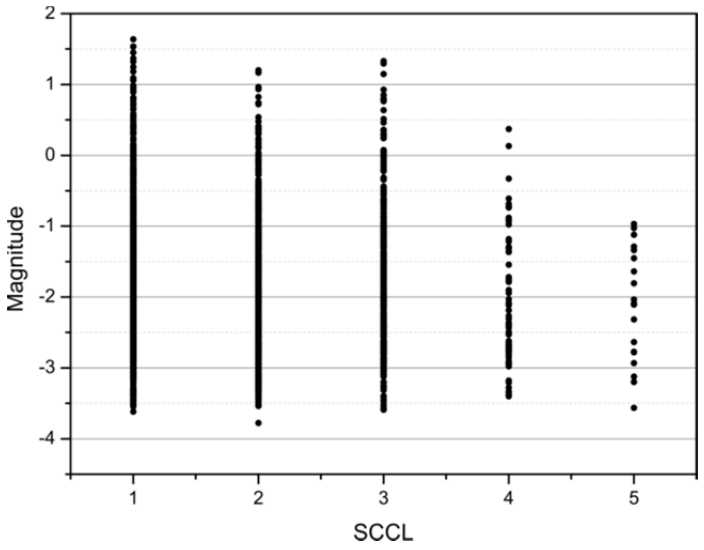

Figure 6-9: SCCL versus magnitude of induced seismic events during GPK1 and GPK3 stimulation. Seismic events with large magnitudes are restricted to low SCCL values, i.e. intervals with little clay inside fractures. With increasing clay content (higher SCCL), the maximum magnitudes of seismic events are smaller

There is evidence that hydrothermally altered zones not only affect the magnitude, but also the evolution of seismicity. The seismic clouds of the GPK1 and GPK3 stimulation move downhole or uphole in steps, when the injection pressure is increased (Figure 6-10). Each pressure increase is marked by colored rectangles in Figure 6-10. The SCCL logs provide a possible explanation of the reason of these steps. Each of these steps starts with a clay-rich zone and ends with an interval with little clay. As mentioned before, clay-rich intervals do not support large stresses and could act as small stress decoupling horizons as observed by Cornet and Roeckel [2012] in the Paris Basin. They might therefore prevent the occurrence of seismic events or shear movements or the events in such zones are very low magnitude events, thus being too small to be measured, i.e. those slips are aseismic. With each pressure increase, the pressure front penetrates the decoupling horizon without inducing seismicity and the seismic events start just below or above this zone, migrating upward (as in GPK3, Figure 6-10b) or downward (as in GPK1, Figure 6-10a) until the next clay-rich zone is reached. This interval will then be overcome by the next pressure increase and so on, leading to a stepwise migration of microseismicity.

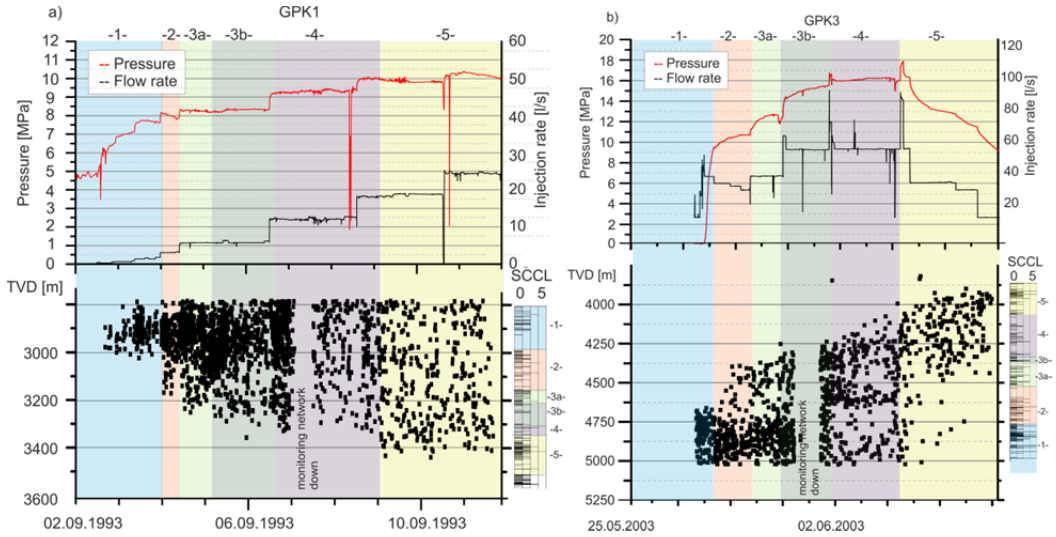

Figure 6-10: Evolution of seismicity in a radius of 100 m around the boreholes during stimulation and SCCL. The upper part of the diagrams show the stimulation pressure and below, the time-evolution of induced seismicity is shown versus depth. The lower part of the diagrams shows the SCCL for the respective depth intervals. Different sections are marked by numbers and colors indicating the pressure steps of injection. With increasing stimulation pressure, seismicity migrates downwards (a) GPK1) and upwards (b) GPK3), respectively. The steps might be caused by clay-rich intervals, which rather promote creep than seismic shearing. After each pressure increase, seismicity begins at depths, where the clay-content is low until the pressure front reaches a clay-rich interval. This interval is overcome during the next pressure increase and seismicity starts just after the clay-rich zone migrating towards the next clay-rich zone and so on. From step 5 on we assume that the pressure front migrated too far away from the borehole so that a correlation with the (2 dimensional) SCCL is not possible any more.

6.5 CONCLUSION AND OUTLOOK

The present SCCL method is an important basis to localize clay rich zones as target zones for hydraulic stimulation and to identify fractures as candidates for aseismic movements. In order to optimally use the properties of hydrothermally altered zones, further effort has to be done on the understanding of processes affecting the geomechanical behavior of a geothermal reservoir. Once such processes are understood, it might become possible to exploit the properties of altered zones in order to increase the reservoir performance, while mitigating perceptible seismicity.

The occurrence of hydrothermally altered zones inside a geothermal reservoir can have large effects on many physical aspects, which are important for the performance of a geothermal system, and especially those related to induced seismicity. The observations at Soultz-sous-Forêts revealed that hydrothermal alteration lowers the mechanical strength of the Soultz granite and its fractures, which results in an inhomogeneously distributed friction coefficient. Geological units with low mechanical

strength promote the occurrence of breakouts and can rotate the stress field as much as 90° from the mean orientation, which is indicated by high breakout densities in clay rich intervals and a deviation of their mean orientation.

A major result of this study is that hydrothermally altered zones can act as decoupling horizons, which change the local stress regime and thus significantly affect the seismicity induced during hydraulic stimulation at Soultz. It has been shown that large seismic events are restricted to fresh granite, whereas only small seismic events occur in clay rich intervals. While this behavior has often been observed on the crustal scale, the present study for the first time confirms this effect on the scale of a geothermal reservoir.

Due to their low frictional strength and increased pore pressures, hydrothermally altered zones represent major target zones for hydraulic stimulation. In future, EGS projects need to be structured that prevention of large seismic events becomes a major achievement. Future stimulations could foster the creation of aseismic instead of seismic slip to increase the reservoir permeability, which requires knowledge on the location of such zones and advanced research towards the evolution of aseismic movements.

ACKNOWLEDGEMENTS

This research was conducted within the portfolio topic GEOENERGIE of the Helmholtz Association of German Research Centres and was funded by Energie Baden-Wuerttemberg (EnBW), Germany. Thanks are given to GEIE Exploitation minière de la chaleur for providing the Soultz borehole data.

7 CHARACTERIZATION OF THE CRITICAL PRESSURE OF FRACTURES AND INDUCED SEISMICITY DURING GPK1 STIMULATION

7.1 INTRODUCTION AND DATABASE

Previous studies reveal the significance of alteration zones in granite for its mechanical behavior. A major aspect in terms of EGS systems is the role of clay zones for the evolution of induced seismicity during hydraulic stimulation and during water circulation in the production phase of a geothermal power plant. In order to investigate the role of clay inside fractures for the hydro-mechanical characteristics of a hydraulic stimulation, a sound analysis of the relationship between fractures, fracture mechanics and seismicity of the Soultz geothermal well GPK1 was conducted. GPK1 was selected due to the good quality of the SCCL logs in this well and the availability of a reliable database of seismic events locations. The massive stimulation of the GPK1 borehole was the first stimulation applied on the Soultz geothermal reservoir and therefore penetrated the most original rock mass.

The mechanical weakness of clay-filled fractures has been demonstrated in several studies [e.g. *Dolan et al.*, 1995; *Schleicher et al.*, 2006b; *Wu*, 1978]. Observations at the San Andreas Fault revealed the mechanical significance of clay minerals in terms of aseismic fault creeping. Several laboratory studies suggest that even small amounts of clay on fracture surfaces determine the mechanical properties of the fault zone, when an external stress is applied [*Tembe et al.*, 2010; *Zoback et al.*, 2012]. On the basis of these results and the findings of the previous chapters, the question arises if and how clay on fractures affects seismicity induced during reservoir stimulation.

It has been shown in chapter 6 that the maximum magnitude seismic events induced during the GPK1 stimulation at Soultz is lower for clay-rich faults than for faults in unaltered rock. Also, the occurrence of aseismic movements in clay rich intervals is suggestive of a correlation between clay and the characteristics of fault slips. I assume that the critical pressure, which is the pressure required to rupture a fault, depends significantly on the clay inside the fault. It is expected that the characteristics of induced seismicity reflect the presence of weak faults. If this is the case, a model of the critical pressure of fractures can be created from fracture orientations and clay content, predicting the occurrence of seismic events. This study aims at creating probabilistic models of the critical pressure of fractures in and around GPK1 taking into consideration the clay content of the fractures. These models are compared to induced seismicity recorded during the 1993 stimulation of GPK1.

7.2 PROBABILISTIC MODEL OF CRITICAL PRESSURE

7.2.1 METHODOLOGY

According to the Mohr-Coulomb failure criterion, the critical pressure of a fracture indicates its distance from the failure envelope, i.e. it represents the pressure, which is required to shear the fault during hydraulic stimulation, where only the pore pressure is assumed to vary. It can be calculated after

$$P_c = \sigma - \frac{(\tau - c)}{\tan \varphi} \qquad (7\text{-}1)$$

where P_c is the critical pressure, σ is the effective normal stress acting on the fracture, τ is the effective shear stress acting on the fracture, c is its cohesion and φ the friction angle. In a reservoir, which is in equilibrium, all fractures exhibit positive critical pressure. Negative values for the critical pressure implicate that the fractures are beyond the failure envelope and would have already sheared under the present conditions, i.e. they are supercritical and the reservoir is not in equilibrium. The critical pressure is controlled by the orientation of the fracture in the prevailing stress field, the mechanical properties of the rock represented by its internal friction and cohesion, and by the pore pressure. The orientation of fractures in Soultz is known from borehole logging and the clay content can be derived from SCCL logs. Friction and cohesion parameters can be defined according to the clay content of a fracture. The creation of the probabilistic model of fracture orientations and clay content and the derived critical pressure is described in the following section.

Fracture network

The orientation and distribution of fractures (Figure 7-1) along the borehole GPK1 is well known from FMI, FMS and UBI logs. The fractures are generally oriented between N10°E and N170°E with a (sub-)vertical dip and are thus largely parallel to the principal stresses S_H, which is oriented N169±21°E [*Cornet et al.*, 2007] and S_v. A total of 1381 fractures have been identified in the granitic section below ~1400 m (Figure 7-1a) and 671 in the open-hole section between 2850 and 3590 m (Figure 7-1b). The dip of the fractures in the open-hole section is representative of the dip in the whole granitic section with a more NNE-SSW oriented dip direction.

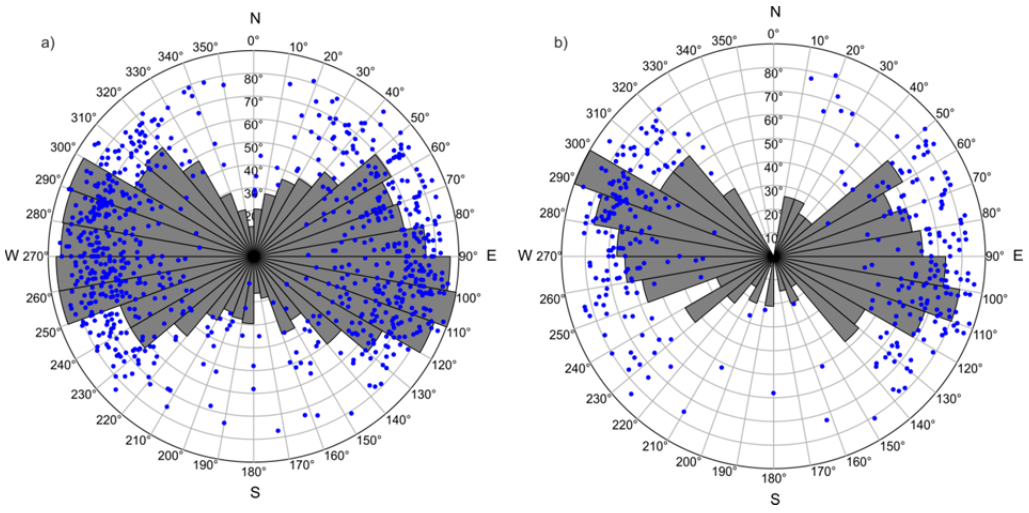

Figure 7-1: Orientation of the fracture normals in the well GPK1 and rose plot of the azimuths of the dip direction for a) the whole granitic section (1400 m-3590 m) and b) for the open-hole section (2850 m-3590 m).

SCCL logs

In a previous study by Meller et al. [2014b], spectral gamma ray logs and fracture density logs were used to create synthetic clay content logs (SCCL), which are a semi-quantitative model of the clay content along the Soultz boreholes. They were created with a neural network, which was previously trained on reference data derived from core material of the well EPS1. The application of the trained network on the deep wells generated logs, which represent the clay content inside fractures in five groups. SCCL group 1 represents the fractures without clay and SCCL group 5 applies to fractures with the highest amount of clay. The resolution of these logs is between several decimeters and 1 meter [*Meller et al.*, 2014b] and they are thus a sound basis for detailed rock mechanical analyses. The synthetic log for the well GPK1 is presented in Figure 7-2. It clearly shows depth intervals of high and low clay content.

Probabilistic distribution of fractures and clay

The fractures identified on UBI logs of the open-hole section of the well GPK1 were used to determine the distribution of fracture orientations. Due to the large number of sub-vertical fractures, a Terzaghi-correction was applied [*Terzaghi*, 1965]. With this correction, the sampling bias of steeply dipping faults in borehole imaging logs is taken into account by weighting fractures according to their orientation to the borehole axis, thus giving subvertical fractures higher weights. The resulting distribution of dip and dip direction is illustrated in Figure 7-3a (dip) and b (dip direction). It is supposed that the orientation distribution of fractures at the borehole wall is representative of fractures in the whole reservoir in the depth interval 2850-3590 m. It is therefore used to create a probability distribution of fracture orientations.

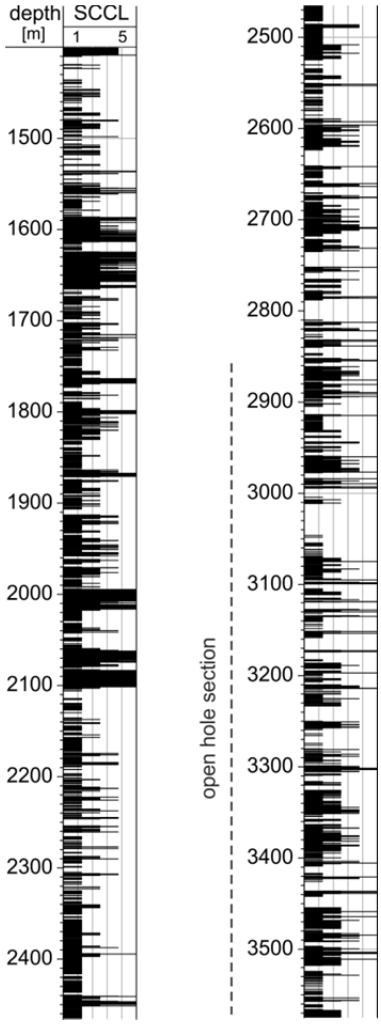

Figure 7-2: SCCL log for the well GPK1. SCCL group 1 represents the fractures without clay filling, whereas SCCL group 5 contains fractures with the highest amount of clay. The open-hole section of the well between 2847 and 3590 m is marked by the dashed line.

Figure 7-4, where the orientation of the fractures in GPK1 is illustrated together with the SCCL group of the fractures shows that there is no correlation between the dip, strike and clay content of the fractures. Therefore, it is reasonable to assume independently of fracture orientation and associated amount of clay a random distribution of SCCL groups over the fractures. Hence, in a probabilistic model, the proportion of fractures for each clay content can be derived from the SCCL logs.

The relative proportion of fractures with different amounts of clay in the open-hole section of GPK1 is provided in Table 7-1. The SCCL groups 1-5 are randomly distributed to the fractures in 25 draws, whereas 42.85 % of the fractures are assigned to SCCL group 1, 32.69 % are assigned to SCCL group 2 and so on. On the basis of various rock mechanical laboratory studies, it is expected that clay rich fractures have lower friction coefficients than unaltered fractures. Therefore, the different SCCL groups are representative of fractures with different friction coefficients and presumably also cohesion.

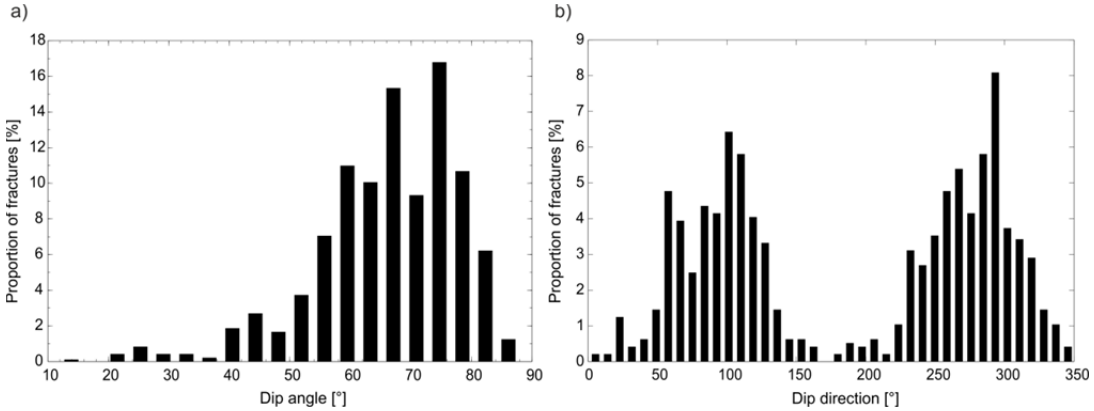

Figure 7-3: Distribution of a) dip and b) dip direction in the open-hole section of GPK1 after Terzaghi correction of the fractures. This distribution is regarded as representative of the whole reservoir around GPK1 in the depth interval of the open-hole section.

As experimental studies on the frictional properties of the Soultz granite are missing, a lower bound for the friction coefficient and the cohesion of the granite must be estimated. Based on previous studies from other researchers, I defined the maximum friction of the Soultz granite for the unaltered rock mass (SCCL 1) as 0.98 [*Cornet et al.*, 2007; *Evans*, 2005]. The most commonly observed clay mineral in Soultz is illite, which has a friction coefficient of ~0.4. However, experimental studies showed that fractures filled with illite have a higher friction coefficient than pure illite [*Blanpied et al.*, 1995]. Following to the experiments of Blanpied et al. [1995], a friction coefficient of 0.58 is defined for SCCL group 5. According to the linear relationship between clay content and friction coefficient observed by Zoback et al. [2012], the friction coefficient is linearly interpolated between SCCL1 and SCCL5 resulting in friction coefficients 0.88 for SCCL2, 0.78 for SCCL3 and 0.68 for SCCL4 (Table 7-1).

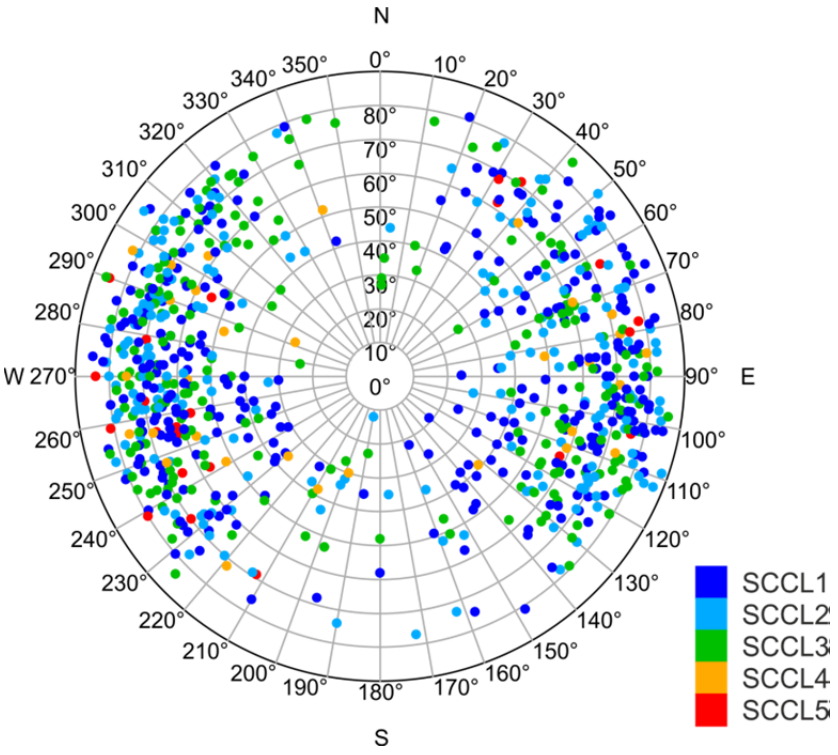

Figure 7-4: Fracture orientations in the well GPK1. The SCCL group of each fracture is color-coded as indicated by the legend.

Although it is often assumed that existing fractures have no cohesion, Cornet et al. [2007] and Evans [2005] found that there must be cohesion on the fractures in the Soultz granite to keep them stable under the present stress conditions. Based on observations from Evans [2005] and Cornet [2007], a cohesion between 4 and 9 MPa can be assumed for the Soultz granite, depending on the stress model. Here, a cohesion of 6 MPa is chosen.

Table 7-1: Proportions of the SCCL groups 1-5 their friction coefficient and cohesion. Group 1 represents the fractures with no clay filling, whereas group 5 contains the fractures with high clay content and large alteration halos.

SCCL group	Proportion	Friction coefficient	Cohesion [MPa]
1	42.85% (~288 fractures)	0.98	6
2	32.69% (~220 fractures)	0.88	6
3	16.84% (~110 fractures)	0.78	6
4	3.16% (~21 fractures)	0.68	6
5	4.45% (~30 fractures)	0.58	6

Stress field

In addition to the fracture orientation, the orientation and magnitude of the principal stress components are required to calculate the critical pressure for a fracture. The stress field in Soultz has been thoroughly investigated by various techniques including borehole breakouts, drilling induced fractures, leak-off tests and fault plane solutions of microseismic events. Valley [2007] and Cornet [2007] provided the most recent solution for the stress field magnitude and orientation at Soultz, which are given in the following equations:

$$S_V = -1.3 + 0.0255 \cdot z \quad (7\text{-}2)$$
$$S_H = 0.98(-1.3 + 0.0255 \cdot z) \quad (7\text{-}3)$$
$$S_h = -1.78 + 0.01409 \cdot z \quad (7\text{-}4)$$
$$P_p = 0.9 + 0.0098 \cdot z \quad (7\text{-}5)$$

with P_p the pore pressure and z the depth in m. The S_H orientation is approximately north-south and the vertical stress S_V is equivalent to the overburden.

7.2.2 RESULTS

According to the stress field, the friction coefficients and the fracture orientation distribution, the critical pressure is calculated for each fracture orientation. Thus, the proportion of fractures with a certain critical pressure is obtained. As the stress magnitudes vary from the top of the open-hole section to its bottom (ΔS_v=18.9 MPa, ΔS_H=18.5 MPa, ΔS_h=10.5 MPa, ΔP_P=7.3 MPa), the critical pressure was calculated for three depths: 2850 m, 3220 m, and 3590 m, which corresponds to the top, the center, and the bottom of the open-hole section. Figure 7-5 shows the cumulative number of fractures versus their critical pressure. The critical pressure was calculated several times using different friction coefficients. For the first three curves (Figure 7-5a), a homogeneous friction coefficient of 0.98 and a cohesion of 6 MPa were used whatever the fracture clay content. Hereafter, this model is referred to as uniform friction model (UFM). For the second set of curves (Figure 7-5b) the friction coefficient was chosen according to the SCCL group of the fractures (see Table 7-1). This model is referred to as distinct friction model (DFM). The cohesion was fixed to 6 MPa for all SCCL groups according to Evans [2005] and Cornet [2007].

A homogeneous friction coefficient for the whole granitic reservoir yields a steep onset of the cumulative curve of fractures versus their critical pressure. If it is assumed that a fracture shears, when the overpressure inside the reservoir exceeds its critical pressure, the steep onset shows that there is a limit, under which no seismic event occurs. Above this limit, about half of the fractures shear within a pressure increase of 0.5 MPa. The remaining 50 % of fractures require a pressure increase of another 4-6 MPa to shear. The highest critical pressure of 15 MPa is far beyond the pressure

reached during the September 1993 stimulation of GPK1, which was maximum 10.57 MPa downhole at the top of the open-hole section. The curves for the three depths mainly differ in the minimum magnitude of the critical pressure (between 8.5 and 10 MPa) and their range, but their shape remains the same. The onset of the curve calculated at the top of the open-hole section deviates ~1.5 MPa from the curve calculated for the bottom of the hole, indicating that a higher minimum pressure is needed for shearing deeper fractures. The large pressure differences between the three selected depths highlight the importance of constraining the stress field.

The DFM curves are significantly different from those obtained from the UFM. This is especially the case at low pressures. Several fractures have critical pressures lower than 8.5 MPa, which was the minimum P_c of fractures at 2850 m, when selecting a homogeneous friction coefficient of 0.98 (Figure 7-5a). Between ~2.5-4 and 8-9 MPa the curve is only moderately rising before its gradient increases and the curve flattens again at ~9-10.5 MPa. The maximum critical pressure is around 15-16 MPa. The main difference between Figure 7-5a and Figure 7-5b is that in the UFM (Figure 7-5a), pressure has to be significantly increased until a seismic event happens, but then, all fractures shear within a very narrow pressure range. The DFM (Figure 7-5b) rather suggests shearing initiation at lower pressure, but the number of shearing events for a given pressure increase is smaller.

In order to investigate the effect of different frictional and cohesion parameters, several model curves are computed. Characteristic values of the curves are their minimum critical pressure ($P_{c,\,min}$), their maximum critical pressure ($P_{c,\,max}$), which is the smallest pressure leading to shearing of 100 % of the fractures, and the smallest pressure, which leads to shearing of 50 % of the fractures ($P_{c,\,50\%}$). The three values are used to compare the results for the top of the open-hole section (2850 m) and are listed in Table 7-2. Figure 7-6 illustrates the corresponding cumulative curves. Curves a) and b) are calculated with a uniform friction coefficient of 0.98, but while the cohesion is kept constant (6 MPa) for curve a), it decreases from SCCL1 to SCCL5 for curve b). The effect of decreasing cohesion is a flattening of the cumulative curve at its onset. The minimum $P_{c,\,min}$ is 2.5 MPa instead of 8.6 MPa. $P_{c,50\%}$ and $P_{c,\,max}$ in contrast do not change. If the friction coefficient instead of the cohesion decreases with increasing SCCL group, the curve is similarly flattened at its onset. Yet, it remains steeper than in curve b). The cohesion has been chosen according to the upper limit of 9 MPa as defined by Evans [2005]. The effect of higher cohesion is a shift of the curve to higher P_c. The minimum P_c in this case is 8.7 MPa and $P_{c,\,max}$ is 53.5 MPa.

It is often assumed that cohesion is a characteristic of intact rock, but fractures have no cohesive component. Curve d) is therefore calculated with decreasing friction coefficients and no cohesion. $P_{c,\,min}$ is negative in this case, which shows that the combination of these parameters is not possible. The shape of the curve is similar to curve b), but with a flatter onset, which is attributed to the combination of low friction coefficients and no cohesion for high clay contents. The parameters, which were

selected for curve e) are similar to those from curve c), but with a higher friction coefficient for SCCL5 and a linear interpolation of the friction coefficients between SCCL1 and SCCL5. Compared to curve c), $P_{c,\ min}$ is higher (5.6 MPa), but $P_{c,\ 50\%}$ and $P_{c,\ max}$ are very similar.

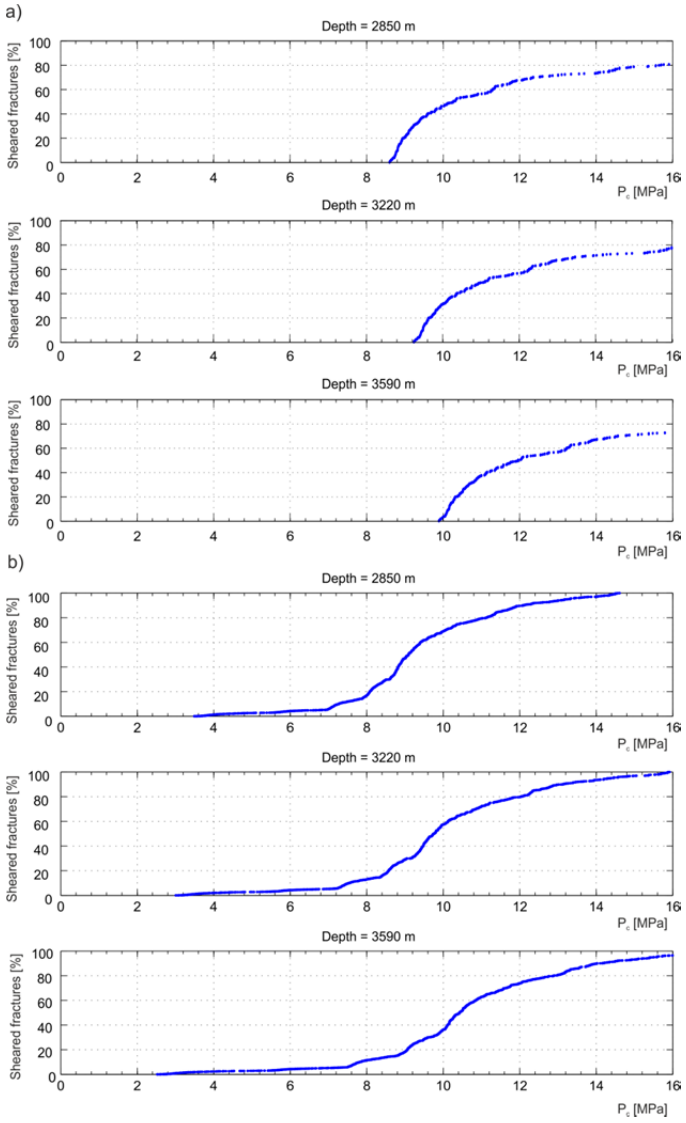

Figure 7-5: Percentage of fractures versus their critical pressure. P_c was calculated according to the Mohr-Coulomb failure criterion after Terzaghi correction of the fracture distribution. a) A uniform friction coefficient of 0.98 and a cohesion of 6 MPa is chosen for all fractures. b) Friction coefficients are different for the 5 SCCL groups (SCCL1: 0.98; SCCL2: 0.88; SCCL3: 0.78; SCCL4: 0.68; SCCL5: 0.58). The stress field is fixed to depths of 2850, 3220 and 3590 m, which corresponds to the top, the center and the bottom of the open-hole section.

The effect of a smaller range of friction coefficients is therefore most visible for low P_c. A further possible scenario is that the friction coefficient below a certain clay content is dominated by the friction of the intact rock, whereas at high clay contents, the clay minerals control the frictional properties of the fracture. This case is represented by curve f), where the groups SCCL1-3 have a friction coefficient of 0.98 and SCCL4-5 have friction coefficients of 0.75 and 0.68. The resulting curve is characterized by a flat onset and a kink at 8 MPa. The onset of the curve is similar to curve e), where the friction coefficients of SCCL4-5 are equal. The part of the curve after the kink is similar to curve a), where the friction coefficients and cohesion are the same for SCCL1-3. This suggests that the onset of the curve is dominated by the influence of SCCL4-5, whereas the higher P_c part is dominated by SCCL1-3. If an equal proportion of all SCCL groups is chosen, the resulting curve g) can be subdivided into 5 sections, each beginning with an increasing gradient, a turning point and a decreasing gradient. Ignoring SCCL5 fractures results in a curve with 4 sections, which is very similar to curve g), but with higher $P_{c,\,min}$, representing the 4 SCCL groups.

To sum up the observations, it can be stated that

- the lowest P_c fractures are dominated by the highest SCCL groups,
- a decrease of the frictional or cohesive properties of the fracture lowers the gradient of the onset of the cumulative curve and lowers the $P_{c,\,min}$, which means that fractures shear at lower critical pressure and that the ΔP_c until 50 % of the fractures have sheared is larger than for uniform friction/cohesion,
- the proportion of fractures in each SCCL group determines the curvature of the curve between $P_{c,\,min}$ and $P_{c,\,50\%}$.

These observations show that clay has a significant influence on the minimum overpressure required to shear fractures and on the number of fractures shearing within a certain pressure increase.

Table 7-2: Comparison of the minimum Pc, the Pc to shear 50 % of the fractures and the maximum Pc for different frictional parameters and proportions of the SCCL groups. A) is corresponding to the UFM. These values are computed for a depth of 2850 m.

corresponding curve		a)	b)	c)	d)	e)	f)	g)	h)
SCCL1	μ	0.98	0.98	0.98	0.98	0.98	0.98	0.98	0.98
	c [MPa]	6	6	9	0	6	6	6	6
	[%]	42.85	42.85	42.85	42.85	42.85	42.85	20	25
SCCL2	μ	0.98	0.98	0.88	0.88	0.91	0.98	0.91	0.91
	c [MPa]	6	4	9	0	6	6	6	6
	[%]	32.69	32.69	32.69	32.69	32.69	32.69	20	25
SCCL3	μ	0.98	0.98	0.78	0.78	0.82	0.98	0.82	0.82
	c [MPa]	6	2	9	0	6	6	6	6
	[%]	16.8	16.8	16.8	16.8	16.8	16.8	20	25
SCCL4	μ	0.98	0.98	0.68	0.68	0.75	0.75	0.75	0.75
	c [MPa]	6	0	9	0	6	6	6	6
	[%]	3.16	3.16	3.16	3.16	3.16	3.16	20	25
SCCL5	μ	0.98	0.98	0.58	0.58	0.68	0.68	0.68	0.68
	c [MPa]	6	0	9	0	6	6	6	6
	[%]	4.45	4.45	4.45	4.45	4.45	4.45	20	0
$P_{c\text{-}min}$	[MPa]	8.6	2.5	8.7	-6.9	5.6	5.6	5.6	6.6
$P_{c,50\%}$	[MPa]	10.3	10.2	13.0	3.2	9.8	10.2	9.2	9.4
$P_{c,\,max}$	[MPa]	45.9	45.9	53.5	39.8	47.4	47.4	47.4	47.0

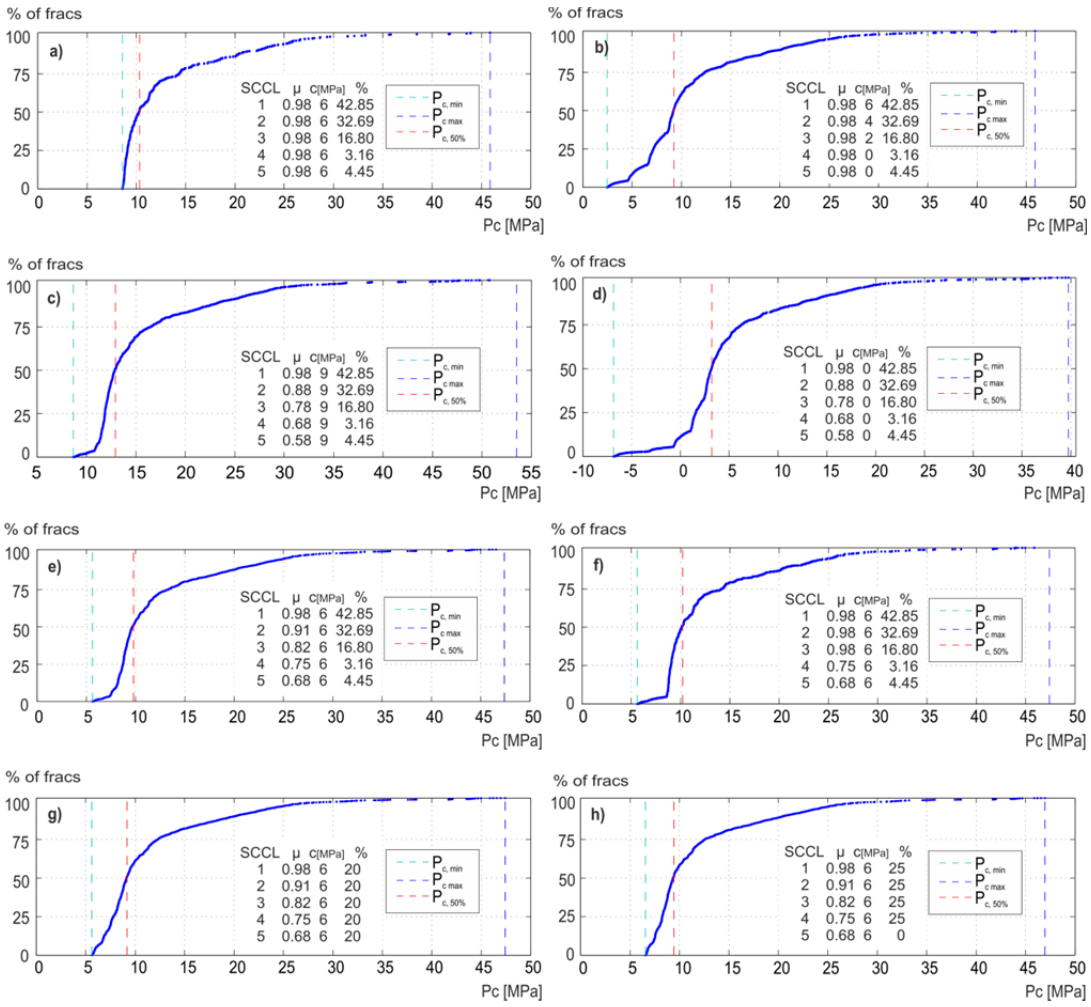

Figure 7-6: Cumulative curves of fractures versus their critical pressure. The parameters chosen for the calculation of the curves are given in the small tables inside the graphs and in Table 7-2. Curves c) and d) have a different scale on the x-axis. The depth reference of the curves is 2850 m.

7.3 SEISMICITY INDUCED DURING STIMULATION OF GPK1

The critical pressure represents the overpressure, which is required to shear a fracture. During stimulation a pressure is applied to the reservoir. This pressure acts on a fracture in addition to the prevailing pore pressure. Therefore, the overpressure in a reservoir corresponds to the wellhead pressure, which has been corrected for a frictional term related to friction of the stimulation fluid along the borehole. Provided that the overpressure in the reservoir corresponds to the critical pressure of fractures, each fracture with a P_c smaller than the applied overpressure shears. If it is assumed that the overpressure inside the reservoir corresponds to the downhole pressure and each shearing fracture induces exactly one seismic event, the previously calculated distribution of P_c can be directly transferred to a seismic event curve with increasing stimulation pressure. This allows investigating the role of clay for the evolution of microseismicity during GPK1 stimulation. In this chapter, the frictional characteristics of the fractures around GPK1 are assessed by comparing the characteristics of recorded seismic events with the probabilistic curves of the distribution of P_c.

7.3.1 SEISMICITY CHARACTERISTICS

The well GPK1 is 3580 m deep with an open-hole section spanning the lowermost 730 m of the borehole. In September 1993, hydraulic stimulation of the open-hole section has been performed in 8 steps approaching a maximum injection rate of 37.8 ls^{-1}. During and shortly after the stimulation operations downhole, which continued 15 days from September 2, the downhole seismic network recorded ~12'000-13'000 seismic events (Figure 7-7). Shut-in was on September 17, but the record of pressure and induced seismicity continued for another 13 days until the wellhead pressure reached zero. Seismicity continued after shut-in, albeit with a lower rate. The seismic cloud propagated ~800 m in horizontal direction as well as 900 m upward and 250 m downward from the open-hole section.

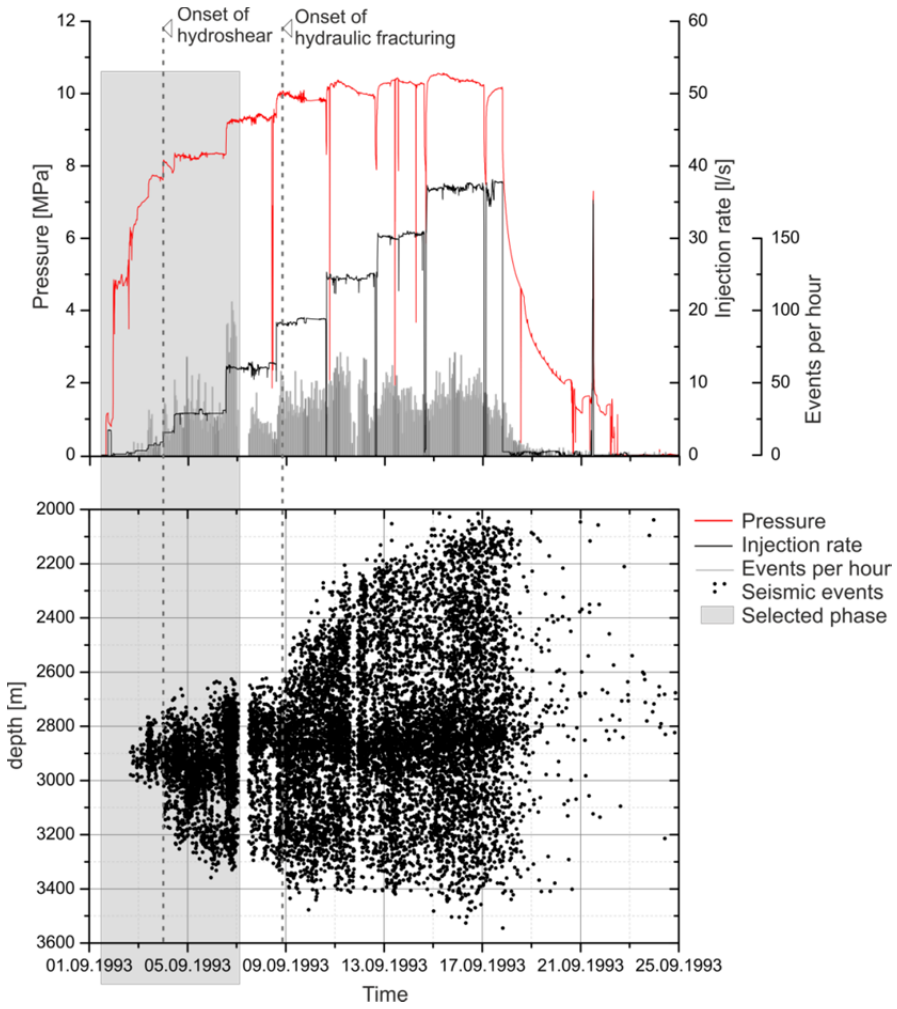

Figure 7-7: Characteristics of the stimulation of the geothermal well GPK1 in 1993. The upper graph shows the injection rate and wellhead pressure (lines) and the event rate. In the lower part, the depth of recorded events is plotted versus time. The x-axis representing the time applies for both graphs. The onset of hydroshear and hydraulic fracturing during stimulation is from Schmittbuhl et al. [2013a]. The grey area represents the selected stimulation phase used for this study. Hydraulic fracturing was excluded as well as the gap in the seismic recording.

7.3.2 METHODS

In a first step, the wellhead pressure applied during stimulation has to be converted into downhole pressure. The correction for the wellhead pressure is derived from the pressure gradient. It consists of a frictional term (subscript f), a hydrostatic term (subscript H) and an acceleration term (subscript A).

$$-\left(\frac{\partial p}{\partial z}\right) = \left(\frac{\partial p}{\partial z}\right)_f + \left(\frac{\partial p}{\partial z}\right)_H + \left(\frac{\partial p}{\partial z}\right)_A \qquad (7\text{-}6)$$

The acceleration term is generally very small in boreholes and can be neglected. The frictional term can be calculated after

$$\left(\frac{\partial p}{\partial z}\right)_f = \frac{4 f \rho v^2}{2D} \qquad (7\text{-}7)$$

with f the Moody friction factor, which is a function of the Reynolds number, ρ is the density of the fluid, which is 1.18 kg m^{-1} for the 1993 stimulation, v the velocity derived from the flow rate and D the hydraulic diameter of the borehole, which is 0.2159 m to a depth of 2847 m and 0.13335 m in the lower part of the well. As for this study only the overpressure inside the reservoir is of interest, the hydrostatic term is removed from equation (7-6). The downhole overpressure (Bhp) is therefore calculated from the wellhead pressure (Whp) after

$$Bhp = Whp - \frac{4 f \rho v^2}{2D} \qquad (7\text{-}8).$$

Hereafter the term bottom hole pressure or downhole pressure refers to the overpressure produced in the reservoir during injection.

In order to create a cumulative number of events vs. overpressure curve, only the increasing pressure steps during stimulation are considered as well as the total number of events, which occurred until the pressure levels were reached.

7.3.3 RESULTS

Due to the dependence of the frictional term of the pressure gradient on depth, the downhole pressure is depth dependent. However, the downhole pressures for the top, the center and the bottom of the open-hole section are very similar and only vary by maximum 20 Pa. Hereafter, the downhole pressure at 2850 m is used, when referred to the bottom hole pressure (*Bhp*). Figure 7-8 shows the cumulative number of events recorded during the September 1993 stimulation of GPK1 versus wellhead and downhole stimulation pressure.

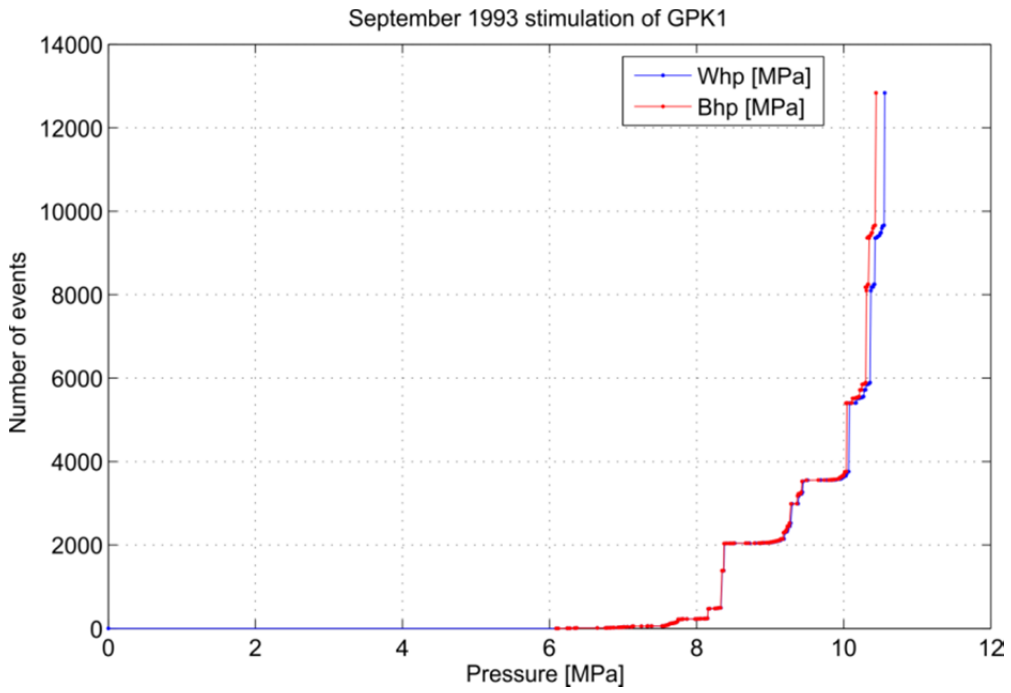

Figure 7-8: Number of events recorded during the September 1993 stimulation of GPK1 versus wellhead (Whp) and downhole pressure (Bhp) (at 2850 m). For higher flow rates (higher pressure) the differences between the curves become larger.

The stimulation starts with a minimum pressure of 6 MPa, where the first seismic event occurs. Until 7 MPa *Bhp*, the number of events is only slowly increasing. Above 8 MPa, the gradient of the curve significantly increases. Between 8 and 10 MPa, about 3500 seismic events occur. At 10.4 MPa, 50 % of recorded seismicity has occurred. The remaining 50 % occur within a small pressure increase of ~0.5 MPa. The curve shows that in order to induce the first 50 % of events, a pressure increase of ~4 MPa is required, whereas the pressure range for the last 50 % is ~0.4 MPa.

7.4 DISCUSSION

7.4.1 COMPARISON BETWEEN PROBABILISTIC CURVES OF P_C AND INDUCED SEISMICITY

Comparison between recorded seismicity and the probabilistic curves of P_c may deliver insight into the frictional properties of the reservoir. However, several assumptions have to be made for such a comparison. One of the strongest is that time variation of the pressure and the pressure decrease with distance from the well is not taken into account here. Indeed, to do so, a correct model of pressure propagation would be necessary. This not a simple task, as identified by Cornet [2012]. For the 1993 stimulation, he identifies 4 phases. At the beginning of stimulation, the propagation of the pressure front depends on the rock diffusivity, thus increasing the ambient pore pressure. According to Cornet, seismic events happen within the elastic domain of the rock in this phase. When the pressure is high enough, slip along pre-existing fractures occurs, which changes the diffusivity of the rock and the growth of the microseismic cloud. At higher pressures, Cornet assumes the generation of new fracture zones related to the local stress field. When the pore pressure reaches the minimum principal stress, the faulting mechanism is hydraulic fracturing. All faulting mechanisms are characterized by different stress-pressure conditions and propagation modes of the microseismic cloud. For Soultz, Schmittbuhl et al. [2013a] postulate that the onset of hydroshearing is at ~8 MPa wellhead pressure and hydraulic fracturing begins at ~10 MPa wellhead pressure. In the hydroshearing phase, flow inside the reservoir is fracture dominated and the pore pressure is high enough to shear along a major structure. As there is a gap in seismic recording above ~9.3 MPa and therefore the number of seismic events is biased between the period before and after this technical problem, the stimulation phase between 0 and 9.3 MPa wellhead pressure is selected for this analysis.

In order to better characterize the evolution of seismicity at low pressures, semi-logarithmic curves are used to illustrate the amount of seismic events versus downhole pressure, which can be compared to the amount of fractures shearing vs. their critical pressure as described in the previous section. Figure 7-9a shows the evolution of seismicity during the 1993 stimulation between 0 and 9.3 MPa. It is compared to 5 probabilistic curves, which have been obtained using different friction and cohesion parameters (Figure 7-9b-f).

The cumulative curve of seismic events during the September 1993 stimulation of GPK1 reveals an onset of seismicity at around 6 MPa downhole pressure. Between 6 and 8.3 MPa the number of events is approximately exponentially increasing, resulting in a sub-linear curve in the semi-logarithmic plot. Noticeable are the 5 steps of

increasing event numbers followed by a pressure increase without or with very few seismic events. The five steps are attributed to large structures inside the reservoir, which affect the propagation of fluid and seismicity. These structures could be either large fracture zones focusing fluid flow and microseismicity as postulated by Evans [2005b] or very clay-rich zones, which hamper the spreading of the seismic cloud [*Meller and Kohl*, 2014].

By selecting different friction and cohesion parameters for the probabilistic curves of critical pressure, I tried to reconstruct the seismic event curve by varying the mechanical parameters. In Figure 7-9b, homogeneous friction coefficients and cohesion are used for the calculation of P_c. It is obvious that the evolution of seismicity as illustrated by Figure 7-9a and b are totally different. Whereas the number of seismic events is exponentially increasing in Figure 7-9a, the uniform friction and cohesion curve of Figure 7-9b shows a rapid increase in the number of sheared fractures with increasing pressure. In this curve, 40 % of all fractures have a critical pressure between 6.5 and 7.5 MPa, implicating that 40 % of all fractures would shear within a pressure increase of 1 MPa at the beginning of the stimulation. In Figure 7-9c, the friction coefficient is decreasing linearly between 0.98 for SCCL1 and 0.58 for SCCL5 (DFM). With these parameters, 1 % of the fractures would shear within a pressure increase from 3.5 to 4 MPa, followed by an exponential increase of the number of shear events. The gradient of the linear section in the semi-logarithmic plot is smaller than that of the real seismic event curve of Figure 7-9a. A steeper gradient is obtained, when the range of friction coefficients between SCCL1 and SCCL5 is smaller. In Figure 7-9d, the friction coefficient was linearly interpolated between 0.98 for SCCL1 and 0.68 for SCCL5. A similar result is obtained, when the friction coefficient is kept constant, but the cohesion decreases with increasing clay content (Figure 7-9e). The gradient of the linear section in this curve is depending on the range between maximum and minimum cohesion. If both, cohesion and friction coefficient are decreasing with increasing clay content, the gradient of the linear section in the semi-log plot is even smaller.

From these curves, it is obvious that in this model, the evolution of seismicity cannot be explained by a uniform friction and cohesion throughout the reservoir. With uniform cohesion and friction, seismic events would be induced above a certain pressure level, which is depending on their mechanical strength, whereas all seismic events happen within a small pressure range in the order of 1 MPa. This is not observed during the September 1993 stimulation. The exponential increase in the number of seismic events, which has been recorded during stimulation, could be caused by the spatial and time variation of pressure. However, the exponential increase can also be reconstructed by distinguishing between fractures with different cohesion/friction, which emphasizes the potential importance of weak zones for the evolution of seismicity. Especially at low stimulation pressures, the time and space variation of the pressure cannot explain the occurrence of seismic events. The fractures shearing at low stimulation pressures must have low friction coefficients, because the onset of their shearing at 6 MPa cannot be explained by a favorable orientation in the ambient stress field alone.

A common feature of the probabilistic curves created with distinct friction and cohesion parameters is the step at the onset of the curve, where the proportion of fractures is quickly increasing to ~1 % within a small pressure increase of 0.3-0.5 MPa, which is not observed in the real seismic event curve. Several reasons for the absence of this section are following discussed.

When comparing the probabilistic curves to the evolution of seismicity during GPK1 stimulation, it is assumed that all fractures inside the reservoir shear and produce a seismic event. This is not necessarily the case. Fractures with high clay contents for example might shear without producing microseismicity. Borehole image logs run before and after the stimulation of GPK1 in 1993 revealed the occurrence of aseismic movements along some fractures cutting the borehole [*Cornet et al.*, 1997]. Meller and Kohl [2014] describe a relationship between the clay content of a fracture and the occurrence of aseismic slips. It was shown in their study that weak, clay rich fractures dominate the occurrence of seismic events at the beginning of stimulation. If several of the weak fractures had sheared aseismically, they would have not been recorded by the seismic network, which is also a possible explanation for the missing steep part in the recorded seismic event curve.

A second reason for the absence of this section in the recorded seismic events could be the Terzaghi correction applied on the fracture distribution model. Very steeply dipping fractures are weighted maximum 5-fold, which increases the number of sub-vertical fractures in the model. Yet, a comparison between the curves created with Terzaghi-corrected fracture models and uncorrected models showed that there is little difference between the curves and the vertical section in the semi-log plot is only insignificantly reduced by less than 0.01 %. Therefore, it is concluded that the Terzaghi correction is not generating the steep increase in shear events at the onset of the probabilistic curves.

A further possible reason is a packer test conducted in GPK1 in August 1993, before stimulation activities started. Water was injected into a fault at 3500 m with a maximum pressure of 20 MPa and 158 seismic events were recorded between 3410 and 3576 m depth. This stimulation started on 19th of August and continued for only 20 hrs. Although the pressure of this packer stimulation was much higher than in the following stimulation of the whole open-hole section, it is assumed that only a small part of the reservoir around the packered fault zone was affected by the high pressure. However, several fractures, which have sheared during this packer test could not shear again during the September stimulation.

A further point, which could affect the cumulative curve at minimum stimulation pressures, is the magnitude of completeness of the seismic catalog, which is around $M_{L,c}$=-1 [*Bachmann et al.*, 2012]. Big differences in magnitudes occur for the events recorded during the 1993 stimulation and a significant number of small events might have been missed by the seismic network. As a previous study showed (chapter 6), the magnitude of seismic events is affected by the clay content. In the probabilistic

analysis, the magnitude of seismic events was not taken into account, but fractures with high clay contents exhibit the lowest critical pressure. If those fractures produce seismic events with magnitudes below the detection limit, they are not recorded and are missing in the cumulative curve. 7.6 % of the fractures are in SCCL groups 4 and 5, and 50 % of them are optimally oriented in the stress field, i.e. their dip and dip direction are within 20° of the orientation of the principal stress components. Thus, they could affect the cumulative curve below 3.9 % of the fractures and could therefore be responsible for the missing steep part at the beginning of the real seismic event curve.

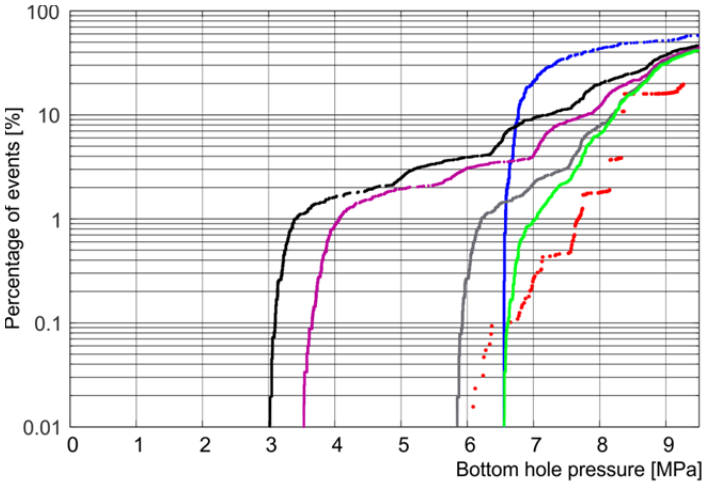

	a)	b)		c)		d)		e)		f)	
SCCL	recorded events	μ	c	μ	c	μ	c	μ	c	μ	c
1		0.98	4	0.98	6	0.98	6	0.98	6	0.98	6
2		0.98	4	0.88	6	0.90	6	0.98	5.5	0.90	5.5
3		0.98	4	0.78	6	0.84	6	0.98	5	0.84	5
4		0.98	4	0.68	6	0.77	6	0.98	4.5	0.77	4.5
5		0.98	4	0.58	6	0.68	6	0.98	4	0.68	4

Figure 7-9: Semi-logarithmic cumulative curves of the events during the September 1993 stimulation of GPK1 (a) and fractures vs their critical pressure calculated with the probabilistic fracture model (b-f) between 0 and 9 MPa. In curve b), the friction coefficient and cohesion are constant. In c) and d), the friction coefficient is decreasing with increasing clay content. In e), cohesion is decreasing with increasing clay content and in f) both, cohesion and friction coefficient, are decreasing with increasing clay content.

Despite the modelling uncertainties and simplifications, the results show that there have to be several fractures with a friction coefficient below 0.98, which was suggested by Cornet et al. [2007] and Evans [2005]. Even a low number of such weak fractures could significantly affect the evolution of induced seismicity. Considering that only 8 % of all fractures are SCCL4-5 and three thirds of the fractures are SCCL1-2, the effect of this small proportion of clay rich fractures completely changes the characteristics of induced seismic events, especially for low overpressures. One of the goals of this study was to find out, if the critical pressure significantly depends on the clay inside the fault. The results have shown that most of the fractures with low critical pressure are SCCL4-5 and therefore fractures with high amounts of clay inside. Without these weak fractures, the minimum P_c would be ~3-5 MPa higher and the evolution of induced seismicity would be most likely different from what is observed during the 1993 stimulation of GPK1. The onset of induced seismicity at low overpressures and the slow increase in the seismic rate until 8.5 MPa clearly indicate that weak fractures dominate the evolution of induced seismicity in the initial stage of hydraulic stimulation.

7.5 CONCLUSION

The study shows that probabilistic curves of the distribution of the critical pressure around the well GPK1 are a reasonable approximation to the distribution of P_c in the reservoir. The P_c distribution can be directly transferred to the overpressure required to induce shear on fractures during hydraulic stimulation. The comparison between the model and recorded seismicity implicates the presence of weak fractures inside the reservoir. The study shows that 1) clay-filled fractures are most likely a weak link inside the reservoir, exhibiting lower frictional and/or cohesive parameters than unaltered rock and 2) the presence of such clay rich fractures significantly affects the pressure dependent evolution of induced seismicity. This indicates that the role of clay and the lowering of the mechanical friction cannot be neglected in models of induced seismicity. Specifying the frictional properties of fractures according to their clay content is a new approach to explain the characteristics of induced seismicity. In future, this approach could be integrated into more complex structural and hydraulic models in order to develop stimulation strategies for geothermal wells. Especially for soft stimulation, where large seismic events are supposed to be mitigated, the P_c distribution in time and space is a necessary input to specify the stimulation pressure.

8 COMPREHENSIVE DISCUSSION

In this thesis, I present four studies towards a better understanding of the correlation between clay as a fracture filling and microseismicity during reservoir stimulation at the Soultz geothermal site. The neural network method to localize zones with different clay contents yields a substantial basis for geomechanical analyses, which is an important step towards the characterization of induced seismicity. Chapter 7 demonstrated that a possible explanation for the exponential increase of the number of events, which have been recorded during the 1993 stimulation of GPK1, is the contrast of mechanical friction and/or cohesion of the fractures related to their clay content. By attributing decreasing friction coefficients to increasing clay contents (increasing SCCL), the model reveals an exponential increase in the number of fractures vs. their critical pressure, which reproduces the evolution of events recorded during the September 1993 stimulation. These results raise several questions concerning the applicability of the critical pressure method:

1) Can this method be applied to wells at other geothermal sites?
2) Does the clay filling inside fractures affect induced seismicity?
3) Is it possible to estimate the occurrence of seismicity during stimulation?

These issues are discussed below.

8.1 APPLICATION TO OTHER SITES

Chapter 4 showed that the application of a neural network to create SCCLs from borehole data yields excellent results, when the neural network is trained on reference data from drill cores. However, the recovery of drill cores is unusual in geothermal drilling. Therefore, the availability of core material for creating reference datasets is an exceptional case. Usually, the only available data to reconstruct the clay content is borehole logs and cuttings. In order to transfer the method to other wells it is therefore necessary to test its performance without using reference datasets. The creation of SCCLs without reference data requires the application of an unsupervised neural network method. According to chapter 2, this method allows finding patterns in input data and forms clusters according to the similarity of input vectors. The performance of the unsupervised Kohonen algorithm for the creation of SCCLs is tested on the EPS1 logs and is then compared to the results obtained from the supervised network.

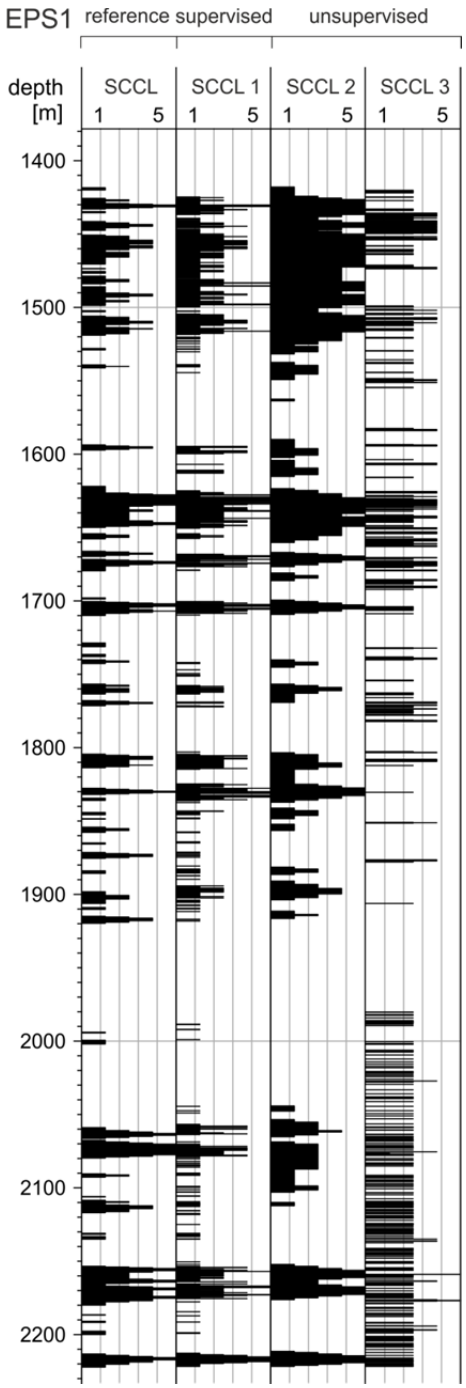

Figure 8-1: Comparison of the SCCL from different combinations of input logs with the reference SCCL from real data (left log). The SCCL1 log was created using the supervised method and the remaining SCCL logs are results of the unsupervised method. SCCL2: Spectral gamma ray and fracture density are used; SCCL3: Only spectral gamma ray logs are used.

The input parameters for the network are chosen in accordance to the settings described in chapter 4. The basis for the analysis are spectral gamma ray logs and fracture density logs. The self-organizing map is a squared 25x25 nodes map and 5'000'000 iterations are run in the training phase. Three different SCCL are compared. SCCL1 is the log created with the supervised learning. SCCL2 is created on the basis of spectral gamma ray and fracture density logs. SCCL3 is created from SGR logs only. For each of the logs, the accordance with the reference dataset is determined.

The SCCLs from the supervised and unsupervised neural network applications are shown in Figure 8-1. In the reference SCCL, which is obtained from the drill core, intervals with different densities of clay-filled fractures and intervals without clay can be clearly discriminated. SCCL1 retrieved with a supervised neural network matches the reference log to 74 %, whereas 91 % of the log deviate maximum one SCCL group from the reference. SCCL2, which was created with the unsupervised neural network applied on SGR and fracture density, matches the reference log to 53 % and 77 % of the log deviate less than one SCCL group from the reference. The resolution of this log is lower so that the differences in clay content for small depth intervals in the order of tens of meters cannot be discriminated. The main clay rich zones and zones without clay are clearly distinguishable from each other, as for example the clay-rich zone at the top of the granite between 1420 and 1520 m or the absence of clay between 1920 and 2050 m. The amount of clay is generally overestimated compared to the reference log. When only spectral gamma ray logs are used as an input for the training of the network, the resulting SCCL3 provides only little details about the location and the amount of clay along the borehole. Only the largest clay rich zones can be reconstructed, whereas there is no reliable information about the amount of clay in these zones. The accordance with the reference log is only 31 % for SCCL3.

The supervised neural network application is able to produce synthetic logs of very high quality. The accordance with real data is worse when the unsupervised method is used, yet the results are convincing. The unsupervised SCCLs can be correctly interpreted, when the geological background is known, as the influence of the matrix lithology is probably the main reason for deviations of the unsupervised SCCLs from the reference. In kalifeldspar cumulates for example (e.g. at 1610 m depth), where the potassium content is increased, the unsupervised SCCLs predict higher clay contents than those indicated by the reference logs.

The main challenge for the interpretation of the results in the unsupervised mode is the assignment of the defined groups to SCCL units 1-5. The output of the neural network is a grouping of the nodes of the self-organizing map into 5 classes, yet it is unknown, which of these clusters corresponds to which SCCL group. So, further information about the lithology is needed, which helps to interpret the results. This information can for example be derived from the petrographic and magnetic investigation of cuttings, which allow identifying highly altered zones based on their mineralogical content. Other logs like resistivity or spontaneous potential logs, which

are sensitive to clay minerals, can also help assigning the right groups. Here, short intervals of additional logs can be sufficient, but several methods should be combined in order to correctly assign the classes to SCCL groups. The more output clusters are defined, the more challenging is the interpretation. Therefore, the number of output groups should be kept as small as possible.

This study shows, the unsupervised neural network method applied on spectral gamma ray and fracture density data can provide sufficiently detailed information about the appearance of clay filled fractures along boreholes in crystalline rock to make geomechanical investigations. This technique can be used in wells, where no reference dataset can be created to train the neural network due to the lack of core material. The interpretation of the results can be accomplished with the help of cutting material or additional logs. With the unsupervised method, 77 % of the real dataset can be reconstructed with a deviation of ≤1 SCCL group provided that the fracture density is known.

As more and more EGS target the crystalline basement, it is worthwhile to further improve this method and to expand it to other crystalline geothermal reservoirs, for which it is equally applicable. In sedimentary geothermal reservoirs, the localization of clay is easier due to the lower matrix influence on spectral gamma ray logs. The application on crystalline rock is challenging, but the previous results show that it is feasible.

8.2 ESTIMATION OF INDUCED SEISMICITY

The importance of clay filling for reservoir mechanics was demonstrated in laboratory studies and by large-scale field observations (chapter 2). The SCCL method is an indirect approach, which is based on statistical evaluation of borehole measurements. Hence, the SCCLs provide a unique high-resolution basis for interpretation of visible geomechanical processes in a reservoir. In chapter 6, the significance of clay on geomechanics was demonstrated on the basis of breakout analyses, borehole image logs and the evolution of the seismic cloud during stimulation. In chapter 7, it was analyzed whether the evolution of induced seismicity also reflects the presence of clay-bearing fractures, which would imply conversely that clay affects the occurrence of induced seismic events.

It was demonstrated that decreasing friction or cohesion with increasing clay content of fractures could explain the evolution of induced seismicity during stimulation of GPK1. According to chapter 7, even a small number of weak fractures could have significant effects on the occurrence of seismic events at low stimulation pressure. In Soultz, the SCCLs indicate that only 8 % of all fractures are SCCL4-5 and two thirds of the fractures are SCCL1-2. Yet, the effect of this small proportion of clay rich fractures can completely change the increase of induced seismic events, especially for low

overpressures. One of the goals of this study was to find out, if the critical pressure significantly depends on the clay inside the fault. I have shown that most of the fractures with low critical pressure are SCCL4-5 and therefore fractures with high clay content. Without these weak fractures, the minimum P_c would be ~3-5 MPa higher and the evolution of induced seismicity would be most likely different from what is observed during the 1993 stimulation of GPK1. The onset of induced seismicity at low overpressures and the slow increase in the seismicity rate until the overpressure reaches 8.5 MPa indicate that weak fractures dominate the evolution of induced seismicity in the initial stage of hydraulic stimulation. The approach to determine the failure probability was primarily developed to understand the occurrence of seismic events upon pore pressure changes. In this context the mechanical contrast between fractures of different alteration grades was taken into account. If this approach is suited to characterize and model the evolution of induced seismicity, it should also be possible to assess the occurrence of seismic events.

The model described in chapter 7 is a simplified representation of the processes in the underground and several uncertainties exist. For the calculation of the critical pressure, Mohr-Coulomb failure is supposed to be the prevailing failure mechanism throughout the reservoir and it is assumed that the seismic events happen on pre-existing structures. Cornet [2012] however observed different faulting mechanisms during hydraulic stimulation, which also involve the formation of new fractures inside the reservoir rock. Including such mechanisms, seismicity cannot be explained by Mohr-Coulomb alone, but needs the combination of different faulting mechanisms and the corresponding failure criteria. This requires detailed knowledge about the reservoir and the surface structure of fractures, which is not easy to obtain and in most cases can only be approximated.

Furthermore, it is assumed that the pressure is homogeneously distributed and equal to the downhole pressure in the area of investigation. This is not the case under in situ conditions as the propagation of the pressure front into the reservoir is controlled by the reservoir permeability. In fractured reservoirs, fractures are the main fluid pathways. As the stimulation fluid is preferentially migrating along fractures, the pressure front is certainly not isotropic throughout the reservoir and the pressure is not necessarily homogeneously distributed around the borehole. The model assumes steady-state conditions and it is supposed that each pressure step instantaneously reached the reservoir, thus inducing shear on fractures with a critical pressure below the stimulation pressure. This approximation could be justified for the stimulation of the well GPK2, where the wellhead pressure curve was rather flat during stimulation and the seismic cloud reached its maximum extension in an early stimulation stage [*Schoenball and Kohl*, 2013]. For GPK1 in contrast, the seismic cloud continuously expanded during stimulation, which rather suggests a time and space dependence of pore overpressure. This effect could also contribute to the exponential increase of the number of seismic events, yet it cannot explain the occurrence of seismic events at low stimulation pressure.

A further simplification in the approach is that a single friction coefficient is attributed to each fracture. This would require a homogeneous fracture structure over its whole length. In reality, the parameters characterizing fracture surfaces vary over distance [*Schleicher et al.*, 2006b; *Schorlemmer et al.*, 2005]. This is for example the case for its roughness, its alteration grade and its filling. Together with these parameters, the friction coefficient of the fracture can also vary locally inside fractures, thus causing also a variation of its critical pressure. For the selection of a uniform friction coefficient for each fracture it was considered that the clay inside fractures has formed during hydrothermal alteration, which is induced by circulating fluids. The altered fractures must have been permeable, when clay minerals have formed. So, if the geothermal fluid was flowing through the fracture, the whole fracture surface was exposed to hydrothermal alteration. Therefore, it was regarded reasonable to specify an average friction coefficient representative for the whole fracture on the reservoir scale.

Another source of approximation is the depth dependence of the critical pressure due to the variation in stress that can reach several MPa over a depth range of 500 m. For the Soultz reservoir this means for example that a fracture at the top of the open-hole section has a critical pressure of 9.6 MPa, whereas the same fracture at the bottom of the open-hole section with dip direction N104°E and dip 72° has a critical pressure of 11.1 MPa. Therefore, the model should be adjusted to the depth at which the stress field is considered. An improved pressure and stress model therefore integrates over the whole depth range of the stimulated rock mass.

Finally, recent studies reveal a correlation between aseismic movements and the triggering of seismic events. Schmittbuhl et al. [2013a] demonstrated in laboratory experiments that creeping events on rough faults control acoustic emissions on the same fracture. They conclude that fluids are not necessarily the driving force of the fault activity, but they affect local creep acceleration, which in turn triggers acoustic emissions. The presence of both, seismic and aseismic slip on faults was observed earlier on the San Andreas Fault [*Schleicher et al.*, 2006b; *Schorlemmer and Wiemer*, 2005]. The same process might also take place on clay-filled fractures in Soultz or in other geothermal reservoirs as it was also demonstrated in chapter 6 of this thesis. If the pore overpressure is not the only driving force to induce seismic events, the present approach cannot capture the whole induced microseismicity.

For an estimation of induced seismicity, all those parameters have to be taken into account, which makes the geomechanical model rather complex. Yet, the independent SCCL method provides a novel and high-resolution basis for the estimation of mechanical properties of fractures, which can be included into new models developed on the basis of the presented simplified critical pressure model.

9 CONCLUSIONS AND OUTLOOK

Hydrothermally altered zones are a weak link inside rock masses, affecting both, the geomechanical, and the hydraulic properties of fractures. Their localization is a basic requirement for reservoir characterization. It has long been assumed that hydrothermal alteration in the Soultz reservoir plays an important role for reservoir mechanics and hydraulics, but sound studies on the mechanical significance of the clay zones were missing. With this thesis, I demonstrated the mechanical significance of clay inside fractures. On the basis of statistical evaluation of geophysical borehole logs, I developed an indirect method to localize clay-rich hydrothermally altered zones in the crystalline reservoir with a vertical resolution in the decimeter scale. The SCCL method for the first time provided a high-resolution profile of the occurrence of clay along a borehole.

So far, hydrothermally altered zones could only be identified from the analysis of drilled rock cuttings, which involves large uncertainties with respect to depth assignment of the samples, and elution, dilution, or enrichment of certain minerals. The SCCLs provided the possibility to investigate both, on the borehole scale, and on the reservoir scale, hydro-mechanical effects related to hydrothermal alteration in the Soultz granite. Finally, the logs could be used as a basis for the analysis of effects of clay-filled fractures on induced seismicity, which is a rather unexplored task on the scale of geothermal reservoirs. The lack of information about the mechanical properties of the heterogeneous Soultz granite gave the incentive to investigate the structure of the granite with respect to zones with different mechanical properties according to their clay content.

The objective of the first study (chapter 4) was to develop a method to localize clay zones in crystalline rock using a restricted number of logs, which are typically available at geothermal sites. Due to their complex mineralogical content, it is a major challenge to identify clay sections in crystalline rock. With a neural network, it was possible to extract information about the clay content of the granite from spectral gamma ray and fracture density logs, which are standard borehole measurements. The resulting synthetic clay content logs are a semi-quantitative measure of the density of clay bearing fractures along a borehole. This method allowed the identification of more than 90 % of the clay bearing fracture zones with a deviation of ≤1 SCCL group from reference core data. Compared to previous techniques for the localization of altered zones, the resolution of the SCCL logs is in the order of few decimeters, because it corresponds to the resolution of the geophysical logs. Beyond that, the logs are not only qualitative, but semi-quantitative measures of the clay content inside the granite. Even, if no reference data is available, an unsupervised neural network method can provide high-quality results.

Synthetic clay content logs were created for all geothermal wellbores at Soultz. Based on these SCCL logs, further methods were tested to characterize hydrothermal alteration. The second study described the magnetic mineralogical characterization of the hydrothermal alteration in Soultz performed on the basis of drilled rock cuttings. The analysis revealed a correlation between magnetic susceptibility carried by magnetite and the SCCL alteration grade of the granite. Generally, fresh granite is characterized by high magnetic susceptibility and magnetite contents of ~1 wt-%. Beside the formation of clay minerals, rock alteration involves the transformation of magnetite into hematite accompanied by a reduction of magnetic susceptibility. Hence, altered granite has a low magnetic susceptibility and magnetite contents <<1wt-%, depending on the grade of alteration. An alteration index derived from temperature-dependent susceptibility measurements of the cuttings could be used as a measure for the alteration grade of the granite. Taking into consideration the petrographic changes during the granite alteration process, the magnetic mineralogical investigation of cuttings allowed characterization of the hydrothermal alteration and calibration of the synthetic clay content logs. The possibility to localize clay zones with two independent geophysical methods (i.e. magnetic susceptibility and spectral gamma ray) attested, firstly, the quality of the neural network mapping of clay bearing fractures, and secondly, it underpinned the usefulness of drilled rock cuttings for analyses of petrography, magnetic mineralogy and granite alteration.

The main focus of the third analysis was on the influence of clay inside crystalline rocks on rock stability, on the stress field, and, finally, on the shearing of fractures including the occurrence of microseismic events. By combining borehole breakout analyses of the well GPK3 with the respective SCCL logs I could demonstrate an increased breakout concentration in clay-rich intervals, thus providing evidence of a weakening of rock by the occurrence of clay. Such zones are also characterized by a deviation of the orientation of breakouts from their mean orientation, indicative of a rotation of the stress field in clay-rich zones. For the first time, I could demonstrate a correlation between the appearance of aseismic movements and hydrothermal alteration. The SCCLs revealed a high clay content on the fractures, where aseismic slips were identified by Cornet et al. [1997] during the 1993 stimulation of GPK1. It was also shown that the mechanical weakness of altered granite affects the evolution of induced seismicity during hydraulic stimulation. Using stimulation data from GPK1 and GPK3, I showed that the magnitude of induced seismic events is inversely correlated to the SCCL group, indicating that clay inside fractures prevents the accumulation of large differential stresses and thus, the occurrence of large earthquakes. This has been earlier demonstrated by e.g. Schorlemmer et al. [2005], who found high *b*-values on creeping faults. In this thesis, I first showed the correlation between earthquake magnitude and clay on the scale of a geothermal reservoir.

The results of this study gave evidence for the influence of clay-rich fracture zones on the occurrence and the evolution of seismicity. In the fourth study, the SCCL analyses were used to create a model of the failure probability. A probabilistic model of the

critical pressure of fractures in the well GPK1 was created representative of induced seismic events at a certain stimulation pressure. Using the probabilistic model, a critical pressure distribution was obtained by introducing varying frictional and cohesive properties of the different SCCL groups, with lower friction and cohesion respectively for the higher clay contents. With the resulting model, the evolution of microseismicity during the 1993 stimulation could be retraced with a slow increase in the seismic event rate with increasing pressure beginning at 6 MPa, before the event rate significantly increases above 8 MPa downhole pressure. This study revealed that the fractures with the highest clay contents, hence those most susceptible to aseismic deformation, shear at the lowest stimulation pressures and might therefore be responsible for the slow increase in the seismic rate. If all fractures had the same friction and cohesion characteristics, all seismic events during stimulation would occur upon a pressure increase in the order of 1 MPa, which is not observed during the Soultz stimulations. It is concluded that clay-rich fractures significantly affect the evolution of microseismicity during geothermal reservoir stimulation and they are a key factor towards a better understanding of induced seismicity during hydraulic stimulation.

One of the major goals for EGS systems is the application of soft stimulation techniques on geothermal reservoirs in order to minimize the environmental impact while optimizing the profitability of a geothermal power plant. This involves the injection of fluids with limited pressure to enhance fluid pathways while mitigating the occurrence of large seismic events. This concept necessitates the establishment of sophisticated hydro-mechanical models of geothermal reservoirs allowing a control of induced seismicity. The foundation for such models is the petrophysical, geological, and mineralogical description of different facies of the reservoir rock and their geomechanical and hydraulic characterization. The SCCL logs provide a sound basis for the discrimination of different geomechanical facies. Yet, the identification of their mechanical properties, especially with respect to hydrothermal alteration, remains a challenging task. To determine the frictional and cohesion parameters of reservoir rocks and fractures, both, in-situ, and geomechanical laboratory studies on various scales are required. I suggest a combination of stress and strain experiments to investigate the role of strong and weak fracture zones on the stress conditions and the resulting deformation of the rock. Recent approaches by Schmittbuhl et al. [2014; 2013b] on the relationship between creep and brittle processes on fractures are a basis for understanding not only the occurrence of microseismicity, but also that of aseismic movements. There is evidence that seismic and aseismic movements are not two separate processes, but their occurrence is strongly interdependent. As aseismic processes could contribute to a large part to the permeability creation in a reservoir during hydraulic stimulation [e.g. *Garagash and Germanovich*, 2012; *Gischig et al.*, 2014; *Zoback et al.*, 2012], it is desirable to get a deeper insight into their nature. The focus of future stimulations could be on targeted creation of aseismic shear to optimize the reservoir productivity while mitigating induced seismicity.

The SCCL logs combined with probabilistic assessment of the reservoir structure, laboratory-derived mechanical parameters and hydraulic data including pore pressure diffusion through the reservoir provide a sound basis to establish a long-term operational concept for EGS systems. Such a concept will contribute to a more efficient and safer development and operation of geothermal reservoirs. In future, the method could be transferred to other applications, which involve processes related to pore pressure changes in a rock mass, like Carbon Capture and Storage, Oil and Gas production, or radioactive waste disposal.

10 REFERENCES

Akayuli, C., B. Ofosu, S. O. Nyako, and O. O. Kwabena (2013), The Influence of Observed Clay Content on Shear Strength and Compressibility of Residual Sandy Soils, *International Journal of Engineering Research and Applications (IJERA)*, **3** (4), 2538-2542.

Ali, J. K. (1994), Neural Networks: A New Tool for the Petroleum Industry?, paper presented at European Petroleum Computer Conference, Society of Petroleum Engineers, Aberdeen, United Kingdom, 15-17 March.

Alves, E. I. (2006), Earthquake Forecasting Using Neural Networks: Results and Future Work, *Nonlinear Dyn*, **44** (1-4), 341-349, doi: 10.1007/s11071-006-2018-1.

Amelung, F., and G. King (1997), Earthquake scaling laws for creeping and non-creeping faults, *Geophysical Research Letters*, **24** (5), 507-510, doi: 10.1029/97gl00287.

Amitrano, D. (2003), Brittle-ductile transition and associated seismicity: Experimental and numerical studies and relationship with the b value, *Journal of Geophysical Research: Solid Earth*, **108** (B1), 2044, doi: 10.1029/2001jb000680.

Angerer, T., R. O. Greiling, and D. Avigad (2011), Fabric development in a weathering profile at a basement–cover interface, the sub-Cambrian peneplain, Israel: Implications for decollement tectonics, *Journal of Structural Geology*, **33** (5), 819-832, doi: 10.1016/j.jsg.2011.03.010.

Antics, M., and B. Sanner (2007), Status of Geothermal Energy Use and Resources in Europe, paper presented at European Geothermal Congress, Unterhaching, Germany, 30 May - 1 June 2007.

Ayala Marín, C.-A., and C.-C. García-Yela (2010), Methodology to design of synthetic sonic logs (SSL) using artificial neural networks. Colorado field application., *CT&F - Ciencia, Tecnología y Futuro*, **4**, 21-31.

Babcock, E. A. (1978), Measurement of subsurface fractures from dipmeter logs, *AAPG Bulletin*, **62** (7), 15.

Bachmann, C., S. Wiemer, B. Goertz-Allmann, J. Woessner, and B. Mena (2012), Why geothermal energy research needs statistical seismology, paper presented at Thirty-Seventh Workshop on Geothermal Reservoir Engineering, Stanford University, Stanford, California, January 30 - February 1.

Baillieux, P. (2012), Multidisciplinary approach to understand the localization of geothermal anomalies in the Upper Rhine Graben from regional to local scale, PhD Thesis thesis, 131 pp, University of Neuchâtel, Neuchâtel.

Baisch, S., R. Voros, E. Rothert, H. Stang, R. Jung, and R. Schellschmidt (2010), A numerical model for fluid injection induced seismicity at Soultz-sous-Forets, *International Journal of Rock Mechanics and Mining Sciences*, **47** (3), 405-413, doi: 10.1016/j.ijrmms.2009.10.001.

Baldwin, J. L., C. L. Wheatley, and R. M. Bateman (1990), Application Of A Neural Network To The Problem Of Mineral Identification From Well Logs, *The Log Analyst*, **31** (5), 279-293.

Bartier, D., B. Ledésert, N. Clauer, A. Meunier, N. Liewig, G. Morvan, and A. Addad (2008), Hydrothermal alteration of the Soultz-sous-Forêts granite (Hot Fractured Rock geothermal exchanger) into a tosudite and illite assemblage, *Eur J Mineral*, **20**, 131–142, doi: 10.1127/0935-1221/2008/0020-1787.

Baumgärtner, J., R. Jung, T. Hettkamp, and D. Teza (2004), The status of the hot dry rock scientific power plant at Soultz-sous-Forêts, *Zeitschrift für angewandte Geologie*, **50** (2), 5.

Benaouda, D., G. Wadge, R. B. Whitmarsh, R. G. Rothwell, and C. MacLeod (1999), Inferring the lithology of borehole rocks by applying neural network classifiers to downhole logs: an example from the Ocean Drilling Program, *Geophys J Int*, **136** (2), 477-491, doi: 10.1046/j.1365-246X.1999.00746.x.

Biegel, R. L., C. G. Sammis, and J. H. Dieterich (1989), The frictional properties of a simulated gouge having a fractal particle distribution, *Journal of Structural Geology*, **11** (7), 827-846, doi: 10.1016/0191-8141(89)90101-6.

Blanpied, M. L., D. A. Lockner, and J. D. Byerlee (1995), Frictional slip of granite at hydrothermal conditions, *Journal of Geophysical Research: Solid Earth*, **100** (B7), 13045-13064, doi: 10.1029/95jb00862.

Boness, N. L., and M. D. Zoback (2006), A multiscale study of the mechanisms controlling shear velocity anisotropy in the San Andreas Fault Observatory at Depth, *Geophysics*, **71** (5), F131-F146, doi: 10.1190/1.2231107.

Bourouis, S., and P. Bernard (2007), Evidence for coupled seismic and aseismic fault slip during water injection in the geothermal site of Soultz (France), and implications for seismogenic transients, *Geophys J Int*, **169** (2), 723-732, doi: 10.1111/j.1365-246X.2006.03325.x.

Boussinesq, J. (1877), Essai sur la théorie des eaux courantes, *Mémoires présentés par divers savants à l'Académie des Sciences de l'Institut national de France*, **23**, 681.

Brousse, R., and H. Bellon (1983), Réflexions chronologiques et pétrologiques sur le volcanisme associé au développement des rifts de France, *Bull. Centres Rech. Explor.-Prod. Elf-Aquitaine*, **7** (1), 409-424.

Brudy, M., M. D. Zoback, K. Fuchs, F. Rummel, and J. Baumgartner (1997), Estimation of the complete stress tensor to 8 km depth in the KTB scientific drill holes: Implications for crustal strength, *Journal of Geophysical Research - Solid Earth*, **102** (B8), 18453-18475, doi: 10.1029/96jb02942.

Brune, J. N. (1968), Seismic moment, seismicity, and rate of slip along major fault zones, *Journal of Geophysical Research*, **73** (2), 777-784, doi: 10.1029/JB073i002p00777.

Byerlee, J. D. (1978), Friction of rocks, *Pure and Applied Geophysics*, **116** (4), 615-626, doi: 10.1007/bf00876528.

Byerlee, J. D., and J. C. Savage (1992), Coulomb plasticity within the fault zone, *Geophys. Res. Lett.*, **19** (23), 2341-2344, doi: 10.1029/92gl02370.

Calò, M., C. Dorbath, and M. Frogneux (2014), Injection tests at the EGS reservoir of Soultz-sous-Forêts. Seismic response of the GPK4 stimulations, *Geothermics*, **52** (0), 50-58, doi: 10.1016/j.geothermics.2013.10.007.

Calò, M., C. Dorbath, F. H. Cornet, and N. Cuenot (2011), Large-scale aseismic motion identified through 4-D P-wave tomography, *Geophys J Int*, **186** (3), 1295-1314, doi: 10.1111/j.1365-246X.2011.05108.x.

Cappa, F., and J. Rutqvist (2012), Seismic rupture and ground accelerations induced by CO2 injection in the shallow crust, *Geophys J Int*, **190** (3), 1784-1789, doi: 10.1111/j.1365-246X.2012.05606.x.

Cataldi, F., M. A. Meier, and S. Wiemer (2013), The role of Coulomb stress changes for injection-induced seismicity: The Basel enhanced geothermal system, *Geophysical Research Letters*, **40** (1), 72-77, doi: 10.1029/2012gl054147.

Chang, S.-H., J.-P. Avouac, S. Barbot, and J.-C. Lee (2013), Spatially variable fault friction derived from dynamic modeling of aseismic afterslip due to the 2004 Parkfield earthquake, *Journal of Geophysical Research: Solid Earth*, **118** (7), 3431-3447, doi: 10.1002/jgrb.50231.

Charléty, J., N. Cuenot, L. Dorbath, C. Dorbath, H. Haessler, and M. Frogneux (2007), Large earthquakes during hydraulic stimulations at the geothermal site of Soultz-sous-Forêts, *International Journal of Rock Mechanics and Mining Sciences*, **44** (8), 1091-1105, doi: 10.1016/j.ijrmms.2007.06.003.

Charlez, P., P. Lemonnier, C. Ruffet, M. J. Bouteca, and C. Tan (1996), Thermally Induced Fracturing: Analysis of a Field Case in North Sea, in *European Petroleum Conference*, edited, Society of Petroleum Engineers, Milan, Italy.

Chawathe, A. (1994), The Application of Kohonen Type Self Organization Algorithm to Formation Evaluation, paper presented at SPE Eastern Regional Meeting, , Society of Petroleum Engineers, Inc., Charleston, West Virginia, 8-10 November.

Chéry, J., M. D. Zoback, and S. Hickman (2004), A mechanical model of the San Andreas fault and SAFOD Pilot Hole stress measurements, *Geophysical Research Letters*, **31** (15), L15S13, doi: 10.1029/2004gl019521.

Cho, W.-J., J.-O. Lee, and S. Kwon (2010), Analysis of thermo–hydro–mechanical process in the engineered barrier system of a high-level waste repository, *Nuclear Engineering and Design*, **240** (6), 1688-1698, doi: 10.1016/j.nucengdes.2010.02.027.

Cochocki, A., and R. Unbehauen (1993), *Neural Networks for Optimization and Signal Processing*, 1 ed., 544 pp., John Wiley & Sons, Inc.

Cornell, R. M., and U. Schwertmann (2003), *The Iron Oxides: Structure, Properties, Reactions, Occurrences and Uses*, 2 ed., 703 pp., Wiley-VCH, Weinheim.

Cornet, F. H. (2012), The relationship between seismic and aseismic motions induced by forced fluid injections, *Hydrogeol J*, **20** (8), 1463-1466, doi: 10.1007/s10040-012-0901-z.

Cornet, F. H., and T. Roeckel (2012), Vertical stress profiles and the significance of "stress decoupling", *Tectonophysics*, **581**, 13, doi: 10.1016/j.tecto.2012.01.020.

Cornet, F. H., T. Bérard, and S. Bourouis (2007), How close to failure is a granite rock mass at a 5 km depth?, *International Journal of Rock Mechanics and Mining Sciences*, **44** (1), 47-66, doi: 10.1016/j.ijrmms.2006.04.008.

Cornet, F. H., J. Helm, H. Pointrenaud, and A. Etchecopar (1997), Seismic and Aseismic Slips Induced by Large-scale Fluid Injections, *Pure and Applied Geophysics*, **150** (3), 563-583, doi: 10.1007/s000240050093.

Crawford, B. R., D. R. Faulkner, and E. H. Rutter (2008), Strength, porosity, and permeability development during hydrostatic and shear loading of synthetic quartz-clay fault gouge, *Journal of Geophysical Research: Solid Earth*, **113** (B3), B03207, doi: 10.1029/2006jb004634.

Cuenot, N., C. Dorbath, and L. Dorbath (2008), Analysis of the Microseismicity Induced by Fluid Injections at the EGS Site of Soultz-sous-Forêts (Alsace, France): Implications for the Characterization of the Geothermal Reservoir Properties, *Pure and Applied Geophysics*, **165** (5), 797-828, doi: 10.1007/s00024-008-0335-7.

Dezayes, C., S. Gentier, and A. Genter (2005a), Deep Geothermal Energy in Western Europe: The Soultz Project, *Rep. RP-54227*, 48 pp.

Dezayes, C., A. Genter, and B. Valley (2010a), Overview of the Fracture Network at Different Scales Within the Granite Reservoir of the EGS Soultz Site (Alsace, France), paper presented at World Geothermal Congress, Bali, Indonesia, 25-29th April, 2010.

Dezayes, C., A. Genter, and B. Valley (2010b), Structure of the low permeable naturally fractured geothermal reservoir at Soultz, *Cr Geosci*, **342** (7-8), 517-530, doi: 10.1016/j.crte.2009.10.002.

Dezayes, C., T. Villemin, A. Genter, and J. Angelier (1996), Origin and significance of relaxation fractures in EPS1 granite core sections (Soultz-sous-Forets, Rhinegraben), *Cr Acad Sci Ii A*, **323** (4), 333-340.

Dezayes, C., B. Valley, E. Maqua, G. Syren, and A. Genter (2000), Natural Fracture System of the Soultz Granite Based on UBI Data in the GPK3 and GPK4 Wells, *Rep.*, 11 pp, BRGM.

Dezayes, C., A. Genter, G. Homeier, M. Degouy, and G. Stein (2003), Geological study of GPK3 HFR borehole (Soultz-sous-Forêts, France), *Public Document Rep.*, 128 pp, BRGM, Orleans.

Dezayes, C., P. Chèvremont, B. Tourlière, G. Homeier, and A. Genter (2005b), Geological study of the GPK4 HFR borehole and correlation with the GPK3 borehole (Soultz-sous-Forêts, France), *Public Document Rep.*, 94 pp, BRGM, Orleans.

Dèzes, P., S. M. Schmid, and P. A. Ziegler (2004), Evolution of the European Cenozoic Rift System: interaction of the Alpine and Pyrenean orogens with their foreland lithosphere, *Tectonophysics*, **389** (1–2), 1-33, doi: 10.1016/j.tecto.2004.06.011.

Dieterich, J. H. (1978), Time-dependent friction and the mechanics of stick-slip, *Pure and Applied Geophysics*, **116** (4-5), 790-806, doi: 10.1007/bf00876539.

Dingding, C., J. Quirein, H. Smith, S. Hamid, J. Grable, and S. Reed (2006), Variable Input Neural Network Ensembles in Generating Synthetic Well Logs, paper presented at IJCNN '06. International Joint Conference on Neural Networks, July 16-21.

Dolan, J. F., K. Sieh, T. K. Rockwell, R. S. Yeats, J. Shaw, J. Suppe, G. J. Huftile, and E. M. Gath (1995), Prospects for Larger or More Frequent Earthquakes in the Los Angeles Metropolitan Region, *Science*, **267** (5195), 199-205, doi: 10.1126/science.267.5195.199.

Dorbath, L., N. Cuenot, A. Genter, and M. Frogneux (2009), Seismic response of the fractured and faulted granite of Soultz-sous-Forets (France) to 5 km deep massive water injections, *Geophys J Int*, **177** (2), 653-675, doi: 10.1111/j.1365-246X.2009.04030.x.

Dubois, M., B. Ledésert, J.-L. Potdevin, and S. Vançon (2000), Détermination des conditions de précipitation des carbonates dans une zone d'altération du granite de Soultz (soubassement du fossé Rhénan, France) : l'enregistrement des inclusions fluides, *Comptes Rendus de l'Académie des Sciences - Series IIA - Earth and Planetary Science*, **331** (4), 303-309, doi: 10.1016/S1251-8050(00)01429-4.

Dubois, M., M. Ayt Ougougdal, P. Meere, J.-J. Royer, M.-C. Boiron, and M. Cathelineau (1996), Temperature of paleo- to modern self-sealing within a continental rift basin; the fluid inclusion data (Soultz-sous-Forets, Rhine Graben, France), *Eur J Mineral*, **8** (5), 1065-1080.

Duebendorfer, E. M., J. Vermilye, P. A. Geiser, and T. L. Davis (1998), Evidence for aseismic deformation in the western Transverse Ranges, southern California: Implications for seismic risk assessment, *Geology*, **26** (3), 271-274, doi: 10.1130/0091-7613(1998)026.

Dunlop, D. J., and Ö. Özdemir (1997), *Rock Magnetism*, 1 ed., 595 pp., Cambridge University Press.

Dyer, B. C., R. Baria, and S. Michelet (2003), Soultz GPK3 stimulation and GPK3-GPK2 circulation May to July 2003 seismic monitoring report, *Rep.*, 69 pp, GEIE

Economides, M. J., K. G. Nolte, and U. Ahmed (1989), *Reservoir stimulation*, 2 ed., 416 pp., Prentice Hall, Michigan.

Edel, J. B., K. Schulmann, E. Skrzypek, and A. Cocherie (2013), Tectonic evolution of the European Variscan belt constrained by palaeomagnetic, structural and anisotropy of magnetic susceptibility data from the Northern Vosges magmatic arc (eastern France), *Journal of the Geological Society*, **170** (5), 785-804, doi: 10.1144/jgs2011-138.

EGEC (2011), Deep Geothermal Market Report 2011, *Rep.*, 48 pp, Bruxelles.

Ellis, D. V., and J. M. Singer (2007), *Well Logging for Earth Scientists*, second edition ed., 692 pp., Springer, Dordrecht, The Netherlands.

Evans, K. F. (2005), Permeability creation and damage due to massive fluid injections into granite at 3.5 km at Soultz: 2. Critical stress and fracture strength, *J. Geophys. Res.*, **110** (B4), B04204, doi: 10.1029/2004jb003169.

Evans, K. F., A. Genter, and J. Sausse (2005a), Permeability creation and damage due to massive fluid injections into granite at 3.5 km at Soultz: 1. Borehole observations, *J Geophys Res-Sol Ea*, **110** (B04203), 19, doi: 10.1029/2004jb003168.

Evans, K. F., H. Moriya, H. Niitsuma, R. H. Jones, W. S. Phillips, A. Genter, J. Sausse, R. Jung, and R. Baria (2005b), Microseismicity and permeability enhancement of hydrogeologic structures during massive fluid injections into granite at 3 km depth at the Soultz HDR site, *Geophys J Int*, **160** (1), 389-412, doi: 10.1111/j.1365-246X.2004.02474.x.

Fabriol, H., A. Beauce, A. Genter, and R. Jones (1994), Induced Microseismicity and Its Relation with Natural Fractures - the HDR Example of Soultz (France), in *Geothermal Resources Council*, edited, pp. 423-430.

Faulkner, D. R., and E. H. Rutter (1998), The gas permeability of clay-bearing fault gouge at 20°C, *Geological Society, London, Special Publications*, **147** (1), 147-156, doi: 10.1144/gsl.sp.1998.147.01.10.

Faulkner, D. R., and E. H. Rutter (2000), Comparisons of water and argon permeability in natural clay-bearing fault gouge under high pressure at 20°C, *Journal of Geophysical Research: Solid Earth*, **105** (B7), 16415-16426, doi: 10.1029/2000jb900134.

Faulkner, D. R., and E. H. Rutter (2003), The effect of temperature, the nature of the pore fluid, and subyield differential stress on the permeability of phyllosilicate-rich fault gouge, *Journal of Geophysical Research: Solid Earth*, **108** (B5), 2227, doi: 10.1029/2001jb001581.

Faulkner, D. R., C. A. L. Jackson, R. J. Lunn, R. W. Schlische, Z. K. Shipton, C. A. J. Wibberley, and M. O. Withjack (2010), A review of recent developments concerning the structure, mechanics and fluid flow properties of fault zones, *Journal of Structural Geology*, **32** (11), 1557-1575, doi: 10.1016/j.jsg.2010.06.009.

Fourcade, S., J. L. Michelot, S. Buschaert, M. Cathelineau, R. Freiberger, Y. Coulibaly, and J. F. Aranyossy (2002), Fluid transfers at the basement/cover interface: Part I. Subsurface recycling of trace carbonate from granitoid basement rocks (France), *Chemical Geology*, **192** (1–2), 99-119, doi: 10.1016/S0009-2541(02)00192-4.

Freund, D. (1992), Ultrasonic compressional and shear velocities in dry clastic rocks as a function of porosity, clay content, and confining pressure, *Geophys J Int*, **108** (1), 125-135, doi: 10.1111/j.1365-246X.1992.tb00843.x.

Fritz, B., E. Jacquot, B. Jacquemont, A. Baldeyrou-Bailly, M. Rosener, and O. Vidal (2010), Geochemical modelling of fluid-rock interactions in the context of the Soultz-sous-Forêts geothermal system, *Cr Geosci*, **342** (7-8), 653-667, doi: 10.1016/j.crte.2010.02.005.

Galushkin, A. I. (2007), *Neural Network Theory*, 420 pp., Springer.

Garagash, D. I., and L. N. Germanovich (2012), Nucleation and arrest of dynamic slip on a pressurized fault, *Journal of Geophysical Research: Solid Earth*, **117** (B10), B10310, doi: 10.1029/2012jb009209.

Gendler, T. S., V. P. Shcherbakov, M. J. Dekkers, A. K. Gapeev, S. K. Gribov, and E. McClelland (2005), The lepidocrocite–maghemite–haematite reaction chain—I. Acquisition of chemical remanent magnetization by maghemite, its magnetic properties and thermal stability, *Geophys J Int*, **160** (3), 815-832, doi: 10.1111/j.1365-246X.2005.02550.x.

Genter, A., and H. Traineau (1991), Geological survey of the HDR borehole EPS-1, Soultz-sous-Forêts, Alsace-France, *Rep.*, 25 pp, BRGM, Orléans.

Genter, A., and H. Traineau (1992), Hydrothermally altered and fractured granite as an HDR reservoir in the EPS-1 borehole, Alsace, France, paper presented at Seventeenth Workshop on Geothermal Reservoir Engineering, Stanford University, Stanford, California, January, 1992.

Genter, A., and H. Traineau (1993), Deepening of GPK-1 HDR borehole 2000-3600m (Soultz-sous-Forêts, France), Geological Monitoring, *Rep.*, 25 pp, BRGM, Orléans.

Genter, A., and H. Tenzer (1995), Geological monitoring of GPK-2 HDR borehole, 1420-3880m, (Soultz-sous-Forêts, France), *Rep.*, 46 pp.

Genter, A., and H. Traineau (1995), Fracture analysis in Granite in the HDR Geothermal EPS-1 Well, Soultz-Sous-Forets, France, *BRGM Rapport* (R-38598), 53.

Genter, A., and H. Traineau (1996), Analysis of macroscopic fractures in granite in the HDR geothermal well EPS-1, Soultz-sous-Forêts, France, *J Volcanol Geoth Res*, **72** (1-2), 121-141, doi: 10.1016/0377-0273(95)00070-4.

Genter, A., H. Traineau, B. Ledésert, B. Bourgine, and S. Gentier (2000), Over 10 Years of Geological Investigations withing the HDR Soultz Project, France, paper presented at World Geothermal Congress 2000, Kyushu - Tohoku, Japan, May 28 - June 10.

Genter, A., K. Evans, N. Cuenot, D. Fritsch, and B. Sanjuan (2010), Contribution of the exploration of deep crystalline fractured reservoir of Soultz to the knowledge of enhanced geothermal systems (EGS), *Cr Geosci*, **342** (7-8), 502-516, doi: 10.1016/j.crte.2010.01.006.

Genter, A., L. Guillou-Frottier, J.-L. Feybesse, N. Nicol, C. Dezayes, and S. Schwartz (2003), Typology of potential Hot Fractured Rock resources in Europe, *Geothermics*, **32** (4-6), 701-710, doi: 10.1016/s0375-6505(03)00065-8.

Genter, A., N. Cuenot, B. Melchert, W. Moeckes, G. Ravier, B. Sanjuan, R. Sanjuan, J. Scheiber, E. Schill, and J. Schmittbuhl (2013), Main achievements from the multi-well EGS Soultz project during geothermal exploitation from 2010 and 2012, paper presented at European Geothermal Congress 2013, Pisa, Italy, 3-7 June.

Gischig, V., S. Wiemer, and A. Alcolea (2014), Balancing reservoir creation and seismic hazard in enhanced geothermal systems, *Geophys J Int*, **198** (3), 1585-1598, doi: 10.1093/gji/ggu221.

Groos, J., J. Zeiß, M. Grund, and J. Ritter (2013), Microseismicity at two geothermal power plants in Landau and Insheim in the Upper Rhine Graben, Germany, paper presented at EGU General Assembly 2013, Vienna, 7-12 April.

Guillou-Frottier, L., C. Carre, B. Bourgine, V. Bouchot, and A. Genter (2013), Structure of hydrothermal convection in the Upper Rhine Graben as inferred from corrected temperature data and basin-scale numerical models, *J Volcanol Geoth Res*, **256**, 29-49, doi: 10.1016/j.jvolgeores.2013.02.008.

Gutenberg, B., and C. F. Richter (1942), Earthquake magnitude, intensity, energy, and acceleration, *Bulletin of the Seismological Society of America*, **32** (3), 163-191.

Gutenberg, B., and C. Richter (1954), *Seismicity of the Earth and Associated Phenomena*, 1 ed., 310 pp., Princeton University Press, Princeton.

Haas, I. O., and R. Hoffmann (1929), Temperature Gradient in Pechelbronn Oil-Bearing Region, Lower Alsace: Its Determination and Relation to Oil Reserves, *AAPG Bulletin*, **13** (10), 16.

Häring, M. O., U. Schanz, F. Ladner, and B. C. Dyer (2008), Characterisation of the Basel 1 enhanced geothermal system, *Geothermics*, **37** (5), 469-495, doi: 10.1016/j.geothermics.2008.06.002.

Haykin, S. S. (1999), *Neural Networks: A Comprehensive Foundation*, Prentice Hall International.

Heinicke, J., T. Fischer, R. Gaupp, J. Götze, U. Koch, H. Konietzky, and K.-P. Stanek (2009), Hydrothermal alteration as a trigger mechanism for earthquake swarms: the Vogtland/NW Bohemia region as a case study, *Geophys J Int*, **178** (1), 1-13, doi: 10.1111/j.1365-246X.2009.04138.x.

Holmes, R. R., et al. (2013), U.S. Geological Survey natural hazards science strategy—Promoting the safety, security, and economic well-being of the Nation, *Rep.*, 79 pp.

Hooijkaas, G. R., A. Genter, and C. Dezayes (2006), Deep-seated geology of the granite intrusions at the Soultz EGS site based on data from 5 km-deep boreholes, *Geothermics*, **35** (5-6), 484-506, doi: 10.1016/j.geothermics.2006.03.003.

Hrouda, F. (2003), Indices for Numerical Characterization of the Alteration Processes of Magnetic Minerals Taking Place During Investigation of Temperature Variation of Magnetic Susceptibility, *Studia Geophysica et Geodaetica*, **47** (4), 847-861, doi: 10.1023/a:1026398920172.

IEA (2011), Technology Roadmap - Geothermal Heat and Power, *Rep.*, 52 pp, OECD/IEA, Paris, France.

Ikari, M. J., D. M. Saffer, and C. Marone (2009), Frictional and hydrologic properties of clay-rich fault gouge, *Journal of Geophysical Research: Solid Earth*, **114** (B5), B05409, doi: 10.1029/2008jb006089.

Ikari, M. J., C. Marone, and D. M. Saffer (2011), On the relation between fault strength and frictional stability, *Geology*, **39** (1), 83-86, doi: 10.1130/g31416.1.

Illies, H. (1975), Intraplate tectonics in stable Europe as related to plate tectonics in the Alpine system, *Geol Rundsch*, **64** (1), 677-699, doi: 10.1007/bf01820690.

Inoue, A., M. Utada, and K. Wakita (1992), Smectite-to-illite conversion in natural hydrothermal systems, *Applied Clay Science*, **7** (1-3), 131-145, doi: 10.1016/0169-1317(92)90035-l.

IPCC (2014), Mitigation of Climate Change. Contribution of Working Group III to the Fifth Assessment Report of the Intergovernmental Panel on Climate Change, *Rep.*, Cambridge, United Kingdom and New York, NY, USA.

Ishihara, S. (1977), The Magnetite-series and Ilmenite-series Granitic Rocks, *Mining Geology*, **27** (145), 293-305.

Jaeger, J. C., N. G. W. Cook, and R. W. Zimmermann (2007), *Fundamentals of Rock Mechanics*, 4th edition ed., 475 pp., Blackwell Publishing, Malden MA, USA.

Janecke, S. U., and J. P. Evans (1988), Feldspar-influenced rock rheologies, *Geology*, **16** (12), 1064-1067, doi: 10.1130/0091-7613(1988)016.

Jones, R. H., A. Beauce, A. Jupe, H. Fabriol, and B. C. Dyer (1995), Imaging Induced Microseismicity During the 1993 Injection Tests at Soultz-Sous-forets, France paper presented at World Geothermal Congress, Florence, Italy, 18-31 May 1995.

Just, J. (2005), Modification of magnetic properties in granite during hydrothermal alteration (EPS-1 borehole, Upper Rhine Graben), PhD Thesis thesis, 105 pp, University of Heidelberg, Heidelberg.

Just, J., and A. Kontny (2012), Thermally induced alterations of minerals during measurements of the temperature dependence of magnetic susceptibility: a case study from the hydrothermally altered Soultz-sous-Forêts granite, France, *Int J Earth Sci (Geol Rundsch)*, **101** (3), 819-839, doi: 10.1007/s00531-011-0668-9.

Just, J., A. Kontny, H. De Wall, A. M. Hirt, and F. Martín-Hernández (2004), Development of magnetic fabrics during hydrothermal alteration in the Soultz-sous-Forêts granite from the EPS-1 borehole, Upper Rhine Graben, *Geological Society, London, Special Publications*, **238** (1), 509-526, doi: 10.1144/gsl.sp.2004.238.01.26.

Kalfayan, L. (2008), *Production Enhancement with Acid Stimulation*, PennWell.

Kanamori, H., and E. E. Brodsky (2004), The physics of earthquakes, *Reports on Progress in Physics*, **67** (8), doi: 10.1088/0034-4885/67/8/R03.

Kohl, T., and T. Mégel (2007), Predictive modeling of reservoir response to hydraulic stimulations at the European EGS site Soultz-sous-Forêts, *International Journal of Rock Mechanics and Mining Sciences*, **44** (8), 1118-1131, doi: 10.1016/j.ijrmms.2007.07.022.

Kohl, T., K. F. Evans, R. J. Hopkirk, R. Jung, and L. Rybach (1997), Observation and simulation of non-Darcian flow transients in fractured rock, *Water Resources Research*, **33** (3), 407-418, doi: 10.1029/96wr03495.

Kohl, T., S. Signorelli, I. Engelhardt, N. A. Berthoud, S. Sellami, and L. Rybach (2005), Development of a regional geothermal resource atlas, *Journal of Geophysics and Engineering*, **2** (4), 372-385.

Kohli, A. H., and M. D. Zoback (2013), Frictional properties of shale reservoir rocks, *Journal of Geophysical Research: Solid Earth*, **118** (9), 5109-5125, doi: 10.1002/jgrb.50346.

Kohonen, T. (1984), *Self-organization and associative memory*, 1 ed., 255 pp., Springer, Berlin.

Kohonen, T. (2001), *Self-Organizing Maps*, 1 ed., 528 pp., Springer-Verlag New York, Inc.

Koleini, M., J. Rooy, and A. Bumby (2012), Slope stability modelling and landslide hazard zonation at the Seymareh dam and power plant project, west of Iran, *Bull Eng Geol Environ*, **71** (4), 691-701, doi: 10.1007/s10064-012-0437-4.

Kontny, A., H. de Wall, T. G. Sharp, and M. Pósfai (2000), Mineralogy and magnetic behavior of pyrrhotite from a 260 °C section at the KTB drilling site, Germany, *Am Mineral*, **85** (10), 1416-1427.

Lagoeiro, L. E. (1998), Transformation of magnetite to hematite and its influence on the dissolution of iron oxide minerals, *Journal of Metamorphic Geology*, **16** (3), 415-423, doi: 10.1111/j.1525-1314.1998.00144.x.

Langenbruch, C., and S. A. Shapiro (2014), Gutenberg-Richter relation originates from Coulomb stress fluctuations caused by elastic rock heterogeneity, *Journal of Geophysical Research: Solid Earth*, **119** (B2), 15, doi: 10.1002/2013jb010282.

Lawrence, S., C. L. Giles, T. Ah Chung, and A. D. Back (1997), Face recognition: a convolutional neural-network approach, *Neural Networks, IEEE Transactions on*, **8** (1), 98-113, doi: 10.1109/72.554195.

Ledésert, B., G. Berger, A. Meunier, A. Genter, and A. Bouchet (1999), Diagenetic-type reactions related to hydrothermal alteration in the Soultz-sous-Forets granite, France, *Eur J Mineral*, **11** (4), 731-741, doi: 10.1127/ejm/11/4/0731.

Ledésert, B., J. Joffre, A. Amblès, P. Sardini, A. Genter, and A. Meunier (1996), Organic matter in the Soultz HDR granitic thermal exchanger (France): natural tracer of fluid circulations between the basement and its sedimentary cover, *J Volcanol Geoth Res*, **70** (3-4), 235-253, doi: 10.1016/0377-0273(95)00058-5.

Ledésert, B., R. Hebert, A. Genter, D. Bartier, N. Clauer, and C. Grall (2010), Fractures, hydrothermal alterations and permeability in the Soultz Enhanced Geothermal System, *Cr Geosci*, **342** (7-8), 607-615, doi: 10.1016/j.crte.2009.09.011.

Maiti, S., R. Krishna Tiwari, and H.-J. Kümpel (2007), Neural network modelling and classification of lithofacies using well log data: a case study from KTB borehole site, *Geophys J Int*, **169** (2), 733-746, doi: 10.1111/j.1365-246X.2007.03342.x.

Majer, E. L., R. Baria, M. Stark, S. Oates, J. Bommer, B. Smith, and H. Asanuma (2007), Induced seismicity associated with Enhanced Geothermal Systems, *Geothermics*, **36** (3), 185-222, doi: 10.1016/j.geothermics.2007.03.003.

Meixner, J., E. Schill, E. Gaucher, and T. Kohl (2014), Inferring the in situ stress regime in deep sediments: an example from the Bruchsal geothermal site, *Geothermal Energy*, **2** (1), 1-17, doi: 10.1186/s40517-014-0007-z.

Meller, C., and T. Kohl (2014), The significance of hydrothermal alteration zones for the mechanical behavior of a geothermal reservoir, *Geothermal Energy*, **2** (12), 21, doi: 10.1186/s40517-014-0012-2.

Meller, C., A. Kontny, and T. Kohl (2014a), Identification and characterization of hydrothermally altered zones in granite by combining synthetic clay content logs with magnetic mineralogical investigations of drilled rock cuttings, *Geophys J Int*, **199** (1), 465-479, doi: 10.1093/gji/ggu278.

Meller, C., A. Genter, and T. Kohl (2014b), The application of a neural network to map clay zones in crystalline rock, *Geophys J Int*, **196** (2), 837-849, doi: 10.1093/gji/ggt423.

Meller, C., T. Kohl, E. Gaucher, and A. Genter (2012), Approach for determination of the failure probability of fractures at the Soultz-sous-Forêts EGS project, paper presented at Thirty-Seventh Workshop on Geothermal Reservoir Engineering, Stanford University, Stanford, California, January 30 - February 1, 2012.

Meunier, A. (2005), *Clays*, 1 ed., 472 pp., Springer, Berlin.

Mokni, N., S. Olivella, J. Carrera, and B. Otto (2012), Surface movements in a rock massif induced by drainage associated to tunnel excavation, *International Journal for Numerical and Analytical Methods in Geomechanics*, **37** (9), 1162-1188, doi: 10.1002/nag.2082.

Moore, D. E., and D. A. Lockner (2007), Friction of the Smectite Clay Montmorillonite: A review and interpretation of data, in *The Seismogenic Zone of Subduction Thrust Faults*, edited by T. Dixon, pp. 317-345, Columbia Univ. Press, New York.

Moore, D. E., and D. A. Lockner (2013), Chemical controls on fault behavior: Weakening of serpentinite sheared against quartz-bearing rocks and its significance for fault creep in the San Andreas system, *J Geophys Res-Sol Ea*, **118** (5), 2558-2570, doi: 10.1002/jgrb.50140.

Morrow, C., B. Radney, and J. Byerlee (1992), Chapter 3 Frictional Strength and the Effective Pressure Law of Montmorillonite and lllite Clays, in *International Geophysics*, edited by E. Brian and W. Teng-fong, pp. 69-88, Academic Press.

Morrow, C. A., D. E. Moore, and D. A. Lockner (2001), Permeability reduction in granite under hydrothermal conditions, *Journal of Geophysical Research: Solid Earth*, **106** (B12), 30551-30560, doi: 10.1029/2000jb000010.

Mulargia, F., S. Castellaro, and M. Ciccotti (2004), Earthquakes as three stage processes, *Geophys J Int*, **158** (1), 98-108, doi: 10.1111/j.1365-246X.2004.02262.x.

Nami, P., R. Schellschmidt, M. Schindler, and T. Tischner (2008), Chemical Stimulation Operations for Reservoir Development of the Deep Crystalline HDR/EGS System at Soultz-sous-Forêts (France) paper presented at Thirty-Second Workshop on Geothermal Reservoir Engineering, Stanford University, Stanford, California, January 28-30, 2008.

Nikravesh, M. (1998), Neural Network Knowledge-Based Modeling of Rock Properties Based on Well Log Databases, paper presented at SPE Western Regional Meeting, Society of Petroleum Engineers Inc., Bakersfield, California, 10-13 May 1998.

Oliva-Urcia, B., A. Kontny, C. Vahle, and A. M. Schleicher (2011), Modification of the magnetic mineralogy in basalts due to fluid–rock interactions in a high-temperature geothermal system (Krafla, Iceland), *Geophys J Int*, **186** (1), 155-174, doi: 10.1111/j.1365-246X.2011.05029.x.

Pandarinath, K., R. Shankar, I. Torres-Alvarado, and A. Warrier (2013), Magnetic susceptibility of volcanic rocks in geothermal areas: application potential in geothermal exploration studies for identification of rocks and zones of hydrothermal alteration, *Arab J Geosci*, 1-10, doi: 10.1007/s12517-013-1013-3.

Petronis, M. S., B. O'Driscoll, and J. Lindline (2011), Late stage oxide growth associated with hydrothermal alteration of the Western Granite, Isle of Rum, NW Scotland, *Geochemistry, Geophysics, Geosystems*, **12** (1), Q01001, doi: 10.1029/2010gc003246.

Reches, Z. e., G. Baer, and Y. Hatzor (1992), Constraints on the strength of the upper crust from stress inversion of fault slip data, *Journal of Geophysical Research: Solid Earth*, **97** (B9), 12481-12493, doi: 10.1029/90jb02258.

REN21 (2013), Renewables 2013 Global Status Report, *Rep.*, 178 pp, Renewable Energy Policy Network for the 21st Century, Paris.

Revil, A., D. Hermitte, M. Voltz, R. Moussa, J. G. Lacas, G. Bourrié, and F. Trolard (2002), Self-potential signals associated with variations of the hydraulic head during an infiltration experiment, *Geophysical Research Letters*, **29** (7), 10-11-10-14, doi: 10.1029/2001gl014294.

Rey, G. D., and K. F. Wender (2011), *Neuronale Netze: eine Einführung in die Grundlagen, Anwendungen und Datenauswertung*, Huber.

Rice, J. R. (1992), Chapter 20 Fault Stress States, Pore Pressure Distributions, and the Weakness of the San Andreas Fault, in *International Geophysics*, edited by E. Brian and W. Teng-fong, pp. 475-503, Academic Press.

Rolon, L., S. D. Mohaghegh, S. Ameri, R. Gaskari, and B. McDaniel (2009), Using artificial neural networks to generate synthetic well logs, *Journal of Natural Gas Science and Engineering*, **1** (4–5), 118-133, doi: 10.1016/j.jngse.2009.08.003.

Ruina, A. (1983), Slip instability and state variable friction laws, *Journal of Geophysical Research: Solid Earth*, **88** (B12), 10359-10370, doi: 10.1029/JB088iB12p10359.

Rummel, F., and E. König (1991), Physical Properties of Core Samples Borehole EPS1 Soultz-sous-Forêts, Velocity-, Density- and Magnetic Susceptibility-Logs, Depth Interval 933-2227m, *Rep.*, 58 pp, Ruhr-University, Bochum.

Rummel, F., and D. Schreiber (1993), Physical Properties of the Core K21 Borehole GPK1 Soultz-sous-Forêts Depth Interval 3522.58-3525.88m, *Rep.*, 11 pp, Ruhr-University, Bochum.

Rummel, F., E. König, and E. Rybacki (1991), Physical Properties of Core Samples Borehole EPS1 Soultz-sous-Forêts, Velocity-, Density- and Magnetic Susceptibility-Logs, Depth Interval 1410-1980m, *Rep.*, 35 pp, Ruhr-University, Bochum.

Rummel, F., Klee, G. (1995), State of Stress at the European HDR Candidate Sites Urach and Soultz, in *World Geothermal Congress*, edited by E. e. a. Barbier, pp. 2639-2642, International Geothermal Association, Florence, Italy.

Sahara, D., M. Schoenball, T. Kohl, and B. Mueller (2014), Impact of fracture networks on borehole breakout heterogeneities in crystalline rock, *International Journal of Rock Mechanics and Mining Sciences*, **71**, 301-309, doi: 10.1016/j.ijrmms.2014.07.001.

Sausse, J. (2002), Hydromechanical properties and alteration of natural fracture surfaces in the Soultz granite (Bas-Rhin, France), *Tectonophysics*, **348** (1–3), 169-185, doi: 10.1016/s0040-1951(01)00255-4.

Sausse, J., and A. Genter (2005), Types of permeable fractures in granite, *Geological Society, London, Special Publications*, **240** (1), 1-14, doi: 10.1144/gsl.sp.2005.240.01.01.

Schill, E., T. Kohl, J. Geiermann, C. Baujard, S. Koch, H. Deckert, G. Munoz, and Y. Abdelfettah (2011), Multi-disciplinary prospection approach for EGS reservoirs in the German Variscan Basement, paper presented at Thirty-Sixth Workshop on Geothermal Reservoir Engineering, Stanford University, Stanford, California, 31 January - 2 February.

Schleicher, A., L. Warr, B. Kober, E. Laverret, and N. Clauer (2006a), Episodic mineralization of hydrothermal illite in the Soultz-sous-Forêts granite (Upper Rhine Graben, France), *Contributions to Mineralogy and Petrology*, **152** (3), 349-364, doi: 10.1007/s00410-006-0110-7.

Schleicher, A. M. (2005), Clay mineral formation and fluid-rock interaction in fractured crystalline rocks of the Rhine rift system : case studies from the Soultz-sous-Forêts granite (France) and the Schauenburg Fault (Germany), Inaugural Dissertation thesis, 114 pp, Ruprecht-Karls-Universität, Heidelberg.

Schleicher, A. M., B. A. Van der Pluijm, J. B. Solum, and L. N. Warr (2006b), Origin and significance of clay-coated fractures in mudrock fragments of the SAFOD borehole (Parkfield, California), *Geophysical Research Letters*, **33** (L16313), pp. 5, doi: 10.1029/2006GL026505.

Schmittbuhl, J., O. Lengliné, F. Cornet, N. Cuenot, and A. Genter (2013a), Seismic and aseismic slip in EGS reservoir: an experimental approach, in *Presentation at the 2nd European Geothermal Workshop*, edited, LABEX, G-EAU-THERMIE PROFONDE, Strasbourg.

Schmittbuhl, J., O. Lengliné, F. Cornet, N. Cuenot, and A. Genter (2014), Induced seismicity in EGS reservoir: the creep route, *Geothermal Energy* (in press).

Schmittbuhl, J., O. Lengliné, Zaepfel, F. H. Cornet, N. Cuenot, and A. Genter (2013b), Seismic and aseismic slip in EGS reservoir: an experimental approach, paper presented at European Geothermal Congress, Pisa, Italy, 3-7 June.

Schoenball, M., and T. Kohl (2013), The Peculiar Shut-In Behavior of the Well GPK2 at Soultz-sous-Forêts, in *37th Geothermal Resources Council*, edited, p. 4, Las Vegas.

Schoenball, M., C. Baujard, T. Kohl, and L. Dorbath (2012), The role of triggering by static stress transfer during geothermal reservoir stimulation, *Journal of Geophysical Research: Solid Earth*, **117** (B9), B09307, doi: 10.1029/2012jb009304.

Schoenball, M., L. Dorbath, E. Gaucher, J. F. Wellmann, and T. Kohl (2014), Change of stress regime during geothermal reservoir stimulation, *Geophysical Research Letters*, **41** (4), 1163-1170, doi: 10.1002/2013gl058514.

Scholz, C., P. Molnar, and T. Johnson (1972), Detailed studies of frictional sliding of granite and implications for the earthquake mechanism, *Journal of Geophysical Research*, **77** (32), 6392-6406, doi: 10.1029/JB077i032p06392.

Scholz, C. H. (2010), *The Mechanics of Earthquakes and Faulting*, 2 ed., 496 pp., Cambridge University Press, Cambridge.

Schorlemmer, D., and S. Wiemer (2005), Earth science Microseismicity data forecast rupture area, *Nature*, **434** (7037), 1086-1086, doi: 10.1038/4341086a.

Schorlemmer, D., S. Wiemer, and M. Wyss (2005), Variations in earthquake-size distribution across different stress regimes, *Nature*, **437** (7058), 539-542, doi: 10.1038/nature04094.

Schumacher, M. E. (2002), Upper Rhine Graben: Role of preexisting structures during rift evolution, *Tectonics*, **21** (1), 6-1-6-17, doi: 10.1029/2001tc900022.

Sharma, M. M., P. B. Gadde, R. Sullivan, R. Sigal, R. Fielder, D. Copeland, L. Griffin, and L. Weijers (2004), Slick Water and Hybrid Fracs in the Bossier: Some Lessons Learnt, in *SPE Annual Technical Conference and Exhibition*, edited, Society of Petroleum Engineers, Houston, Texas.

Sibson, R. H. (2009), Rupturing in overpressured crust during compressional inversion—the case from NE Honshu, Japan, *Tectonophysics*, **473** (3–4), 404-416, doi: 10.1016/j.tecto.2009.03.016.

Singh, S. (2005), Permeability Prediction Using Artificial Neural Network (ANN): A Case Study of Uinta Basin, paper presented at SPE Annual Technical Conference and Exhibition, Society of Petroleum Engineers, Dallas, Texas, 9-12 October 2005.

Smith, S. A. F., R. E. Holdsworth, C. Collettini, and J. Imber (2007), Using footwall structures to constrain the evolution of low-angle normal faults, *Journal of the Geological Society*, **164** (6), 1187-1191, doi: 10.1144/0016-76492007-009.

Stober, I., and K. Bucher (2012), *Geothermie*, 1 ed., 287 pp., Springer Verlag, Heidelberg.

Takahashi, M., K. Mizoguchi, K. Kitamura, and K. Masuda (2007), Effects of clay content on the frictional strength and fluid transport property of faults, *Journal of Geophysical Research: Solid Earth*, **112** (B8), B08206, doi: 10.1029/2006jb004678.

Tauxe, L. (1998), *Paleomagnetic Principles and Practice*, 1 ed., 301 pp., Springer Netherlands, Dordrecht, the Netherlands.

Taylor, R. M., and U. Schwertmann (1974), Maghemite in soils and its origin - II. Maghemite syntheses at ambient temperature and pH7, *Clay Minerals*, **10** (4), 13.

Tembe, S., D. A. Lockner, and T.-F. Wong (2010), Effect of clay content and mineralogy on frictional sliding behavior of simulated gouges: Binary and ternary mixtures of quartz, illite, and montmorillonite, *Journal of Geophysical Research: Solid Earth*, **115** (B3), B03416, doi: 10.1029/2009jb006383.

Tembe, S., D. A. Lockner, J. G. Solum, C. A. Morrow, T. F. Wong, and D. E. Moore (2006), Frictional strength of cuttings and core from SAFOD drillhole phases 1 and 2, *Geophysical Research Letters*, **33** (23), pp. 5, doi: 10.1029/2006gl027626.

Terzaghi, R. D. (1965), Sources of Error in Joint Surveys, *Geotechnique*, **15** (3), 287 – 304, doi: 10.1680/geot.1965.15.3.287

Tischner, T., M. Schindler, R. Jung, and P. Nami (2007), HDR Project Soultz: Hydraulic and seismic observations during stimulation of the 3 deep wells by massive water injections, paper presented at Thirty-Second Workshop on Geothermal Reservoir Engineering, Stanford University, Stanford, California, 22-24 January.

Titov, K., A. Tarasov, Y. Ilyin, N. Seleznev, and A. Boyd (2010), Relationships between induced polarization relaxation time and hydraulic properties of sandstone, *Geophys J Int*, **180** (3), 1095-1106, doi: 10.1111/j.1365-246X.2009.04465.x.

Valley, B. (2007), The relation between natural fracturing and stress heterogeneities in deep-seated crystalline rocks at Soultz-sous-Forêts (France) Dissertation thesis, 277 pp. pp, ETH Zürich, Zürich.

Valley, B., and K. Evans (2000), Stress estimates from analysis of breakouts and drilling-induced tension fractures in GPK1 and GPK4, *Rep.*, 5 pp, ETH, Zurich.

Valley, B., and K. Evans (2003), Strength and Elastic Properties of the Soultz Granite, *Rep.*, 6 pp, ETH Zürich, Zürich, Switzerland.

Valley, B., and K. F. Evans (2006), Strength and elastic properties of the Soultz granite, paper presented at EHDRA scientific conference, Soultz-sous-Forêts, France, 15-16 June 2006.

Valley, B., and K. F. Evans (2007), Stress state at Soultz-sous-Forêts to 5 km depth from wellbore failure and hydraulic observations, paper presented at 32nd workshop on geothermal reservoir engineering, Stanford.

Valley, B., and K. F. Evans (2010), Stress Heterogeneity in the Granite of the Soultz EGS Reservoir Inferred from Analysis of Wellbore Failure, paper presented at World Geothermal Congress, Bali, Indonesia.

Velde, B. (1977), *Clays and clay minerals in natural and synthetic systems*, 1 ed., 218 pp., Elsevier, Amsterdam [u.a.].

Velde, B. (Ed.) (1995), *Origin and Mineralogy of Clays*, 1 ed., Springer, Heidelberg.

Voisin, C., F. Cotton, and S. Di Carli (2004), A unified model for dynamic and static stress triggering of aftershocks, antishocks, remote seismicity, creep events, and multisegmented rupture, *Journal of Geophysical Research: Solid Earth*, **109** (B6), B06304, doi: 10.1029/2003jb002886.

Warpinski, N. R., M. J. Mayerhofer, M. C. Vincent, C. L. Cipolla, and E. P. Lolon (2009), Stimulating Unconventional Reservoirs: Maximizing Network Growth While Optimizing Fracture Conductivity, *Journal of Canadian Petroleum Technology*, **48** (10), 39-51, doi: 10.2118/114173-pa.

Wilkinson, M., and R. S. Haszeldine (2002), Fibrous illite in oilfield sandstones – a nucleation kinetic theory of growth, *Terra Nova*, **14** (1), 56-60, doi: 10.1046/j.1365-3121.2002.00388.x.

Wu, F. T. (1978), Mineralogy and physical nature of clay gouge, *Pure and Applied Geophysics*, **116** (4-5), 655-689, doi: 10.1007/bf00876531.

Wu, F. T., L. Blatter, and H. Roberson (1975), Clay gouges in the San Andreas Fault System and their possible implications, *Pure and Applied Geophysics*, **113** (1), 87-95, doi: 10.1007/bf01592901.

Zoback, M. D., and H.-P. Harjes (1997), Injection-induced earthquakes and crustal stress at 9 km depth at the KTB deep drilling site, Germany, *J. Geophys. Res.*, **102** (B8), 18477-18491, doi: 10.1029/96jb02814.

Zoback, M. D., A. Kohli, I. Das, and M. McClure (2012), The Importance of Slow Slip of Faults During Hydraulic-Fracturing Stimulation of Shale Gas Reservoirs in *Americas Unconventional Resources*, edited, p. 9, SPE, Stanford University, Pittsburgh, Pennsylvania.

A- DECLARATION OF AUTHORSHIP

APPROACH FOR DETERMINATION OF THE FAILURE PROBABILITY OF FRACTURES

Citation:

Meller, C., Kohl, T. and Gaucher, E. [2012] Approach for Determination of the Failure Probability at the Soultz-sous-Forêts EGS Project, in *Proceedings 37th Workshop on Geothermal Reservoir* Engineering, Stanford University, pp. 8, Stanford, California.

The first study was conducted as a feasibility study to determine the failure probability of fractures. The fracture data is courtesy of GEIE Soultz and BRGM, France. I analyzed the evolution of the critical pressure of fractures with depth using a Matlab-Code, using the Mohr-Coulomb criterion. The Matlab code was mainly developed in cooperation with Emmanuel Gaucher. I wrote the manuscript.

THE APPLICATION OF A NEURAL NETWORK TO MAP CLAY ZONES IN CRYSTALLINE ROCK

Citation:

Meller, C., Genter, A. and Kohl, T. [2014] The application of a neural network to map clay zones in crystalline rock. *Geophys J Int* **196** (2): 837-849. doi:10.1093/gji/ggt423.

This study was conducted within the portfolio topic GEOENERGIE of the Helmholtz Association of German Research Centres and was funded by Energie Baden-Wuerttemberg (EnBW), Germany. I created the synthetic logs using a neural network code implemented into the software Techlog (Schlumberger). The borehole logs are courtesy of GEIE Soultz and BRGM. I interpreted the results and wrote the manuscript.

IDENTIFICATION AND CHARACTERIZATION OF HYDROTHERMALLY ALTERED ZONES IN GRANITE

Citation:

Meller, C., Kontny, A. and Kohl, T. [2014] Identification and characterization of hydrothermally altered zones in granite by combining synthetic clay content logs with magnetic mineralogical investigations of drilled rock cuttings. *Geophys J Int* **199** (1), 465-479. doi: 10.1039/gji/ggu278.

This study was conducted within the portfolio topic GEOENERGIE of the Helmholtz Association of German Research Centres and was funded by Energie Baden-Wuerttemberg (EnBW), Germany. The cutting material and the borehole data is courtesy of BRGM, France and GEIE Soultz. I applied magnetic mineralogical methods following the thesis of Jana Just (2005) to characterize hydrothermal alteration of cuttings. The magnetic devices were provided by the Division Structural Geology at KIT and the electron microscopic analyses were conducted at LEM (KIT) supported by Volker Zibat (LEM). Thin sections were prepared for optical microscopic investigation by the preparators Stephan Unrein and Kristian Nikoloski (KIT). I conducted the measurements and made the microscopic investigations and created the SCCL logs with the neural network code of the previous study. Supported by Agnes Kontny I interpreted the magnetic measurements and microscopic analyses. I wrote the manuscript.

THE SIGNIFICANCE OF HYDROTHERMAL ALTERATION ZONES FOR THE MECHANICAL BEHAVIOR OF A GEOTHERMAL RESERVOIR

Citation:

Meller, C. and Kohl, T. [2014]. The significance of hydrothermal alteration zones for the mechanical behavior of a geothermal reservoir, *Geothermal Energy*, **2** (12): 21p. doi: 10.1186/s40517-014-0012-2

This study was conducted within the portfolio topic GEOENERGIE of the Helmholtz Association of German Research Centres and was funded by Energie Baden-Wuerttemberg (EnBW), Germany. I interpreted the SCCL logs on the basis of borehole breakout analyses by Sahara et al. [2014] and of the thesis of Valley [2000] and on borehole analyses mainly conducted by Evans [2005], Evans et al [2005a; 2005b] and Cornet et al. [1997]. Basis for the analysis were the seismic catalogues of GPK1 [*Jones et al.*, 1995] and GPK3 [*Dorbath et al.*, 2009]. Finally, I wrote the manuscript.

B- PUBLICATIONS

Meller, C. and Kohl, T. (2014) How synthetic clay content logs from well logs can help to assess the behavior of a geothermal reservoir upon hydrothermal stimulation, Proceedings World Geothermal Congress, 2015, *accepted* ***(Peer-reviewed)***

Meller, C. and Kohl, T (2014) The significance of hydrothermal alteration zones for the mechanical behavior of a geothermal reservoir, Geothermal Energy, 2 (12): 21. doi: 10.1186/s40517-014-0012-2 ***(Peer-reviewed)***

Meller, C., Kontny, A. and Kohl, T. (2014) Identification and characterization of hydrothermally altered zones in granite by combining synthetic clay content logs with magnetic mineralogical investigations of drilled rock cuttings. Geophys J Int 199 (1), 465-479. doi: 10.1039/gji/ggu278 ***(Peer-reviewed)***

Meller, C., Genter, A. and Kohl, T. (2014) The application of a neural network to map clay zones in crystalline rock. Geophys J Int 196 (2): 837-849. doi: 10.1093/gji/ggt423 ***(Peer-reviewed)***

Meller, C., Genter, A. and Kohl, T. (2013) A method to map clay zones in crystalline geothermal reservoirs-A Neural Network Based Approach Towards a Better Mechanical and Hydraulic Understanding of the Reservoir (trans: Jahrestagung des KITZE, Zentrum E). Impulse für die Zukunft der Energie: Wissenschaftliche Beiträge des KIT zur 2. Jahrestagung des KIT-Zentrums Energie. Doktorandensymposium, vol. 2. KIT Scientific Publishing, ISBN: 978-3-7315-0097-1

Meller, C., Kohl, T. and Gaucher, E (2012) Approach for Determination of the Failure Probability at the Soultz-sous-Forêts EGS Project, in Proceedings 37th Workshop on Geothermal Reservoir Engineering, Stanford University, pp. 8, Stanford, California

Meller, C., Kohl, T., Genter, A. and Gaucher, E. (2011) Abschätzung der Scherwahrscheinlichkeit von Klüften während der hydraulischen Stimulation, Proc. Geothermiekongress 2011, 10 S., Bochum

C- PRESENTATIONS WITH ABSTRACTS

C. Meller, E. Gaucher, T. Kohl (2014) The geomechanical significance of clay in geothermal reservoirs, 3rd European Geothermal Workshop, 15–16 October 2014, Karlsruhe, Germany.

C. Meller, T. Kohl (2014) Synthetic clay content logs- Implications for the hydro-mechanical properties of crystalline rock, 1st International Symposium on Energy Challenges and Mechanics, 8-10 July, Aberdeen, UK **(invited talk)**

C. Meller, A. Genter, T. Kohl (2014) The mapping of clay bearing fractures from well logs with a neural network and their implications for rock mechanics, 74. Jahrestagung der Deutschen Geophysikalischen Gesellschaft, 10-13 March 2014, Karlsruhe, Germany

C. Meller, A. Genter, T. Kohl (2013) The Application of a Neural Network to Identify Clay Bearing Fractures from Well Logs, 2nd European Geothermal Workshop, 24-25 October, Strasbourg, France

C. Meller, T. Kohl (2013) A Method to Map Clay Zones in Crystalline Geothermal Reservoirs - A Neural Network Based Approach Towards a Better Mechanical and Hydraulic Understanding of the Reservoir, 1st European Geothermal Workshop, 19 March 2013, Karlsruhe, Germany

C. Meller, A. Genter, T. Kohl (2013) The identification of clay bearing fractures from well logs and their implications for rock mechanics, EAGE-Sustainable Earth Sciences, 30 September-4 October, Pau, France

C. Meller, A. Genter, T. Kohl (2013) The identification of clay bearing fractures from well logs and their implication for rock mechanics, Sedimentary Basins Jena, 23-25 September, Jena, Germany

C. Meller, T. Kohl, A. Genter (2012) Synthetic clay content logs from borehole data-a neural network approach. Geothermiekongress 2012, 13-16 November, Karlsruhe, Germany (Poster)

C. Meller, T. Kohl, A. Genter, Emmanuel Gaucher (2012) Estimation of the Failure Probability during EGS Stimulation – Geological and Mechanical Processes, European Geosciences Union General Assembly, 22-27 April, Vienna, Austria

C. Meller, T. Kohl, A. Genter, E. Gaucher (2011) Abschätzung der Scherwahrscheinlichkeit von Klüften während der hydraulischen Stimulation, Geothermiekongress 2011, 15-16 November, Bochum, Germany

C. Meller, E. Gaucher, T. Kohl (2011) First steps towards determining the failure probability at the Soultz-sous-Forêts EGS project, Soultz Geothermal Conference, 5-6 October, Soultz-sous-Forêts, France

D- ACKNOWLEDGEMENTS

Many people played their very specific and important role during this PhD project. I would like to say thank you to all of them.

First of all, I would like to thank my supervisor Thomas Kohl for providing me the possibility to work on this interesting and challenging topic. With fruitful discussions and provoking questions, he contributed to my personal and scientific development and he pushed me further, when I could not to see the wood for the trees.

I would like to thank Béatrice Ledésert, who took the responsibility to be the co-examiner of my thesis.

Many thanks to the members of the Petrotherm working group for being a motivating team, which encouraged me in difficult phases during this thesis. Special people of this group have to be explicitly mentioned by name, as they contributed to a large part to the progress of this thesis.

Thank you Emmanuel for your great help and lively discussions, for the Frac-Dance, and for your good humor.

Thanks to overseas, Martin, for your integrating works at the beginning of my thesis, for several fruitful discussions, for eating my cakes, and for proofreading. I hope we will stay in contact.

Special thanks to Silke for assisting me through the bureaucratic jungle of KIT, for the lunchtime chats and occasional coffee and cocktail evenings.

Thank you, Hannah, for keeping the overview in organizational matters. Thank you, Judith, for proofreading and 'women's talks'. Thank you, Agnes, for your scientific and interpersonal support. Thank you, Niklas, for plundering my tea and 'Bonsche' supplies.

Finally, I would like to say thank you to Jens for being there for me in every situation. Many thanks to my parents for their unconditional support in all aspects and for providing me the possibility to establish my way.

THANK YOU ALL!

E- DECLARATION IN LIEU OF OATH

I herewith declare in lieu of oath that I have composed this thesis without any inadmissible help of a third party and without the use of aids other than those listed. The data and concepts that have been taken directly or indirectly from other sources have been acknowledged and referenced.

I further declare that I have followed the rules for ensuring good scientific practice at the Karlsruhe Institute of Technology (KIT), passed on 5th May 2010 by the executive committee of KIT.

This thesis has not been submitted, wholly or substantially, neither in this country nor abroad for another degree at any university or institute.

I have said nothing but the truth to the best of my knowledge and I have not withheld any information.

Karlsruhe, 29th October, 2014 _____

Carola Meller